

Advances in Experimental Medicine and Biology 820

Panayiotis Vlamos  
Athanasios Alexiou *Editors*

# GeNeDis 2014

Computational Biology and  
Bioinformatics

 Springer

# Advances in Experimental Medicine and Biology

Volume 820

---

Editorial Board:

IRUN R. COHEN, *The Weizmann Institute of Science, Rehovot, Israel*

N.S. ABEL LAJTHA, *Kline Institute for Psychiatric Research, Orangeburg, NY, USA*

RODOLFO PAOLETTI, *University of Milan, Milan, Italy*

JOHN D. LAMBRIS, *University of Pennsylvania, Philadelphia, PA, USA*

More information about this series at <http://www.springer.com/series/5584>



Panayiotis Vlamos • Athanasios Alexiou  
Editors

# GeNeDis 2014

Computational Biology and Bioinformatics

 Springer

*Editors*

Panayiotis Vlamos  
Department of Informatics  
Ionian University  
Corfu, Greece

Athanasios Alexiou  
Department of Informatics  
Ionian University  
Corfu, Greece

ISSN 0065-2598

ISBN 978-3-319-09011-5

DOI 10.1007/978-3-319-09012-2

Springer Cham Heidelberg New York Dordrecht London

ISSN 2214-8019 (electronic)

ISBN 978-3-319-09012-2 (eBook)

Library of Congress Control Number: 2014954992

© Springer International Publishing Switzerland 2015

This work is subject to copyright. All rights are reserved by the Publisher, whether the whole or part of the material is concerned, specifically the rights of translation, reprinting, reuse of illustrations, recitation, broadcasting, reproduction on microfilms or in any other physical way, and transmission or information storage and retrieval, electronic adaptation, computer software, or by similar or dissimilar methodology now known or hereafter developed. Exempted from this legal reservation are brief excerpts in connection with reviews or scholarly analysis or material supplied specifically for the purpose of being entered and executed on a computer system, for exclusive use by the purchaser of the work. Duplication of this publication or parts thereof is permitted only under the provisions of the Copyright Law of the Publisher's location, in its current version, and permission for use must always be obtained from Springer. Permissions for use may be obtained through RightsLink at the Copyright Clearance Center. Violations are liable to prosecution under the respective Copyright Law.

The use of general descriptive names, registered names, trademarks, service marks, etc. in this publication does not imply, even in the absence of a specific statement, that such names are exempt from the relevant protective laws and regulations and therefore free for general use.

While the advice and information in this book are believed to be true and accurate at the date of publication, neither the authors nor the editors nor the publisher can accept any legal responsibility for any errors or omissions that may be made. The publisher makes no warranty, express or implied, with respect to the material contained herein.

Printed on acid-free paper

Springer is part of Springer Science+Business Media ([www.springer.com](http://www.springer.com))

# Contents

<b>1</b>	<b>Optoacoustics as a Bioengineering Model for Neuroscience Discovery</b> . . . . .	<b>1</b>
	Vasilis Ntziachristos	
<b>2</b>	<b>Respiratory Particle Deposition Probability Due to Sedimentation with Variable Gravity and Electrostatic Forces</b> . . . . .	<b>3</b>
	Ioannis Haranas, Ioannis Gkigkitzis, George D. Zouganelis, Maria K. Haranas, and Samantha Kirk	
<b>3</b>	<b>Sequence Patterns Mediating Functions of Disordered Proteins</b> . . . . .	<b>49</b>
	Konstantinos P. Exarchos, Konstantina Kourou, Themis P. Exarchos, Costas Papaloukas, Michalis V. Karamouzis, and Dimitrios I. Fotiadis	
<b>4</b>	<b>Management and Modeling of Balance Disorders Using Decision Support Systems: The EMBALANCE Project</b> . . . .	<b>61</b>
	Themis P. Exarchos, Christos Bellos, Iliana Bakola, Dimitris Kikidis, Athanasios Bibas, Dimitrios Koutsouris, and Dimitrios I. Fotiadis	
<b>5</b>	<b>A Computer-Aided Diagnosis System for Geriatrics Assessment and Frailty Evaluation</b> . . . . .	<b>69</b>
	Charalampos Vairaktarakis, Vasilis Tsiamis, Georgia Soursou, Filippos Lekkas, Markella Nikolopoulou, Emmanouilia Vasileiadou, Konstantinos Premtsis, and Athanasios Alexiou	

<b>6</b>	<b>Exploiting Expert Systems in Cardiology: A Comparative Study</b> . . . . .	79
	George-Peter K. Economou, Efrosini Sourla, Konstantina-Maria Stamatopoulou, Vasileios Syrimpeis, Spyros Sioutas, Athanasios Tsakalidis, and Giannis Tzimas	
<b>7</b>	<b>Modeling Protein Misfolding in Charcot–Marie–Tooth Disease</b> . . .	91
	Georgia Theocharopoulou and Panayiotis Vlamos	
<b>8</b>	<b>The Effect of the Shape and Size of Gold Seeds Irradiated with Ultrasound on the Bio-Heat Transfer in Tissue</b> . . . . .	103
	Ioannis Gkigkitzis, Carlos Austerlitz, Ioannis Haranas, and Diana Campos	
<b>9</b>	<b>Clinical Decision Support System for the Diagnosis of Adolescence Health</b> . . . . .	125
	Irene Moutsouri, Amalia Nikou, Machi Pampalou, Maria Lentza, Paulos Spyridakis, Natassa Mathiopoulou, Dimitris Konsoulas, Marianna Lampou, and Athanasios Alexiou	
<b>10</b>	<b>Mitochondrial Fusion Through Membrane Automata</b> . . . . .	163
	Konstantinos Giannakis and Theodore Andronikos	
<b>11</b>	<b>A Mathematical Model for the Blood Plasma Flow Around Two Aggregated Low-Density Lipoproteins</b> . . . . .	173
	Maria Hadjinicolaou	
<b>12</b>	<b>Translation of Two Aggregated Low-Density Lipoproteins Within Blood Plasma: A Mathematical Model</b> . . . . .	185
	Maria Hadjinicolaou and Eleftherios Protopapas	
<b>13</b>	<b>Chaotic Attractors in Tumor Growth and Decay: A Differential Equation Model</b> . . . . .	193
	Michael Harney and Wen-sau Yim	
<b>14</b>	<b>Modeling <math>k</math>-Noncrossing Closed RNA Secondary Structures via Meandric Compression</b> . . . . .	207
	Antonios Panayotopoulos and Panayiotis Vlamos	
<b>15</b>	<b>Exploring the Online Satisfaction Gap of Medical Doctors: An Expectation-Confirmation Investigation of Information Needs</b> . . . . .	217
	Panos E. Kourouthanassis, Patrick Mikalef, Margarita Ioannidou, and Adamantia Pateli	
<b>16</b>	<b>A Cloud-Based Data Network Approach for Translational Cancer Research</b> . . . . .	229
	Wei Xing, Dimitrios Tsoumakos, and Moustafa Ghanem	
	<b>Index</b> . . . . .	239

# GeNeDis 2014 Information: Springer AEMB

## GeNeDis 2014 Overview

The 1st World Congress on Geriatrics and Neurodegenerative Disease Research, GeNeDis 2014 focused on recent advances in Geriatrics and Neurodegeneration, ranging from basic science to clinical and pharmaceutical developments, providing also an international forum for the latest scientific discoveries, medical practices, and care initiatives. Leading scientists and experts, students, physicians and nurses, professionals as well as industries representatives, and many other participants discussed the latest major challenges, new drug targets, the development of new biomarkers, imaging techniques, novel protocols for early diagnosis of neurodegenerative diseases, bioinformatics methods, and several other scientific achievements. While the European Union aims to strengthen the research and innovation towards Horizon 2020, the translational research for healthy aging and neurodegeneration will remove any barrier on multidisciplinary collaboration. Novel approaches including biomarkers, stem cell therapy, protein misfolding, immunotherapy, as well as developments in our understanding of the genetics, the molecular mechanisms and signaling pathways contributing to neuronal dysfunction, nanotechnological products, and innovative computational methods will offer new research directions and strategies on future preclinical and clinical studies on neurodegenerative diseases and further improvement of quality services on rehabilitation and health education. Advanced information technologies have been discussed concerning the various research, implementation, and policy, as well as European and global issues in the funding of long-term care and medico-social policies regarding elderly people.

We can resume the major objectives of the 1st World Congress on Geriatrics and Neurodegenerative Disease Research, GeNeDis 2014 as follows:

- To promote the scientific and research results to the research community through sharing and exchanging ideas, experiences, and expectations focusing on Healthy Aging and Mental Wellness in the new digital era.



- To explore the beneficial (and not only) impact of scientific and technological achievements and future challenges that may affect the Healthy Aging and Mental Wellness process.
- To enhance the co-operation and the exchange of experiences and resources among organizers of events and the research community, increasing further the European dimension and added value of the activities of the Europe 2020 and HORIZON 2020.
- To increase the interest of all the stakeholders in contributing to the research in the field, while mental health is a basic human right, and is fundamental to all human and social progress. It is a prerequisite to a happy and fulfilled life for individual citizens, starting at birth, for functioning families and for societal cohesion.

### **The Organizers**

- Ionian University, Department of Informatics, Bioinformatics and Human Electrophysiology, Greece
- Ionian University, Department of Informatics, Computational Modeling Laboratory, Greece
- Science View, Member of the European Science Journalists EUSJA, Greece

### **The Co-organizers**

- Hellenic Open University, School of Science and Technology, Greece
- University of Salento, Department of Innovation Engineering, Laboratory of Applied Mechanics, Section of Mechatronics, Italy
- Ionian University, Department of History, M.Sc., in Historical Research, Teaching and New Technologies, Greece
- Region of Ionian Islands, Greece

## **Scientific Program Committee**

### **Conference Chair**

Vlamos Panayiotis, Department of Informatics, Ionian University, Greece

### **Conference Vice-Chair**

Alexiou Athanasios, Department of Informatics, Ionian University, Greece

- Acosta Sandra, Institut de Recherche Interdisciplinaire en Biologie Humaine et Moléculaire, Belgium
- Aigner Ludwig, Paracelsus Medizinische Privatuniversität, Austria

- Alexopoulos Dimitrios, Dental Surgeon, Editorial Director Dentorama, Dental Journal and Dental Tribune, Hygeia Hospital
- Anagnostopoulos Dimosthenis, Harokopeio University of Athens, Greece
- Ashraf Md Ghulam, King Fahd Medical Research Center, King Abdulaziz University, Saudi Arabia
- Bilensoy Erem, Hacettepe Üniversitesi Eczacılık Fakültesi Farmasötik Teknoloji Anabilim Dalı, Turkey
- Bottalico Barbara, University of Pavia, European Center for Law, Science and New Technologies, University of Pavia, Italy
- Chrissikopoulos Vassileios, Ionian University, Greece
- Chatzidaki Georgia, Corfu General Hospital, Greece
- De Castro Fernando, Grupo de Neurobiología del Desarrollo-GNDe Hospital Nacional de Paraplégicos-SESCAM, Spain
- Delabar JM, Université Paris Diderot, France
- Demetzos Costas, Dept. of Pharmaceutical Technology, Faculty of Pharmacy, National and Kapodistrian University of Athens, Greece
- D’Mello Santosh R., University of Texas, USA
- Exarchos Themis, Department of Computer Science, University of Ioannina, Greece
- Fjeldsted Katrin, President Standing Committee of European Doctors
- Fotiadis Dimitrios, University of Ioannina, Greece
- Geoghegan-Quinn Maire, Commissioner of Research, Innovation and Science, EU
- Georgiadis Adonis, Minister For Health, Greece
- Giannakopoulos Panteleimon, Professor, Chairman of the Department of Mental Health and Psychiatry, University Hospitals of Geneva, Switzerland
- Ghiatas Abraham, University of Texas, USA
- Gkigkitzis Ioannis, Departments of Mathematics and Biomedical Physics, East Carolina, USA
- Gonos Efstathios, National Hellenic Research Foundation, Institute of Biological Research and Biotechnology, Greece
- Hadjinicolaou Maria, Hellenic Open University, Greece
- Haranas Ioannis, VDG Research and Development in Electromagnetic Theory Applications, Department of Mathematics, East Carolina University, USA
- Huotilainen Minna, University of Helsinki, Finland
- Ifantis Ilias, Hellenic Naval Academy, Piraeus, Greece
- Karabatsas Kostantinos, Governor of General Hospital Achillopouleion of Volos
- Karalis Vangelis, Faculty of Pharmacy, National Kapodistrian University of Athens, Greece
- Kariotou Foteini, Hellenic Open University, Greece
- Kontogeorgis Georgios, Technical University of Denmark
- Koumoutsakos Georgios, Commissioner, EU
- Knyazeva Maria, Lausanne University Hospital, Switzerland
- Lefkimmiatis Konstantinos, Department of Physiology Anatomy and Genetics, University of Oxford

- Logothetis Nikos, Max-Planck-Institute for Biological Cybernetics, Germany
- Luhan Petru Constantin, Commissioner, EU
- Marambaud Philippe, The Feinstein Institute for Medical Research
- Matsas Rebecca, Hellenic Pasteur Institute, Greece
- Nääätänen Risto, University of Helsinki, Finland
- Oertel Wolfgang, Neurological Clinic Institution, Philipps-Universität Marburg, Germany
- Orban Guy, KU Leuven, Belgium
- Pasinetti Giulio, Icahn School of Medicine at Mount Sinai, Department of Neurology and Friedman Brain Institute, New York
- Pateli Adamantia, Ionian University, Greece
- Priyadarshini Madhusmita, University of Helsinki, Finland
- Protopappas Vasilios, University of Ioannina, Greece
- Psiha Maria, Ionian University, Greece
- Ratana Rajiv R., Burke Medical Research Institute, Cornell University, USA
- Robakis Nikolaos, Mount Sinai Hospital, New York
- Sakka Paraskevi, Athens Alzheimer's Association, Dementia Society, Greece
- Serrano Alberto, University Autonoma Madrid, Spain
- Sattler Wolfgang, University of Graz, Austria
- Simou Panagiota, Department of Audio and Visual Arts, Ionian University, Greece
- Sioutas Spyros, Ionian University, Greece
- Tabrez Shams, King Fahd Medical Research Center, King Abdulaziz University, Saudi Arabia
- Takashima Akihito, Department of Aging Neurobiology
- Tarnanas Ioannis, Universität Bern, Germany
- Tiligadis Konstantinos, Department of Audio and Visual Arts, Ionian University, Greece
- Tripoliti Evi, University of Ioannina, Greece
- Tsamis Konstantinos, University of Ioannina, Greece
- Tsantili-Kakoulidou Anna, President of the Society of Hellenic Medicinal Chemistry, Greece
- Tsolaki Magda, Aristotle University of Thessaloniki, Greece
- Tsoumakos Dimitrios, Ionian University, Greece
- Velayudhan Latha, Department of Health Science, University of Leicester, England
- Van der Jeugd Anneke, Laboratory of Biological Psychology, KU Leuven, Belgium
- Villringer Arno, Max Planck Institute for Human Cognitive and Brain Sciences, Germany
- Volikas Kimon, University of Nicosia, Cyprus
- Wolozin Benjamin, Department of Pharmacology Boston University Alzheimer's Disease Center
- Xiang Zhao, Neuroscience Center, University of Helsinki, Finland
- Xing Wei, Scientific Computing/PI, University of Manchester, United Kingdom

- Yapijakis Christos, Department of Oral and Maxillofacial Surgery, University of Athens Medical School “Attikon” Hospital, Greece
- Zaidi Syed Kashif, Center of Excellence in Genomic Medicine Research, King Abdulaziz University, Saudi Arabia
- Zaganas Ioannis, Department of Neurology, Medical School, University of Crete, Greece
- Zouganelis George, Bournemouth and Poole College, United Kingdom

### **Keynote Lectures**

- Professor Nikolaos Robakis, Professor of Psychiatry, Neuroscience and experimental therapeutics. First A.P. Slaner Professor for Alzheimer disease research. Mount Sinai School of Medicine, NYU, USA, Title: Molecular neuropathology of Alzheimer dementia and therapeutic approaches
- Professor George Paxinos, A.O., D.Sc., F.A.S.S.A., F.A.A., N.H.M.R.C., Australia Fellow, Neuroscience Research Australia, Barker St and Hospital Rd, Randwick, Sydney, Australia, Title: Brain, Behaviour and Evolution
- Professor Vasilis Ntziachristos, Chair Institute for biological and medical imaging (IBMI) Technische Universität München, Germany, Title: Biomedical optics and optoacoustics as a model for scientific discovery and economic growth
- Dr. Akihito Takashima, Department of Aging Neurobiology, National Center for Geriatrics and Gerontology, Japan, Title: Toxic tau aggregation in AD
- Professor Benjamin Wolozin, Department of Pharmacology Boston University Alzheimer’s Disease Center, USA, Title: Stress granules and Neurodegeneration: A new paradigm for mechanisms of neurodegeneration
- Professor Panteleimon Giannakopoulos, Chairman of the Department of Mental Health and Psychiatry, University Hospitals of Geneva, Switzerland, Title: Mental health in a global world: moving from illness to individual vulnerability
- Dr. Efstathios Gonos, Director of Research IUBMB, National Hellenic Research Foundation, Institute of Biology, Medicinal Chemistry and Biotechnology, Greece, Title: Proteasome activation delays ageing and minimizes deficiencies underlying neurodegenerative diseases
- Dr. Ioannis Haranas, VDG Research and Development in Electromagnetic Theory Applications, Department of Mathematics, East Carolina University, USA, Title: Respiratory Particle Deposition Probability due to Sedimentation with Variable Gravity and Electrostatic Forces
- Professor Dimitrios Fotiadis, Unit of Medical Technology and Intelligent Information Systems, University of Ioannina, Title: Sequence patterns mediating functions of disordered proteins
- Professor Arno Villringer, Max Planck Institute for Human Cognitive and Brain Sciences, Germany, Title: The path from obesity and hypertension to dementia
- Professor Constantin Bouras, University Hospitals, Geneva, Department of Psychiatry, Switzerland, Title: Individual severity of AD-type lesions, A $\beta$  oligomers and comorbidity in the brain aging

**Invited Talks: Workshops and Round Tables**

- Professor Theodosia Vallianatou, Department of Pharmaceutical Chemistry, School of Pharmacy, University of Athens, Greece, Title: The impact of physicochemical and molecular properties in drug design. Navigation in the “drug-like” chemical space
- Professor Costas Demetzos, Faculty of Pharmacy, National and Kapodistrian University of Athens, Title: Advanced Drug Delivery nano Systems: perspectives and regulatory issues
- Dr. Paraskevi Sakka, Neurologist-Psychiatrist, Director at Hygeia Hospital, Neurodegenerative Brain Conditions – Memory Clinic, Chairwoman at Athens Association of Alzheimer’s Disease, and Related Disorders, Greece, Title: Non-pharmacological treatments of dementia. The encouraging results of SOCIABLE

# Chapter 1

## Optoacoustics as a Bioengineering Model for Neuroscience Discovery

Vasilis Ntziachristos

We present the development of novel biomedical imaging methods based on optoacoustics. These novel tools can revolutionize biomedical discovery and clinical healthcare. We focus in particular in multispectral optoacoustic tomography (MSOT). This technology, now recipient of numerous awards and acclaim, shows two important developments: on one hand on how it can break through the limits of conventional optical imaging to shift the paradigm of biomedical observation and on the other how biomedical technology offers a necessary leverage point in scientific discovery but also economic growth, even at moderate investments.

---

V. Ntziachristos (✉)  
Technische Universität München, Munich, Germany  
e-mail: [vntziachristos@gmail.com](mailto:vntziachristos@gmail.com)

# Chapter 2

## Respiratory Particle Deposition Probability Due to Sedimentation with Variable Gravity and Electrostatic Forces

Ioannis Haranas, Ioannis Gkigkitzis, George D. Zouganelis,  
Maria K. Haranas, and Samantha Kirk

**Abstract** In this chapter, we study the effects of the acceleration gravity on the sedimentation deposition probability, as well as the aerosol deposition rate on the surface of the Earth and Mars, but also aboard a spacecraft in orbit around Earth and Mars as well for particles with density  $\rho_p = 1,300 \text{ kg/m}^3$ , diameters  $d_p = 1, 3, 5 \text{ }\mu\text{m}$ , and residence times  $t = 0.0272, 0.2 \text{ s}$ , respectively. For particles of diameter  $1 \text{ }\mu\text{m}$  we find that, on the surface of Earth and Mars the deposition probabilities are higher at the poles when compared to the ones at the equator. Similarly, on the surface of the Earth we find that the deposition probabilities exhibit 0.5 and 0.4 % higher percentage difference at the poles when compared to that of the equator, for the corresponding residence times. Moreover in orbit equatorial orbits result to higher deposition probabilities when compared to polar ones. For both residence times particles with the diameters considered above in circular and elliptical orbits around Mars, the deposition probabilities appear to be the same for all orbital inclinations. Sedimentation probability increases drastically with particle diameter and orbital eccentricity of the orbiting spacecraft. Finally, *as an alternative framework for the study of interaction and the effect of gravity in biology, and in particular gravity*

---

I. Haranas (✉)

Physics and Computer Science, Wilfrid Laurier University, Science Building, Room N2078  
75 University Ave. W, Waterloo, ON, N2L 3C5, Canada  
e-mail: [yiannis.haranas@gmail.com](mailto:yiannis.haranas@gmail.com)

I. Gkigkitzis • S. Kirk

Departments of Mathematics and Biomedical Physics, East Carolina University,  
124 Austin Building, East Fifth Street, Greenville, NC, 27858-4353, USA  
e-mail: [gkigkitzisi@ecu.edu](mailto:gkigkitzisi@ecu.edu)

G.D. Zouganelis

Health and Medical Sciences, Bournemouth and Poole College, North Road, Poole,  
Dorset BH14-OLS, United Kingdom  
e-mail: [zouganelisg@bpc.ac.uk](mailto:zouganelisg@bpc.ac.uk)

M.K. Haranas

Department of Informatics with Applications in Medicine, University of Thessaly,  
Argonafton & Filellinon, 38221 Volos, Magnesia, Greece  
e-mail: [maria\\_h1692@hotmail.com](mailto:maria_h1692@hotmail.com)

*and the respiratory system we introduce is the term information in a way Shannon has introduced it, considering the sedimentation probability as a random variable. This can be thought as a way in which gravity enters the cognitive processes of the system (processing of information) in the cybernetic sense.*

**Keywords** Deposition probability • Sedimentation • Gravitational acceleration • Zonal harmonic • Information • Respiratory system • Cybernetics

## 2.1 Introduction

Airborne particles have always been around in the history of mankind. Human population has been exposed to the inhalation of airborne particle clouds, clouds that have been created by various natural processes that include volcanic eruptions and forest fires. The severity of corresponding exposures can be hazardous or even fatal, if the particle air concentration, size, and composition of the suspended materials. In a pioneering paper by Watkins Pitchford and Moir [33] the authors understand the importance of that, and they find that 80 % of the particles in silicotic human lungs are smaller than  $2 \mu\text{m}$  in diameter. Next, Hatch and Gross [14] report that inhalation exposure to aerosols of fine zinc oxide particles of diameter less  $0.6 \mu\text{m}$  can cause the so called “metal fume fever,” where exposure to similar air concentrations of zinc oxide that results from bulk material is not toxic. The measured concentration of the corresponding contaminant particles and their total inhaled volume was found to be insufficient to predict the pathological effects of inhalation exposure, and also to predict the relative hazard to a particular aerosol, that might be dust or mist. It is the size distribution and also the density of particular aerosol particles which determines their penetration depth as well as their fractional deposition in the respiratory track which results in the determination of the location of their critical sites of action and finally their translocational mechanisms. The use of the term aerosol simply refers to particles that might be solid or liquid in nature, with a sufficiently small diameter that can be suspended in the air as it is defined by Green and Lane [9].

To describe any possible risks associated with the inhalation of aerosol particles, one must know how much is deposited in a particular region of the respiratory track as well as how much is left after a physiological clearance from that region. Any remaining material can constitute a potential effective dose which can produce an acute or a chronic pulmonary disease. Deposition of the aerosol material within the respiratory track is predicted by models and also experimental evaluation and they important in the case of soluble aerosols, because their contaminants reach the bloodstream but also the lymphatic channels from several places of the respiratory track. Deposition is an important step in determining various clearance processes. In Morrow et al. [21] a discussion on lung dynamics the respiratory track can be described in terms of three compartments that are based upon a clearance mechanism associated with each place separately. Inhaled particles deposited in the



posterior nares will be caught in the mucus and conveyed by mucocilliary action through the nasopharynx, and into the gastrointestinal track [15].

In this contribution we examine the effect of variable gravity might have on the deposition probability of aerosol particles on the surface of the Earth and also above an orbiting spacecraft. For that we correct the acceleration of gravity on the surface for the Earth's rotation and for its oblateness via the  $J_2$  harmonic coefficient of the gravitational field. The effect of various latitudes is examined and compared, for particles of various sizes and a particular density. Similarly, in orbiting spacecraft this is achieved by transforming the gravitational acceleration at the orbital altitude of the spacecraft as a function of the orbital elements, and for three orbits of three different inclinations the sedimentation probabilities are examined and compared. Next, we modify the acceleration of gravity by adding an electrostatic deposition acceleration caused by the image force acting on the particles. This acceleration is responsible for the deposition increase within the respiratory track, and therefore the deposition probability is again calculated on the surface of the Earth and in an orbiting spacecraft experiment. After that, the aerosol deposition rate on the surface of the Earth and Mars as well as aboard an orbiting spacecraft is also calculated. Finally, *as an alternative framework for the study of interaction of the effect of gravity in biology, and in particular gravity and respiratory system we introduce, is the term information in a way Shannon has introduced it, considering the sedimentation probability as a random variable.* This can be thought as a way in which gravity enters the cognitive processes of the system (processing of information) in the cybernetic sense.

## 2.2 Mechanisms of Deposition

Aerosol particles are inhaled and deposited in the human respiratory track. Inertial impaction of the inhaled particles is the main mechanism of large particle deposition in the upper part of the respiratory track. Inertial impaction can act on particles ranging from 2 to 3  $\mu\text{m}$  to greater than 20  $\mu\text{m}$  in diameter, i.e., 50  $\mu\text{m}$ . It is the inertia of the large airborne particles that tend to maintain their initial path when the supporting air stream is deflected suddenly by nasal turbinates or branching of the airways. The probability of inertial deposition  $P_{\text{dep}_i}$  is proportional to the product of the terminal settling velocity  $v_{\text{ter}}$ , which is higher for larger diameter particles, and  $v_{\text{air}}$ , is the entrained particle velocity which is inversely proportional to the radius  $R$  of the airway (Gussman 1969a):

$$P_{\text{dep}_i} \propto \frac{v_{\text{ter}} v_{\text{air}} \sin \theta}{(gR + v_{\text{ter}} v_{\text{air}} \sin \theta)}, \quad (2.1)$$

where  $g$  is the acceleration of gravity. In the case of a large increasing air velocity, smaller airway radius and large bending angle  $\theta$  implies a large inertial impaction probability  $P_i$  becomes ideally large (Fig. 2.1).

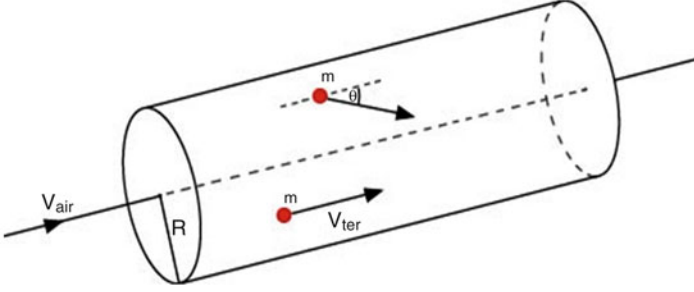


**Fig. 2.1** Particles entering the airway at an angle  $\theta$  with terminal velocity  $v_{ter}$  and air velocity  $v_{air}$ , at an angle  $\theta$  to the horizontal

Settling terminal velocity is related to sedimentation, and it is very important for particle deposition in the respiratory track. A particle falling under gravity, acquires a terminal velocity that is given by [13]

$$v_{ter} = \frac{gd^2(\rho_p - \rho_{air})}{18\eta_{air}}, \quad (2.2)$$

where  $\eta_{air}$  is the viscosity of the air,  $\rho_p$  is the density of the particle,  $\rho_{air}$  is the density of the air, and  $d$  is the diameter of the particle. When the particle's diameter becomes very small and of the same order with the air molecule mean free path  $L$ , the corresponding drag increases and the following correction must be applied [5]:

$$v_{ter}(\text{cor}) = v_{ter}(\text{cal}) \left[ 1 + \frac{2C_c}{d}L \right], \quad (2.3)$$

where  $v_{ter}(\text{cor})$  and  $v_{ter}(\text{cal})$  are the corrected and calculated terminal velocities, respectively [10], and where  $C_c$  is given by the following expression (Hinds 1999):

$$C_c = 1 + \frac{\lambda}{d_p} \left[ 2.34 + 1.05e^{-\left(\frac{0.39}{\lambda}d_p\right)} \right], \quad (2.4)$$

$C_c$  is the so-called Cunningham correction or “slip correction factor” that must be taken into account when the size of the aerosol particles is comparable to the mean free path of the atmospheric molecules, discontinuities in the medium become important consideration, and particle mobility increases.  $\lambda$  is the mean free path of the air, and its inversely proportional to its density  $\lambda = 7.91 \times 10^{-8}/\rho_{air}$  for  $\lambda$  in meters and  $\rho_{air}$  in  $\text{kg/m}^3$ , and  $d_p$  in meters. In a time  $t$ , the inhaled particles travel a distance  $d_{ter} = v_{ter}t$ , and therefore, if the particles enter the airway at an angle  $\theta$  with the horizontal then the deposition probability  $P_{dep}$  due to sedimentation becomes (Landhal 1950)

$$P_{\text{sed}} = 1 - e^{-\left(\frac{\tau(\rho_p - \rho_{\text{air}})d_p^2 C_c}{18\eta_{\text{air}}R} g \cos \theta\right)}. \quad (2.5)$$

The time it takes for a particle to travel in the trachea is

$$\tau = \frac{L_{\text{tr}}}{v_{\text{air}}}, \quad (2.6)$$

Eliminating this traveling time  $\tau$  in Eq. (2.5) we obtain that the sedimentation probability takes the form

$$P_{\text{sed}} = 1 - e^{-\left(\frac{(\rho_p - \rho_{\text{air}})d_p^2 C_c}{18\eta_{\text{air}}R} \frac{L}{v_{\text{air}}} g \cos \theta\right)} \quad (2.7)$$

where  $L$  is the length of trachea,  $v$  the velocity of the air, and  $R$  the radius of the airway. Sedimentation is the basic mechanism via which inhaled particles in the range  $0.1 \mu\text{m} \leq d_p \leq 50 \mu\text{m}$  are deposited. We can write the particle's effective distance at right angles to the direction of travel in the following way:

$$h_s = \frac{v_{\text{ter}}\eta_{\text{air}}}{g} \sin \theta, \quad (2.8)$$

where  $\theta$  is the same angle defined before. Finally, the ratio  $r$  of the fall distance or the distance that the particle travels in time  $t$  moving with terminal velocity  $v_t$  to the max distance of deposition or the physical distance of the diameter of object (trachea) in our case that the particle has to travel becomes

$$h_{\text{max}} = \frac{v_{\text{ter}}\tau}{2R} \cos \theta = \frac{v_{\text{ter}}}{2R} \left(\frac{L_{\text{tr}}}{v_{\text{air}}}\right) \cos \theta. \quad (2.9)$$

When a particle enters our respiratory system is subject to the deposition mechanism described above. The actual deposition efficiency of a given particle size has been determined experimentally. Various models have been developed to predict the deposition based on experimental data. The most advanced and widely used is the one developed by the International Commission on Radiological Protection (ICRP) and the National Council on Radiation Protection and Measurement (NCRP). The total deposition fraction (DF) in the respiratory system according to ICRP model is given by [16]

$$DF = \left[ 1 - 0.5 \left[ 1 - \frac{1}{1 + 0.00076d_p^{2.8}} \right] \right] \left[ 0.0587 + \frac{0.911}{1 + e^{(4.77+1.485\ln d_p)}} + \frac{0.943}{1 + e^{(0.53-2.58\ln d_p)}} \right]. \quad (2.10)$$

where  $d_p$  is the particle diameter in microns.

### 2.3 The Gravitational Acceleration on the Surface of the Earth and at Orbital Point

In our effort to study the effect of gravity on the respiratory system, let us consider the acceleration of gravity  $g$  at the orbital altitude of the spacecraft in which a respirator type of experiment is taking place under controlled conditions. Following Haranas et al. [12] we write the acceleration of gravity as the sum of three different components namely

$$V_{\text{tot}}(r') = -\frac{GM_E}{r'} + \frac{GM_ER_E^2J_2}{2r'^3} (3 \sin^2\phi_E - 1) - \frac{1}{2}\omega_E^2 r'^2 \cos^2\phi_E. \quad (2.11)$$

where  $r'$  is the radial distance from the center of the Earth to an external surface point,  $M_E$  is the mass of the Earth,  $R_E$  is the radius of the Earth,  $J_2$  is the zonal harmonic coefficient that describes the oblateness of the Earth,  $\omega_E$  is the angular velocity of the Earth, and  $\phi_E$  is the geocentric latitude of the designed experiment. Zonal harmonics are simply bands of latitude, whose boundaries are the roots of a Legendre polynomial. Spherical harmonics in general are very important concept in solar system research and in particular in the modeling of planetary gravity fields. For example in Hadjifotinou [11] the author uses a gravitational potential that includes a  $J_2$  as well as a  $J_4$  harmonics in predicting numerically the motion of Saturn's satellites. Similarly, in Iorio [17] the author derives the precession of the ascending node of a satellite due to Lense-Thirring effect as a function of the  $J_2$  harmonic. This particular gravitational harmonic coefficient is a result of the Earth's shape and is about 1,000 times larger than the next harmonic coefficient  $J_3$  and its value is equal to  $J_2 = -0.0010826260$  (Kaula 2000). At the orbital point of the spacecraft the rotational potential on the surface of the earth does not affect the orbit of spacecraft. Therefore the gravitational acceleration as it is given by Eq. (2.2) can be transformed as a function of orbital elements, using standard transformations given by Kaula (2000) and Vallado (2007) namely  $\sin\phi_E = \sin i \sin(u) = \cos\theta_E$ , where,  $\phi_E$  is the geocentric latitude, measured from the Earth's equator to the poles, and  $\theta_E$  is the corresponding colatitude measured from the poles down to the equator ( $\theta_E = 90 - \phi_E$ ),  $u = \omega + f$  is the argument of latitude that defines the position of a body moving along a Kepler orbit,  $i$  its orbital inclination,  $\omega$  is the argument of the perigee of the spacecraft (not to be confused with angular velocity, which we write with subscripts),  $f$  is its true

anomaly (an angle defined between the orbital position of the spacecraft and its perigee). The orbital elements are shown in Fig. 2.2 below.

To familiarize the reader with the orbital elements used here let us define the orbital elements appearing in our Eq. (2.4) below.  $a_s$  is the semi-major axis that defines the size of the orbital ellipse. It is the distance from the center of the ellipse to an apsis, i.e., the point where the radius vector is maximum or minimum (i.e., apogee and perigee points). Similarly,  $e$  is the eccentricity, that defines the shape of the orbital ellipse (minor to major axis ratio),  $i$  is the inclination of the orbit defined as the angle between the orbital and equatorial planes, and  $\omega$  is the argument of the perigee, the angle between the direction of the ascending node (the point on the equatorial plane at which the spacecraft crosses from south to north) and the direction of the perigee. Finally, the true anomaly  $f$  is the angle that locates the spacecraft in the orbital ellipse and is measured in the direction of motion from the perigee to the position vector of the satellite. Assuming an elliptical orbit the geocentric orbital distance  $r'$  is given by (Vallado 2007)

$$r' = \frac{a_s(1 - e^2)}{(1 + e \cos f)}, \quad (2.12)$$

and therefore Eq. (2.11) becomes a function of the spacecraft orbital elements:

$$g_{\text{tot}} = -\frac{GM_E(1 + e \cos f)^2}{a_s^2(1 - e^2)^2} + \frac{3GM_ER_E^2J_2(1 + e \cos f)^4}{2a_s^4(1 - e^2)^4}(3 \sin^2 i \sin^2 f - 1). \quad (2.13)$$

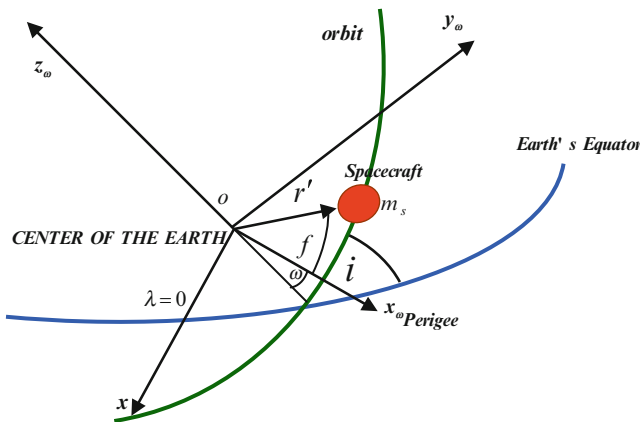


**Fig. 2.2** Explanation of the orbital elements: inclination  $i$ , argument of latitude  $u = \omega + f$ , and the radial vector  $r'$  of the spacecraft, and  $\lambda = 0$  is the zero longitude point on the Earth's equator, and  $x_\omega, y_\omega, z_\omega$  define a right-handed coordinate system (Haranas et al. [12])

First, let us consider a sedimentation experiment that takes place on the surface of the Earth  $r = R_E$ . In this case from Eq. (2.11) we obtain the following expression for the acceleration of gravity corrected for the oblateness and the rotation of the Earth on the Earth's surface and therefore the gravitational acceleration  $g_s$  becomes

$$-g_s = \frac{GM_E}{R_E^2} - \frac{3GM_E J_2}{2R_E^2} (3 \sin^2 \phi - 1) - R_E \omega_E^2 \cos^2 \phi. \quad (2.14)$$

Furthermore, thinking the Earth to be an ellipsoid of revolution we can write that (Kaula 2000)

$$\begin{aligned} R_E &= R_{\text{eq}} \left( 1 - \left( f' + \frac{3}{2} f'^2 \right) \sin^2 \phi_E + \frac{3}{2} f'^2 \sin^4 \phi_E - \dots \right) \\ &\approx R_{\text{eq}} \left( 1 - f' \sin^2 \phi_E \right), \end{aligned} \quad (2.15)$$

where  $\phi$  is the planetocentric latitude, and  $f'$  is the Earth's flattening that it is given by

$$f' = \frac{R_{\text{eq}} - R_{\text{pol}}}{R_{\text{eq}}} = \frac{3J_2}{2} + \frac{R_E^3 \omega_E^2}{2GM_E}, \quad (2.16)$$

where  $R_{\text{eq}}$  and  $R_{\text{pol}}$  is the Earth's equatorial and polar radii and therefore. Eq. (2.14) becomes

$$\begin{aligned} g_s &= \frac{GM_E}{R_{\text{eq}}^2 (1 - f' \sin^2 \phi)^2} \\ &- \frac{3GM_E J_2}{2R_{\text{eq}}^2 (1 - f' \sin^2 \phi)^2} (3 \sin^2 \phi - 1) - R_{\text{eq}} (1 - f' \sin^2 \phi) \omega_E^2 \cos^2 \phi. \end{aligned} \quad (2.17)$$

On the surface of the Earth and for the geocentric latitude  $\phi = 0^\circ, 45^\circ, 90^\circ$  Eq. (2.17) results in the following expressions for the gravitational acceleration:

$$g_{\phi=0} = \frac{GM_E}{R_{\text{eq}}^2} + \frac{3GM_E J_2}{2R_{\text{eq}}^2} - R_{\text{eq}} \omega_E^2. \quad (2.18)$$

$$g_{\phi=45} = \frac{GM_E}{R_{\text{eq}}^2 (1 - f')^2} - \frac{3GM_E J_2}{4R_{\text{eq}}^2 (1 - \frac{f'}{2})^2} - \frac{1}{2} \left( 1 - \frac{f'}{2} \right) R_{\text{eq}} \omega_E^2, \quad (2.19)$$

$$g_{\phi=90} = \frac{GM_E}{R_{\text{eq}}^2 (1 - f')^2} - \frac{3GM_E J_2}{R_{\text{eq}}^2 (1 - f')^2}. \quad (2.20)$$

## 2.4 Modified Gravity Probability Deposition Due to Sedimentation

First let us now consider Eq. (2.7) for the deposition probability of particles on the surface of the Earth, where the gravitational acceleration has been corrected for the rotation of the Earth and also for its oblateness via the  $J_2$  harmonic coefficient. Using Eqs. (2.6) and (2.18–2.20) we can write that the deposition probability becomes

$$P_{\text{sed}} = 1 - e^{-\left(\frac{(\rho_p - \rho_{\text{air}})d_p^2 C_c}{18\eta_{\text{air}}R} \frac{L}{v_{\text{air}}} \left(\frac{GM_E}{R_{\text{eq}}^2} + \frac{3GM_E J_2}{2R_{\text{eq}}^2} - R_{\text{eq}}\omega_E^2\right) \cos\theta\right)}, \quad (2.21)$$

$$P_{\text{sed}} = 1 - e^{-\left(\frac{(\rho_p - \rho_{\text{air}})d_p^2 C_c}{18\eta_{\text{air}}R} \frac{L}{v_{\text{air}}} \left(\frac{GM_E}{R_{\text{eq}}^2(1-f')^2} - \frac{3GM_E J_2}{4R_{\text{eq}}^2(1-f')^2} - \frac{1}{2}\left(1-\frac{f'}{2}\right)R_{\text{eq}}\omega_E^2\right) \cos\theta\right)}, \quad (2.22)$$

$$P_{\text{sed}} = 1 - e^{-\left(\frac{(\rho_p - \rho_{\text{air}})d_p^2 C_c}{18\eta_{\text{air}}R} \frac{L}{v_{\text{air}}} \left(\frac{GM_E}{R_{\text{eq}}^2(1-f')^2} - \frac{3GM_E J_2}{R_{\text{eq}}^2(1-f')^2}\right) \cos\theta\right)}. \quad (2.23)$$

For circular orbits, i.e.,  $e = 0$ , of inclinations  $i = 0^\circ, 45^\circ, 90^\circ$  we obtain

$$P_{\text{sed}} = 1 - e^{-\left(\frac{(\rho_p - \rho_{\text{air}})d_p^2 C_c}{18\eta_{\text{air}}R} \frac{L}{v_{\text{air}}} \left(\frac{GM_E}{a^2} + \frac{3GM_E R_{\text{eq}}^2 J_2}{2a^4}\right) \cos\theta\right)}. \quad (2.24)$$

$$P_{\text{sed}} = 1 - e^{-\left(\frac{(\rho_p - \rho_{\text{air}})d_p^2 C_c}{18\eta_{\text{air}}R} \frac{L}{v_{\text{air}}} \left(\frac{GM_E}{a^2} + \frac{3GM_E R_{\text{eq}}^2 J_2}{2a^4} \left(\frac{3\sin^2 u}{2} - 1\right)\right) \cos\theta\right)}, \quad (2.25)$$

$$P_{\text{sed}} = 1 - e^{-\left(\frac{(\rho_p - \rho_{\text{air}})d_p^2 C_c}{18\eta_{\text{air}}R} \frac{L}{v_{\text{air}}} \left(\frac{GM_E}{a^2} + \frac{3GM_E R_{\text{eq}}^2 J_2}{2a^4} \left(\frac{3\sin^2 u - 1}{2}\right)\right) \cos\theta\right)}. \quad (2.26)$$

Similarly, for elliptical orbits of the same inclinations the deposition probability of particles takes the form

$$P_{\text{sed}} = 1 - e^{-\left( \frac{(\rho_p - \rho_{\text{air}})d_p^2 C_c}{18\eta_{\text{air}}R} \frac{L}{v_{\text{air}}} \left( \frac{GM_E(1 + e \cos f)^2}{a^2(1 - e^2)} + \frac{3GM_E R_{\text{eq}}^2 J_2 (1 + e \cos f)^4}{2a^4(1 - e^2)^4} \right) \cos \theta \right)}. \quad (2.27)$$

$$P_{\text{sed}} = 1 - e^{-\left( \frac{(\rho_p - \rho_{\text{air}})d_p^2 C_c}{18\eta_{\text{air}}R} \frac{L}{v_{\text{air}}} \left( \frac{GM_E(1 + e \cos f)^2}{a^2(1 - e^2)} + \frac{3GM_E R_{\text{eq}}^2 J_2 (1 + e \cos f)^4}{2a^4(1 - e^2)^4} \left( \frac{3 \sin^2 f}{2} - 1 \right) \right) \cos \theta \right)}. \quad (2.28)$$

$$P_{\text{sed}} = 1 - e^{-\left( \frac{(\rho_p - \rho_{\text{air}})d_p^2 C_c}{18\eta_{\text{air}}R} \frac{L}{v_{\text{air}}} \left( \frac{GM_E(1 + e \cos f)^2}{a^2(1 - e^2)} + \frac{3GM_E R_{\text{eq}}^2 J_2 (1 + e \cos f)^4}{2a^4(1 - e^2)^4} \left( \frac{3 \sin^2 f - 1}{2} \right) \right) \cos \theta \right)}. \quad (2.29)$$

## 2.5 Modified Gravity Ratio of the Fall Distance to the Maximum Distance for Deposition

In Eq. (2.7) we have given the ratio  $r$  of the fall distance to the max distance for deposition. In this section we correct Eq. (2.7) by correcting the gravitational acceleration on the surface of the Earth for the rotation of the Earth, and also for its oblateness, we give expressions for three different geocentric latitudes, taking Earth's flattening into account. Similarly, we extend the expression for the maximum height when in orbit around a planetary body in our case the Earth and therefore we obtain

$$h_{\text{max}} = \frac{(\rho_p - \rho_{\text{air}})d_p^2 C_c}{18\eta_{\text{air}}R} \frac{L}{v_{\text{air}}} \left( \frac{GM_E}{R_{\text{eq}}^2} + \frac{3GM_E J_2}{2R_{\text{eq}}^2} - R_{\text{eq}} \omega_E^2 \right) \cos \theta, \quad (2.30)$$

$$h_{\text{max}} = \frac{(\rho_p - \rho_{\text{air}})d_p^2 C_c}{18\eta_{\text{air}}R} \frac{L}{v_{\text{air}}} \left( \frac{GM_E}{R_{\text{eq}}^2 (1 - f')^2} - \frac{3GM_E J_2}{4R_{\text{eq}}^2 (1 - \frac{f'}{2})^2} - \frac{1}{2} \left( 1 - \frac{f'}{2} \right) R_{\text{eq}} \omega_E^2 \right) \cos \theta, \quad (2.31)$$

$$h_{\text{max}} = \frac{(\rho_p - \rho_{\text{air}})d_p^2 C_c}{18\eta_{\text{air}}R} \frac{L}{v_{\text{air}}} \left( \frac{GM_E}{R_{\text{eq}}^2 (1 - f')^2} - \frac{3GM_E J_2}{R_{\text{eq}}^2 (1 - f')^2} \right) \cos \theta. \quad (2.32)$$

For circular orbits, i.e.,  $e = 0$ , of inclinations  $i = 0^\circ, 45^\circ, 90^\circ$  we obtain

$$h_{\text{max}} = \frac{(\rho_p - \rho_{\text{air}})d_p^2 C_c}{18\eta_{\text{air}}R} \frac{L}{v_{\text{air}}} \left( \frac{GM_E}{a^2} + \frac{3GM_E R_{\text{eq}}^2 J_2}{2a^4} \right) \cos \theta, \quad (2.33)$$



$$h_{\max} = \frac{(\rho_p - \rho_{\text{air}})d_p^2 C_c}{18\eta_{\text{air}}R} \frac{L}{v_{\text{air}}} \left( \frac{GM_E}{a^2} + \frac{3GM_E R_{\text{eq}}^2 J_2}{2a^4} \left( \frac{3 \sin^2 u}{2} - 1 \right) \right) \cos \theta, \quad (2.34)$$

$$h_{\max} = \frac{(\rho_p - \rho_{\text{air}})d_p^2 C_c}{18\eta_{\text{air}}R} \frac{L}{v_{\text{air}}} \left( \frac{GM_E}{a^2} + \frac{3GM_E R_{\text{eq}}^2 J_2}{2a^4} \left( \frac{3 \sin^2 u}{2} - 1 \right) \right) \cos \theta. \quad (2.35)$$

Similarly, for elliptical orbits of the same inclinations the ratio takes the form

$$h_{\max} = \frac{(\rho_p - \rho_{\text{air}})d_p^2 C_c}{18\eta_{\text{air}}R} \frac{L}{v_{\text{air}}} \left( \frac{GM_E(1 + e \cos f)^2}{a^2(1 - e^2)} + \frac{3GM_E R_{\text{eq}}^2 J_2 (1 + e \cos f)^4}{2a^4(1 - e^2)^4} \right) \cos \theta, \quad (2.36)$$

$$h_{\max} = \frac{(\rho_p - \rho_{\text{air}})d_p^2 C_c}{18\eta_{\text{air}}R} \frac{L}{v_{\text{air}}} \left( \frac{GM_E(1 + e \cos f)^2}{a^2(1 - e^2)} + \frac{3GM_E R_{\text{eq}}^2 J_2 (1 + e \cos f)^4}{2a^4(1 - e^2)^4} \left( \frac{3 \sin^2 f}{2} - 1 \right) \right) \cos \theta, \quad (2.37)$$

$$h_{\max} = \frac{(\rho_p - \rho_{\text{air}})d_p^2 C_c}{18\eta_{\text{air}}R} \frac{L}{v_{\text{air}}} \left( \frac{GM_E(1 + e \cos f)^2}{a^2(1 - e^2)} + \frac{3GM_E R_{\text{eq}}^2 J_2 (1 + e \cos f)^4}{2a^4(1 - e^2)^4} \left( \frac{3 \sin^2 f}{2} - 1 \right) \right) \cos \theta. \quad (2.38)$$

## 2.6 The Inclusion of Electrostatic Deposition Forces

Up to Eq. (2.38) we have dealt with the effect of a variable gravity on the surface of a planetary body and also in an experiment above an orbiting spacecraft. Next, we consider dust particle electrostatic forces first in the absence of an electric field  $E$  falling in the trachea. Following Yu [35] we say that there are two electric forces which cause particles to deposit on the surface of an enclosure. One is the image force due to the interaction between a particle and the wall. The other is the space charge force due to the mutual repulsion between particles of the same charge. The image force is a single particle effect, while the space charge force depends on the particle concentration of the system. In order to find out which of these two forces is important in lung deposition, the interparticle distance must be estimated in relation to the airways. Because most environmental aerosols have low concentration numbers, we will assume that the primary deposition force is the image force acting on the particles, which is also responsible for the deposition increase within the respiratory track. Because the particle is acted upon by the vector sum of many forces, for the determination of an exact image deposition acceleration will be a very hard task. We simplify the analysis by following the idea give in Yu [35] where the total acceleration acted upon the particle is a superposition of the gravitational and that resulted by the image force, and therefore we have that

$$a_{\text{tot}} = g \cos \theta + a_{\text{image}} \cos \xi, \quad (2.39)$$

where  $a_{\text{image}} \xi$  is the vertical component of  $a_{\text{image}}$ , where  $\xi$  is the angle between the vertical component of the image acceleration and the direction of the acceleration of gravity. Therefore Eq. (2.1) can be modified to

$$P_i \propto \frac{v_{\text{ter}} v_{\text{air}} \sin \theta}{((g + a_{\text{image}} \cos \xi)R + v_{\text{ter}} v_{\text{air}} \sin \theta)}. \quad (2.40)$$

Therefore using the expression for the image force given by Yu [35] we obtain the vertical component of the image acceleration to

$$a_{\text{image}} = \frac{F_{\text{image}}}{m} = \frac{q^2 r^2 \cos \xi}{16\pi\epsilon_0 m (R - r)^2}, \quad (2.41)$$

where  $R$  is the tracheal radius,  $r$  is the distance of the particle from the axis,  $m$  is the mass of the particle, and  $q$  is its charge, and  $\epsilon_0$  is the permittivity of the air. Therefore the sedimentation probability in Eq. (2.7) takes the form

$$P_{\text{sed}} = 1 - e^{-\left(\frac{(\rho_p - \rho_{\text{air}})d_p^2 C_c}{18\eta_{\text{air}}R} \frac{L}{v_{\text{air}}} (g \cos \theta + a_{\text{image}} \cos \xi)\right)}. \quad (2.42)$$

Next, we can write a particle effective distance at right angles to the direction of travel to be

$$h_s = \frac{v_{\text{ter}} \eta_{\text{air}}}{(g + a_{\text{image}} \cos \xi)} \sin \theta. \quad (2.43)$$

First let us now consider Eq. (2.1) for the deposition probability of particles on the surface of the Earth, where the gravitational acceleration has been corrected for the rotation of the Earth and also for its oblateness via the  $J_2$  harmonic coefficient. Using Eqs. (2.9–2.11) we can write that

$$P_{\text{sed}} = 1 - e^{-\left(\frac{(\rho_p - \rho_{\text{air}})d_p^2 C_c}{18\eta_{\text{air}}R} \frac{L}{v_{\text{air}}} \left(\left(\frac{GM_E}{R_{\text{eq}}^2} + \frac{3GM_E J_2}{2R_{\text{eq}}^2} - R_{\text{eq}} \omega_E^2\right) \cos \theta + \frac{q^2 r^2 \cos \xi}{16\pi\epsilon_0 m (R - r)^2}\right)\right)}, \quad (2.44)$$

$$P_{\text{sed}} = 1 - e^{-\left(\frac{(\rho_p - \rho_{\text{air}})d_p^2 C_c}{18\eta_{\text{air}}R} \frac{L}{v_{\text{air}}} \left(\left(\frac{GM_E}{R_{\text{eq}}^2 (1 - f')^2} - \frac{3GM_E J_2}{4R_{\text{eq}}^2 (1 - \frac{f'}{2})^2} - \frac{1}{2} \left(1 - \frac{f'}{2}\right) R_{\text{eq}} \omega_E^2\right) \cos \theta + \frac{q^2 r^2 \cos \xi}{16\pi\epsilon_0 m (R - r)^2}\right)\right)}, \quad (2.45)$$

$$P_{\text{sed}} = 1 - e^{-\left( \frac{(\rho_p - \rho_{\text{air}})d_p^2 C_c}{18\eta_{\text{air}}R} \frac{L}{v_{\text{air}}} \left( \left( \frac{GM_E}{R_{\text{eq}}^2(1-f')^2} - \frac{3GM_E J_2}{R_{\text{eq}}^2(1-f')^2} \right) \cos\theta + \frac{q^2 r^2 \cos\xi}{16\pi\epsilon_0 m(R-r)^2} \right) \right)} \quad (2.46)$$

For circular orbits, i.e.,  $e=0$ , of inclinations  $i=0^\circ, 45^\circ, 90^\circ$  we obtain

$$P_{\text{sed}} = 1 - e^{-\left( \frac{(\rho_p - \rho_{\text{air}})d_p^2 C_c}{18\eta_{\text{air}}R} \frac{L}{v_{\text{air}}} \left( \left( \frac{GM_E}{a^2} + \frac{3GM_E R_{\text{eq}}^2 J_2}{2a^4} \right) \cos\theta + \frac{q^2 r^2 \cos\xi}{16\pi\epsilon_0 m(R-r)^2} \right) \right)} \quad (2.47)$$

$$P_{\text{sed}} = 1 - e^{-\left( \frac{(\rho_p - \rho_{\text{air}})d_p^2 C_c}{18\eta_{\text{air}}R} \frac{L}{v_{\text{air}}} \left( \left( \frac{GM_E}{a^2} + \frac{3GM_E R_{\text{eq}}^2 J_2}{2a^4} \left( \frac{3\sin^2 u}{2} - 1 \right) \right) \cos\theta + \frac{q^2 r^2 \cos\xi}{16\pi\epsilon_0 m(R-r)^2} \right) \right)} \quad (2.48)$$

$$P_{\text{sed}} = 1 - e^{-\left( \frac{(\rho_p - \rho_{\text{air}})d_p^2 C_c}{18\eta_{\text{air}}R} \frac{L}{v_{\text{air}}} \left( \left( \frac{GM_E}{a^2} + \frac{3GM_E R_{\text{eq}}^2 J_2}{2a^4} \left( \frac{3\sin^2 u - 1}{2} \right) \right) \cos\theta + \frac{q^2 r^2 \cos\xi}{16\pi\epsilon_0 m(R-r)^2} \right) \right)} \quad (2.49)$$

Similarly, for elliptical orbits of the same inclinations the particle deposition probability takes the form

$$P_{\text{sed}} = 1 - e^{-\left( \frac{(\rho_p - \rho_{\text{air}})d_p^2 C_c}{18\eta_{\text{air}}R} \frac{L}{v_{\text{air}}} \left( \left( \frac{GM_E(1+e\cos f)^2}{a^2(1-e^2)} + \frac{3GM_E R_{\text{eq}}^2 J_2(1+e\cos f)^4}{2a^4(1-e^2)^4} \right) \cos\theta + \frac{q^2 r^2 \cos\xi}{16\pi\epsilon_0 m(R-r)^2} \right) \right)} \quad (2.50)$$

$$P_{\text{sed}} = 1 - e^{-\left( \frac{(\rho_p - \rho_{\text{air}})d_p^2 C_c}{18\eta_{\text{air}}R} \frac{L}{v_{\text{air}}} \left( \left( \frac{GM_E(1+e\cos f)^2}{a^2(1-e^2)} + \frac{3GM_E R_{\text{eq}}^2 J_2(1+e\cos f)^4}{2a^4(1-e^2)^4} \left( \frac{3\sin^2 f}{2} - 1 \right) \right) \cos\theta + \frac{q^2 r^2 \cos\xi}{16\pi\epsilon_0 m(R-r)^2} \right) \right)} \quad (2.51)$$

$$P_{\text{sed}} = 1 - e^{-\left( \frac{(\rho_p - \rho_{\text{air}})d_p^2 C_c}{18\eta_{\text{air}}R} \frac{L}{v_{\text{air}}} \left( \left( \frac{GM_E(1+e\cos f)^2}{a^2(1-e^2)} + \frac{3GM_E R_{\text{eq}}^2 J_2(1+e\cos f)^4}{2a^4(1-e^2)^4} \left( \frac{3\sin^2 f - 1}{2} \right) \right) \cos\theta + \frac{q^2 r^2 \cos\xi}{16\pi\epsilon_0 m(R-r)^2} \right) \right)} \quad (2.52)$$

Similarly, we extend the expression for the maximum height when in orbit around a planetary body in our case the Earth and therefore we obtain

$$h_{\text{max}} = \frac{(\rho_p - \rho_{\text{air}})d_p^2 C_c}{18\eta_{\text{air}}R} \frac{L}{v_{\text{air}}} \left[ \left( \frac{GM_E}{R_{\text{eq}}^2} + \frac{3GM_E J_2}{2R_{\text{eq}}^2} - R_{\text{eq}}\omega_E^2 \right) \cos\theta + \frac{q^2 r^2 \cos\xi}{16\pi\epsilon_0 m(R-r)^2} \right] \quad (2.53)$$

$$h_{\max} = \frac{(\rho_p - \rho_{\text{air}})d_p^2 C_c}{18\eta_{\text{air}}R} \frac{L}{v_{\text{air}}} \left[ \left( \frac{GM_E}{R_{\text{eq}}^2(1-f')^2} + \frac{3GM_E J_2}{4R_{\text{eq}}^2 \left(1 - \frac{f'}{2}\right)^2} - \frac{1}{2} \left(1 - \frac{f'}{2}\right) R_{\text{eq}} \omega_E^2 \right) \cos \theta + \frac{q^2 r^2 \cos \xi}{16\pi\epsilon_0 m(R-r)^2} \right], \quad (2.54)$$

$$h_{\max} = \frac{(\rho_p - \rho_{\text{air}})d_p^2 C_c}{18\eta_{\text{air}}R} \frac{L}{v_{\text{air}}} \left[ \left( \frac{GM_E}{R_{\text{eq}}^2(1-f')^2} + \frac{3GM_E J_2}{R_{\text{eq}}^2(1-f')^2} \right) \cos \theta + \frac{q^2 r^2 \cos \xi}{16\pi\epsilon_0 m(R-r)^2} \right]. \quad (2.55)$$

For circular orbits, i.e.,  $e = 0$ , of inclinations  $i = 0^\circ, 45^\circ, 90^\circ$  we obtain

$$h_{\max} = \frac{(\rho_p - \rho_{\text{air}})d_p^2 C_c}{18\eta_{\text{air}}R} \frac{L}{v_{\text{air}}} \left[ \left( \frac{GM_E}{a^2} + \frac{3GM_E R_{\text{eq}}^2 J_2}{2a^4} \right) \cos \theta + \frac{q^2 r^2 \cos \xi}{16\pi\epsilon_0 m(R-r)^2} \right], \quad (2.56)$$

$$h_{\max} = \frac{(\rho_p - \rho_{\text{air}})d_p^2 C_c}{18\eta_{\text{air}}R} \frac{L}{v_{\text{air}}} \left[ \left( \frac{GM_E}{a^2} + \frac{3GM_E R_{\text{eq}}^2 J_2}{2a^4} \left( \frac{3 \sin^2 u}{2} - 1 \right) \right) \cos \theta + \frac{q^2 r^2 \cos \xi}{16\pi\epsilon_0 m(R-r)^2} \right], \quad (2.57)$$

$$h_{\max} = \frac{(\rho_p - \rho_{\text{air}})d_p^2 C_c}{18\eta_{\text{air}}R} \frac{L}{v_{\text{air}}} \left[ \left( \frac{GM_E}{a^2} + \frac{3GM_E R_{\text{eq}}^2 J_2}{2a^4} \left( \frac{3 \sin^2 u}{2} - 1 \right) \right) \cos \theta + \frac{q^2 r^2 \cos \xi}{16\pi\epsilon_0 m(R-r)^2} \right]. \quad (2.58)$$

Similarly, for elliptical orbits of the same inclinations the ratio takes the form

$$h_{\max} = \frac{(\rho_p - \rho_{\text{air}})d_p^2 C_c}{18\eta_{\text{air}}R} \frac{L}{v_{\text{air}}} \left[ \left( \frac{GM_E(1+e \cos f)^2}{a^2(1-e^2)} + \frac{3GM_E R_{\text{eq}}^2 J_2 (1+e \cos f)^4}{2a^4(1-e^2)^4} \right) \cos \theta + \frac{q^2 r^2 \cos \xi}{16\pi\epsilon_0 m(R-r)^2} \right], \quad (2.59)$$

$$h_{\max} = \frac{(\rho_p - \rho_{\text{air}})d_p^2 C_c}{18\eta_{\text{air}}R} \frac{L}{v_{\text{air}}} \left[ \left( \frac{GM_E(1+e \cos f)^2}{a^2(1-e^2)} + \frac{3GM_E R_{\text{eq}}^2 J_2 (1+e \cos f)^4}{2a^4(1-e^2)^4} \left( \frac{3 \sin^2 f}{2} - 1 \right) \right) \cos \theta + \frac{q^2 r^2 \cos \xi}{16\pi\epsilon_0 m(R-r)^2} \right], \quad (2.60)$$

$$h_{\max} = \frac{(\rho_p - \rho_{\text{air}})d_p^2 C_c}{18\eta_{\text{air}}R} \frac{L}{v_{\text{air}}} \left[ \left( \frac{GM_E(1+e \cos f)^2}{a^2(1-e^2)} + \frac{3GM_E R_{\text{eq}}^2 J_2 (1+e \cos f)^4}{2a^4(1-e^2)^4} \left( \frac{3 \sin^2 f}{2} - 1 \right) \right) \cos \theta + \frac{q^2 r^2 \cos \xi}{16\pi\epsilon_0 m(R-r)^2} \right]. \quad (2.61)$$

## 2.7 Aerosol Deposition Rate on the Surface of a Planetary Body and in a Spacecraft in Orbit Around It

Following García [8] we can write the deposition rate  $D$  in the following way:

$$D = P_{\text{sed}} C_s v_{\text{sed}}, \quad (2.62)$$

where  $P_{\text{sed}}$  is the sedimentation probability,  $v_s$  is its vertical sedimentation velocity, and  $C_s$  is the suspending particle concentration. Using Eqs. (2.2), (2.7), and (2.17) we write that on the surface of the Earth the dose takes the form

$$D = \frac{(\rho_p - \rho_{\text{air}}) d_p^2 C_c}{18\eta_{\text{air}}} \left( \begin{array}{c} \frac{GM_E}{R_{\text{eq}}^2 (1 - f' \sin^2 \phi)^2} \\ - \frac{3GM_E J_2}{2R_{\text{eq}}^2 (1 - f' \sin^2 \phi)^2} (3 \sin^2 \phi - 1) \\ - R_{\text{eq}} (1 - f' \sin^2 \phi) \omega_E^2 \cos^2 \phi + \frac{q^2 r^2 \cos \xi}{16\pi \epsilon_0 m (R - r)^2} \end{array} \right) \times \left( \begin{array}{c} \frac{GM_E}{R_{\text{eq}}^2 (1 - f' \sin^2 \phi)^2} \\ - \frac{(\rho_p - \rho_{\text{air}}) d_p^2 C_c L_{\text{tr}}}{18\eta_{\text{air}} R v_{\text{air}}} \left( \begin{array}{c} \frac{GM_E}{R_{\text{eq}}^2 (1 - f' \sin^2 \phi)^2} \\ - \frac{3GM_E J_2}{2R_{\text{eq}}^2 (1 - f' \sin^2 \phi)^2} (3 \sin^2 \phi - 1) \\ - R_{\text{eq}} (1 - f' \sin^2 \phi) \omega_E^2 \cos^2 \phi \end{array} \right) \cos \theta + \frac{q^2 r^2 \cos \xi}{16\pi \epsilon_0 m (R - r)^2} \end{array} \right) C_s, \quad (2.63)$$

which for the geocentric latitudes of  $\phi = 0^\circ, 45^\circ, 90^\circ$ , respectively, becomes

$$D = \frac{(\rho_p - \rho_{\text{air}}) d_p^2 C_c}{18\eta_{\text{air}}} \left( \begin{array}{c} \left( \frac{GM_{\text{eq}}}{R_{\text{eq}}^2} + \frac{3GM_{\text{eq}} J_2}{2R_{\text{eq}}^2} - R_{\text{eq}} \omega_E^2 \right) \cos \theta \\ + \frac{q^2 r^2 \cos \xi}{16\pi \epsilon_0 m (R - r)^2} \end{array} \right) \times \left( \begin{array}{c} \frac{(\rho_p - \rho_{\text{air}}) d_p^2 C_c L_{\text{tr}}}{18\eta_{\text{air}} R v_{\text{air}}} \left( \begin{array}{c} \left( \frac{GM_{\text{eq}}}{R_{\text{eq}}^2} + \frac{3GM_{\text{eq}} J_2}{2R_{\text{eq}}^2} - R_{\text{eq}} \omega_E^2 \right) \cos \theta \\ + \frac{q^2 r^2 \cos \xi}{16\pi \epsilon_0 m (R - r)^2} \end{array} \right) \\ + \frac{q^2 r^2 \cos \xi}{16\pi \epsilon_0 m (R - r)^2} \end{array} \right) C_s, \quad (2.64)$$

$$\begin{aligned}
D &= \frac{(\rho_p - \rho_{\text{air}})d_p^2 C_c}{18\eta_{\text{air}}} \left( \begin{array}{c} \left( \frac{GM_{\text{eq}}}{R_{\text{eq}}^2 (1-f')^2} + \frac{3GM_{\text{eq}}J_2}{4R_{\text{eq}}^2 \left(1 - \frac{f'}{2}\right)^2} \right) \cos \theta \\ -\frac{1}{2} \left(1 - \frac{f'}{2}\right) R_{\text{eq}} \omega_{\text{E}}^2 \\ + \frac{q^2 r^2 \cos \xi}{16\pi\epsilon_0 m (R-r)^2} \end{array} \right) \\
&\times \left( \begin{array}{c} - \left( \frac{GM_{\text{E}}}{R_{\text{eq}}^2 (1-f')^2} + \frac{3GM_{\text{E}}J_2}{4R_{\text{eq}}^2 \left(1 - \frac{f'}{2}\right)^2} \right) \cos \theta \\ - \frac{(\rho_p - \rho_{\text{air}})d_p^2 C_c L_{\text{tr}}}{18\eta_{\text{air}} R v_{\text{air}}} \left( \begin{array}{c} \frac{GM_{\text{E}}}{R_{\text{eq}}^2 (1-f')^2} + \frac{3GM_{\text{E}}J_2}{4R_{\text{eq}}^2 \left(1 - \frac{f'}{2}\right)^2} \\ -\frac{1}{2} \left(1 - \frac{f'}{2}\right) R_{\text{eq}} \omega_{\text{E}}^2 \\ + \frac{q^2 r^2 \cos \xi}{16\pi\epsilon_0 m (R-r)^2} \end{array} \right) \cos \theta \\ 1 - e \end{array} \right) C_{\text{S}}, \quad (2.65)
\end{aligned}$$

$$\begin{aligned}
D &= \frac{(\rho_p - \rho_{\text{air}})d_p^2 C_c}{18\eta_{\text{air}}} \left( \begin{array}{c} \left( \frac{GM_{\text{E}}}{R_{\text{eq}}^2 (1-f')^2} + \frac{3GM_{\text{E}}J_2}{R_{\text{eq}}^2 (1-f')^2} \right) \cos \theta \\ + \frac{q^2 r^2 \cos \xi}{16\pi\epsilon_0 m (R-r)^2} \end{array} \right) \\
&\times \left( \begin{array}{c} - \left( \frac{(\rho_p - \rho_{\text{air}})d_p^2 C_c L_{\text{tr}}}{18\eta_{\text{air}} R v_{\text{air}}} \left( \frac{GM_{\text{E}}}{R_{\text{eq}}^2 (1-f')^2} + \frac{3GM_{\text{E}}J_2}{R_{\text{eq}}^2 (1-f')^2} \right) \cos \theta \right) \\ + \frac{q^2 r^2 \cos \xi}{16\pi\epsilon_0 m (R-r)^2} \\ 1 - e \end{array} \right) C_{\text{S}}. \quad (2.66)
\end{aligned}$$

Similarly, in circular and elliptical orbits of inclination  $i = 0^\circ, 45^\circ, 90^\circ$  we, respectively, obtain that

$$\begin{aligned}
D &= \frac{(\rho_p - \rho_{\text{air}})d_p^2 C_c}{18\eta_{\text{air}}} \left( \begin{array}{c} \left( \frac{GM_{\text{E}}}{a^2} + \frac{3GM_{\text{E}}R_{\text{eq}}^2 J_2}{2a^4} \right) \cos \theta \\ + \frac{q^2 r^2 \cos \xi}{16\pi\epsilon_0 m (R-r)^2} \end{array} \right) \\
&\times \left( \begin{array}{c} - \left( \frac{(\rho_p - \rho_{\text{air}})d_p^2 C_c L_{\text{tr}}}{18\eta_{\text{air}} R v_{\text{air}}} \left( \frac{GM_{\text{E}}}{a^2} + \frac{3GM_{\text{E}}R_{\text{eq}}^2 J_2}{2a^4} \right) \cos \theta \right) \\ + \frac{q^2 r^2 \cos \xi}{16\pi\epsilon_0 m (R-r)^2} \\ 1 - e \end{array} \right) C_{\text{S}}, \quad (2.67)
\end{aligned}$$

$$D = \frac{(\rho_p - \rho_{\text{air}})d_p^2 C_c}{18\eta_{\text{air}}} \left( \frac{\left( \frac{GM_E}{a^2} + \frac{3GM_E R_{\text{eq}}^2 J_2}{2a^4} \left( \frac{3 \sin^2 u}{2} - 1 \right) \right) \cos \theta}{+\frac{q^2 r^2 \cos \xi}{16\pi\epsilon_0 m(R-r)^2}} \right) \times \left( \frac{- \left( \frac{(\rho_p - \rho_{\text{air}})d_p^2 C_c L_{\text{tr}}}{18\eta_{\text{air}} R v_{\text{air}}} \left( \frac{GM_E}{a^2} + \frac{3GM_E R_{\text{eq}}^2 J_2}{2a^4} \left( \frac{3 \sin^2 u}{2} - 1 \right) \right) \cos \theta}{+\frac{q^2 r^2 \cos \xi}{16\pi\epsilon_0 m(R-r)^2}} \right)}{1 - e} \right) C_s, \quad (2.68)$$

$$D = \frac{(\rho_p - \rho_{\text{air}})d_p^2 C_c}{18\eta_{\text{air}}} \left( \frac{\left( \frac{GM_E}{a^2} + \frac{3GM_E R_{\text{eq}}^2 J_2}{2a^4} \left( \frac{3 \sin^2 u}{2} - 1 \right) \right) \cos \theta}{+\frac{q^2 r^2 \cos \xi}{16\pi\epsilon_0 m(R-r)^2}} \right) \times \left( \frac{- \left( \frac{(\rho_p - \rho_{\text{air}})d_p^2 C_c L_{\text{tr}}}{18\eta_{\text{air}} R v_{\text{air}}} \left( \frac{GM_E}{a^2} + \frac{3GM_E R_{\text{eq}}^2 J_2}{2a^4} \left( \frac{3 \sin^2 u}{2} - 1 \right) \right) \cos \theta}{+\frac{q^2 r^2 \cos \xi}{16\pi\epsilon_0 m(R-r)^2}} \right)}{1 - e} \right) C_s. \quad (2.69)$$

For elliptical orbits the dose becomes

$$D = \frac{(\rho_p - \rho_{\text{air}})d_p^2 C_c}{18\eta_{\text{air}}} \left( \frac{\left( \frac{GM_E(1 + e \cos f)^2}{a^2(1 - e^2)} + \frac{3GM_E R_{\text{eq}}^2 J_2 (1 + e \cos f)^4}{2a^4(1 - e^2)^4} \right) \cos \theta + \frac{q^2 r^2 \cos \xi}{16\pi\epsilon_0 m(R-r)^2}}{\right) \times \left( \frac{- \left( \frac{(\rho_p - \rho_{\text{air}})d_p^2 C_c L_{\text{tr}}}{18\eta_{\text{air}} R v_{\text{air}}} \left( \frac{GM_E(1 + e \cos f)^2}{a^2(1 - e^2)} + \frac{3GM_E R_{\text{eq}}^2 J_2 (1 + e \cos f)^4}{2a^4(1 - e^2)^4} \right) \cos \theta}{+\frac{q^2 r^2 \cos \xi}{16\pi\epsilon_0 m(R-r)^2}} \right)}{1 - e} \right) C_s, \quad (2.70)$$

$$D = \frac{(\rho_p - \rho_{\text{air}})d_p^2 C_c}{18\eta_{\text{air}}} \left( \left( \frac{GM_E(1+e\cos f)^2}{a^2(1-e^2)} + \frac{3GM_E R_{\text{eq}}^2 J_2 (1+e\cos f)^4}{2a^4(1-e^2)^4} \left( \frac{3\sin^2 f}{2} - 1 \right) \right) \cos \theta + \frac{q^2 r^2 \cos \xi}{16\pi \epsilon_0 m (R-r)^2} \right) \times \left( \frac{(\rho_p - \rho_{\text{air}})d_p^2 C_c L_{\text{tr}}}{18\eta_{\text{air}} R v_{\text{air}}} \left( \frac{GM_E(1+e\cos f)^2}{a^2(1-e^2)} + \frac{3GM_E R_{\text{eq}}^2 J_2 (1+e\cos f)^4}{2a^4(1-e^2)^4} \left( \frac{3\sin^2 f}{2} - 1 \right) \right) \cos \theta + \frac{q^2 r^2 \cos \xi}{16\pi \epsilon_0 m (R-r)^2} \right) \Bigg|_{1-e}^{C_s}, \quad (2.71)$$

$$D = \frac{(\rho_p - \rho_{\text{air}})d_p^2 C_c}{18\eta_{\text{air}}} \left( \left( \frac{GM_E(1+e\cos f)^2}{a^2(1-e^2)} + \frac{3GM_E R_{\text{eq}}^2 J_2 (1+e\cos f)^4}{2a^4(1-e^2)^4} \left( \frac{3\sin^2 f}{2} - 1 \right) \right) \cos \theta + \frac{q^2 r^2 \cos \xi}{16\pi \epsilon_0 m (R-r)^2} \right) \times \left( \frac{(\rho_p - \rho_{\text{air}})d_p^2 C_c L_{\text{tr}}}{18\eta_{\text{air}} R v_{\text{air}}} \left( \frac{GM_E(1+e\cos f)^2}{a^2(1-e^2)} + \frac{3GM_E R_{\text{eq}}^2 J_2 (1+e\cos f)^4}{2a^4(1-e^2)^4} \left( \frac{3\sin^2 f}{2} - 1 \right) \right) \cos \theta + \frac{q^2 r^2 \cos \xi}{16\pi \epsilon_0 m (R-r)^2} \right) \Bigg|_{1-e}^{C_s}. \quad (2.72)$$

## 2.8 Discussion and Numerical Results

To proceed with our numerical calculation let us assume the following values for our numerical parameters, i.e., all particles have density  $\rho_p = 1,300 \text{ kg/m}^3$  [30], unless range of densities is specified,  $\eta_{\text{air}} = 1.8 \times 10^{-8} \text{ kg/m/s}$ , is the viscosity of the air,  $R_{\text{trachea}} = d_{\text{trachea}}/2 = 25 \text{ mm} = 12.5 \text{ mm}$  [2], is the radius of the trachea,  $\lambda = (0.8-1.0) \times 10^{-7} \text{ m}$  is the air mean free path, and  $\theta = 2/\pi$  [19]. In Fig. 2.3 we plot of the deposition probability on the surface of the Earth as a function of the particle diameter  $d$  and density  $\rho$ , at geocentric latitude  $\phi = 90^\circ$ , for particles with diameters and densities in the range  $1 \text{ }\mu\text{m} \leq d \leq 40 \text{ }\mu\text{m}$  and  $800 \text{ kg/m}^3 \leq \rho \leq 2,300 \text{ kg/m}^3$ , respectively. Similarly, for Mars the Cunningham factor for particles of  $1 \text{ }\mu\text{m}$  in a  $\text{CO}_2$  atmosphere is given to be  $C_M = 15$  [4].  $J_2 = 0.0010826269$  is the Earth's harmonic coefficient,  $J_2 = 0.001964$



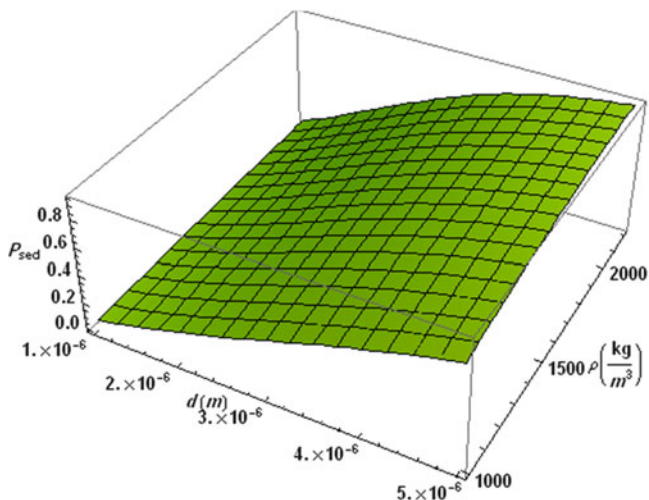


**Fig. 2.3** Plot of the deposition probability on the surface of the Earth as a function of the particle diameter  $d$  and density  $\rho$ , at geocentric latitude  $\phi = 90^\circ$ , for particles of diameters  $d$  in the ranges  $1 \mu\text{m} \leq d \leq 5 \mu\text{m}$  and  $1,000 \text{ kg/m}^3 \leq \rho \leq 2,200 \text{ kg/m}^3$ , and residence time  $t = 0.0272 \text{ s}$

(Vallado 2007) is Mars' harmonic coefficient,  $R_M = 3397.2 \text{ km}$  is Mars' radius,  $M_M = 6.4191 \times 10^{23} \text{ kg}$  is its mass, with a flattening coefficient (Vallado 2007),  $\rho_M = 0.02 \text{ kg/m}^3$  is Mars' surface atmospheric density and viscosity, and finally  $\eta_{\text{air}} = 1.47 \times 10^{-5} \text{ kg/m/s}$  [4] is Mars' atmospheric viscosity. The deposition probabilities between the poles and the equator for particles of density  $\rho_p = 1,300 \text{ kg/m}^3$  of various diameters  $d$  and residence time  $t$  are related according to the relation

$$P_E(\phi = 90^\circ) = \left[ \frac{1 - e^{-\frac{6413.7(3.2803 \times 10^{-33} + 7.85859d^3)e^{-7.85714 \times 10^6 d} (2.8 + (8.82 + 5 \times 10^7 d)e^{7.85714 \times 10^6 d}) t}{d^2}}}{1 - e^{-\frac{6413.7(3.2803 \times 10^{-33} + 7.81686d^3)e^{-7.85714 \times 10^6 d} (2.8 + (8.82 + 5 \times 10^7 d)e^{7.85714 \times 10^6 d}) t}{d^2}}} \right] P_E(\phi = 0^\circ). \quad (2.73)$$

Similarly, on Mars we find that

$$P_M(\phi = 90^\circ) = \left[ \frac{1 - e^{-\left(3.00435 + \frac{3.8742 \times 10^{-32}}{d^3}\right) d^2 t}}{1 - e^{-\left(2.97821 + \frac{3.8742 \times 10^{-32}}{d^3}\right) d^2 t}} \right] P_M(\phi = 0^\circ). \quad (2.74)$$

Next, for the deposition rates on Earth and Mars we, respectively, obtain

$$D_E(\phi = 90^\circ) = 1.00534 \left[ \frac{1 - e^{-\frac{-3.20685 \times 10^{11} \left( \frac{3.28059 \times 10^{-33}}{d^3} \right) \left( \frac{7(1.26 + 0.4e^{-7.85714 \times 10^6 d})}{5 \times 10^7 d} \right)^{d^2 t}}}{1 - e^{-\frac{-3.20685 \times 10^{11} \left( \frac{3.28059 \times 10^{-33}}{d^3} \right) \left( \frac{7(1.26 + 0.4e^{-7.85714 \times 10^6 d})}{5 \times 10^7 d} \right)^{d^2 t}}}} \right] D_E(\phi = 0^\circ), \quad (2.75)$$

$$D_M(\phi = 90^\circ) = 1.00001 \left[ \frac{1 - e^{-\frac{-6.28864 \times 10^9 \left( \frac{3.8742 \times 10^{-32}}{d^3} \right) \left( \frac{2.97823 + \frac{3.8742 \times 10^{-32}}{d^3}}{d^3} \right)^{d^2 t}}}{1 - e^{-\frac{-6.28864 \times 10^9 \left( \frac{3.8742 \times 10^{-32}}{d^3} \right) \left( \frac{2.97823 + \frac{3.8742 \times 10^{-32}}{d^3}}{d^3} \right)^{d^2 t}}}} \right] D_M(\phi = 0^\circ). \quad (2.76)$$

From Table 2.1 we see that particles of a given density and diameter have a greater deposition probability at the poles when compared with that of the equator. On the surface of the Earth, and for a particles of diameter 1, 3, and 5  $\mu\text{m}$ , density 1,300  $\text{kg/m}^3$ , and residence times  $t = 0.0272$  s we find the following percentage differences for the corresponding deposition probabilities between the poles and the equator to be 0.5 %, 0.4 %, and 0.2 %, respectively. Similarly, and for the same particles a residence time  $t = 0.2$  results to a percentage difference equals to 0.4 %, 0.02 %, and 0 % between the poles and the equator. From Tables 2.2 and 2.3 we find that in circular and elliptical orbits around Earth, equatorial orbits i.e.  $i = 0^\circ$  result to higher deposition probabilities than the polar orbits, i.e.,  $i = 90^\circ$ . In particular for particles of the same diameter, density and residence time  $t = 0.0272, 0.2$  s we find the following percentage differences  $-0.1$  %,  $-0.08$  %,  $-0.04$  %,  $-0.09$  %,  $-0.007$  %, 0 % and  $-0.17$  %,  $-0.09$  %,  $-0.05$  % and  $-0.09$  %,  $-0.006$  %,  $-0.0001$  %, respectively. Furthermore, on the surface of the Earth and for the same residence times and particles of diameters  $d = 1, 3, 5$   $\mu\text{m}$  we find that the

**Table 2.1** Sedimentation probability geocentric latitude effect for an experiment taking place on the surface of the Earth and for particles of various diameters and density  $\rho = 1,300$   $\text{kg/m}^3$

Geocentric latitude $\phi$ [°]	Particle diameter $d$ [ $\mu\text{m}$ ]	Sedimentation probability $t = 0.0272$ s	Sedimentation probability $t = 0.2$ s
0	1.0	0.077080	0.445561
45		0.077277	0.446434
90		0.077475	0.447304
0	3.0	0.477816	0.991583
45		0.478722	0.991689
90		0.479624	0.991795
0	5.0	0.828767	0.999998
45		0.829572	0.999998
90		0.830372	0.999998

**Table 2.2** Sedimentation probability inclination and eccentricity effect for an experiment taking place in a circular orbit above the Earth for particle of various diameters and density  $\rho = 1,300 \text{ kg/m}^3$ 

Orbital inclination $i$ [°] and eccentricity $e = 0$	Particle diameter $d$ [ $\mu\text{m}$ ]	Sedimentation probability $t = 0.0272 \text{ s}$	Sedimentation probability $t = 0.2 \text{ s}$
0	1.0	0.0707827	0.4171340
45		0.0707096	0.4167970
90		0.0707020	0.4167620
0	3.0	0.4482460	0.9873800
45		0.4478950	0.9873210
90		0.4478580	0.9873140
0	5.0	0.8011340	0.9999930
45		0.8007890	0.9999930
90		0.8007590	0.9999930

**Table 2.3** Sedimentation probability inclination and eccentricity effect for an experiment taking place in an elliptical orbit above the Earth for particle of various diameters and density  $\rho = 1,300 \text{ kg/m}^3$ 

Orbital inclination $i$ [°] and eccentricity $e = 0.1$	Particle diameter $d$ [ $\mu\text{m}$ ]	Sedimentation probability $t = 0.0272 \text{ s}$	Sedimentation probability $t = 0.2 \text{ s}$
0	1.0	0.07216880	0.4324970
45		0.07209280	0.4321500
90		0.07208500	0.4231140
0	3.0	0.45487800	0.9884530
45		0.45481700	0.9883970
90		0.45447900	0.9883910
0	5.0	0.80755900	0.9999950
45		0.80721200	0.9999940
90		0.80717600	0.9999940

deposition probabilities at the poles are related to those at the equator in following way:  $P_{\phi=90^\circ} \cong 1.005 P_{\phi=0^\circ}$ ,  $P_{\phi=90^\circ} \cong 1.003 P_{\phi=0^\circ}$  and  $P_{\phi=90^\circ} \cong 1.002 P_{\phi=0^\circ}$ . In Earth circular and elliptical orbits of eccentricity  $e = 0, 0.1$  and for particles of the same diameters as the ones given above we find that the deposition probabilities are related in the following way:  $P_{\phi=90^\circ} \cong 0.998 P_{\phi=0^\circ}$  or  $P_{\phi=90^\circ} \cong 0.999 P_{\phi=0^\circ}$  and  $P_{\phi=90^\circ} \cong 0.999 P_{\phi=0^\circ}$  and  $P_{\phi=90^\circ} \cong 0.999 P_{\phi=0^\circ}$  or  $P_{\phi=90^\circ} \cong 0.999 P_{\phi=0^\circ}$  and  $P_{\phi=90^\circ} \cong P_{\phi=0^\circ}$  and for residence time  $t = 0.0272 \text{ s}$  and  $0.2 \text{ s}$ , respectively. Similarly, Table 2.4 demonstrates that on the surface of Mars and for the same particle diameters there is an approximately 0.9 % percentage difference between the deposition probabilities at the poles and that at the equator. From Tables 2.5 and 2.6, we see that for particles of diameters  $d = 1, 3, 5 \mu\text{m}$ , of the same residence times Martian circular and elliptical orbits at the orbital altitude 300 km with

**Table 2.4** Sedimentation probability geocentric latitude effect for an experiment taking place on surface of the Mars and for particles of diameter  $d$  and density  $\rho = 1,300 \text{ kg/m}^3$ 

Geocentric latitude $\phi$ [°]	Particle diameter $d$ [ $\mu\text{m}$ ]	Sedimentation probability $t = 0.0272 \text{ s}$	Sedimentation probability $t = 0.2 \text{ s}$
0	1.0	0.000509296	0.00373877
45		0.000511533	0.00375516
90		0.000513765	0.00377152

**Table 2.5** Sedimentation probability geocentric latitude effect for an experiment taking place in a Mars circular orbit and for particles of diameter  $d$  and density  $\rho = 1,300 \text{ kg/m}^3$ 

Orbital inclination $i$ [°] and eccentricity $e = 0$	Particle diameter $d$ [ $\mu\text{m}$ ]	Sedimentation probability $t = 0.0272 \text{ s}$	Sedimentation probability $t = 0.2 \text{ s}$
0	1.0	0.000431798	0.00317063
45		0.000431798	0.00317063
90		0.000431798	0.00317063

**Table 2.6** Sedimentation probability geocentric latitude effect for an experiment taking place in a Mars elliptical orbit and for particles of diameter  $d$  and density  $\rho = 1,300 \text{ kg/m}^3$ 

Orbital inclination $i$ [°] and eccentricity $e = 0.1$	Particle diameter $d$ [ $\mu\text{m}$ ]	Sedimentation probability $t = 0.0272 \text{ s}$	Sedimentation probability $t = 0.2 \text{ s}$
0	1.0	0.00173888	0.0127155
45		0.00173888	0.0127155
90		0.00173888	0.0127155

**Table 2.7** Sedimentation probability geocentric latitude effect for an experiment taking place in a Mars elliptical orbit of high orbital eccentricity  $e = 0.3$  for particles of diameter and density  $\rho = 1,300 \text{ kg/m}^3$ 

Orbital inclination $i$ [°] and eccentricity $e = 0.3$	Particle diameter $d$ [ $\mu\text{m}$ ]	Sedimentation probability $t = 0.0272 \text{ s}$	Sedimentation probability $t = 0.2 \text{ s}$
0	1.0	0.00173888	0.0190125
45		0.00173888	0.0190125
90		0.00173888	0.0190125

eccentricities, i.e.,  $e = 0, 0.1$ , respectively, result to similar relations for the deposition probabilities i.e.  $P_{\phi=90^\circ} = P_{\phi=45^\circ} = P_{\phi=0^\circ}$ . This demonstrates that the inclination of the orbit does not really affect the deposition probability. On the other hand if the eccentricity increases then the deposition probability increases as well. On the surface of the Earth/Mars and also in orbit the sedimentation probability becomes zero when angle  $\theta$  takes the following value (Table 2.7):

$$\theta = \pm \cos^{-1} \left[ \left( \frac{q^2 R^2 x^2 (1 + 2f \sin^2 \phi + f^2 \sin^4 \phi) \cos \xi}{m \epsilon_0 (x - R)^2 Q_0} \right) \right] \quad (2.77)$$

where in the case of the Earth is equal to

$$Q_0 = 50.2655 GM_E - 37.699 GM_E J_2 + 113.097 GM_E J_2 \cos 2\phi + R_E^2 \omega_E^2 \left( \cos^2 \phi \begin{pmatrix} -50.2655 \\ +f^2 \sin^4 \phi (-150.796 + 50.2655 f \sin^2 f) \\ +37.6991 f \sin^2 2\phi \end{pmatrix} \right). \quad (2.78)$$

This angle is independent of the residence time  $t$ , the particle density  $\rho$ , and the particle diameter  $d$  and depends only on the planetary parameters indicated. Furthermore, it is the same for any geocentric latitude on the Earth and Mars. Numerically for Earth and Mars if the bending angle is equal to  $\theta = \pm 1.5708^\circ$  the deposition probability/deposition rate becomes equal to zero. On the Earth's surface the deposition probability becomes equal to one if the residence time of a particle of diameter  $d_p$  takes the following value:

$$t_{\text{res}} = \frac{18\eta R}{d_p^2 (\rho_p - \rho_{\text{air}}) \left( 1 + \frac{2\lambda}{d} \left( \alpha + \beta e^{-\frac{0.55d}{\lambda}} \right) \right)} \times \left( \left( \frac{GM_E}{R_E^2 (1 - f \sin^2 \phi)^2} - \frac{3GM_E J_2 (1 - 3 \sin^2 \phi)}{2R_E^2 (1 - f \sin^2 \phi)^2} \right) \cos \theta + \frac{0.0198944 q^2 x^2}{m \epsilon (x - R)^2} \cos \xi \right). \quad (2.79)$$

Similarly, zero deposition probability will imply that  $t_{\text{res}} = 0$ . For particles of diameter  $d = 1 \mu\text{m}$ , and density  $\rho_p = 1,300 \text{ kg/m}^3$  at the geocentric latitudes of  $\phi = 0^\circ, 45^\circ$ , and  $90^\circ$  a deposition probability equal to one will require residence times  $t_{\text{res}} = 0.764528, 0.762491$ , and  $0.760468$  s, respectively. Similarly, for a particle with diameter  $d_p = 3 \mu\text{m}$  of the same density we obtain the following residence times  $t_{\text{res}} = 0.0943844, 0.0941329$ , and  $0.0938832$  s which make the deposition probability equal to one. Thus we see that at the poles the required residence time is smaller than that of the equator. Similarly, on the surface of Mars  $1 \mu\text{m}$  particles result to deposition probability equal to one if the residence time is given by the following expression:

$$t_{\text{res}} = \frac{18\eta R}{d_p^2 (\rho_p - \rho_{\text{air}}) \left( 1 + \frac{32\lambda}{d} \right) \left( \left( \frac{GM_M}{R_M^2 (1 - f_M \sin^2 \phi)^2} - \frac{3GM_M J_2 (1 - 3 \sin^2 \phi)}{2R_M^2 (1 - f_M \sin^2 \phi)^2} \right) \cos \theta + \frac{0.0198944 q^2 x^2}{m \epsilon (x - R)^2} \cos \xi \right)}. \quad (2.80)$$

For dust particles of diameter  $d = 1 \mu\text{m}$  and mean free path is given by the following expression:  $\lambda = 1.6 \times 10^{-5} \left( \frac{T}{p} \right)$  [23], where  $T$  is the absolute temperature in Kelvin,

and  $p$  is the atmospheric pressure in Pascal. Taking the surface temperature and pressure equals to 210 K and the 610 pa, we find that the mean free path  $\lambda = 5.508 \times 10^{-6}$  m = 5.508  $\mu$ m. Therefore the corresponding residence times become  $t_{\text{res}} = 3.88128, 3.86430, 3.84751$  s respectively. Finally, for an experiment above a spacecraft in an elliptical orbit around Earth the residence time is given by

$$t_{\text{orbM}} \cong \frac{18R\eta}{d_p^2(\rho_p - \rho_{\text{air}}) \left[ \frac{q^2 x^2 \cos \xi}{\pi m \epsilon (x - R)^2} + \frac{8GM_E \cos \theta (1 + e \cos f)^2 (2a^2 (1 - e^2) - 3J_2 R_E^2 (1 + e \cos f)^2 (\sin^2 f \sin^2 i - 1))}{a^4 (1 - e^2)^4} \right]}. \quad (2.81)$$

The electrostatic image force contributes an extra acceleration, that for particles of diameter  $d = 1$   $\mu$ m is equal to  $1.891 \times 10^{-5}$   $\mu$  gal, and increases significantly as the particle diameter decreases. For a particle of the same density but with a diameter  $d = 0.0017$   $\mu$ m, the image force acceleration is equal to approximately 3,849  $\mu$  gal.

Planetary geophysical parameters can be in principle calculated once a deposition rate can be measured. Using Eq. (2.63) and expanding the exponential to first order we solve for  $J_2$  once the particle concentration  $C_{\text{sed}}$  and rate of deposition  $D$  are known or measured experimentally. Therefore we obtain

$$J_2 = \frac{(A_0 - C_0)}{B_0} \pm \frac{1}{B_0} \left[ H_0 \sec \theta \cos \xi + \frac{18B_0 R \eta_{\text{air}}^2 D}{B_0 C_c d_p^2 \eta_{\text{air}} \cos \theta \sqrt{RC_{\text{sed}} D (\rho^2 - \rho_{\text{air}}^2) t}} \right]. \quad (2.82)$$

Similarly, for a given deposition rate and particle concentration  $C_{\text{sed}}$ , we can obtain solutions for particle diameters  $d_p$ . Solving Eq. (2.63) we obtain the following real solution:

$$d_p = 3\sqrt{2\eta_{\text{air}}} \left[ \frac{RD}{C_{\text{sed}} t (\rho - \rho_{\text{air}})^2 (C_c (A_0 - B_0 J_2 - C_0) \cos \theta + C_c H_0 \cos^2 \xi)} \right]^{1/4}, \quad (2.83)$$

where

$$A_0 = \frac{GM_E}{R_{\text{eq}}^2 (1 - f \sin^2 \phi)^2}, \quad (2.84)$$

$$B_0 = \frac{3GM_E(3 \sin^2 \phi - 1)}{2R_{eq}^2(1 - f \sin^2 \phi)^2}, \quad (2.85)$$

$$C_0 = R_{eq} \omega_E^E (1 - f \sin^2 \phi) \cos^2 \phi, \quad (2.86)$$

$$H_0 = \frac{q^2 r^2}{16\pi \epsilon_0 m_p (R_{tr} - r)^2}. \quad (2.87)$$

In Fig. 2.3 we plot of the deposition probability on the surface of the Earth as a function of the particle diameter  $d$  and density  $\rho_p$ , at the geocentric latitude  $\phi = 90^\circ$ , for particles with diameters and densities in the range  $1 \mu\text{m} \leq d_p \leq 5 \mu\text{m}$  and  $1,000 \text{ kg/m}^3 \leq \rho_p \leq 2,200 \text{ kg/m}^3$  and residence time  $t = 0.0272 \text{ s}$ . The deposition probability increases gradually as the diameter and the particle density increases starting at diameter  $d_p \approx 1 \mu\text{m}$  and  $\rho = 1,000 \text{ kg/m}^3$ . Similarly, in Fig. 2.4 we plot the deposition probability as a function of the particle diameter  $d_p$  and geocentric latitude  $\phi$  for particles of diameters in the range  $1 \mu\text{m} \leq d_p \leq 5 \mu\text{m}$  on the surface of the Earth for the residence time  $t = 0.2 \text{ s}$ . We find that the deposition probability gradually increases starting at  $d_p \approx 1.5 \mu\text{m}$  approaching the higher value plateau but does become not one as the diameter of the particles increase. Therefore, particles in the range of  $2 \mu\text{m}$  and above have a grater deposition probability to be affected by sedimentation, and therefore can end up easily down in the tracheal path. In Fig. 2.5 we plot of the sedimentation probability on the surface of the Earth as a function of the particle diameter  $d_p$  and geocentric latitude  $\phi$  for particle diameters and densities in the range  $1 \mu\text{m} \leq d_p \leq 1.0013 \mu\text{m}$  for residence time  $t = 0.2 \text{ s}$ .

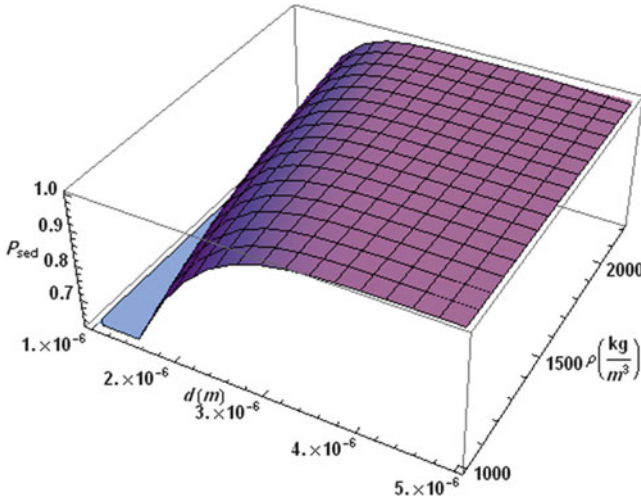


**Fig. 2.4** Plot of the deposition probability on the surface of the Earth as a function of the particle diameter  $d$  and density  $\rho$ , at geocentric latitude  $\phi = 90^\circ$ , for particles of diameter  $d$  in the ranges  $1 \mu\text{m} \leq d \leq 5 \mu\text{m}$  and density  $\rho$  in the range  $1,000 \text{ kg/m}^3 \leq \rho \leq 2,200 \text{ kg/m}^3$ , and residence time  $t = 0.2 \text{ s}$

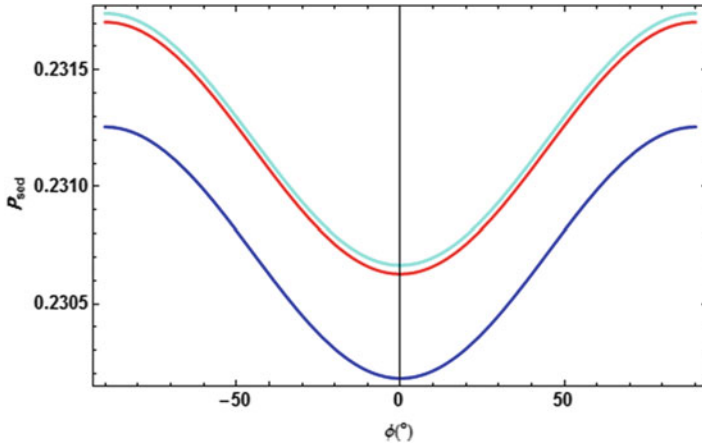


**Fig. 2.5** Plot of the deposition probability on the surface of the Earth as a function of geocentric latitude  $\phi$  for particles of various diameters in the range  $1 \mu\text{m} \leq d \leq 1.0013 \mu\text{m}$  of density  $\rho = 1,300 \text{ kg/m}^3$ , and residence time  $t = 0.2 \text{ s}$

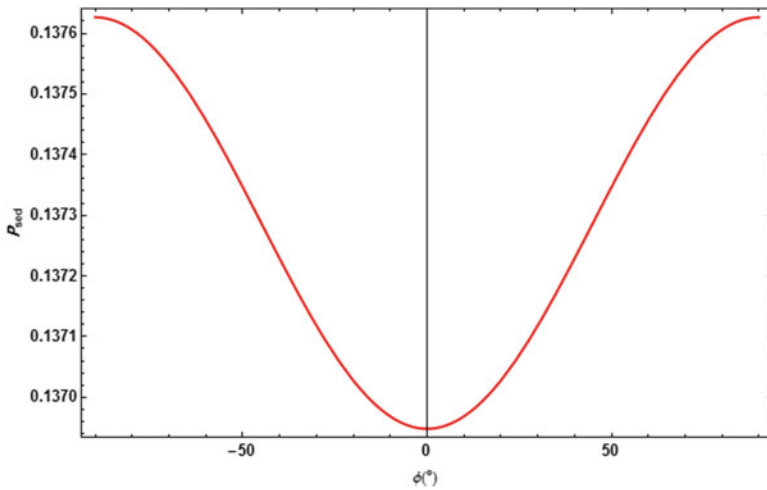


**Fig. 2.6** Plot of the deposition probability on the surface of the Earth as a function and geocentric latitude  $\phi$  for particles of diameters  $2 \mu\text{m}$ , density  $\rho = 1,300 \text{ kg/m}^3$ , and residence time  $t = 0.2 \text{ s}$

This figure exhibits the periodic nature of the deposition probability as a function of geocentric latitude when the particle diameter increases by  $0.0013 \mu\text{m}$ , being larger at  $\phi = 90^\circ$  and smaller at  $\phi = 0^\circ$ . In Fig. 2.6, we plot of the deposition probability on the surface of the Earth as a function of the geocentric latitude  $\phi$  for particles of diameters  $2 \mu\text{m}$ , density  $\rho = 1,300 \text{ kg/m}^3$ , and residence time  $t = 0.2 \text{ s}$ . We find a difference of  $0.0006$  in the probability of deposition between the latitudes of  $90^\circ$  to  $0^\circ$ . In Fig. 2.7 we plot the deposition probability for an experiment taking place



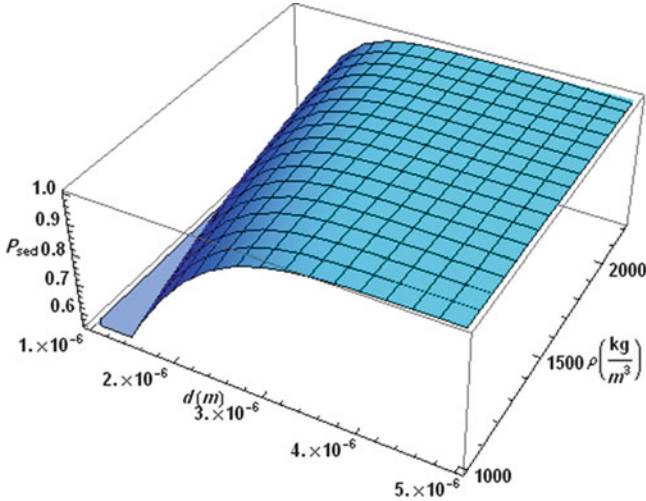


**Fig. 2.7** Plot of the deposition probability in an experiment taking place in spacecraft in a circular polar orbit  $e = 0$  and  $i = 90^\circ$ , 300 km above the surface of the Earth as a function of the particle diameter  $d$  and density  $\rho$  for particles of diameters  $d$  in the ranges  $1 \mu\text{m} \leq d \leq 5 \mu\text{m}$  and density in the range  $1,000 \text{ kg/m}^3 \leq \rho \leq 2,200 \text{ kg/m}^3$ , and for residence time  $t = 0.2$  s

300 km above the surface of the Earth in a circular polar orbit i.e.  $e = 0$  and  $i = 90^\circ$ , as a function of the particle diameter  $d$  and density  $\rho$  for particles of diameters in the ranges  $1 \mu\text{m} \leq d \leq 5 \mu\text{m}$  and density in the range  $1,000 \text{ kg/m}^3 \leq \rho \leq 2,200 \text{ kg/m}^3$ , and residence time  $t = 0.2$  s. We find that the sedimentation probability increases significantly for particles of diameters  $d > 1.4 \mu\text{m}$ , reaching a plateau at approximate diameters  $d \geq 3.4 \mu\text{m}$  and for the given density range. In Fig. 2.8 we plot the deposition probability in a spacecraft experiment 300 km above the surface of the Earth in a circular equatorial orbit  $e = i = 0$ , as a function of particle diameter and density and for particles in the diameter in the ranges  $1 \mu\text{m} \leq d \leq 5 \mu\text{m}$  and  $1,000 \text{ kg/m}^3 \leq \rho \leq 2,200 \text{ kg/m}^3$  and residence time  $t = 0.2$  s. We find that the deposition probability increases for particles with diameter  $d \geq 1.5 \mu\text{m}$  reaching gradually a plateau with values less than one at higher densities. In Fig. 2.9 we plot deposition probability as a function of residence time  $t$  and particle diameter  $d$ , for particles of densities  $1,300 \text{ kg/m}^3$ , in an experiment taking place in a circular orbit of inclination  $i = 45^\circ$ . We find that a plateau of higher probabilities is reached at  $d \approx 3 \mu\text{m}$  as the residence time increases. In Fig. 2.10 we plot of the deposition probability for an experiment taking place 300 km above the surface of the Earth in a elliptical polar orbit of eccentricity  $e = 0.1$ , as a function of the particle diameter  $d$ , and spacecraft's orbital true anomaly  $f$ , and residence time  $t = 0.2$  s and density  $\rho = 1,300 \text{ kg/m}^3$ . We find that the deposition probability demonstrates a week periodicity in the true anomaly and reaches a plateau of higher probability values for particles of diameter  $d \approx 4 \mu\text{m}$ . In Fig. 2.11 we plot the deposition probability for an experiment taking place 300 km above the surface of the Earth in a highly eccentric elliptical polar orbit of eccentricity  $e = 0.38$ , as a function of the particle

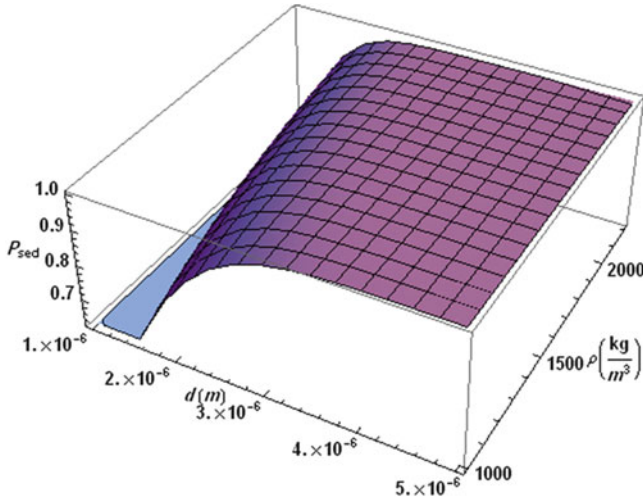


**Fig. 2.8** Plot of the deposition probability in an experiment taking place in spacecraft in a circular equatorial orbit  $e = 0$  and  $i = 0^\circ$ , 300 km above the surface of the Earth as a function of the particle diameter  $d$  and density  $\rho$ , for particles of diameters  $d$  in the ranges  $1 \mu\text{m} \leq d \leq 5 \mu\text{m}$  and density in the range  $1,000 \text{ kg/m}^3 \leq \rho \leq 2,200 \text{ kg/m}^3$ , and for residence time  $t = 0.2 \text{ s}$

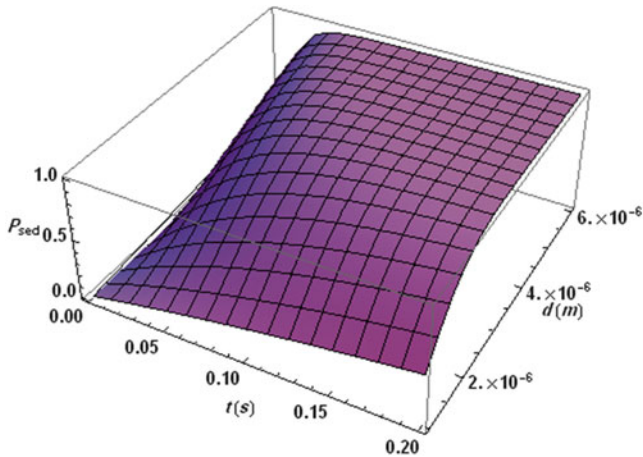


**Fig. 2.9** Plot of the deposition probability in an experiment taking place in spacecraft in a circular orbit  $e = 0$  and  $i = 45^\circ$ , 300 km above the surface of the Earth as a function of the particle residence time  $t$ , and diameter  $d$ , particle density used  $\rho = 1,300 \text{ kg/m}^3$

diameter  $d$ , and spacecraft’s orbital true anomaly  $f$ , and for the residence a time  $t = 0.2 \text{ s}$  and for particles of density  $\rho = 1,300 \text{ kg/m}^3$ . We find that that the deposition probability exhibits a strong periodicity in the true anomaly  $f$ , between the true anomaly values of  $80^\circ \leq f \leq 300^\circ$ , reaching a probability plateau at particle diameters  $d \geq 4 \mu\text{m}$ . Next, in Fig. 2.12 we plot of the deposition probability for an

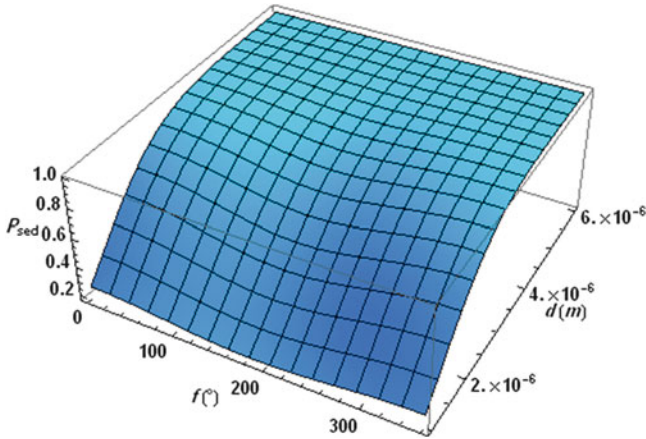


**Fig. 2.10** Plot of the deposition probability for an experiment taking place 300 km above the surface of the Earth in a elliptical polar orbit, as a function of the particle diameter  $d$ , and spacecraft's orbital true anomaly  $f$ , eccentricity used  $e = 0.1$ , residence time  $t = 0.2$  s and particle density  $\rho = 1,300 \text{ kg/m}^3$

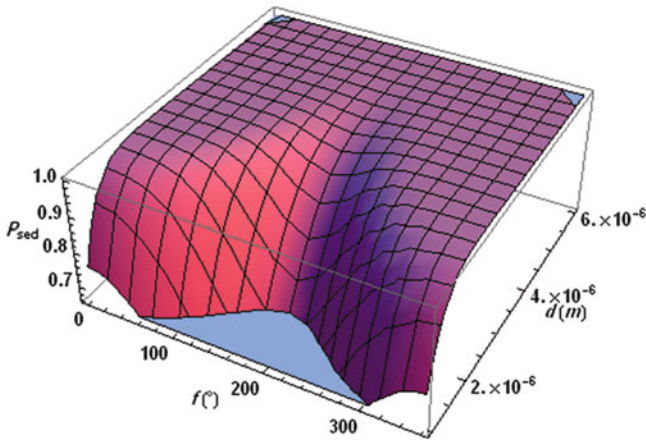


**Fig. 2.11** Plot of the deposition probability for an experiment taking place 300 km above the surface of the Earth in a elliptical polar orbit, as a function of the particle diameter  $d$ , and spacecraft's orbital true anomaly  $f$ , orbital eccentricity used  $e = 0.38$ , residence time  $t = 0.2$  s for particle density  $\rho = 1,300 \text{ kg/m}^3$

experiment taking place 300 km above the surface of the Earth as a function of the spacecraft's orbital true anomaly  $f$  and eccentricity  $e$  and for the residence time  $t = 0.2$  s for particles of density  $\rho = 1,300 \text{ kg/m}^3$ . We find that the deposition probability demonstrates a periodic effect in the true anomaly effect. The effect demonstrates a plateau effect that is bounded by specific values of the true anomaly namely  $20^\circ \leq f \leq 80^\circ$  and  $160^\circ \leq f \leq 340^\circ$ , and for values of eccentricity in the range  $0.6 \leq e \leq 0.8$  and higher. In Fig. 2.13 we lot of the deposition probability as a

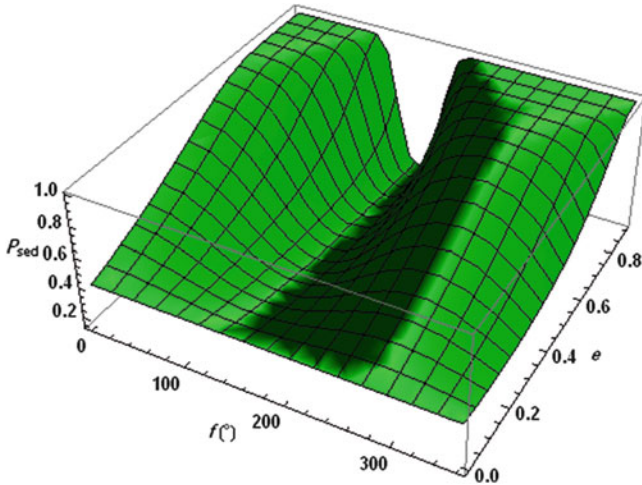
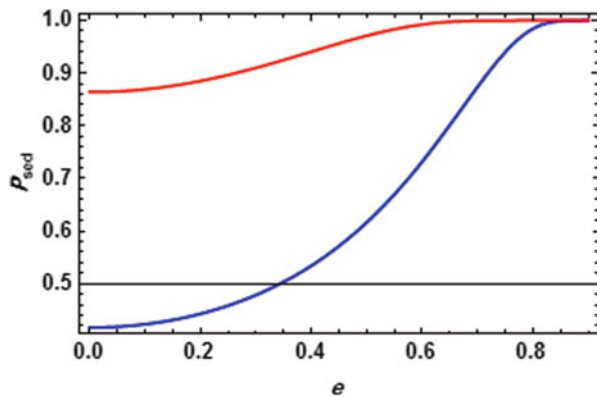


**Fig. 2.12** Plot of the deposition probability for an experiment taking place 300 km above the surface of the Earth in an elliptical polar orbit, as a function of the spacecraft's orbital true anomaly  $f$  and eccentricity  $e$  for residence time  $t = 0.2$  s and density  $\rho = 1,300$  kg/m<sup>3</sup>

**Fig. 2.13** Plot of the deposition probability as a function of orbital eccentricity  $e$  in an experiment taking place in a spacecraft 300 km above the surface of the Earth in an elliptical polar orbit for particles of diameters blue = 1  $\mu$ m red = 2  $\mu$ m and density  $\rho = 1,300$  kg/m<sup>3</sup>



function of orbital eccentricity  $e$  in an experiment taking place in a spacecraft 300 km above the surface of the Earth in elliptical polar orbits for particles of diameters blue = 1  $\mu$ m, red = 2  $\mu$ m and density  $\rho = 1,300$  kg/m<sup>3</sup>. We find that for the same residence time  $t = 0.2$  s the deposition probability increases with particle diameter  $d$  and eccentricity  $e$ . In particular for particles of diameter 1  $\mu$ m the high probability plateau is reached for eccentricities in the range  $0.7 \leq e \leq 0.8$  and higher, and for particles of 2  $\mu$ m in diameter in the range  $0.6 \leq e \leq 0.8$ . Next in Fig. 2.14 we plot of the deposition probability as a function of orbital eccentricity  $e$  for particles of diameters  $d = 3$  and 3.5  $\mu$ m of the same density. We find that increasing eccentricity increases the deposition probability for the particles of the above diameters. Larger diameters reach a constant higher probability plateau at

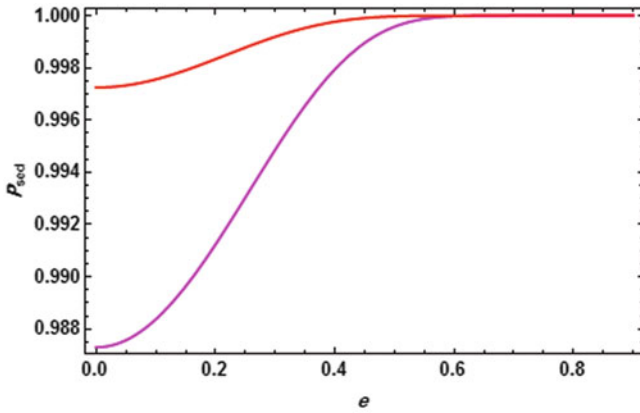


**Fig. 2.14** Plot of the deposition probability as a function of orbital eccentricity  $e$  in an experiment taking place in a spacecraft 300 km above the surface of the Earth in a elliptical polar for particles of diameters *magenta* = 3  $\mu\text{m}$  and *red* = 3.5  $\mu\text{m}$  and density  $\rho = 1,300 \text{ kg/m}^3$

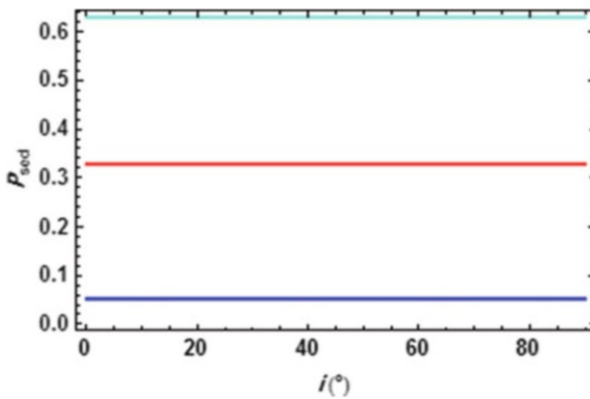


**Fig. 2.15** Plot of the deposition probability as a function of orbital inclination  $i$  in an experiment taking place in a spacecraft 300 km above the surface of the Earth in a elliptical polar orbit of eccentricity  $e = 0.1$  for particles of the same diameter  $d = 1.3 \mu\text{m}$  and density  $\rho = 1,300 \text{ kg/m}^3$ , and corresponding residence times  $t = 0.0272, 0.2,$  and  $0.5 \text{ s}$ , respectively, from the bottom up  $d = 1.3 \mu\text{m}$

smaller eccentricities. In Fig. 2.15 we plot the deposition probability as a function of orbital inclination  $i$  in an experiment taking place in a spacecraft 300 km above the surface of the Earth in a elliptical polar orbit of eccentricity  $e = 0.1$  for particles of the same diameter  $d = 1.3 \mu\text{m}$  and density  $\rho = 1,300 \text{ kg/m}^3$ , and corresponding residence times  $t = 0.0272, 0.2,$  and  $0.5 \text{ s}$ , respectively, from the bottom up. We find that the orbital inclination does not affect the deposition probability which appears to be constant for the various residence times indicated. Next, in Fig. 2.16 we plot of the deposition probability on the surface of the Mars as a function of the particle diameter  $d$  and density  $\rho$ , at areocentric latitude  $\phi = 90^\circ$ , for particles in the

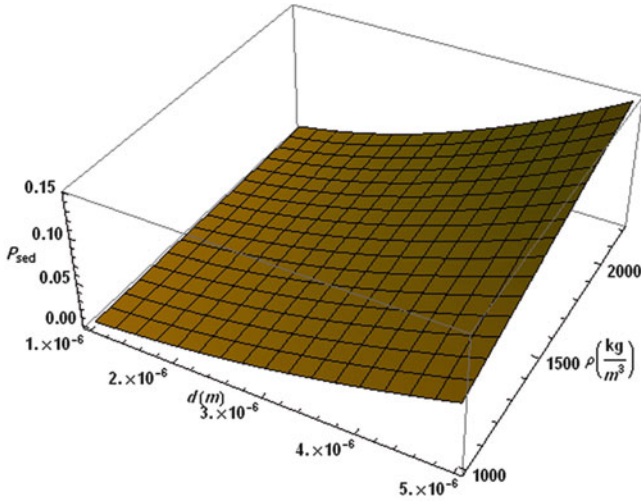


**Fig. 2.16** Plot of the deposition probability on the surface of the Mars as a function of the particle diameter  $d$  and density  $\rho$ , at areocentric latitude  $\phi = 90^\circ$ , for particles in the diameter/density range of  $1 \mu m \leq d \leq 5 \mu m$  and  $1,000 \text{ kg/m}^3 \leq \rho \leq 2,200 \text{ kg/m}^3$  and residence time  $t = 0.2 \text{ s}$  respectively

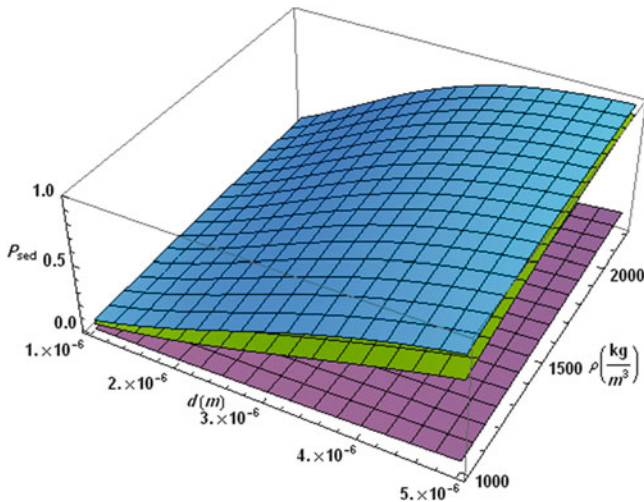


**Fig. 2.17** Plot of the deposition probability on the surface of the Mars as a function of the particle diameter  $d$  and density  $\rho$ , at areocentric latitude  $\phi = 90^\circ$ , for particles in the diameter/density range of  $1 \mu m \leq d \leq 5 \mu m$  and  $1,000 \text{ kg/m}^3 \leq \rho \leq 2,200 \text{ kg/m}^3$  and residence times  $t = 0.2, 3, \text{ and } 5 \text{ s}$ , respectively

diameter range of  $1 \mu m \leq d \leq 5 \mu m$  residence time  $t = 0.2 \text{ s}$  and density  $1,300 \text{ kg/m}^3$ . We find that at the areocentric latitude of  $90^\circ$  the deposition probability increases with particle diameter  $d$  and density  $\rho$  in a much slower way than the corresponding Earth one. In Fig. 2.17 we plot of the deposition probability on the surface of the Mars as a function of the particle diameter  $d$  and density  $\rho$ , at



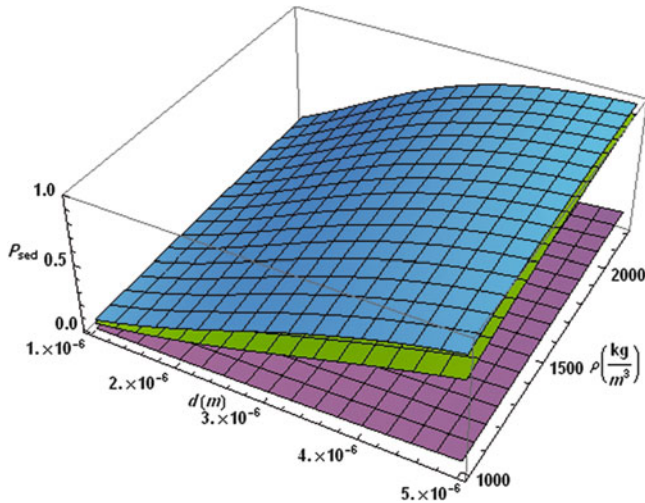


**Fig. 2.18** Plot of the deposition probability on the surface of the Mars as a function of the particle diameter  $d$  and density  $\rho$ , at areocentric latitude  $\phi = 45^\circ$  for particles for particles in the diameter/density range of  $1 \mu\text{m} \leq d \leq 5 \mu\text{m}$  and  $1,000 \text{ kg/m}^3 \leq \rho \leq 2,200 \text{ kg/m}^3$  and residence times  $t = 0.2, 3, \text{ and } 5 \text{ s}$ , respectively

areocentric latitude  $\phi = 90^\circ$ , for particles in the diameter range of  $1 \mu\text{m} \leq d \leq 5 \mu\text{m}$ , density  $1,300 \text{ kg/m}^3$  and residence time  $t = 0.2, 3, \text{ and } 5 \text{ s}$ , respectively. We find that higher particle diameters combined with high densities and higher residence times can easily ensure deposition probabilities that can be equal to one. For example a residence time of  $5 \text{ s}$  can easily ensure  $P_{dep} = 1.0$  if the density and diameter are high enough. Figure 2.18 we plot the deposition probability as in Fig. 2.16 but for the areocentric latitude of  $45^\circ$  demonstrates a similar behavior at a lesser degree. In Fig. 2.19, we plot deposition probability versus particle diameter and density and for exactly the same particles with diameter and density ranges of  $1 \mu\text{m} \leq d \leq 5 \mu\text{m}$  and  $1,000 \text{ kg/m}^3 \leq \rho \leq 2,200 \text{ kg/m}^3$ , respectively. We find that circular orbits result to a smaller deposition probabilities with a plateau that has a max probability range of approximately half of that of the elliptical orbits. In Figs. 2.20 and 2.21 we plot of the deposition probability on the surface of the Mars as a function of the particle diameter  $d$  and density  $\rho$ , in an experiment taking place in a spacecraft  $300 \text{ km}$  above the surface of Mars in an elliptical polar orbits of orbital inclination  $i = 90^\circ$ , and eccentricities  $e = 0.1, 0.4$  and residence time  $t = 0.2, 3, \text{ and } 5 \text{ s}$ , respectively. We find that the higher inclination considerably affects particle of large diameter/density that fall for higher residence times. Higher residence times reach a probability plateau at small particle diameters. In Fig. 2.22 we plot of the deposition probability on the surface of Earth and Mars as a function of particle density  $\rho$  for the geocentric and areocentric latitude  $\phi = 45^\circ$  and for particles with diameters in the range  $1, 2, 3, \text{ and } 4 \mu\text{m}$  for residence time  $t = 0.2 \text{ s}$ . The bottom bundle of straight lines corresponds to Martian deposition probabilities where the upper bundle corresponds to Earth deposition probabilities that are significantly higher when compared to the Martian ones. Figure 2.23 gives the deposition rate in an experiment taking place on the surface of Earth as a function particle density  $\rho$  and

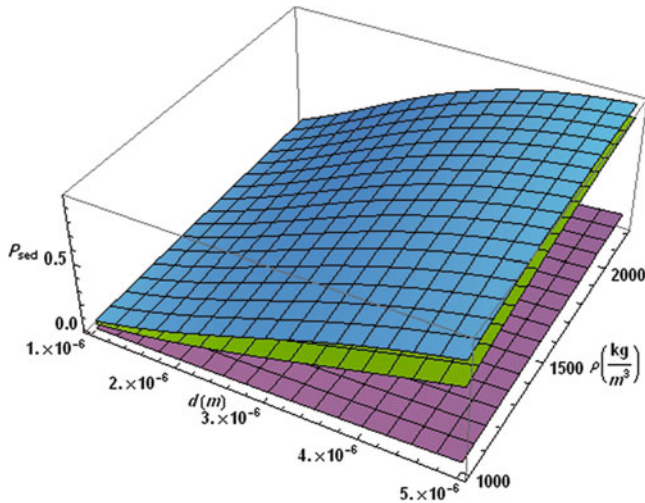


**Fig. 2.19** Plot of the deposition probability on the surface of the Mars as a function of the particle diameter  $d$  and density  $\rho$ , in an experiment taking place in a spacecraft 300 km above the surface of Mars in a circular polar orbit of orbital inclination  $i = 90^\circ$ , eccentricity  $e = 0$ , and residence time  $t = 0.2, 3, 5$  s respectively, and for particles in the in the diameter/density range of  $1 \mu\text{m} \leq d \leq 5 \mu\text{m}$  and  $1,000 \text{ kg/m}^3 \leq \rho \leq 2,200 \text{ kg/m}^3$

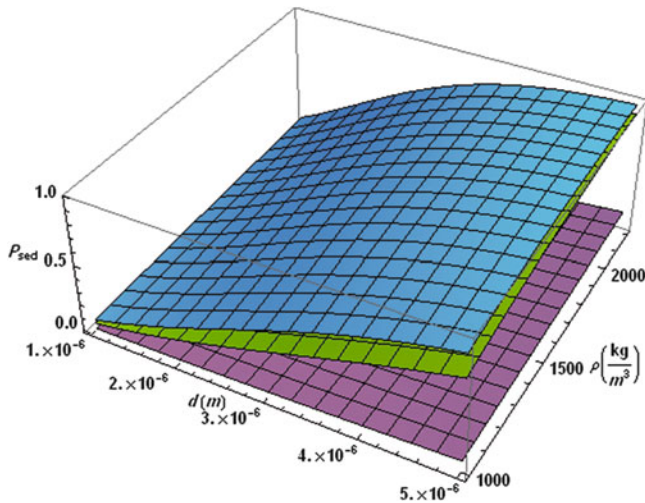


**Fig. 2.20** Plot of the deposition probability on the surface of the Mars as a function of the particle diameter  $d$  and density  $\rho$ , in an experiment taking place in a spacecraft 300 km above the surface of Mars in an elliptical polar orbit of orbital inclination  $i = 90^\circ$ , eccentricity  $e = 0.1$  and residence time  $t = 0.2, 3, 5$  s respectively, respectively, and for particles in the diameter/density range of  $1 \mu\text{m} \leq d \leq 5 \mu\text{m}$  and  $1,000 \text{ kg/m}^3 \leq \rho \leq 2,200 \text{ kg/m}^3$



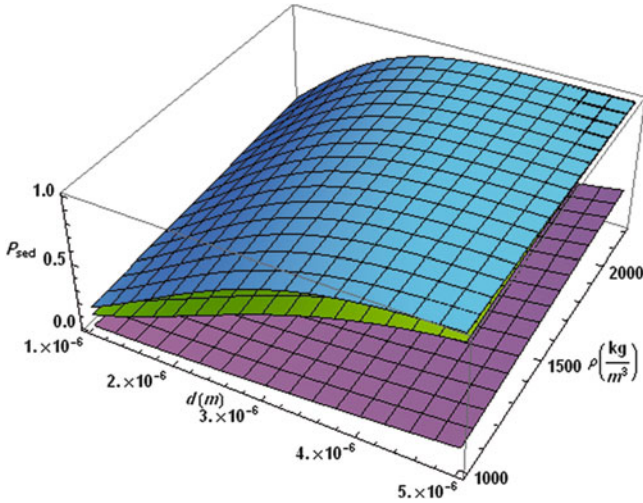


**Fig. 2.21** Plot of the deposition probability on the surface of the Mars as a function of the particle diameter  $d$  and density  $\rho$ , in an experiment taking place in a spacecraft 300 km above the surface of Mars in a elliptical polar orbit of orbital inclination  $i = 90^\circ$ , eccentricity  $e = 0.4$  and residence time  $t = 0.2, 3, \text{ and } 5$  s, respectively, and for particles in the diameter/density range of  $1 \mu\text{m} \leq d \leq 5 \mu\text{m}$  and  $1,000 \text{ kg/m}^3 \leq \rho \leq 2,200 \text{ kg/m}^3$

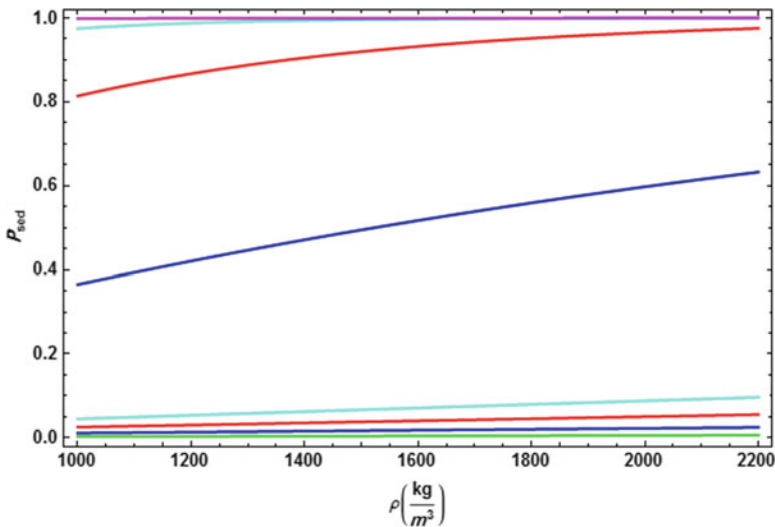


**Fig. 2.22** Plot of the deposition probability on the surface of Earth and Mars as a function of particle density  $\rho$  for the geocentric and areocentric latitude  $\phi = 45^\circ$  for particles of diameters in the range  $1 \mu\text{m} \leq d \leq 4 \mu\text{m}$  for residence time  $t = 0.2$  s. The *bottom bundle of straight lines* corresponds to Mars

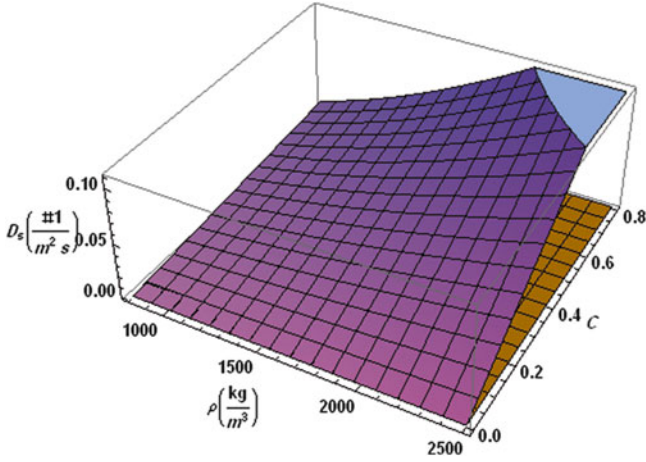


**Fig. 2.23** Plot of the deposition rate in an experiment taking place on the surface of Earth as a function particle density  $\rho$  and particle concentration  $C$  for particles of diameter  $d = 1 \mu m$  and residence times  $t = 0.0272, 0.2$  s correspondingly

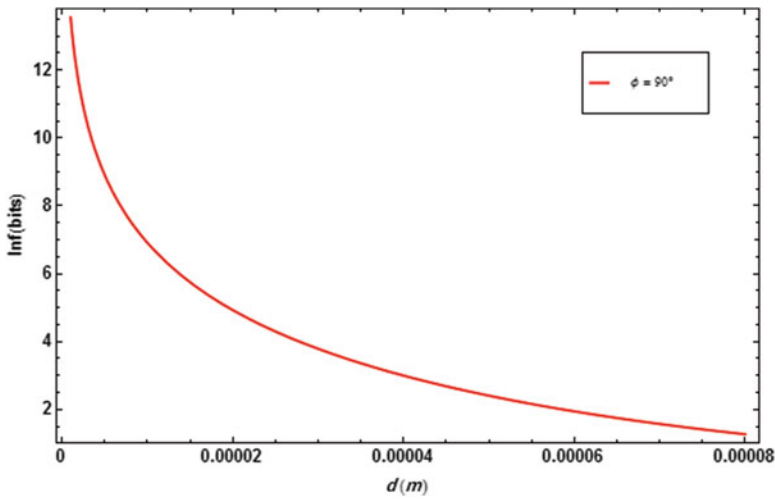


**Fig. 2.24** Plot of the information content required in an experiment taking place on the surface of Earth at geocentric latitude  $\phi = 90^\circ$  as a function particle diameter  $d$  for particles of density  $\rho = 1,300 \text{ kg/m}^3$

particle concentration  $C$  for particles of diameter  $d = 1 \mu m$  and residence time  $t = 0.0272, 0.2$  s. Higher residence times result to higher deposition rates at higher deposition coefficients and densities. For a  $t = 0.2$  s deposition plateau it's reached at about  $0.10 \text{ particles/m}^2 \text{ s}$  bounded by the density and particle concentration ranges of  $2,100 \text{ kg/m}^3 \leq \rho \leq 2,500 \text{ kg/m}^3$  and  $0.6 \leq C \leq 0.8$  respectively. In Fig. 2.24 we plot the information content required in an experiment taking place

on the surface of Earth at geocentric latitude  $\phi = 90^\circ$  as a function particle diameter  $d_p$  for particles of density  $\rho = 1,300 \text{ kg/m}^3$ . Similarly, in Fig. 2.25 we plot of the information content required in relation to particles of diameter  $d_p$  in a deposition probability experiment on the surface of Mars as a function particle diameter  $d_p$ . Furthermore, in Fig. 2.26 we plot of the information content required in an

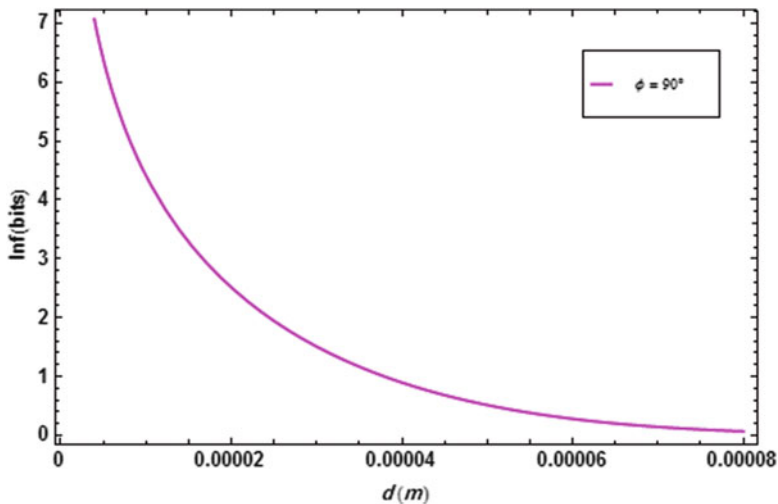


Fig. 2.25 Plot of the information content required in relation to particles of diameter  $d$  in the sedimentation probability experiment surface of Mars as a function particle diameter  $d$  particles of density  $\rho = 1,300 \text{ kg/m}^3$

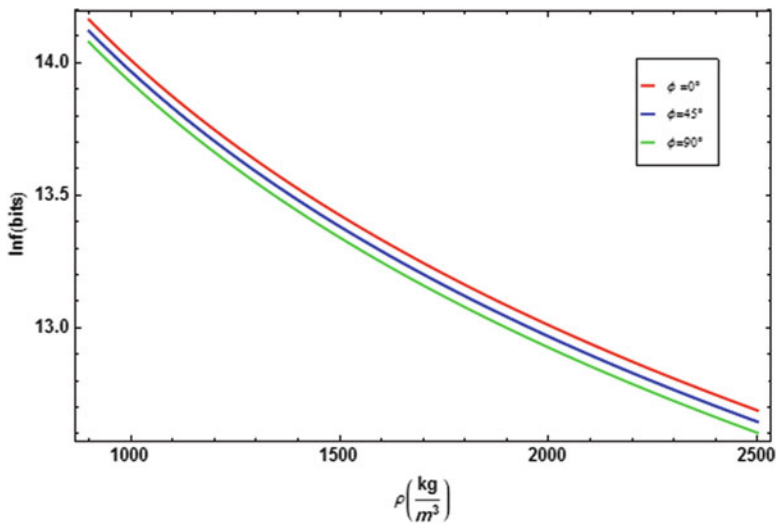
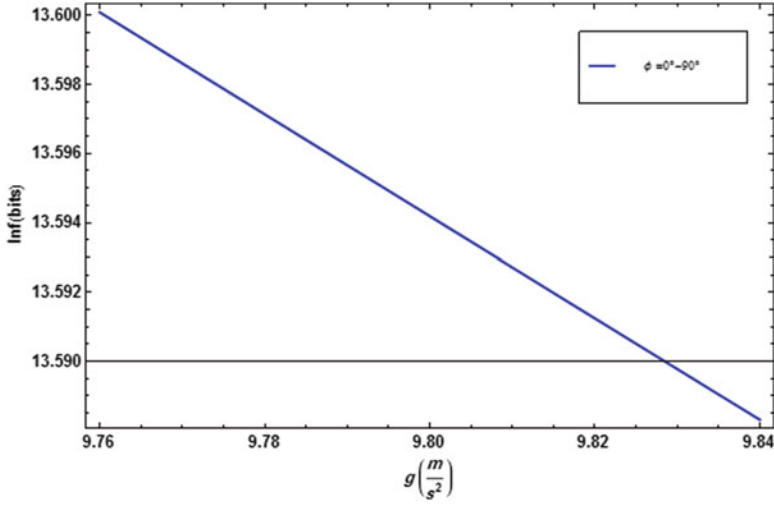


Fig. 2.26 Plot of the information content required in an experiment taking place at various geocentric latitudes on the surface of Earth as a function particle density  $\rho$



**Fig. 2.27** Plot of the information content required in an experiment taking place on the surface of Earth as a function the acceleration of gravity  $g$  in the range of geocentric latitude  $\phi = 0^\circ - 90^\circ$

experiment taking place on the surface of Earth as a function particle density  $\rho_p$ . In Fig. 2.26 we plot the information content required in an experiment taking place at various geocentric latitudes on the surface of Earth as a function particle density  $\rho$ . Finally, in Fig. 2.27 we plot the information content required in an experiment taking place on the surface of Earth as a function the acceleration of gravity  $g$  in the range of geocentric latitude  $\phi = 0^\circ - 90^\circ$ .

For residence time  $t = 0.2$  s and particles of diameter  $d_p = 1 \mu\text{m}$  on the surface of the Earth the deposition rates numerically become

$$D_{\phi=0^\circ} = 0.262792C_s, \quad (2.88)$$

$$D_{\phi=45^\circ} = 0.264010C_s, \quad (2.89)$$

$$D_{\phi=90^\circ} = 0.265228C_s. \quad (2.90)$$

For residence time  $t = 0.2$  s and particles of diameter  $d_p = 5 \mu\text{m}$  on the surface of the Earth the deposition rates numerically become

$$D_{\phi=0^\circ} = 12.9759C_s, \quad (2.91)$$

$$D_{\phi=45^\circ} = 13.0106C_s, \quad (2.92)$$

$$D_{\phi=90^\circ} = 13.0452C_s. \quad (2.93)$$

For residence time  $t = 0.2$  s and particles of diameter  $d_p = 1 \mu\text{m}$  on the surface of Mars the deposition rates numerically become

$$D_{\phi=0^\circ} = 1.74163 \times 10^{-5} C_s, \quad (2.94)$$

$$D_{\phi=45^\circ} = 1.74164 \times 10^{-5} C_s, \quad (2.95)$$

$$D_{\phi=90^\circ} = 1.74165 \times 10^{-5} C_s. \quad (2.96)$$

For both Earth and Mars and for a particular concentration  $C_s$  we find that the deposition rate is higher at the poles comparing to that of the equator. In reference to a spacecraft environment, we say that the atmosphere of spacecraft will contain aerosols (both biological and non-biological) in concentrations which represent the balance between the rates of aerosol particle generation and particle removal by various processes. Physically, the microbial particles while suspended will behave similarly to other particles of various sizes, and at this point there is no need to distinguish about their generation and translocation. In fact, it can be expected that viable microbial particles will physically adhere to nonviable material quite often. During spaceflight there will be the transfer of microbes between crew members. Microbial exchange commonly occurs amongst astronauts. Several bacterial associated diseases were experienced by the crew in Skylab 1 [31]. The microbial contamination in the Skylab was found to be very high. *Staphylococcus aureus* and *Aspergillus* spp. have commonly been isolated from the air and surfaces during several space missions. During one mission an increase in the number and spread of fungi and pathogenic streptococci were found in many American Spacecrafts [26]. This constitutes an important issue for future extended missions in the Moon or Mars. This consideration could be of particular importance at filter surfaces or in impinger fluids because the nonviable material may serve as substrate permitting the growth of large microbial concentrations on these surfaces. In microgravity conditions it might be necessary to redefine the term ‘‘aerosol.’’ Aerosols consist of particles suspended in gas, and the particles are small enough to stay in suspension for appreciable periods of time. In microgravity, this distinction disappears. However, in the atmosphere of the spacecraft there is still an important difference between the behavior of large and small particles. The small particles have a relatively ratio of surface-to-mass ratio, and as a result, move through the atmosphere primarily by the influence of viscous drag forces. Large particles, on the other hand, are affected primarily by inertial forces, and are relatively unresponsive to gas flows at moderate velocities. In addition to small particles characteristic of aerosols, the atmosphere of the spacecraft may at times contain relatively large objects from food or equipment. Some of these could lodge in various locations and become potential microbial growth sites. Debris also may enter the equipment used for aerosol control, and interfere in the operation of that equipment. This problem is not encountered in dust collectors in gravitational fields. Coarse objects settle out in the air. In designing aerosol control equipment for the spacecraft environment special attention must be given to means for excluding coarse debris and avoiding interference from this source. Air environments can be important in the dissemination of microbial cells. These are cells, of various sizes that vary in size from a few microns to a fraction of a micron, become

suspended in air through a variety of mechanisms. The organisms once suspended remain in air for long periods of time and they can be dispersed over a wide area by atmospheric diffusion. For example a microorganism with diameter  $d = 1 \mu\text{m}$ , i.e., the size of some bacteria, settles downward in the air at a rate of only 0.217 m/h or  $3.52 \times 10^{-5}$  m/s. Furthermore, small air currents such as those caused by thermal convection are sufficient to propel them in the absence of gravitational attraction. In a spacecraft atmosphere a certain portion of the organisms suspended will remain viable and these organisms can be transported from the interior of space suits and carried by cabin air currents originating from the function of the Environmental Control Systems (ECS) as well as from the motion of the crew. In the absence of gravity, aerosol particles are effectively removed from suspension by contacting a fixed surface to which they are held by mechanical restraint and by chemical or physical interaction. Cabin aerosol particles will move toward the walls and other exposed surfaces at a rate which depends on several factors. The most important driving force will be furnished by the "air" currents which can easily reach random local velocities of several cm per second. Small particles will be carried about by the gas at essentially the same velocities. Statistically, a certain fraction of the particles per unit time will approach a surface closely enough for the particle to be "captured" and held by surface attractive forces. The removal of particles on certain sections of the walls can be increased by increasing the "sticking" probability. This may be accomplished by providing an adhesive surface or by using a dielectric material which readily builds up high electrostatic charges. It might also be possible to utilize the "thermal precipitation" effect, whereby small particles are preferentially deposited on a surface which is maintained colder than surroundings. Further detailed study is needed to determine the advantages of inducing such deposits of aerosols on selected portions of the surface of a space vehicle cabin. The problems of inhibiting microbial growth on the surface and of determining relative collection efficiencies need to be considered in relation to the corresponding problems involved in the use of conventional particle collectors. Inhalation of particles generated as a result of thermal degradation from fire or smoke, as may occur on spacecraft, is of major health concern to space-faring countries. Knowledge of lung airflow and particle transport under different gravity environments is required to address this concern by providing information on particle deposition. Similarly deposition of inhaled lunar dust particles will be very important in the case of future moon missions. The extent of the inflammatory response in the lung will depend on where the Lunar and Mars dust particles are deposited. During 1 g deposition in the more central airways will reduce the transport of the fine particles in the periphery of the lung. On the other hand the fractional gravity of the Moon and Mars will deposit the inhaled particles in more peripheral lung regions. Moon's less gravity will also result in a smaller sedimentation rate. As a result fine dust particles will deposit in the alveolar lung region, exacerbating the potential for the lung damage. Lunar dust is known to have a large surface area (i.e., it is porous), and a substantial portion is in the respirable range. The surface of the lunar dust particles is known to be chemically activated by processes ongoing at the surface of the moon.

An alternative framework for the study of gravitational effects in biology, and in particular the interaction of gravity and the respiratory system is the introduction of information. The introduction of this different approach discussed below requires a detailed description of Shannon linear model of communication, and details on the theory of information and cybernetics which can be found in several references such as [1, 27, 28]. In order to formalize the gravity role in the sedimentation process and to help the reader follow the rationale behind it, we provide some interpretations proper to Shannon information model. Information theory, which was originally developed for use in telecommunications, has in recent years been increasingly applied to analyzing biological signaling pathways to answer relative biological questions [22]. For Shannon, anything is a source of information (in our case, the respiratory system of the human organism) if it has a number of alternative states (in our case, states of gravitational interaction) that might be realized on a particular occasion and the method of encoding is based on the presupposition. It is necessary to process, or encode information from a source (in our case the encoder is the gravitational field and the encoding is done through the gravitational acceleration formula which codifies all changes of gravitational interaction) before transmitting it through a given channel. According to Shannon information presupposes the existence of a signal probability, where the signal can be described via a stochastic distribution function [28]. Furthermore, this signal propagates through communicational channels [28]. With reference to the communication channel we say, that this constitutes a composite channel (particles, environment, respiratory system as well as the physiology of the system), where a way of transportation of the signal is the sedimentation (itself), among which the basic regulatory parameters are gravity itself as well as the rest of the variables.

Even though there is still no final definition of the term information, according to Stonier [29] “information exists” and regulates various parameters of the system that they are impossible to be described in a deterministic model, as well as its not possible to quantify via a stochastic model (e.g., in the case of the respiratory system these factors could be the structural form, variation in lung capacities, coordination of muscles for controlling breathing, exchange gases with the circulatory system). The net effect of these parameters can be modeled in the theory of information. According to Shannon [28] information is transferred with an allowable degree of noise. Shannon allows the introduction of noise in the interaction of a biological organism and environment, where noise accounts for biological environment variation [3, 22, 32].

In this paper we do not quantify the effect of noise according to Shannon’s rate distortion theory, but we study how information or the self-information of the system can be reflected and codified via gravity in the natural phenomenon of sedimentation, taking into account that the respiratory system is itself a decoder of the information transmitted and contained in the system of the human body. A decoder is a device which does the reverse operation of an encoder, undoing the encoding so that the original information can be retrieved. In our case the decoder is the respiratory system. Next, according to Shannon, we consider the probability of

sedimentation  $P_{\text{sed}}$  to be a random variable and remind the reader that according to Shannon the amount of the information content, given in [20]

$$I(x = a_i) = -\log_2[P(x = a_i)], \quad (2.97)$$

is a sensible measure of the information content of the outcome  $x = a_i$ . Therefore, let us consider that the sedimentation is the random variable and that the amount of information content associated with the sedimentation of dust particles in the respiratory system is

$$I(P_{\text{sed}}) = -\log_2(P_{\text{sed}}) = -\log_2 \left[ 1 - e^{-\left( \frac{(\rho_p - \rho_{\text{air}})d_p^2 C_c}{18\eta_{\text{air}}R} ig \cos \theta \right)} \right] \text{ bits}, \quad (2.98)$$

from which we can also obtain that the dependence of the acceleration of gravity itself on the amount of information content is given by

$$g(I) = \frac{q^2 r^2 \cos \xi}{16\pi \epsilon m_p (r - R)^2} + \frac{18\eta R \sec \theta}{C_c (\rho_p - \rho_{\text{air}}) d_p^2 t} \log(1 - 2^{-I}). \quad (2.99)$$

Next,  $g = g(I)$  since sedimentation is taking place but also since this sedimentation connects to the acceleration of gravity. The fact that the two variables are correlated is manifested on the phenomenon of sedimentation. Therefore, the spatial-temporal conditions (gravity, time, etc.) serve as substrate for the correlation of gravity  $g$  and information  $I$ . In the case of a dust particle that has diameter  $d = 1 \mu\text{m}$  and density  $\rho = 1,300 \text{ kg/m}^3$  on the surface of the Earth, we obtain that the information related to the sedimentation has a dependence on the acceleration gravity  $g$  that is given by the equation below:

$$I = -1.4427 \ln \left( 1 - e^{-0.000377267(3.8742 \times 10^{-14} + 0.80411g)} \right) \quad (2.100)$$

From Eq. (2.85) we that if the acceleration of gravity  $g$  changes the probability of sedimentation and therefore changes the information contained in the random variable, as it is decoded by the pulmonary system. Thus we say that the pulmonary system is a receiver and a decoder of information. Therefore, the environment is the sender as it sends information on the human body, in other words the biophysics of sedimentation equals to the a communication channel. This communication channel can be designed and based on parameters such as gravity to change. Therefore gravity in our case controls how to transmit the information signal. The pulmonary system is the biological decoder in which information is received and as primordial information it interacts with the structural information of the system, producing a new kind of information which could be interpreted as a kind of meta-information



information of the interaction. This can be thought as a way in which gravity enters the cognitive processes of the system (processing of information) in the cybernetic sense. The “Shannon” approach to sedimentation is a new different approach that is related to the main approach adopted in the paper through the probability of sedimentation. This is a first step towards an approach that aims in a deeper understanding and mathematical and structural description of information processing in human organisms in variable gravitational background.

### Conclusions

We have studied the effect of the acceleration of gravity on the deposition probability due to sedimentation. In doing so, on the surface of the Earth and Mars we have corrected the acceleration of gravity for the zonal harmonic coefficients of both planets as well as for their rotation. On the surface of the Earth/Mars, we have found that deposition probability due to sedimentation at the poles is higher than that at the equator. For  $1\ \mu\text{m}$  particles of density  $1,300\ \text{kg/m}^3$  with residence time of  $0.2\ \text{s}$  exhibit a  $0.4\ \%$  percentage difference, where on Mars the corresponding percentage difference is  $0.9\ \%$ . When orbiting around a planet equatorial orbits result to higher deposition probabilities than the polar ones. In particular for a spacecraft orbiting at  $300\ \text{km}$  above the Earth in a circular orbit we find that  $1\ \mu\text{m}$  particles with corresponding residence times of  $0.0272$  and  $0.2\ \text{s}$  exhibit  $-0.1$  and  $-0.09\ \%$  percentage difference in the deposition probabilities between polar and equatorial orbits. Similarly elliptical orbits of eccentricity  $e = 0.1$  exhibit a percentage difference equal to  $-0.17\ \%$  and  $-0.09\ \%$ , respectively. On the surface of Mars and for the residence time of  $0.2\ \text{s}$  the deposition probability of  $1\ \mu\text{m}$  particles demonstrates an approximately  $0.9\ \%$  percentage difference between poles and the equator. Similarly, and for the same particles there is a  $0\ \%$  difference between circular/elliptical polar and equatorial orbits. We have also found that high eccentricity elliptical orbits result to higher deposition probabilities. Finally, as an alternative framework for the study of interaction and the effect of gravity in biology the term information according to Shannon has been used, and in particular gravity and respiratory system. This can be thought as a way in which gravity enters the cognitive processes of the system (processing of information) in a bio-gravitational cybernetic sense, introducing the possibility of a multidisciplinary approach of the study of the effects of gravity on humans. This may be important also because it could open interesting perspectives to project new kinds of missions having both biological and fundamental physics and bio-engineering goals.

**Acknowledgements** The authors of this chapter would like to thank two anonymous reviewers for their encouraging review of this chapter. The authors want to thank Ivana Haranas for designing Fig. 2.1 in this paper.

## References

1. Berger T (1971) Rate distortion theory; a mathematical basis for data compression, Prentice-Hall series in information and system sciences. Prentice-Hall, Englewood Cliffs, NJ, p xiii, 311
2. Breatnach E, Abbot GC, Fraser RG (1983) Dimensions of the normal human trachea. *AJR AM J Roentgenol* 141:903–906
3. Burton W, Iglesias PA (2007) An information-theoretic characterization of the optimal gradient sensing response of cells. *PLoS Comput Biol* 3(8):e153
4. Calle CI, Thompson SM, Cox ND, Johansen MR, Williams BR, Hogue MD, Clements JS (2011) Electrostatic precipitation of dust in the Martian atmosphere: implications for the utilization of resources during future manned exploration missions. *J Phys Conf Ser* 327:012048
5. Cunningham E (1910) On the velocity of steady fall of spherical particles through fluid medium. *Proc R Soc Lond A Math Phys Sci* A83:357–365
6. García MH (2008) Sedimentation engineering: processes, measurements, modeling, and practice. ASCE Publications, Reston, VA, p 964
7. Green HL, Lane WR (1957) Particulate clouds: dusts, smokers, and mists. D. Van Nostrand, Princeton, NJ
8. Gussman RA (1969) On the aerosol particle slip correction factor. *J Appl Meteorol* 8:999–1001
9. Gussman R A 1969a, Rep No. 170, Cambridge Mass., Bolt Beranek and Newman
10. Hadjifotinou KG (2000) Numerical integration of satellite orbits around an oblate planet. *Astron Astrophys* 354:328–333
11. Haranas I, Gkigkitzis I, Zouganelis DG (2013) A computational study of the mechanics of gravity-induced torque on cells. *Gravit Space Res* 1:79–94
12. Haranas I, Gkigkitzis I, Zouganelis DG (2012)  $g$  Dependent particle concentration due to sedimentation. *Astrophys Space Sci* 342:31–43
13. Hatch T, Gross P (1964) Pulmonary deposition and retention of inhaled aerosols. Academic, New York
14. Holmes TH, Goodell H, Wolf S, Wolff HG (1950) The nose. Charles C Thomas, Springfield, IL
15. ICRP (1994) Human respiratory tract model for radiological protection. Technical report ICRP publication 66, International Commission on Radiological Protection
16. Iorio L et al (2011) Phenomenology of the Lense-Thirring effect in the solar system. *Astrophys Space Sci* 331(2):351–395
17. Kaula William M (2000) Applications of Satellites to Geodesy. *Theory of Satellite Geodesy*, pp. 40
18. Landhall HD (1950) *Bull. Math. Biophysics* 12:43
19. Landhl HD (1963) *Bull Math Biophys* 25:29–39
20. MacKay DJC (2005) Information theory, inference, and learning algorithms. Cambridge University Press, Cambridge, p 67, Version 7.2
21. Morrow PE, Bates DV, Fish BR, Hatch TF, Mercer TT (1966) International commission on radiological protection task group on lung dynamics; deposition and retention models for internal dosimetry of the human respiratory tract. *Health Phys* 12:173–207
22. Porter JR, Andrews BW, Iglesias PA (2012) A framework for designing and analyzing binary decision-making strategies in cellular systems. *Integr Biol* 4(3):310–317
23. Read PL, Lewis SR (2004) The Martian climate revisited: atmosphere and environment of a desert planet. Springer, Berlin, p 197
24. Schuenger AC (1998) Microbial contamination of advanced life support (ALS) systems poses a moderate threat to the long-term stability of space-based bioregenerative systems. *Life Support Biosph Sci* 5(3):325–337
25. Shannon CE, Weaver W (1959) The mathematical theory of communication. University of Illinois Press, Champaign, IL
26. Shannon CE (1948) A mathematical theory of communication. *Bell Syst Tech J* 27(3):379–423

27. Stonier T (1990) Information and the internal structure of the universe: an exploration into information physics. Springer, New York
28. Stuart BO (1984) Deposition and clearance of inhaled particles. *Environ Health Perspect* 55:369–390
29. Taylor GR, Graves RC, Brockett RM, Ferguson JK, Mieszkuc BJ (1977) Skylab environmental and crew microbiology studies. In: Johnston RS, Dietlein LF (eds) *Biomedical results from Skylab*. NASA SP-377. NASA, Washington, DC, p 53, 491 pages
30. Tkačik G, Walczak AM (2011) Information transmission in genetic regulatory networks: A review. *J Phys Condens Matter* 23:153102
31. Vallado D, McClain WD (2007) *Fundamentals of Astrodynamics and Applications*, Space Technology Library, Third Edition
32. Watkins-Pitchford W, Moir J (1916) On the nature of the doubly refracting particles seen in microscopic sections of silicotic lungs, and an improved method for disclosing siliceous particles in such sections. *S Afr Inst Med Res* 1:207–230
33. William C. Hinds (1999) *Aerosol Technology: Properties, Behavior, and Measurement of Airborne Particles*, John Willey & Sons, pp. 45
34. Yu CP (1985) Theories of electrostatic lung deposition of inhaled aerosols. *Ann Occup Hyg* 29 (2):219–227

# Chapter 3

## Sequence Patterns Mediating Functions of Disordered Proteins

**Konstantinos P. Exarchos, Konstantina Kourou, Themis P. Exarchos, Costas Papaloukas, Michalis V. Karamouzis, and Dimitrios I. Fotiadis**

**Abstract** Disordered proteins lack specific 3D structure in their native state and have been implicated with numerous cellular functions as well as with the induction of severe diseases, e.g., cardiovascular and neurodegenerative diseases as well as diabetes. Due to their conformational flexibility they are often found to interact with a multitude of protein molecules; this one-to-many interaction which is vital for their versatile functioning involves short consensus protein sequences, which are normally detected using slow and cumbersome experimental procedures. In this work we exploit information from disorder-oriented protein interaction networks focused specifically on humans, in order to assemble, by means of overrepresentation, a set of sequence patterns that mediate the functioning of disordered proteins; hence, we are able to identify how a single protein achieves such functional promiscuity. Next, we study the sequential characteristics of the extracted patterns, which exhibit a striking preference towards a very limited subset of amino acids; specifically, residues leucine, glutamic acid, and serine are particularly frequent among the extracted patterns, and we also observe a nontrivial propensity towards alanine and glycine. Furthermore, based on the extracted patterns we set off to infer potential functional implications in order to verify our findings and potentially further extrapolate our knowledge regarding the functioning of disordered proteins.

---

K.P. Exarchos • K. Kourou • D.I. Fotiadis (✉)

Unit of Medical Technology and Intelligent Information Systems, Department of Materials Science and Engineering, University of Ioannina, Ioannina, Greece  
e-mail: [kexarcho@gmail.com](mailto:kexarcho@gmail.com); [konstadina.kourou@gmail.com](mailto:konstadina.kourou@gmail.com); [fotiadis@cc.uoi.gr](mailto:fotiadis@cc.uoi.gr)

T.P. Exarchos

Institute of Communication and Computer Systems, National Technical University of Athens, Athens, Greece  
e-mail: [themis.exarchos@gmail.com](mailto:themis.exarchos@gmail.com)

C. Papaloukas

Department of Biological Applications and Technologies, University of Ioannina, Ioannina, Greece  
e-mail: [papalouk@cc.uoi.gr](mailto:papalouk@cc.uoi.gr)

M.V. Karamouzis

Molecular Oncology Unit, Department of Biological Chemistry, Medical School, University of Athens, Athens, Greece  
e-mail: [mkaramouz@med.uoa.gr](mailto:mkaramouz@med.uoa.gr)

We observe that the extracted patterns are primarily involved with regulation, binding and posttranslational modifications, which constitute the most prominent functions of disordered proteins.

**Keywords** Disordered proteins • Pattern extraction • Posttranslational modifications • Human diseases

### 3.1 Introduction

Intrinsically disordered proteins, which are also referred to as intrinsically unstructured, or natively unfolded, have lately attracted growing interest. They are characterized by lack of specific 3D structure either in long stretches of amino acids or in their entirety [1]. Specifically, in their native state they exist in an ensemble of formations with considerable abundance in living organisms. Especially, in the case of eukaryotes, there is a prevalent enrichment of their proteome with disordered proteins, compared to the proteomes of bacteria and archaea, thus pinpointing their essentiality and importance [2].

Disordered proteins can adopt a diverse set of structural conformations with transitions between the states, owed to their inherent disorderliness. Due to this flexibility they are able to interact with multiple partners and have, therefore, been associated with several distinguishable functions [3, 4]. Specifically, numerous disordered regions have been implicated with molecular recognition and binding, and consequently with protein-protein interactions [5]; typically, they are involved in the regulation and signaling of pathway interactions that require high specificity/low affinity. Another crucial functional involvement of disordered proteins is related to transcription regulation as indicated by the abundance of disorder in transcription factors, especially within eukaryotic organisms. Moreover, a high preponderance of disordered regions in sites of posttranslational modifications such as phosphorylation, acetylation and many others has been reported [6].

The implication of disordered proteins in a very broad range of functions, makes them a good candidate for disease associations; indeed, several disease-related pathways have been proven to be affected by disordered proteins, in a manner originating from misidentification, misregulation and missignaling subsequently followed by misfolding [7]. The role of disordered proteins in cancer has been specifically emphasized as several crucial cancer-associated proteins—such as p53, AFP, and BRCA1—contain long stretches of disorder [8]. Furthermore, numerous disordered proteins have shown considerable propensity towards cardiovascular diseases, neurodegenerative diseases (e.g., Parkinson’s disease, Alzheimer’s disease, dementia with Lewy bodies), as well as diabetes [9].

Consequently, the inherent interaction promiscuity of disordered proteins and their subsequent functional anthology as well as disease implications, provides an excellent “target group” for extracting and studying linear motifs (or recognition peptides), i.e. short peptide regions (comprised approximately from three to eight

residues) which frequently exhibit a particular pattern crucial for a wide range of cellular functions [10, 11]. In [10], linear motifs of this kind have been systematically identified, however, by considering a wide set of proteins, without a specific orientation. As previously noted, such functionally important patterns are frequently observed in regions of proteins characterized by intrinsic disorder. Specifically, patterns located in disordered protein regions have been proven to dictate a multitude of critical processes such as cell signaling and regulation, gene expression and others. In general, recognition motifs have been proven to reside primarily in sequence segments characterized by disorder and local flexibility [12].

This work specifically focuses on human-encoded disordered proteins and their interactome. We have specifically focused on disordered proteins due to their binding promiscuity and high content in terms of linear motifs. Subsequently, we put together a set of disordered proteins and additionally formulate their interactome. The driving idea is that among a set of proteins interacting with a common partner—a rather frequent situation in disordered proteins—their protein sequences could well share a common pattern that mediates binding or interaction in general. Our primary aim is to discover those patterns, which serve as recognition peptides and are responsible for the subsequent interaction, as well as to study their sequential characteristics. Thus, we assemble a set of protein patterns, in the form of regular expressions that provides insight into the molecular mechanism mediating the abundance of interactions and functions exhibited by disordered proteins. The proposed methodological analysis may as well serve as a means to systematically identify recognition peptides implicated in the functioning of any protein set.

## 3.2 Materials and Methods

The steps of the proposed methodological analysis are depicted in Fig. 3.1. Initially, we assemble a set of seed proteins, that are all either partially or completely disordered or are additionally encoded in humans; subsequently we exploit information from repositories of protein interactions in order to formulate the interactome among the employed seed proteins. From the resulting network, we identify the disordered nodes that exhibit a relatively higher degree of connectivity and retrieve the sequences of all its interacting partners. Within those sequences we aim to discover overrepresented linear motifs, in the form of regular-expression-type patterns that mediate a variety of cellular functions; prior to the pattern discovery process the employed sequences are subject to a series of preprocessing/filtering steps. The discovered patterns are further validated and compared against negative control sets in order to maintain only a limited number of non-redundant patterns. The retained patterns are then analyzed in terms of sequential composition as well as functional implications.

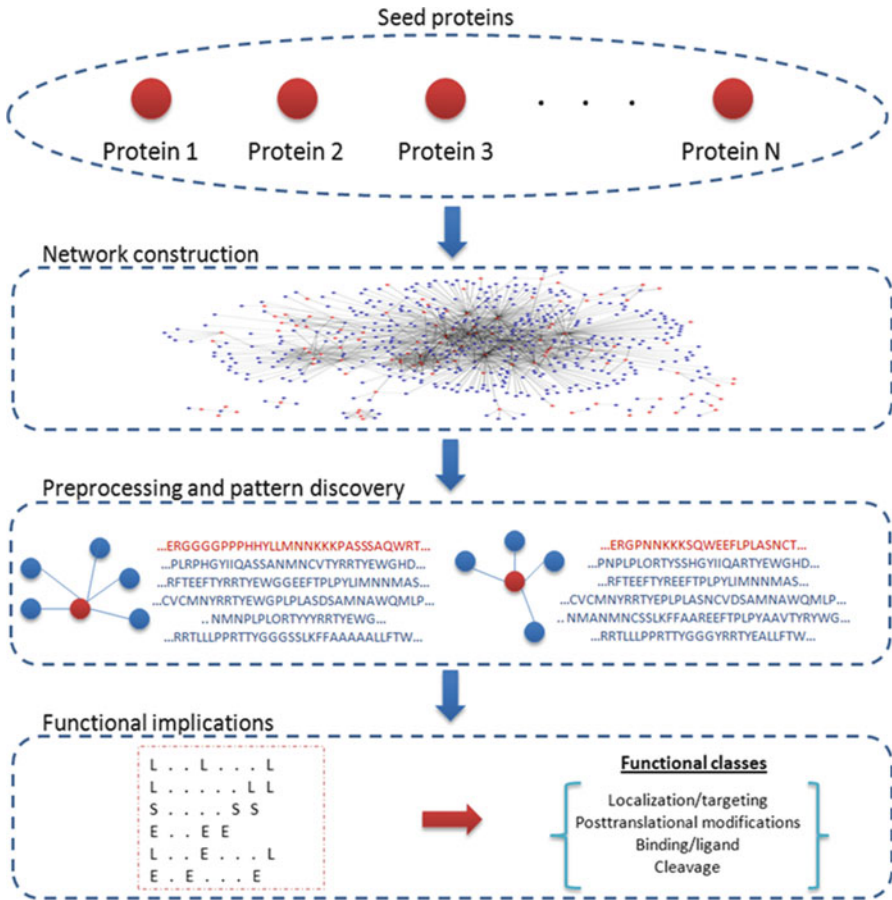


**Fig. 3.1** Flow chart of the proposed methodological analysis

### 3.2.1 Seed Proteins

In order to assemble the initial set of proteins for the construction of the interaction network, we employ the Disprot database [13]. Disprot is currently the largest publicly available database of disordered proteins. Out of this dataset we exclude proteins that are not encoded in humans resulting in 193 proteins. For the remaining list we retrieve the respective genes using the UniProt [14] ID mapping functionality, in order to provide them as input to the next step of our methodological analysis. These proteins/genes (seeds) comprise the core of the disorder-network and are available online as supplementary material (<https://sites.google.com/site/disordernet/>).

### 3.2.2 Network Construction

Although assembling a comprehensive set of disordered proteins is quite useful, we go one step further and elucidate the interactions among the involved proteins; for the construction of the network the MimI [15] repository is employed, which is actually a meta-database of binary interactions merging several resources, such as HPRD [16], IntAct [17], datasets from the Center for Cancer Systems Biology at Harvard [18], as well as many others. Specifically, for the network expansion, we retrieved interacting partners for each of the seed-proteins that we provided as input. The resulting interaction network consists of 3,955 nodes connected with 52,678 edges.

### 3.2.3 Preprocessing and Pattern Discovery

After constructing the network, we calculate the degree for each of the initial disordered genes/proteins, and retain only the nodes that exhibit a relatively higher degree of connectivity, i.e., the so-called *hubs*; specifically, we assemble a set of 43 disordered proteins comprising the top 20 % of the nodes, in terms of degree. The value of 20 % does not pose a “hard” threshold, and has been used elsewhere [19] for the identification of hubs in a protein interaction network. The resulting set of proteins/genes is relatively manageable and all retained hubs exhibit quite high degree of connectivity (i.e. >57 interacting partners) to be considered as hubs. Next, we retrieve from UniProt [14] the sequences that correspond to the interacting partners for each of the 43 proteins under consideration; Table 3.1 contains the names of the retained genes and the respective degree value, i.e., the number of interacting partners.

**Table 3.1** The set of maintained genes and their degree of connectivity

Gene	Degree	Gene	Degree	Gene	Degree	Gene	Degree
MYC	986	NCBP1	169	RPA1	102	HMGA1	70
MAX	950	NCBP2	164	NFKBIA	96	BCL2L1	68
TP53	305	AR	162	CD4	94	VHL	66
GRB2	231	CCNH	147	GSK3B	92	MDM2	64
ESR1	214	HNRNPA1	141	HRAS	90	POU2F1	63
POLRH	208	SHC1	135	PLK1	87	FOS	60
RAC1	206	RAF1	116	BCL2	87	NCOA3	60
EGFR	205	CDKN1A	116	RXRA	82	CTDP1	60
RELA	198	SP1	104	CCNB1	82	SRF	58
SMAD4	184	ETF1	103	ARHGAP1	79	CDKNA	57
BRCA1	178	NR3C1	103	CDKB	78		



Upon each set of interacting partners we perform a series of preprocessing steps: first, we compare sequences to one another, and among the ones that feature more than 25 % sequence identity, we maintain only one representative; thus, we remove any factor (e.g., homology) that would affect the representation of a sequence segment in a biased manner. Next, using Pfilt [20], we remove sequence regions that are unlikely to contain motifs or patterns, but might as well hinder the motif discovery process yielding misleading overrepresentations; such regions are globular domains, transmembrane segments, coiled-coil, and collagen regions [20].

The outcome of the previous step is comprised of 43 “bins,” containing the sequences of the interacting partners for each identified hub, after having been stripped off from all redundant regions that would hinder or bias the next steps of our analysis. According to our initial hypothesis, protein sequences that share a common interacting partner (hub), will also share a small region that mediates interaction and thus allowing for the detection of common features [10]. To this end, we employ the filtered sets of sequences, extracted using the aforementioned analysis, in order to identify protein patterns, in the form of regular expressions, that are overrepresented among the sequences that share a common interacting partner. In the present work, we provide each set of unaligned protein sequences in turn as input to the TEIRESIAS algorithm [21]; during the flow of operation of TEIRESIAS, elementary patterns that exceed a certain support threshold (in our analysis minimum support  $K = 3$ ) are identified and are progressively combined in order to formulate larger and more specific patterns. It should be noted that TEIRESIAS guarantees that all retrieved patterns are maximal, i.e., given a set of threshold and restrictions all conforming patterns have been reported. Specifically, we search for short linear peptide regions spanning from three to eight residues, from which at least three positions need to be occupied by literal characters in order to ensure convergence of the TEIRESIAS algorithm. The reported patterns need to be observed at least three times in the input set (minimum support  $K = 3$ ) and each position may be occupied either from a specific amino acid or the dot (“.”) wild-character which represents any of the 20 standard amino acids.

In the next step, the patterns reported from TEIRESIAS are subject to an evaluation process which is twofold. First, we assess the representation of each pattern in the initial input set, i.e., the number of sequences that actually contain the pattern under consideration; each pattern in order to be maintained must be present in at least 40 % of the initial input set. The threshold is defined as a percentage of the input set, since there are significant perturbations in the number of constituents across the 43 sets. As there is no golden standard, in order to decide upon the representation of a pattern within a set of sequences, the employed threshold has been chosen so that the retained patterns are represented in an adequately large subset of sequences of the input set. Furthermore, we assess the significance of each pattern retrieved from TEIRESIAS by performing a chi-square test (Eq. 3.1),

in order to identify those patterns that are significantly represented in the partners of a certain hub, compared to a control group of random sequences:

$$\chi^2 = \sum_{i=1}^n \frac{(O_i - E_i)^2}{E_i} \quad (3.1)$$

where  $O_i$  and  $E_i$  denote the observed and expected values, respectively, and  $n$  is the number of cells in the contingency table. In order to estimate the expected frequency of observation for each extracted pattern, we have assembled a control set of proteins containing approximately 7,000 proteins sequences, randomly chosen from the Protein Data Bank [22]. All sequences in the control set were subject to the same preprocessing procedure as the initial pool of proteins employed for extracting the patterns. In order to retain the most prominent sequence patterns, we keep only the top scoring ones (i.e., patterns yielding the lowest p-values) but also omit patterns with p-values higher than  $10^{-2}$  [10], thus scrutinizing further the reported patterns.

### 3.2.4 Functional Implications

In the next step of our methodological analysis we compare in turn each retained pattern against a major repository of functionally annotated protein patterns. More specifically, we provide the retained patterns as input to the Comparimotif algorithm [23], in order to search and procure potential functional implications of the extracted patterns by comparing them against the patterns deposited in the ELM repository [24]. ELM is a well-structured and constantly updated repository that contains experimentally validated and annotated protein patterns in terms of four functional classes, namely localization/targeting (TRG), posttranslational modifications (MOD), binding/ligand (LIG), and cleavage (CLV). For each pattern-pattern comparison, Comparimotif calculates a score representing the degree of overlap between the patterns; besides exact matches, Comparimotif can identify a series of relationships between two patterns by employing a sliding window comparison which takes into account and rates all possible overlaps between variants of the patterns under consideration.

## 3.3 Results and Discussion

From the aforementioned methodological analysis, a set of patterns have emerged which mediate interactions of disordered proteins that involve a multitude of different interacting partners. It should be noted that our primary aim is to identify a set of patterns that are overrepresented among the interacting partners of disordered proteins, in a systematic manner, without delving into the cumbersome and normally slow discovery process of linear motif discovery.

### 3.3.1 Patterns

From the extensive list of retrieved patterns we omit the ones that are represented in the input set less than 40 %; moreover, we sort the remaining patterns according to the  $p$ -value returned from the chi-square test and discard patterns yielding a  $p$ -value higher than  $10^{-2}$ . However, for cases that several patterns are maintained even after posing the aforementioned restrictions, we report only the top-five patterns. There are also some cases where none of the retrieved patterns fulfilled those restrictions (e.g., gene ETF1); therefore no patterns are reported as significantly represented.

Table 3.2 contains an indicative list of the most overrepresented patterns yielded after the restrictions. Specifically, the top four hubs are shown along with the respective patterns and their  $p$ -values. The selection was made concerning the patterns' representation percentage observed in the input set of sequences. We only report those patterns that show a representation percentage more than 50 %. The complete list of patterns detected from the TEIRESIAS algorithm as well as specific statistical details such as  $p$ -value and representation percentage, are available in the following URL: <https://sites.google.com/site/disordernet/>.

In the subsequent discussion, all remarks refer to the analysis of the entire list of patterns maintained for each hub, and not to the subset shown in Table 3.2. It is noteworthy that even though we deal with a variety of genes/proteins, we observe that similar patterns have been deduced in their majority, maybe due to their common characteristic which is partial or complete disorder. Overall, we observe that some amino acids clearly stand out among the entire list of patterns, for all hubs. Specifically, leucine (L), serine (S), and glutamic acid (E) appear quite replete in almost all patterns.

Although the extracted patterns are limited in length between three to eight residues in order to detect short linear motifs, there is a clear tendency towards repetitive leucine residues, resembling partially peptide regions of leucine-rich repeats (LRRs) [25]. LRRs are sequence motifs that are primarily involved with protein-protein interactions and have been found to be constituents of recognition

**Table 3.2** Top four hubs with their most overrepresented patterns

Hub	Pattern	$p$ -Value	Re.*(%)	Hub	Pattern	$p$ -Value	Re.*(%)
ARHGAP1	ELL	1.36E-24	79	HRAS	L..L..L	4.05E-16	65
	L.E.L	9.23E-19	79		L..L..L	1.28E-14	61
	E.E..E	4.48E-56	79		L.L..L	2.11E-21	61
	L.L.E	1.07E-25	76		LL..L	3.72E-18	59
	L.EL	1.22E-18	76		L....LL	1.51E-19	57
RAC1	L.L....L	1.17E-34	64	SRF	S..SS	2.54E-26	61
	L.....LL	1.09E-33	64		GS.S	1.48E-24	61
	L..L..L	2.97E-22	61		S.SS	6.50E-24	57
	L..LL	1.10E-24	61		S.S..S	7.18E-29	57
	LL..L	4.64E-25	61		S..SS	2.22E-26	57

and binding peptides. Therefore, the highly reactive nature of disordered proteins, which tend to have multiple interacting partners, is partly attributed to the LRR group comprising a common pattern mediating a series of interactions.

### 3.3.2 Functions

Next, we aim to infer the functional propensities of the extracted patterns. Specifically, we compare the list of patterns extracted for each of the 43 disordered hubs against the ELM repository and calculate the propensities towards each of the four functional classes/groupings considered in ELM, i.e., CLV, LIG, MOD, and TRG. In Fig. 3.2, we present average propensity values of the entire list of extracted patterns towards the ELM functional classes.

Specifically, there is a major thrust towards TRG and LIG functional classes; indeed, the strong association between disordered proteins and functions related to ligand binding and targeting has been well characterized and established. These findings are further verified by our analysis which additionally aims to identify and analyze the specific sequence patterns that mediate those functionalities.

Regarding the MOD class, a slightly decreased yet considerable prevalence is observed in both plots; post-translational modifications have been proven to be strongly correlated with peptide regions where intrinsic disorder is quite abundant. To this end, posttranslational modification sites, besides the grouping in terms of molecular mechanism, are grouped according to their conformational state; specifically, modifications that are primarily associated with disordered regions involve mainly phosphorylation, acetylation, acylation, adenylylation, ADP ribosylation,

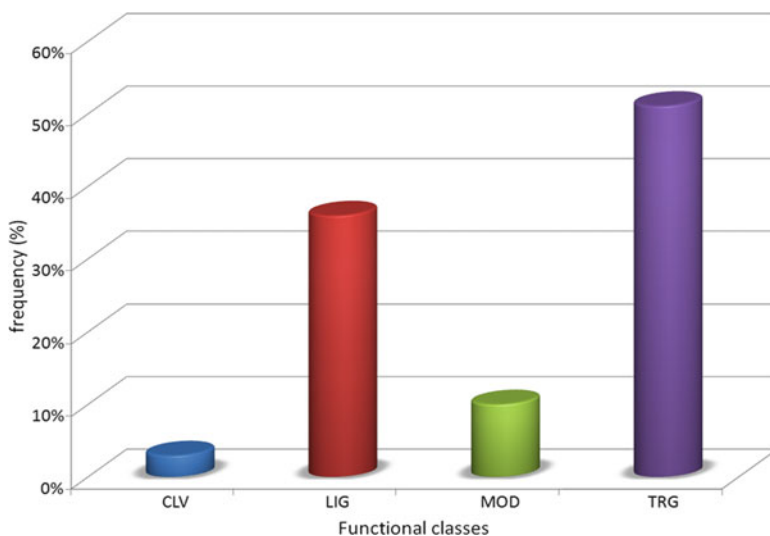


**Fig. 3.2** Functional propensities exhibited by the extracted patterns for all hubs

amidation, carboxylation, formylation, glycosylation, methylation, sulfation, prenylation, ubiquitination, and Ubl-conjugation. Those modifications rely largely on low-affinity, high-specificity interactions between a specific enzyme and a substrate [6]. As for the CLV class, we observe that it is represented to a very limited extent and in several cases not at all; the trivial association with disordered regions, as pinpointed by our methodological analysis is further validated by the literature where no significant relationship has been reported.

### Conclusions

A significant number of cellular processes are dictated by short sequence segments, which have been proven to reside quite frequently in disordered regions of proteins. In this work we propose a methodological analysis for the identification of such patterns by utilizing information from interaction networks, thus, avoiding the normally slow and demanding discovery process. Specifically, we discover sequence patterns that mediate interaction between a single disordered protein and a set of different partners. The extracted patterns exhibit a striking preference towards residues leucine, glutamic acid and serine, as well as alanine and glycine, however, to a far lesser extent. It is noteworthy that the patterns are mostly comprised by exclusive repeats of a single residue or from a couple of residues at most, rather than forming more complex patterns. Those patterns can serve as a reference point for experimental studies in order to verify their potential role in the interaction and functioning of the disordered protein, as well as their specific implication in the induction of diseases where disorder is abundant.

### References

1. Uversky VN (2013) Intrinsic disorder-based protein interactions and their modulator. *Curr Pharm Des* 19(23):4191–4213
2. Dunker AK, Silman I, Uversky VN, Sussman JL (2008) Function and structure of inherently disordered proteins. *Curr Opin Struct Biol* 18(6):756–764
3. Radivojac P, Iakoucheva LM, Oldfield CJ, Obradovic Z, Uversky VN, Dunker AK (2007) Intrinsic disorder and functional proteomics. *Biophys J* 92:1439–1564
4. Uversky VN (2013) A decade and a half of protein intrinsic disorder: biology still waits for physics. *Protein Sci* 22(6):693–724
5. Cozzetto D, Jones DT (2013) The contribution of intrinsic disorder prediction to the elucidation of protein function. *Curr Opin Struct Biol* 23(3):467–472
6. Gao J, Xu D (2012) Correlation between posttranslational modification and intrinsic disorder in protein. *Pac Symp Biocomput*:94–103
7. Moreno-Gonzalez I, Soto C (2011) Misfolded protein aggregates: mechanisms, structures and potential for disease transmission. *Semin Cell Dev Biol* 22(5):482–487
8. Midic U, Oldfield CJ, Dunker AK, Obradovic Z, Uversky VN (2009) Protein disorder in the human diseasome: unfoldomics of human genetic diseases. *BMC Genomics* 10(Suppl 1):S12
9. Uversky VN (2009) Intrinsic disorder in proteins associated with neurodegenerative diseases. *Front Biosci* 14:5188–5238

10. Neduva V, Linding R, Su-Angrand I, Stark A, de Masi F, Gibson TJ, Lewis J, Serrano L, Russell RB (2005) Systematic discovery of new recognition peptides mediating protein interaction networks. *PLoS Biol* 3:e405.18
11. Xue B, Hsu WL, Lee JH, Lu H, Dunker AK, Uversky VN (2010) SPA: short peptide analyzer of intrinsic disorder status of short peptides. *Genes Cells* 15:635–646
12. Davey NE, Van Roey K, Weatheritt RJ, Toedt G, Uyar B, Altenberg B, Budd A, Diella F, Dinkel H, Gibson TJ (2012) Attributes of short linear motifs. *Mol Biosyst* 8(1):268–281
13. Sickmeier M, Hamilton JA, LeGall T, Vacic V, Cortese MS, Tantos A, Szabo B, Tompa P, Chen J, Uversky VN, Obradovic Z, Dunker AK (2007) DisProt: the database of disordered proteins. *Nucleic Acids Res* 35:D786–D793
14. UniProt Consortium (2014) Activities at the Universal Protein Resource (UniProt). *Nucleic Acids Res* 42(1):D191–D198
15. Tarcea VG, Weymouth T, Ade A, Bookvich A, Gao J, Mahavisno V, Wright Z, Chapman A, Jayapandian M, Ozgur A, Tian Y, Cavalcoli J, Mirel B, Patel J, Radev D, Athey B, States D, Jagadish HV (2009) Michigan molecular interactions r2: from interacting proteins to pathways. *Nucleic Acids Res* 37:D642–D646
16. Prasad TS, Kandasamy K, Pandey A (2009) Human Protein Reference Database and Human Proteinpedia as discovery tools for systems biology. *Methods Mol Biol* 577:67–79
17. Aranda B, Achuthan P, Alam-Farouque Y, Armean I, Bridge A, Derow C, Feuermann M, Ghanbarian AT, Kerrien S, Khadake J, Kerssemakers J, Leroy C, Menden M, Michaut M, Montecchi-Palazzi L, Neuhauser SN, Orchard S, Perreau V, Roechert B, van Eijk K, Hermjakob H (2010) The IntAct molecular interaction database in 2010. *Nucleic Acids Res* 38:D525–D531
18. Han JD, Bertin N, Hao T, Goldberg DS, Berriz GF, Zhang LV, Dupuy D, Walhout AJ, Cusick ME, Roth FP, Vidal M (2004) Evidence for dynamically organized modularity in the yeast protein-protein interaction network. *Nature* 430:88–93.19
19. Zotenko E, Mestre J, O’Leary DP, Przytycka TM (2008) Why do hubs in the yeast protein interaction network tend to be essential: reexamining the connection between the network topology and essentiality. *PLoS Comput Biol* 4:e1000140
20. Jones DT, Swindells MB (2002) Getting the most from PSI-BLAST. *Trends Biochem Sci* 27:161–164
21. Rigoutsos I, Floratos A (1998) Combinatorial pattern discovery in biological sequences: the TEIRESIAS algorithm. *Bioinformatics* 14:55–67
22. Rose PW, Bi C, Bluhm WF, Christie CH, Dimitropoulos D, Dutta S, Green RK, Goodsell DS, Prlic A, Quesada M, Quinn GB, Ramos AG, Westbrook JD, Young J, Zardecki C, Berman HM, Bourne PE (2013) The RCSB Protein Data Bank: new resources for research and education. *Nucleic Acids Res* 41:D475–D482
23. Edwards RJ, Davey NE, Shields DC (2008) CompariMotif: quick and easy comparisons of sequence motifs. *Bioinformatics* 24:1307–1309
24. Dinkel H, Van Roey K, Michael S, Davey NE, Weatheritt RJ, Born D, Speck T, Kruger D, Grebnev G, Kuban M, Strumillo M, Uyar B, Budd A, Altenberg B, Seiler M, Chemes LB, Glavina J, Sanchez IE, Diella F, Gibson TJ (2014) The eukaryotic linear motif resource ELM: 10 years and counting. *Nucleic Acids Res* 42(1):D259–D266
25. Bella J, Hindle KL, McEwan PA, Lovell SC (2008) The leucine-rich repeat structure. *Cell Mol Life Sci* 65:2307–2333

## Chapter 4

# Management and Modeling of Balance Disorders Using Decision Support Systems: The EMBALANCE Project

**Themis P. Exarchos, Christos Bellos, Iliana Bakola, Dimitris Kikidis, Athanasios Bibas, Dimitrios Koutsouris, and Dimitrios I. Fotiadis**

**Abstract** In this work, we present the concept, the methodological ideas and the architecture of the EMBALANCE platform. EMBALANCE platform extends existing but generic and currently uncoupled balance modeling activities, leading to a multi-scale and patient-specific balance Hypermodel, which is incorporated to a Decision Support System (DSS), towards the early diagnosis, prediction and the efficient treatment planning of balance disorders. Various data feed the intelligent system increasing the dimensionality and personalization of the system. Human Computer Interaction techniques are utilized in order to develop the required interfaces in a user-intuitive and efficient way, while interoperable web services enhance the accessibility and acceptance of the system. The platform will be validated using both retrospective as well as prospective experimental and clinical data. The final tool will be a powerful web-based platform provided to primary and secondary care physicians across specialties, levels of training and geographical boundaries, targeting wider clinical acceptance as well as the increased confidence in the developed DSS towards the early diagnostic evaluation, behaviour prediction and effective management planning of balance problems. Currently we focus and present the management and modeling of the balance disorders.

**Keywords** Balance disorders • Decision support system • Multi-scale modeling

---

T.P. Exarchos • C. Bellos • D. Koutsouris

Institute of Communication and Computer Systems, National Technical University of Athens, Athens, Greece

e-mail: [Themis.exarchos@gmail.com](mailto:Themis.exarchos@gmail.com); [cbellos@biosim.ntua.gr](mailto:cbellos@biosim.ntua.gr); [dkoutsou@biomed.ntua.gr](mailto:dkoutsou@biomed.ntua.gr)

I. Bakola • D.I. Fotiadis (✉)

Unit of Medical Technology and Intelligent Information Systems, Department of Computer Science, University of Ioannina, Ioannina, Greece

e-mail: [iliana\\_bakola@hotmail.co.uk](mailto:iliana_bakola@hotmail.co.uk); [Fotiadis@cc.uoi.gr](mailto:Fotiadis@cc.uoi.gr)

D. Kikidis • A. Bibas

1st University Department of Otolaryngology, National and Kapodistrian University of Athens, Athens, Greece

e-mail: [dimitriskikidis@yahoo.com](mailto:dimitriskikidis@yahoo.com); [thanosbibas@hotmail.com](mailto:thanosbibas@hotmail.com)

## 4.1 Introduction

Human balance is achieved and maintained by a complex set of sensorimotor systems that include sensory input from vision, proprioception and the vestibular system (motion, equilibrium, spatial orientation); integration of the sensory input and motor output to the muscles of the eye and body. Failure at the level of the sensory inputs or at the integration of the sensory information by the central nervous system may lead to a variety of age spanning diseases which affect balance. This complexity leads to undiagnosed or under-treated patients with balance disorders for long periods and results in large socio-economic costs.

Postural balance is achieved through the integration of visual, vestibular and somatosensory systems, which detect balance deviations, and the generation of corrective motor output through the muscles. According to numerous research articles, the visual system is the primary sensory system used to maintain upright postural control [1–3]. The vestibular system interacts with the proprioceptive system coupled with corollary discharge of a motor plan, allowing the brain to distinguish active from passive head movements [4]. In addition, both visual and proprioceptive systems interact with the vestibular system throughout the central vestibular pathways and are essential for gaze and postural control. The somatosensory system contributes to maintain normal quiet stance and to safely accomplish the majority of activities of daily living.

Currently, there are a few proposed models for human postural balance [5–7], in the scientific literature, combining state feedback control with optimal state estimation. State estimation uses an internal model of body and sensor dynamics to process sensor information and determine body orientation, taking into account the (assumed) uncertainty of the several sensory modalities. Three sensory modalities are usually modelled in [8]: joint proprioception, vestibular organs in the inner ear and vision. The resulting model may be useful for predicting which sensors are most critical for balance, and how much they can deteriorate before posture becomes unstable. Nevertheless, currently existing models of balance are too generic, while the complexity of the balance system calls for both multi-scale modeling and personalized models.

The innovation of the EMBalance DSS is multi-level and the final integrated solution goes beyond state of the art of existing Clinical DSS tools and services, by addressing the following issues:

1. The EMBalance DSS can provide support to clinicians at various stages in the care process, from the early diagnosis of the balance disorders to monitoring, evaluation and prevention of the balance disorders behaviour evolution as well as to follow-up activities, treatment planning and effective management.
2. Publishing the DSS to the web and developing web services to interact with the system and access the generated decision and feedback. Such web-services enhance the accessibility and re-usability of the system by providing: (1) use in rural/smaller/primary care healthcare units; (2) elimination of unnecessary referrals to distant centres of excellence, but also assurance that patients who



- need these referrals will receive them; (3) distance-collaboration of clinicians for better diagnosis; (4) equal access to expert healthcare of the whole population; (5) a common universal database; (6) secure user authentication with different access levels depending on the role of the users and (7) universal standardized data collection for research.
3. The EMBalance introduces the next generation of clinical DSS systems, which will become even more sophisticated when the required expertise is incorporated as part of the system's functionality. This expert would consult with the user to provide an effective and customized use of operations according to the user's specific context information. This would provide an opportunity for the user to employ an expert software agent for managing web assets and performing the desired tasks with minimum effort and time.
  4. Address security and privacy issues that are crucial in dealing with sensitive personal data. Healthcare systems that operate with sensitive clinical data require particular attention and procedures to ensure authorized access in order to prevent privacy and security breaches of clinical data residing in the CDSS. There has been a dramatic increase in reports of security breaches. In particular, since most healthcare systems (including CDSS) are web and service based (e.g. Mashups), preserving the integrity, security and privacy of patient data has utmost importance. Therefore, a research challenge is to target security and privacy issues.

## 4.2 Methodology

### 4.2.1 Description of the Methodology

Upright stance and locomotion are subject to many disturbances, including gravity, Coriolis and centrifugal forces, the body's own inertia, pushes and pulls exerted from the outside and motion of the support surface. In view of all these hazards, one might assume that postural control must be very complicated.

The EMBALANCE hypermodel extends and personalizes existing models by the multi-scale modeling of the three sensory systems/factors of balance (i.e. visual, vestibular and joint proprioceptive) that will be simulated, incorporating to the analysis various physiologic and pathologic data. The different inputs of the EMBALANCE hypermodel are shown in Fig. 4.1. The developed hypermodel is used as input to the Decision Support System, which provides a useful tool to the balance and human posture experts.

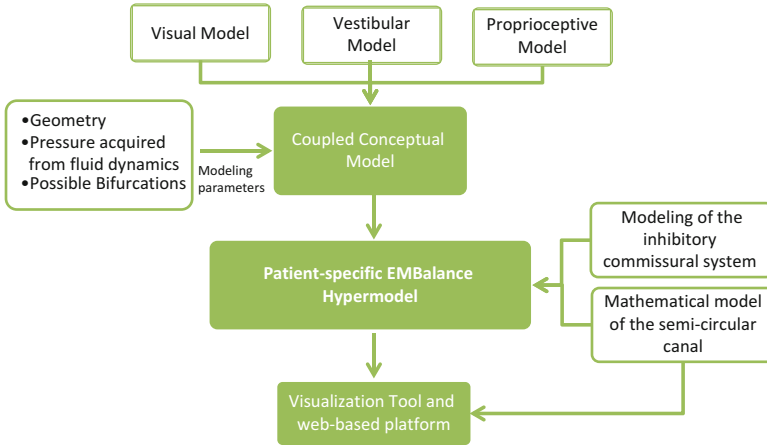


**Fig. 4.1** The input data of the EMBALANCE hypermodel

### 4.2.2 Multi-dimensionality of the Input Feature Vector

Various quantitative and qualitative data are taken under consideration to assist the clinician's diagnosis and decision on appropriate treatment. In addition, the parameters acquired from the EMBalance Hypermodel, the conceptual model of the inhibitory commissural system and the mathematical model of the semi-circular canals (i.e. geometry malfunctions, pressure acquired from fluid dynamics, possible bifurcations) are fused with existing data and indicative parameters provided by the clinicians, to form the Feature Input Vector of the DSS. The features will be annotated in time and the input vector will be accompanied by multi-annotations provided by clinicians that are characterizing the instances of existing data (i.e. normal, ear problem, severe neurological problem).

Moreover, it should be noted that these crucial factors will be recorded under various different conditions increasing the dimensionality of the data. This heterogeneity of the input parameters increases the complexity of the data mining problem and leads to the necessity of the decision support system.

### 4.2.3 Decision Support System Intelligence Core Engine

As being depicted in Fig. 4.2, after forming the Feature Input Vector, annotating each instance with clinicians' assessment and performing secondary but crucial functionalities (i.e. missing values replacement, error probability, sensitivity analysis, feature selection), the DSS is triggered. Several different classification schemes will be studied and a sophisticated system will be developed, incorporating

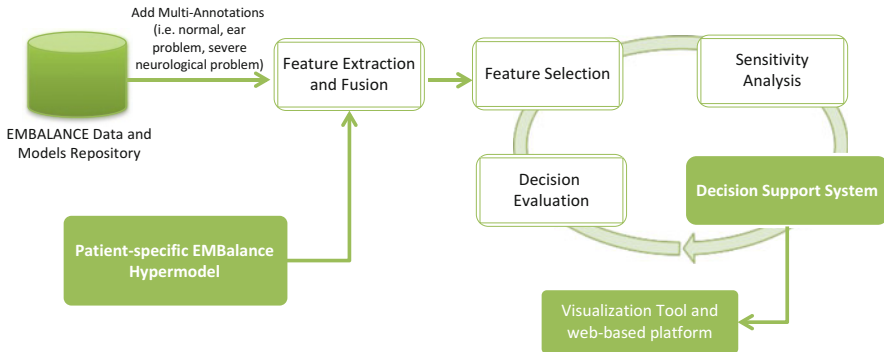


**Fig. 4.2** High-level architecture of the decision support system

intelligent algorithms, to address the multi-factorial problem. The decisions that can be formulated by the DSS are four age-spanning related decisions.

- (a) **Examinations Recommendation:** Towards this outcome, an avatar and the necessary tools of the DSS will be developed in order to guide the clinicians to perform the right tests/assessments.
- (b) **Early Diagnosis of Balance Disorders:** Quantification and weighting of the contribution of the individual system's input pathology for the observed impairment (i.e. visual problem, malfunction of the semicircular canal), and the combination of deficits and impairments in light or current scientific knowledge (literature reviews) will guide the development and further research activities undertaken in order to provide a diagnostic decision of balance disorders to clinicians users.
- (c) **Prediction of Balance Disorders Behaviour:** Range and duration of symptoms can be predicted according to patterns that DSS will process and provide. This can guide on possible referral to other specialties or need for rehabilitation as well as to a potential need for an excellence centre.
- (d) **Treatment Planning:** Efficient treatment planning is achieved at multiple levels (i.e. Medication, Psychological, Rehabilitation and Additional Measures).

#### **4.2.4 Patient-Specific Feedback Engine**

The final decision for patients of all adult ages will be provided as a feedback to the clinicians, closing the loop and assisting the healthcare professionals on diagnosing any possible balance disorders on their patients, assessing their patients' balance disorders status and evolution, planning efficient treatment and management. Furthermore, the DSS will be utilized as a training and educational tool, by selecting some appropriate and representative case studies, for medical students and residents

alike to consolidate their knowledge and clinical skills on the management of vestibular disorders.

### 4.2.5 Web Service Interfaces and Access Engine

It should be noted that the DSS will be structured and developed using an open architecture, addressing a three-layer design that is required to incorporate new follow-up data and predict the behaviour of the human posture and the evolution of the related impairments. The Rich Internet Applications and web services as well as the adoption of standards to encode healthcare data (i.e. Clinical Data Architecture) and knowledge (i.e. Predictive Model Markup Language) will be developed.

## 4.3 Validation Plan

A careful and detailed plan has been defined for the validation of the EMBALANCE platform. The validation includes three phases, as shown also in Fig. 4.3: (1) the clinical validation cycle, (2) the clinical trials cycle and (3) the proof of concept and clinical evaluation.

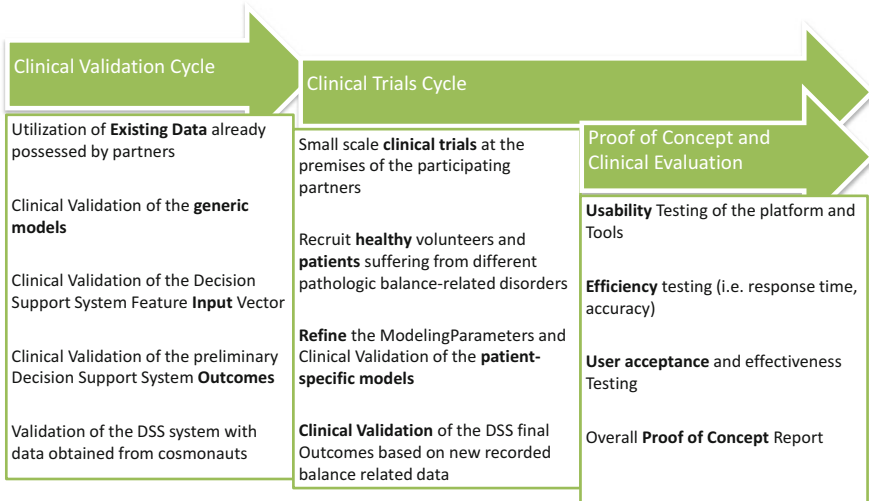


**Fig. 4.3** The three phases of the EMBALANCE planned validation

### Conclusions

Several statistics show the high incidence of balance disorders. A majority of individuals over 70 years of age report problems of dizziness and imbalance, and balance-related falls account for more than one-half of the accidental deaths in the elderly (the American National Institute of Health Statistics). Furthermore, in a sample of persons age 65–75, one-third reported that dizziness and imbalance degraded the quality of their lives, while 40 % of the population over age 40 will experience a dizziness disorder in their lifetime. Also, this impairment is prevalent across life time enhancing the complexity of the required solutions to be patient and age specific. EMBALANCE platform targets the early and accurate diagnosis and prediction of the complex balance disorders as well as the efficient, multifactorial and personalized treatment planning, proving major impact in the patients, the caregivers, the society and the healthcare system.

**Acknowledgments** This research is partly funded by the European Commission as part of the project EMBALANCE “A Decision Support System incorporating a validated patient-specific, multi-scale Balance Hypermodel towards early diagnostic Evaluation and efficient Management plan formulation of Balance Disorders” (Grant Agreement no 610454).

### References

1. Campbell AM, Heyer LJ (2007) *Discovering genomics, proteomics and bioinformatics*. Benjamin Cummings, San Francisco, CA
2. Kapoula Z, Le T (2006) Effects of distance and gaze position on postural stability in young and old subjects. *Exp Brain Res* 173:438–445. doi:[10.1007/s00221-006-0382-1](https://doi.org/10.1007/s00221-006-0382-1)
3. Shaffer S, Harrison A (2007) Aging of the somatosensory system: a translation perspective. *Phys Ther* 87(2):194–207
3. Uchiyama M, Demura S (2009) The role of eye movement in upright postural control. *Sport Sci Health* 5:21–27. doi:[10.1007/s11332-009-0072-z](https://doi.org/10.1007/s11332-009-0072-z)
4. Angelaki D, Cullen K (2008) Vestibular system: the many facets of a multimodal sense. *Annu Rev Neurosci* 31:125–150. doi:[10.1146/annurev.neuro.31.060407.125555](https://doi.org/10.1146/annurev.neuro.31.060407.125555)
5. Mergner T, Schweigart G, Fennell L, Maurer C (2009) Posture control in vestibular loss patients. *Ann N Y Acad Sci* 1164:206–215
6. Maurer C, Mergner T, Peterka RJ (2006) Multisensory control of human upright stance. *Exp Brain Res* 171:231–250
7. van der Kooij H, de Vlugt E (2007) Postural responses evoked by platform perturbations are dominated by continuous feedback. *J Neurophysiol* 98:730–743
8. Kuo AD (2005) An optimal state estimation model of sensory integration in human postural balance. *J Neural Eng* 2(3):S235–S249, Epub 2005 Aug 31

## Chapter 5

# A Computer-Aided Diagnosis System for Geriatrics Assessment and Frailty Evaluation

Charalampos Vairaktarakis, Vasilis Tsiamis, Georgia Soursou, Filippos Lekkas, Markella Nikolopoulou, Emmanouilia Vasileiadou, Konstantinos Premtsis, and Athanasios Alexiou

*“the sixth age shifts into the lean and slipper’d pantaloon,  
with spectacles on nose and pouch on side, his youthful hose  
well sav’d, a world too wide, for his shrunk shank . . .”*

—Shakespeare in As You Like It

**Abstract** It is a common knowledge that frailty is a condition associated with getting older, and it has been considered as highly prevalent as far as falls, disability, hospitalization, and mortality are concerned. At the present time a standardized definition has not yet been established. With that in mind and for frailty being of a vital importance as a term identifying geriatric symptoms, we pursued to embody the well-known 70-scale CSHA Frailty index of the Canadian Study of Health and Aging in a Clinical Decision Support System, after categorizing and expanding it. The proposed categorization in this chapter can be helpful for usage by patients and their relatives, care givers, and medical doctors.

**Keywords** Frailty • Elderly • Geriatric clinical medicine • Clinical decision support system • Computer-aided diagnosis program

---

C. Vairaktarakis (✉) • V. Tsiamis • G. Soursou • F. Lekkas • M. Nikolopoulou  
E. Vasileiadou • K. Premtsis  
Department of Computer Sciences and Biomedical Informatics, University of Thessaly,  
Papasiopoulou 2-4, 53100 Lamia, Greece  
e-mail: [cvairakt@dib.uth.gr](mailto:cvairakt@dib.uth.gr); [vtsiamis@dib.uth.gr](mailto:vtsiamis@dib.uth.gr); [gsoursou@dib.uth.gr](mailto:gsoursou@dib.uth.gr); [flekkas@dib.uth.gr](mailto:flekkas@dib.uth.gr);  
[mnikolop@dib.uth.gr](mailto:mnikolop@dib.uth.gr); [evasilei@dib.uth.gr](mailto:evasilei@dib.uth.gr); [kpremtsi@dib.uth.g](mailto:kpremtsi@dib.uth.g)

A. Alexiou  
Department of Informatics, Ionian University, Plateia Tsirigoti 7, 49100 Corfu, Greece  
e-mail: [alexiou@ionio.gr](mailto:alexiou@ionio.gr)

## 5.1 Introduction

Frailty is a common geriatric syndrome that embodies an elevated risk of catastrophic declines in health and function among elderly people. As our population ages, a central focus of geriatricians and public health practitioners is to understand, and then beneficially intervene on, the factors and processes that put elders in the community at such risk, in particular the increased vulnerability to stressors that characterizes many older adults. Worldwide, at least 35.6 million people have various geriatric symptoms, with just over half (58 %) living in low- and middle-income countries. Every year there are 7.7 million new cases. The estimated proportion of the general population aged 60 and over with geriatric symptoms, centralized by their frailty condition at a given time, is between 2 and 8 per 100 people. The total number of people with geriatric symptoms is projected to almost double every 20 years to 65.7 million in 2030 and 115.4 million in 2050 [1]. Much of this increase is attributable to the fact of the rising numbers of elderly people among the world. Thus, the need for their cure and care is of a highly concern. With no corresponding Clinical Decision Support System (CDSS) in geriatric's discipline, we find it crucial to develop a CDSS to help those in need. A CDSS is a Computer-Aided Diagnosis (CAD) program application that analyzes clinical data and presents it so that users can make clinical decisions more easily. CDSS is interactive decision support computer software, which is designed to assist physicians and other health professionals with decision making tasks, such as determining diagnosis of a patient's data. Physicians, nurses, and other health care professionals can use a CDSS to prepare a diagnosis and to review the diagnosis as a mean of improving the final result. Data mining may be conducted to examine the patient's medical history in conjunction with relevant clinical research. Considering that, the widespread usage of CDSS is already registered [2] and is being used as a means to improve health care and well-being. In this chapter, we extended the well-known 70-scale CSHA Frailty index of the Canadian Study of Health and Aging [3] and formulate a 7-category of elderly geriatric characterization and assessment (7-CoEGCA), in order to evaluate and integrate future clinical studies and identify new biomarkers and correlations, through an intelligent web-based system. Moreover, a website which embodies the 7-COEGCA symptoms and simultaneously considers the patient's risk factors, so as to make the diagnosis more reliable and valid, is under development by our team. Both the website and this new classification of frailty symptoms, which characterize the CDSS as analyzed below, could aid the activity of patients, care givers, medical doctors, and geriatricians in general.

## 5.2 Methods and Materials

### 5.2.1 Frailty 7-CoEGCA Symptoms Analysis

As we have already mentioned, frailty has a biologic basis and is a distinct clinical syndrome. More specifically, estimates of frailty prevalence in older populations may vary according to a number of factors. By taken into consideration some of the latest researches on geriatric medicine and frailty [3–6], we present elderly health as a 7-subsystem living organism according to the following hierarchy (Fig. 5.1):

This hierarchy shows the factors that emerge from elderly health. We classified them from psychological, behavioral, and daily functions to genetic, environmental, cardiovascular, and aging, as well as comorbidities, and neurodegeneration ones.

### 5.2.2 A New CDSS Framework

These entries of the general structure are the seven categories that we propose while disjointing the already expanded 70-scale CSHA Frailty index of the Canadian Study of Health and Aging. The following figure is a sample of the way we analyzed the 7-CoEGCA (Table 5.1). Indicatively, level I factors are analyzed in several symptoms (level II) in order to define the CDSS. For example, a set of factors that we took into consideration, as depicted in the above table is the genetic one. A genetic symptom could be derived from the background of one's family. Particularly, we considered the family's history for degenerative, malignant diseases, and relevant to cognitive impairment or loss. All the above can assist to define the genetic impairments of an older person. Additionally, for what concerns the categorization of cardiovascular diseases having in mind the [7], we basically combined every heart disease from the already expanded 70-scale CSHA Frailty index considering two standpoints. The first one affects heart diseases that are mainly caused due to the buildup of a substance called plaque in the wall of the arteries just like myocardial infarction. On the other hand, the second standpoint, derived from the heart's incompetence of not pumping enough blood through to meet the body's needs for blood and oxygen. Last but not least, the neurodegeneration term refers to the progressive loss of function or structure of



Fig. 5.1 The general structure of the proposed categorization



**Table 5.1** The general structure of the analyzed 7-CoEGCA

Categories—Level I	Symptoms—Level II
Psychological, behavioral, and daily functions	Changes in everyday activities
	Clouding or delirium
	Depression
	Feeling sad, blue, depressed
	Mood problems
	Paranoid features
	Restlessness
	Sleep changes
Genetic	Family history of degenerative disease.
	Family history relevant to cognitive impairment or loss.
	Malignant diseases.
Environmental	Gastrointestinal or abdominal problems due to nutrition or medicines
	Lung problems
	Malignant disease
	Respiratory problems
	Skin problems due to living conditions
Cardiovascular disease	Myocardial infarction
	Arrhythmia
	Arterial hypertension
Aging	Head and neck problems
	Skin problems
	Tiredness all the time
	Urinate incontinence
Comorbidities	Abdominal problems
	Other medical history
	Skin problems due to pathological reasons
Neurodegeneration	Memory changes
	Tremor at rest
	Onset of cognitive symptoms
	Irregular gait patterns
	Seizures

neurons, including neuronal death and is related to a big group of disorders and diseases. Neurodegeneration diseases can be classified according to their causes. Several diseases are caused by genetic mutation, others by protein misfolding which leads to abnormal intracellular functions and mechanisms.

More detailed, diseases caused by protein misfolding are called proteopathies. Each proteopathy can be classified according to the protein that is being misfolded to tauopathies (for example Alzheimer disease) and synucleinopathies (for example Parkinson disorder) [8]. It is commonplace that more and more neurodegeneration

diseases tend to appear in elderly people, and while elderly population is increasing, care givers, medical doctors, and geriatricians in general are assigned to provide medical care for them, with increasing frequency. According to the symptoms of neurodegeneration diseases [8–19], we classified them into two categories, the general mental function symptoms and the general impaired mobility symptoms. As a result of our research, among the symptoms of the expanded 70-scale CSHA Frailty index, in the first neurodegenerative category we classified symptoms such as memory changes and onset of cognitive symptoms, while in the second one we classified symptoms such as tremor at rest and irregular gait patterns. Seizures have mixed symptoms in both categories.

### ***5.2.3 The 7-CoEGCA and a User-Friendly Interface***

A website is under development and testing by our team. Here are some technical characteristics. As far as tools are concerned, the site was developed in the web developing language HTML. All the distinguished pages were in the form of PHP files for better connectivity between them. The language PHP was also utilized to include functions in the site in order to calculate a frailty score. The formatting and styling of the site was implemented with CSS. JavaScript was also utilized in order to make some of the functional parts of the site such as the navigation bar. Furthermore, bootstrap contributed to make the site responsive for all web platforms and screen resolutions.

As far as operation is concerned, in the index page we can see the general information for the project and the team. Using the button labeled “Start the questionnaire” the user is transferred to a page with an initial set of questions to establish his medical history (Fig. 5.2). As a final question the user is being asked whether he/she wants to store his/her data anonymously, for research purposes only, or not. After pressing the “Submit” button he/she is transferred to a list of questionnaires that can be taken in order to calculate the frailty score (Figs. 5.3, 5.4, 5.5, and 5.6). For each completed test, a result is produced and presented to the user in a new page giving him/her also the opportunity to return to the list of questionnaires and take another one.

## **5.3 Result and Discussion**

Undoubtedly, frailty is a term that is hard to define. As population ages, the former plays a significant role in elderly people as a term identifying geriatric symptoms. Overall, there is an outstanding amount of data for geriatric symptoms which makes it challenging to categorize them. We postulate that the already expanded 70-scale Canadian research could face a further extension. As a result, our 7-CoEGCA could also be expanded to 8, 9 or more categories. Future work in our interface also needs

Geriatrics Measurements Project [Home](#) [Features](#) [Contact Us](#) [Frailty Hierarchy](#) [Frailty Questionnaire](#)

## Patient health record and history

All fields marked with an asterisk (\*) are required.

### Health History Record

#### Personal Physiological Characteristics

**First Name**  
 (max 30 characters a-z and A-Z)

**Last Name**  
 (max 30 characters a-z and A-Z)

**Gender\***  
 Male  
 Female

**Age\***  
 (For the algorithm to give accurate results the age should be greater than 60)

#### Diseases\* History

**Input\***  
  (browse computer)

**Fig. 5.2** The user is prompted to complete his/her health record history including Pathophysiological Biomarkers, Electrophysiology Measurements, and Heavy Metals Measurements

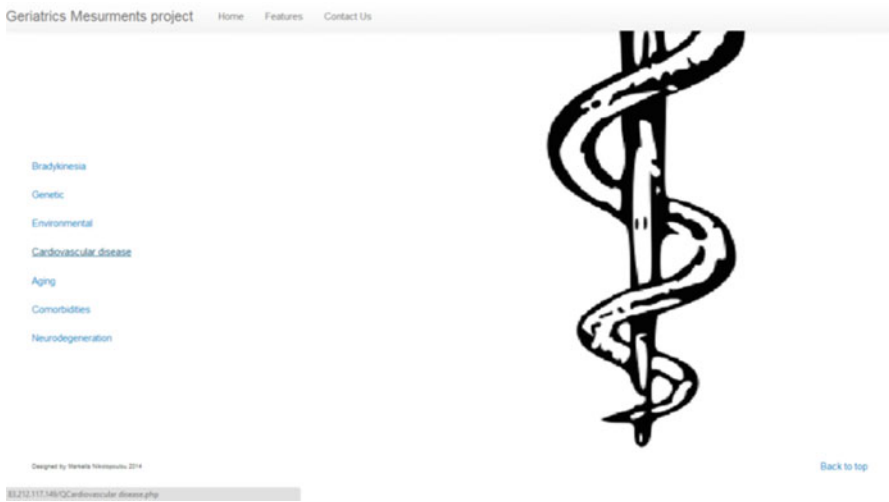


**Fig. 5.3** The user is choosing to complete the Cardiovascular Disease questionnaire

to be done. In the next update of the web platform of this project the user will be able to create an account in order to see past results and compare them with the new ones. Thus, the user interface will become more user friendly. Additionally, the algorithms calculating the frailty score will be improved in order to achieve more reliable and according to new clinical studies scorings. Finally, geriatricians will be able to create an account and manage their patient's scores. As an ultimate perspective, the proposed CDSS in this chapter, which consists of both the

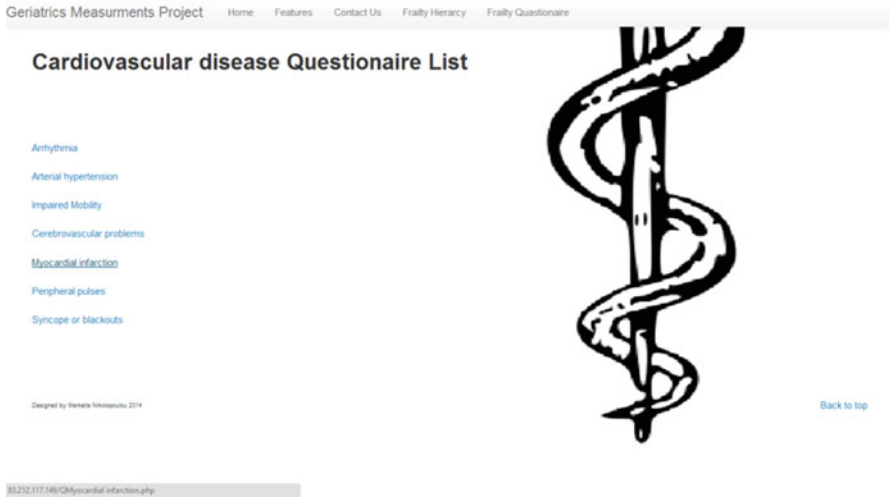


Fig. 5.4 The user is choosing Myocardial Infarction category



Fig. 5.5 The user fills in the various symptoms of the desired category and then he/she can press the submit button at the bottom of the web page. Subsequently, a frailty score is being calculated

7-CoEGCA and the website, is an attempt to present those geriatric symptoms in a simple and understandable way to patients, care givers, and medical doctors and to users regardless of specialty and knowledge so as to help those in need.

Geriatrics Measurements Project   Home   Features   Contact Us   Frailty Hierarchy   Frailty Questionnaire

## Your Myocardial infarction Geriatrics Score is:4/7

### Cardiovascular disease Questionnaire

All fields marked with an asterisk (\*) are required.

**Chest Pain\***

Yes  
 No

**Sorries of Beath\***

Yes  
 No

**Sweating\***

Yes  
 No


**Nausia\***

Yes  
 No

**Vomiting\***

Yes  
 No

**Abnormal Heartbeat\***



**Fig. 5.6** In this figure the user can see the frailty score for the Myocardial Infarction category at the top of his/her screen

## References

1. World Health Organization. <http://www.who.int/en/>
2. EU horizon 2020. <http://ec.europa.eu/programmes/horizon2020/>
3. Espinoza S, Walston JD (2005) Frailty in older adults: insights and interventions. *Cleve Clin J Med* 72(12):1105–1112
4. Rockwood K, Andrew M, Mitnitski A (2007) A comparison of two approaches to measuring frailty in elderly people. *J Gerontol A Biol Sci Med Sci* 62(7):738–743
5. Bowen ME (2012) The relationship between body weight, frailty, and the disablement process. *J Gerontol Ser B Psychol Sci Soc Sci* 67(5):618–626. doi:10.1093/geronb/gbs067
6. Rockwood K, Song X, MacKnight C, Bergman H, Hogan DB, McDowell I, Mitnitski A (2005) A global clinical measure of fitness and frailty in elderly people. *CMAJ* 173(5):489–495
7. American Heart Association. <http://www.heart.org>
8. Taoka T (2013) In Guglielmi G, Peh WCG, Guermazi A (eds) *Geriatric imaging*, Chapter 25. Springer, Berlin. pp 676–706. ISBN 978-3-642-35578-3
9. Riddle DR (ed) (2007) *Brain aging: Models, Methods, and Mechanisms*. CRC Press, Boca Raton, FL, Chapter 1
10. Fillit HM, Rockwood K, Woodhouse K (ed) (2010) *Brocklehurst's textbook of geriatric medicine and gerontology*, 7th edn. Saunders Elsevier, p 172
11. The Epilepsy Foundation of America (Epilepsy therapy project). <http://www.epilepsy.com/>
12. Owen G, Mulley GP (2002) The Palmomenttal reflex: a useful clinical sign? *J Neurol Neurosurg Psychiatry* 73:113–115. doi:10.1136/jnnp.73.2.113
13. Judge JO (2013) *The Merck manual*. Health care professional, geriatrics, gaint disorders in the elderly. [http://www.merckmanuals.com/professional/geriatrics/gaint\\_disorders\\_in\\_the\\_elderly](http://www.merckmanuals.com/professional/geriatrics/gaint_disorders_in_the_elderly)
14. Elble RJ, Thomas SS, Higgins C, Colliver J (1991) Stride-dependent changes in gait of older people. *J Neurol* 238(1):1–5
15. Petersen RC (2004) Mild cognitive impairment as a diagnostic entity. *J Intern Med* 256(3):183–194

16. Wickrematatchi MM, Llewelyn JG (2006) Effects of ageing on touch. *Postgrad Med J* 82 (967):301–304
17. Grimaldi G, Manto M (2008) Tremor: from pathogenesis to treatment. Morgan and Claypool publishers, San Rafael, pp 42–44
18. Manto M (2008) Tremorgenesis: a new conceptual scheme using reciprocally innervated of neurons. *J Transl Med* 6:71
19. Schott JM, Rossor MN (2003) The grasp and other primitive reflexes. *J Neurol Neurosurg Psychiatry* 74:558–560

# Chapter 6

## Exploiting Expert Systems in Cardiology: A Comparative Study

**George-Peter K. Economou, Efrosini Sourla,  
Konstantina-Maria Stamatopoulou, Vasileios Syrimpeis,  
Spyros Sioutas, Athanasios Tsakalidis, and Giannis Tzimas**

**Abstract** An improved Adaptive Neuro-Fuzzy Inference System (ANFIS) in the field of critical cardiovascular diseases is presented. The system stems from an earlier application based only on a Sugeno-type Fuzzy Expert System (FES) with the addition of an Artificial Neural Network (ANN) computational structure. Thus, inherent characteristics of ANNs, along with the human-like knowledge representation of fuzzy systems are integrated. The ANFIS has been utilized into building five different sub-systems, distinctly covering Coronary Disease, Hypertension, Atrial Fibrillation, Heart Failure, and Diabetes, hence aiding doctors of medicine (MDs), guide trainees, and encourage medical experts in their diagnoses centering a wide range of Cardiology. The Fuzzy Rules have been trimmed down and the ANNs have been optimized in order to focus into each particular disease and produce results ready-to-be applied to real-world patients.

**Keywords** Artificial intelligence • Decision making • Cardiovascular diseases

---

G.-P.K. Economou (✉)

Department of Computer Science, Hellenic Open University, 26335 Patras, Greece  
e-mail: [econom@upatras.gr](mailto:econom@upatras.gr)

E. Sourla • Konstantina-Maria Stamatopoulou • A. Tsakalidis  
Computer Engineering & Informatics Department, University of Patras, 26500 Patras, Greece  
e-mail: [sourla@ceid.upatras.gr](mailto:sourla@ceid.upatras.gr); [stamatok@ceid.upatras.gr](mailto:stamatok@ceid.upatras.gr); [tsak@ceid.upatras.gr](mailto:tsak@ceid.upatras.gr)

V. Syrimpeis  
3 General Hospital of Patras Agios Andreas, 26335 Patras, Greece  
e-mail: [siva@upatras.gr](mailto:siva@upatras.gr)

S. Sioutas  
Department of Informatics, Ionian University, 49100 Corfu, Greece  
e-mail: [sioutas@ionio.gr](mailto:sioutas@ionio.gr)

G. Tzimas  
Computer & Informatics Engineering Department, Technological Educational  
Institute of Western Greece, 26334 Patras, Greece  
e-mail: [tzimas@teimes.gr](mailto:tzimas@teimes.gr)

## 6.1 Introduction

Single analysis techniques [7] for many years have been the bases with which engineers worldwide tried to equip Medical Doctors (MDs) with computational means inasmuch as to improve their performance. Yet, those techniques only enhanced Medical Data provided by various examinations and methods; they could not support MDs with their diagnoses. On the other hand, Artificial Intelligence (AI) methodologies have proven to be crucial in utilizing the knowledge of specialized experts in various fields of human activities [10].

Artificial Neural Networks (ANNs), in particular, have been employed so that to process medical information and classify symptoms into diseases and proper treatment, hence reaching correct diagnoses. The general and flexible structure of a Medical Decision Making System (MDMS), composed of ANNs, is capable of being adjusted to different areas of either medical interest or where human knowledge and reasoning prevails simply by providing applicable learning data [10]. Similarly, Fuzzy Logic is considered to be one of the most suitable approximations of decision making, since it deals with reasoning that is approximate rather than fixed and exact, thus closer to human reasoning [2]. Therefore, both AI domains are capable of modeling complex phenomena [8, 12].

In this work, an Adaptive Neuro-Fuzzy Inference System (ANFIS) was developed for the MDMS to be trained, tested, and applied in the field of Cardiovascular Diseases (CDs). The team of MDs also decided that five different and medically critical CDs were to be the focus of the project and five distinctive sub-systems, one for each particular disease, were to be developed. The CDs, namely Coronary Disease, Hypertension, Atrial Fibrillation, Heart Failure, and Diabetes, were chosen due to the number of real-world clinical data that could be analyzed.

Thus, for the MDMS presented in this paper, medical data from real clinical cases were used to model both learning patterns for its ANNs and its fuzzy rules. Medical data, the inputs of the five sub-systems, were converted to the different members of the associated membership functions based on their value, so as to be fuzzy-fied and hence be exploited by the Stage 1 of the MDMS. Stage 2 exploits the necessary fuzzy rules, a direct mapping of MDs expertise, to treat the inputs of the previous stage. Each rule provides for a (fuzzy) output. Stage 3 combines all partial (fuzzy) outputs and Stage 4 de-fuzzy-fies the output into a more medical response. All stages have been implemented by ANNs.

The rest of the paper is organized as follows: Related work to the proposed project is presented in Sect. 6.2. Section 6.3 approaches the implemented ANFIS via a thorough description, followed by the system evaluation and comparison data in Sect. 6.4. Finally, Sect. 6.5 hosts conclusions and future work.



## 6.2 Related Work

A large number of joined MDs and engineers teams' research projects nowadays reflect the manifold integration of artificial intelligence in medicine. MDMSs combined with genome information and biomarkers [10]; cancer biomarker discovery and multiplexed nanoparticle probes for cancer biomarker profiling [14]; molecular diagnosis and individualized therapy of human diseases [9]; identification of potential responders to a certain medication therapy using random forests algorithms [13]; classification of electroencephalogram signals through feature extraction, using the wavelet transform [7].

Most of the abovementioned MDMSs concentrate on MDs requirements for educational reasons or to serve plain advisory roles. More vigorous efforts have also been proposed [4] upon which ANNs play dominant roles, as well as technology evolution and "smart" devices features and potential [3]. As far as it concerns MDMSs in CDs, there are also a number of research projects. One treating hypertension [15] recommends two separate ANNs propagating medical data regarding healthy and possible patients' symptoms and extrapolating the diagnosis by comparing their outputs. Another one employs a multi-layered perceptron neural network and support vector machine, determining Coronary Artery Disease by being fed exercise stress testing data [1]. In [16], ANNs are used as most suitable to outcome prediction trends in post-operative cardiac patients.

Guidi et al. [6] operated a system to assist non-specialists in the analysis of heart failure patients' data. ANNs compete with a support vector machine, a decision tree, and a fuzzy expert system whose rules are produced by a Genetic Algorithm, all AI-techniques contributing to the final outcome. ANNs achieved the best performance with an accuracy of 86%. Health care systems are proposed in [5] that allow patients to self-record Electrocardiograms (ECGs) with "smart" portable devices that analyze the signal inputs and through a set of rules and risk factors can estimate the severity and the condition of life threatening heart episodes. These projects needed extra hardware in order to produce the ECGs and export the final results.

## 6.3 Description of the MDMS

In this section, the proposed MDMS is described. First though, we present an introduction to Fuzzy Logic and ANNs.

### 6.3.1 Introduction to Fuzzy Logic

All computational machines can process crisp data such as either (logical) “0” or “1.” In order to enable them to handle vague language input, the crisp input and output must be converted to linguistic variables, thus forming fuzzy components. A crisp input will be converted to the different members of the associated membership functions based on its value. From this point of view, the output of a fuzzy logic controller is based on its memberships of the different membership functions, which can be considered as a range of inputs [2].

Generally, fuzzy-fication involves two processes: derive the membership functions for input and output variables and represent them with linguistic variables. In practice, membership functions can have multiple different types, such as the triangular waveform, trapezoidal waveform, Gaussian waveform, etc. [2]. In the proposed ANFIS triangular membership functions are used, since significant dynamic variation in a short period of time is needed.

Then, for the Fuzzy Inference Process to begin, fuzzy inputs, and membership functions utilization along with the control rules are combined to derive the fuzzy output. The control rules are the core of the fuzzy inference process and are directly related to a human being’s intuition or expertise [2]. MDs were asked to assess the severity of every rule, according to their experience and knowledge. To make the fuzzy output available to real applications, a de-fuzzy-fication process is needed. A fuzzy output is still a linguistic variable, hence it needs to be converted to the crisp variable via the de-fuzzy-fication process. All proposed CDs sub-systems function on the weighted average de-fuzzy-fication method [2]. Figure 6.1 shows an example of a stored membership function.

### 6.3.2 Introduction to ANNs

ANNs consist of a large number of Artificial Neurons (ANs), similar or not to each other, that form networks by the way they are combined. ANs vary in structure and function and, because of their connections (called *Synapses*), exhibit different characteristics. Figure 6.2a shows a typical AN [4, 11]. Its inputs and outputs generally obey the equation:

$$\psi = \phi(\sum_{i=1}^n \beta_i \cdot \chi_i) \quad (6.1)$$

An AN can accept large number of (digital or analogue) inputs ( $\chi_1, \chi_2, \dots, \chi_n$ ), multiply them by the factors  $\beta_1, \beta_2, \dots, \beta_n$  (called *weights*), and extract an output that can feed similar, or not, neurons. The outputs can be made discrete or analogue and when they have a non-zero value the neuron is said to have *-fired*. The weighted inputs sum up and are expressed in a non-linear function  $\phi(\cdot)$ . The non-linear

**Fig. 6.1** Membership function

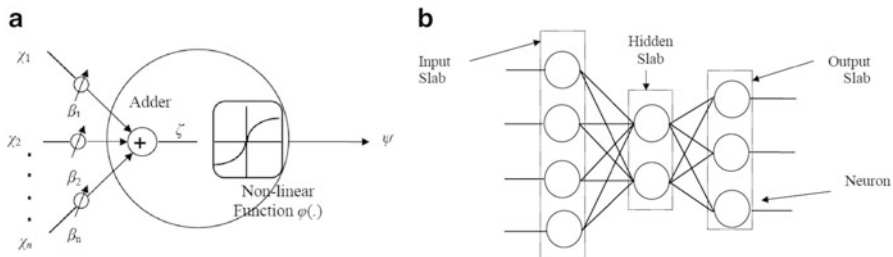
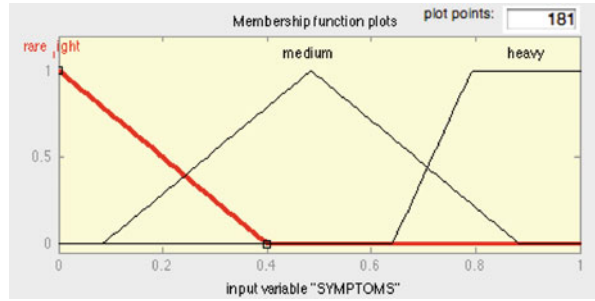


**Fig. 6.2** (a) Typical AN and (b) ANNs Feed forward architecture

function  $\phi(\cdot)$  corresponds to biological models’ performance and is called *Sigmoid* due to its shape (similar to the Hellenic capital letter  $\Sigma$ ). Figure 6.2a shows a usual AN, whereas Fig. 6.2b a typical ANNs architecture (feed forward—fANNs).

In a fANN, the connections are only allowed between ANs belonging to adjacent architecture levels (“Slabs”). Between input and output Slabs and depending on the application, a number of hidden Slabs of ANs intervene in which input vectors do not have access and they do not contribute directly to the output ones.

The number of hidden Slabs/ANs defines the fANNs performance and effectiveness. ANNs can be taught by feeding typical data to their inputs and forcing their outputs to appropriate ones by means of learning algorithms that calculate their weights’ values [11]. Those Input/Output vectors are referred to as learning patterns and each time all ANNs weights are calculated anew denotes an epoch.

### 6.3.3 The ANFIS

Systems integrating the parallel computation and learning capabilities of ANNs with the human-like knowledge representation of fuzzy systems form neuro-fuzzy systems. Those have far better explanation abilities supporting their outputs (and in the case of CDs, medical diagnoses) than either separate AI methodologies. As a result, neural networks mode of operation becomes more understandable and additionally fuzzy systems become adroit of adaptation and of learning.

A neuro-fuzzy system (ANFIS) basically is an ANN which is functionally equivalent to a fuzzy inference model. Moreover, as already stated, it can adapt to virtually every area of human expertise provided with the necessary training patterns (representative pairs of vectors of inputs/outputs used in their learning phase). Thus, an ANFIS can be trained to develop IF-THEN fuzzy rules and determine membership functions for input and output variables of a particular area. Therefore, building the fuzzy inference engine is avoided, which not only entails a substantial computational burden but also depends on experts' subjectivity and knowledge-extraction methodology (see also Sect. 6.4).

The structure of an ANFIS is similar to a multi-layer ANN (Fig. 6.2b): it has input and output slabs; the number of each slab's ANs is dictated by the expert. Also, it is generally provided with three hidden slabs that represent membership functions and fuzzy rules. Each slab in an ANFIS is associated with a particular step in the fuzzy inference process. The first slab is the input layer (or Stage 1 of the MDMS). Each of its ANs is input data that have been through a fuzzy-fication procedure. The second slab (Stage 2) determines the degree to which this input vector belongs to the ANs fuzzy set; the appropriate AN, then fires and its output propagates to the ANs of the next hidden layer, up to the output slab (Stage 3). ANs of that Stage are also especially aggregated (always under an expert's guide when building this whole infrastructure) to produce the closing vector of fuzzy outputs. Lastly, the final AN slab (Stage 4) operates as the de-fuzzy-fication operand, being set to "transform" the MDMS data into an actual diagnosis.

### 6.3.3.1 The MDMSs

- The **Coronary Disease** MDMS sub-system (cMDMS) has five vectors of inputs, namely *Family History*, *Risk Factors*, *Myocarditis Probability*, *Other Reasons for the disease*, and *(older) Clinical Examinations Results (CEX)*. Its outputs are *No Further Evaluation*, *Re-Evaluation after 3 Months*, *Perform a Computerized Tomography (CT)*, *Perform a Magnetic Tomography (MRI)*, and *Perform Surgery -percutaneous coronary intervention (PCI)*, all set by experts.

The severity of the above factors is fuzzy-fied into three membership functions *min*, *med*, and *max* (as shown in Fig. 6.1). The rules constructed for the cMDMS are close to 300 and are established similarly to the following one:

IF *Family History* IS *min* AND *Risk Factors* IS *med* AND *Myocarditis Probability* IS *min* AND *Other Reasons for the disease* IS *min* AND *CEX* IS *med* THEN *Outcome* IS *MRI*.

- The **Hypertension** MDMS sub-system (hMDMS) has three vectors of inputs, namely *Risk Factors*, *Performed Echocardiogram (Echo)*, and *Other (older) Clinical Examinations Results (CEX)*. Its outputs are *No Further Evaluation*, *Re-Evaluation after 3 Months*, *Re-Evaluation after 12 Months*, *Two Consecutive Weeks Evaluation*, and *Therapy*, all set by experts.

The severity of the above factors is fuzzy-fied into three membership functions *min*, *med*, and *max*. The rules constructed for the hMDMS are close to 30 and are established similarly to the one of the cMDMS.

- The **Atrial Fibrillation** MDMS sub-system (afMDMS) has five vectors of inputs, namely *Family History*, *Risk Factors*, *CHA2DS2VASC Score Results*, (*various*) *Symptoms Assessment (SA)*, and *Documentation of Arrhythmia*. Its outputs are *Regular Assessment of Performed Electrocardiography (ECG)*, *Holter Use*, *Perform Echocardiogram (Echo)*, *Perform Cardioversion-Ablation*, *Treatment Underlying Disease*, *Rhythm Control*, *Rate Control*, *Aspirin Use*, and *Oral Anticoagulant Use*, all set by experts.

The severity of the above factors is fuzzy-fied into three membership functions *min*, *med*, and *max* (as shown in Fig. 6.1). The rules constructed for the afMDMS are close to 200 and are established similarly to the one of the cMDMS.

- The **Heart Failure** MDMS sub-system (hfMDMS) has four vectors of inputs, namely *Family History*, *Risk Factors*, *Symptoms Assessment (SA)*, and *Performed Echocardiogram (Echo)*. Its outputs are *No Heart Failure*, *Heart Failure (HF) Class I (NYHA)*, *HF Class II (NYHA)*, *HF Class III (NYHA)*, and *HF Class IV (NYHA)*, all set by experts.

The severity of the above factors is fuzzy-fied into three membership functions *min*, *med*, and *max* (as shown in Fig. 6.1). The rules constructed for the hfMDMS are close to 80 and are established similarly to the one of the cMDMS.

- The **Diabetes** MDMS sub-system (dMDMS) has four vectors of inputs, namely *Family History*, *Risk Factors*, (*older*) *Clinical Examinations results (CEX)*, and (*existing*) *Cardiovascular Problem*. Its outputs are *No Further Evaluation*, *Periodical Fasting Glucose*, *Fasting Glucose and 2 Hours Postprandial Glucose Every 2 Years*, *Fasting Glucose and 2 Hours Postprandial Glucose Every Year* and *HgbA1C*, all set by experts.

The severity of the above factors is fuzzy-fied into three membership functions *min*, *med*, and *max* (as shown in Fig. 6.1). The rules constructed for the dMDMS are close to 80 and are established similarly to the one of the cMDMS.

### 6.3.4 Choosing the Proper Fuzzy Method

There are two types of fuzzy methods widely accepted for capturing expert knowledge: Mamdani and Sugeno. Mamdani method allows for the description of expertise in more intuitive, human-like manner, but it entails a substantial computational burden. On the other hand, Sugeno method is computationally efficient and works well with optimization and adaptive techniques, which makes it very attractive in control problems, particularly for dynamic non-linear systems. These adaptive techniques can be used to customize the membership functions [12].

## 6.4 Evaluation and Comparison Data

### 6.4.1 ANFIS vs. Previous Work

In [17] previous work on building a working MDMS in the field of CDs was presented. Its performance was evaluated by three different teams of experts, specifically Group A (expert MDs that did not participate the design of the MDMS), Group B (general MDs), and Group C (medical students). All groups were asked to grade the system on its Medical Reliability, Assistance in Work, and Usability.

The former MDMS received good/very good grades regarding Medical Reliability and medium/good rating on Assistance in both Work and Usability. The newly proposed MDMS strives to overcome the difficulties and reservations users may have towards handling the system, mostly by the design of a new MDs-to-machine interface and by the application of ANNs to add to its adaptation capabilities and decision support aspects of an expert system designed for MDs.

Since MATLAB [12] was the tool used for developing the former MDMS, it was kept to also design the proposed one. Typical comparison data and diagrams showing divergences between the two systems follow in Table 6.1.

The reader promptly realizes that the performance of the ANFIS is somewhat “worse” of the former one, at least comparing the two systems’ numerical data. Yet, one should carefully contemplate the typical diagrams in Fig. 6.3a, b.

It is clear that no ANFIS was left to generalize its learning inputs into the outputs. The various MDMSs have some epochs left in order to reach their minima. Still, it was decided their number to be kept similar to the previous ones.

### 6.4.2 Fuzzy Rules Reduction

The numbers of fuzzy rules that were employed for the previous MDMS, as already stated (Sect. 6.3), were 300 for the cMDMS; 30 for the hMDMS; 200 for the afMDMS; 80 for the hfMDMS; and 80 for the dMDMS. The engineer team reduced those numbers by first sorting the rules out with respect to their outputs; then, they eliminated the redundant ones that only differed in one of their vector inputs preserving the other vectors, i.e.:

Rule 1	IF $a1$ IS <i>min</i> AND $a2$ IS <i>med</i> AND ... THEN <i>Outcome</i> IS $d11$ .
Rule 2	IF $a1$ IS <i>med</i> AND $a2$ IS <i>med</i> AND ... THEN <i>Outcome</i> IS $d11$ .
Rule 3	IF $a1$ IS <i>max</i> AND $a2$ IS <i>med</i> AND ... THEN <i>Outcome</i> IS $d11$ .
Winning Rule	IF $a2$ IS <i>med</i> AND ... THEN <i>Outcome</i> IS $d11$ .

**Table 6.1** Typical comparison data of former/ANFIS MDMSs

	Hypertension		Heart failure		Diabetes	
	Former	ANFIS	Former	ANFIS	Former	ANFIS
Max error	0.3010	0.3458	0.0514	0.0540	0.0382	0.0446
Min error	-0.3462	-0.7775	-0.0582	-0.0631	-0.0545	-0.0557
Standard deviation	0.0031	0.0039	1.9145e-04	1.9145e-04	8.2153e-05	1.0326e-05

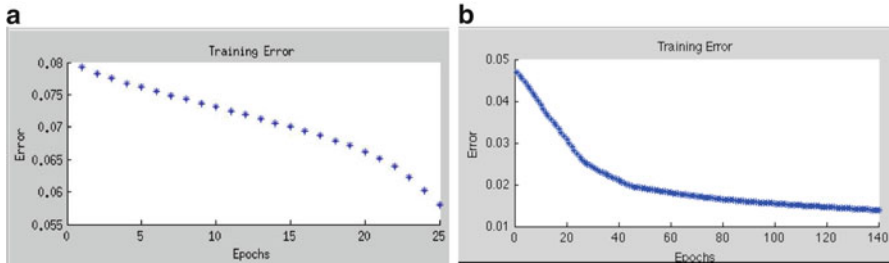
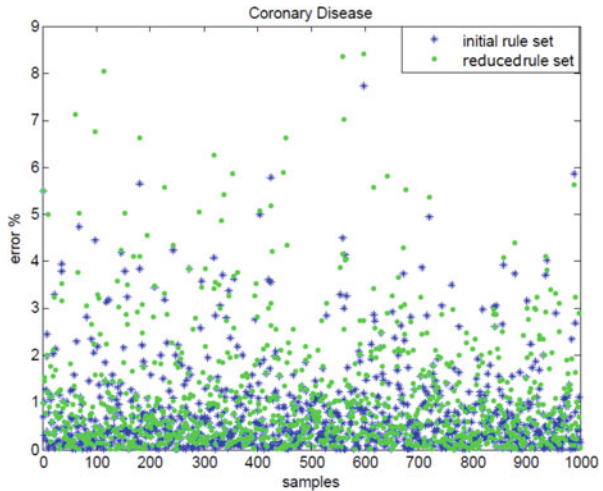


**Fig. 6.3** (a) hMDMS’s learning and (b) hfMDMS’s learning

**Fig. 6.4** cMDMSs’ generalization errors



The input that got all the range of possible values, though the other inputs retained theirs, was eliminated. Figure 6.4 shows the differences between the two cMDMSs when left to generalise un-trained (testing) input patterns into the appropriate output ones.

### Conclusions and Future Work

A new MDMS is proposed in the field of Cardiovascular Diseases. The new system is an improvement of a former one, both in potential and in less computing requirements, whereas its performance is comparable to it. In its next phase, its evaluation by MDs is scheduled, over some period of time, and several aspects of its design architecture are going to be optimized: MDs-to-machine interface, training data, number and quality of fuzzy rules, programming code portability, and porting to “smart” devices using the Android Operating System, thus ensuring its acceptance by MDs on an everyday working basis.

**Acknowledgements** This research has been co-financed by the European Union (European Social Fund ESF) and Greek national funds through the Operational Program “Education and Lifelong Learning” of the National Strategic Reference Framework (NSRF)—Research Funding Program: Heracleitus II. Investing in knowledge society through the European Social Fund.

### References

1. Babaoglu I et al (2010) A comparison of artificial intelligence methods on determining coronary artery disease, advances in information technology. *Commun Comput Inf Sci* 114:18–26
2. Bai Y, Wang D (2006) Fundamentals of fuzzy logic control - fuzzy sets, fuzzy rules and defuzzifications. *Advanced fuzzy logic technologies in industrial applications*. Springer, Berlin, pp 17–36
3. Economou G-PK, Papaioannou V (2013) Medical decision making via artificial neural networks: a smart phone-embedded application addressing pulmonary diseases diagnosis, 2013 mining humanistic data workshop (2013 engineering applications on neural networks). *Commun Comput Inf Sci* 384:156–163
4. Economou G-PK et al (2004) Decision support systems for tele-medicine applications. Research Studies Press Ltd., Hertfordshire
5. Fayn J, Rubel P (2010) Toward a personal health society in cardiology. *IEEE Trans Inf Technol Biomed* 14(2):401–409
6. Guidi G et al (2012) Heart failure artificial intelligence-based computer aided diagnosis telecare system. In: Donnelly M et al (eds) *Impact analysis of solutions for chronic disease prevention and management*, vol 7251. Springer, Berlin, pp 278–281
7. Gulera I, Ubeyli ED (2005) Adaptive neuro-fuzzy inference system for classification of EEG signals using wavelet coefficients. *J Neurosci Methods* 148(2):113–121
8. Honka AM, van Gils MJ, Parkka J (2011) A personalized approach for predicting the effect of aerobic exercise on blood pressure using a fuzzy inference system. In: 2011 annual international conference of the IEEE EMBS, Boston, pp 8299–8302
9. Jones LK et al (2011) Confident predictability: identifying reliable gene expression patterns for individualized tumor classification using a local minimax Kernel algorithm. *BMC Med Genomics* 4:1–10
10. Kouris I et al (2010) E-health towards ecumenical framework for personalized medicine via decision support system. In: 2010 annual international conference of the IEEE EMBS, Buenos Aires, pp 2881–2885



11. Lippmann RP (1987) An introduction to computing with NN, IEEE ASSP, pp 4–22
12. Mathworks Documentation Center, Comparison of Sugeno and Mamdani Systems. <http://www.mathworks.com/help/fuzzy/comparison-of-sugeno-and-mamdani-systems.html>
13. Midorikawa Y et al (2012) Genomic approach towards personalized anticancer drug therapy. *Pharmacogenomics* 13(2):191–199
14. Phan JH et al (2009) Convergence of biomarkers, bioinformatics and nanotechnology for individualized cancer treatment. *Trends Biotechnol* 27(6):350–358
15. Poli R et al (1991) An NN expert system for diagnosing and treating hypertension. *IEEE Comput* 24(3):64–71
16. Rowan M et al (2007) The use of ANNs to stratify the length of stay of cardiac patients based on pre- and initial post-operative factors. *Artif Intell Med* 40(3):211–221
17. Sourla E et al (2013) Exploiting fuzzy expert systems in cardiology. *Commun Comput Inf Sci* 384:80–89

# Chapter 7

## Modeling Protein Misfolding in Charcot–Marie–Tooth Disease

Georgia Theocharopoulou and Panayiotis Vlamos

**Abstract** Charcot–Marie–Tooth (CMT) disease is the most common inherited neuromuscular disorder. Recent advancements in molecular biology have elucidated the molecular bases of this genetically heterogeneous neuropathy. Still, the major challenge lies in determining the individual contributions by malfunctions of proteins to the disease’s pathology. This paper reviews the identified molecular mechanisms underlying major forms of CMT disease. A growing body of evidence has highlighted the role of protein misfolding in demyelinating peripheral neuropathies and neurodegenerative diseases. Several hypotheses have been proposed to explain how misfolded aggregates induce neuronal damage. Current research focuses on developing novel therapeutic targets which aim to prevent, or even reverse the formation of protein aggregation. Interestingly, the role of the cellular defence mechanisms against accumulation of misfolded proteins may play a key role leading to novel strategies for treatment accelerating the clearance of their toxic early aggregates. Based on these findings we propose a model for describing in terms of a formal computer language, the biomolecular processes involving proteins associated with CMT disease.

### 7.1 Introduction

Charcot–Marie–Tooth disease (CMT) refers to the inherited peripheral neuropathies named for the three investigators who described them in the late 1800s (Jean-Martin Charcot, Pierre Marie, Howard Henry Tooth). CMT is also known as hereditary motor and sensory neuropathy (HMSN) and peroneal muscular atrophy (PMA). As CMT diseases affect approximately one in 2,500 people, equating to approximately 23,000 people in the United Kingdom and 125,000 people in the USA, they are among the most common inherited neurological disorders. Most patients show slowly progressive distal and symmetrical muscle weakness and

---

G. Theocharopoulou (✉) • P. Vlamos  
Department of Informatics, Ionian University, Corfu, Greece  
e-mail: [zeta.theo@ionio.gr](mailto:zeta.theo@ionio.gr); [vlamos@ionio.gr](mailto:vlamos@ionio.gr)

atrophy that affects the intrinsic foot and peroneal muscles in combination with sensory problems [3, 47]. Later in the disease, muscles of hands and forearms become affected. Over the past decade remarkable progress has been made toward understanding the genetic causes of many types of CMT. More recently, advances in cell biology have provided clues as to how particular mutations are linked to the disease.

In 1968, CMT was subdivided based on pathologic and physiologic criteria into two types, CMT1 and CMT2; a predominant demyelinating process resulting in low conduction velocities (CMT1) and a predominant axonal process, resulting in low potential amplitudes (CMT2) [11]. Slowing of conduction in motor and sensory nerves was believed to cause weakness and numbness. Scientific studies suggested that neurological dysfunction and clinical disability in CMT1A are caused by loss or damage to large-diameter motor and sensory axons [21]. Nerve signals are conducted by an axon with a myelin sheath wrapped around it. Myelinating Schwann cells wrap around axons of motor and sensory neurons to form the myelin sheath. Schwann cells and neurons exchange molecular signals that regulate cell survival and differentiation. These signals are disrupted in CMT [5]. Demyelinating Schwann cells cause abnormal axon structure and function. They may cause axon degeneration, or they may simply cause axons to malfunction [21]. The degree of axonal damage and loss of fibers are reflected in a reduction in amplitude of compound muscle action potential (CMAP) for motor nerves, and of sensory nerve action potential (SNAP) for sensory nerves. Both axonal and demyelinating CMT eventually result in loss of axons.

## 7.2 Gene Mutations Associate with CMT Disease

As disease-causing mechanisms unravel, there is growing evidence that the distinction between demyelinating and axonal CMT is somewhat artificial. Researchers have identified an increasing number of mutations of the same genes that may result either in a demyelinating type with slow conduction or in an axonal type of the disease. CMT is caused by mutations in genes that produce proteins involved in the structure and function of either the peripheral nerve axon or the myelin sheath. Although different proteins are abnormal in different forms of CMT disease, all of the mutations affect the normal function of the peripheral nerves. Consequently, these nerves slowly degenerate and lose the ability to communicate with their distant targets. Based on molecular diagnosis CMT has been further subdivided and can be regarded as a collection of hereditary peripheral neuropathies. With the advent of genetic testing, all of the different diseases that fall under the heading of CMT syndrome eventually are likely to become distinguishable. Genetic testing allows for definitive diagnosis, even in asymptomatic individuals. Only 50–60 % of cases, however, will be positive. The other 40–50 % of patients with CMT has another genetic type. Approximately 60 % of CMT patients show a predominantly demyelinating peripheral neuropathy and are classified as CMT1

[19]. The main subtype is CMT1A, accounting for 40–50% of all CMT cases, which is associated with an autosomal dominant duplication on chromosome 17p11.2 that includes the peripheral myelin protein 22 gene (PMP22), expressed predominantly in the compact myelin of Schwann cells of the PNS [4, 29]. Research studies revealed that a mechanism of gene dosage (duplicated or deleted PMP22) gives rise to demyelinating neuropathies and secondary axonal loss or abnormalities. When overexpressed in cultured cells or in transgenic mice gene PMP22 reaches late endosomes and forms protein aggregates that are ubiquitinated [15]. Removal of pre-existing aggresomes formed by endogenous PMP22 is aided by autophagy [14]. Although demyelination is the pathological and physiological hallmark of CMT1A, the clinical signs and symptoms of this disease, progressive weakness, and sensory loss are produced by axonal degeneration [21]. CMT1B, which accounts for 5% of patients, is caused by mutations in the major myelin protein zero gene (MPZ), which comprises approximately 50% of myelin protein, and is necessary for both normal myelin structure and function [12, 16]. The mutation may cause abnormal production of myelin and may result in segmental demyelination, leading to uniform slowing of conduction velocity. To date there are more than 150 different mutations in MPZ known to cause CMT1B in patients, which include missense, nonsense, small insertion/deletion, and splice site mutations [19]. Studies in a CMT1B mouse model showed that the unfolded protein response (UPR), activated by overload of misfolded proteins in the endoplasmic reticulum (ER), is associated with demyelination [32].

A key question is whether all these mutated genes associated with CMT play a role which converges at common intermediates and/or crosstalk with one another, or, alternatively each different gene leads to a dysfunctional pathway by a distinct mechanism. Obviously, dysfunction can result from the absence, or accumulation of a specific protein involved in the mechanisms regulating myelination in the peripheral nervous system. Furthermore the canonical protective cell responses to stresses caused by mistargeting of key macromolecules can, in certain circumstances, become accidentally detrimental by activating pathways leading to unregulated programmed cell death. In a recent CMT1B mouse model scientists have reported that mutated MPZ protein is retained in the endoplasmic reticulum of Schwann cells and provokes a transitory, canonical UPR [40]. UPR activation aims to reduce the load of unfolded proteins through upregulation of chaperones and global attenuation of protein synthesis. Moreover, when endoplasmic reticulum stress is overwhelming, the UPR uses destructive outputs to trigger programmed cell death. In this study authors conclude that less activation of the UPR would enable increased myelination to occur in these mice. Identifying which CMT mutations activate the UPR signaling and the mechanisms by which myelination is affected will give us information about therapeutic modulation of ER chaperones and UPR components.

Recent findings suggest that demyelinating CMT may be a protein-misfolding disease of Schwann cells [10, 24]. Misfolded myelin proteins, such as PMP22, MPZ and other proteins such as SIMPLE, which have been identified to cause CMT, have a tendency to sequester chaperones, and hence to induce a prolonged UPR at the

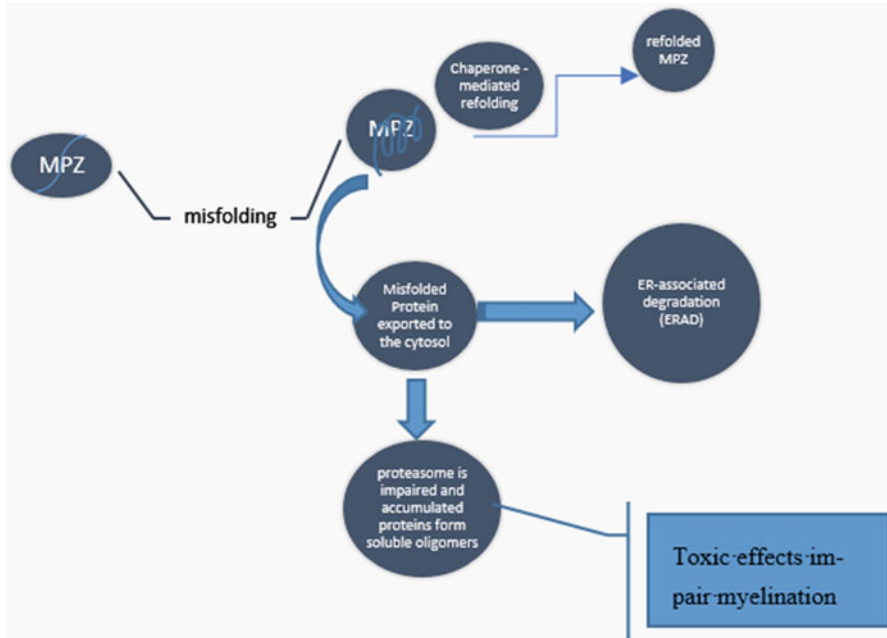


**Fig. 7.1** Hypothesized model of how misfolded MPZ arrests or slows myelination

endoplasmic reticulum (Fig. 7.1). When refolding is not possible, these aberrant proteins in the ER lumen are exported back to the cytosol and degraded by the proteasome, in a process known as ER-associated degradation (ERAD). When proteasome is impaired or overwhelmed, misfolded proteins accumulate and form soluble oligomers with potentially toxic effects and may impair Schwann cell functions including myelination [28, 38]. The aggresome-autophagy pathway sequesters and delivers toxic protein aggregates to autophagy for clearance. Aggresomal pathway has emerged as another crucial protein quality control system in Schwann cells that degrades misfolded and aggregated proteins [9, 38].

Several studies indicate that Schwann cells handle misfolded PMP22 and SIMPLE by sequestering them into perinuclear aggresomes through a mechanism requiring microtubule-dependent retrograde transport [23, 38]. There must be a critical balance in the protein quality control, between retaining and degrading potentially harmful aggregated proteins. The accumulation of misfolded PMP22 and MPZ at the ER suggests that impaired ERAD function and subsequent ER stress may be involved in causing demyelinating CMT [20, 22]. Moreover, proteasome inhibition could contribute to demyelinating CMT pathogenesis. Another major contributing factor of demyelinating peripheral neuropathies is the inhibition of the aggresome-autophagy pathway due to the overload of impaired proteins.

### 7.3 Modeling and Simulating

Over the last years a formal computer language has been proposed for describing the biomolecular processes underlying protein networks. The pi-calculus, a process algebra, originally developed for describing computer processes, has been used to model biomolecular processes [1, 2, 26, 35]. Abstracting biomolecular systems, at the cellular level, as concurrent computation, is a system of interacting molecular entities which is described and modeled by a system of interacting computational entities. Multiple computational processes (molecules, molecular domains) communicate with each other on complementary channels that are identified by specific names. Thus, chemical interaction and subsequent modification are modeled as communication and channel transmission. Two different types of communications can be defined in the pi calculus [34, 35]. In the first type, processes can send empty messages to one another, only if they share the same communication channel. Following communication, each process may either iterate or change its state, becoming another process with different channels and behavior. The second type of communication is more complex. In this case, the content of a message is one or more channel names, which can be used by the receiving process to communicate with other processes. As before, following communication the processes may either iterate or change state. Moreover, the process acquires communication capabilities dynamically that were not specified a priori in its explicit program. Such a change in future communication capabilities as a result of passing messages is termed mobility [34, 35]. Since biochemical interactions may occur in sequence, in parallel with other independent events, or in a mutually exclusive, competitive fashion, there are several alternative interactions in which a molecule may participate. A sequence of interactions is abstracted as a sequence of input and output offers, separated by the comma sign, “,”. Mutually exclusive offers are summed together, using the choice operator (“+” or “;”). Finally, the case where several interactions may occur in parallel, without directly affecting each other, is handled by composing different offers in parallel. Another basic operator is the new operator, indicated by  $\nu$  followed by name or a set of channel. Operator  $\nu$  introduces private channels with restricted communication scopes, i.e. the private channel lives at the scope of that process. A system of processes denotes a collection of molecule processes, occurring in parallel (parallel composition, | PAR operator).

The aim of this work is to provide a theoretical framework of a model that will be able to give insights into the mechanisms underlying the experimental results and will allow to test the validity of several hypotheses that have been proposed. In a recent study scientists have generated a mouse knock-in model of CMT type 1B, where a mutation encoding R98C was targeted to the mouse *Mpz* gene [40]. This study suggests that less activation of the UPR would enable increased myelination to occur in these mice. However, the mechanisms through which the UPR affects myelination are likely to be distinct. The UPR has been implicated in a variety of diseases including metabolic disease, neurodegenerative disease, inflammatory

**Table 7.1** The pi calculus consists of three components: simple syntax for formal descriptions; congruence laws; operational semantics

Processes-channels	Events	Process syntax	Structural congruence
P, Q...process	$x(y)$ receive y along x	$P1 \mid P2$ parallel processes	$P \mid Q \equiv Q \mid P$
x, y, ... channel	$\bar{x}y$ send y along x	$\pi.P1$ sequential prefixing by communication	$P+Q \equiv Q+P$
$\bar{x}$ co-channel	(new x)P new communication	$\pi 1 \cdot P1 + \pi 2 \cdot P2$ mutually exclusive com	$(newx)P$ scope of inert process
	0 inert process		$(newx)(newy)P \equiv (newy)(newx)P$ multiple communication scopes

disease, and cancer. Targeting various signaling components of the UPR are emerging as potential targets for intervention and treatment of human disease.

Using simulation techniques, our overarching aim is to unravel key cellular mechanisms and their distortions, in order to define novel molecular markers for diagnosis and therapeutic intervention. One of the challenges in development of models is the aim to reduce a model's complexity which affects the level of detail at which subsystems are described. Moreover, the ability to compose complex entities from constituent parts according to pre-defined rules offers a unique way to handle such entities (Table 7.1).

In this model we describe in terms of formal language pi-calculus the UPR induced by the accumulation of mutated protein MPZ to the endoplasmic reticulum.

To date, three ER-resident transmembrane proteins have been identified as proximal sensors of the presence of ER stress: inositol requiring enzyme IRE1, the PERK kinase, and the transcription factor ATF6 [37]. Three parameters are usually used to detect UPR activation: XBP1 splicing as an indicator of IRE1 pathway activation, ATF6 cleavage and increase in the levels of the transcription factor CHOP and its translocation to the nucleus, as an indicator of PERK pathway activation [39]. Studies with CMT1B mice showed that ablation of CHOP improved the neuropathy, suggesting that reducing UPR activation caused by endoplasmic reticulum stress is a viable therapeutic strategy for at least some cases of CMT1B [30, 31]. Activation of ATF6, IRE1, and PERK in response to ER stress is thought to occur in parallel, but the timing or duration of each may differ, while the mechanistic details are not yet resolved. In unstressed cells these proteins appear to form complexes with the ER chaperone BiP [41, 42]. The system of biomolecules driving the UPR is implemented as process SYSTEM, given by the parallel composition of seven processes that represent their homonymous molecules:

IRE1, PERK, ATF6, CHAPERONE, MISFOLDED, BIP, EIF2A.

A pathway is defined as a collection of concurrently operating molecules, seen as processes with potential behavior. Concurrency is denoted by the PAR operator.

$$\text{UPRpathway} ::= \text{IRE1} | \text{PERK} | \text{ATF6} | \text{BIP} | \text{MISFOLDED} | \text{EIF2A}$$

Each constituent molecule in the pathway is a process, as are its domains. For example, the extracellular, intra-cellular and transmembranal domains of the receptor molecule will be denoted by Extra, Transmem, and Intra processes. In this model we have called MISFOLDED the pathogenic mutated protein. When misfolded proteins accumulate in the ER, they bind to and sequester BiP, activating the sensors [6, 41]. MISFOLDED process sends a private name to-bip to the process BIP via the shared channel bind-to-bip. The result of this interaction is the complex MISFOLDED-BIP.

$$\text{MISFOLDED} ::= (\nu \text{to} - \text{bip}) \text{bind} - \text{to} - \text{bip}(\text{to} - \text{bip}). \text{MISFOLDED} - \text{BIP}(\text{to} - \text{bip})$$

The interactions of BiP with IRE1 and with PERK are disrupted. Activated PERK phosphorylates eIF2, which in turn attenuates general protein translation to reduce the ER protein-folding load. For simplicity, we handle the enzymatic reaction as a “single-step” reaction, rather than an elaborate model. Protein Kinase PERK sends p-eIF2a as message on to-eIF2a channel. The eIF2 offers to receive on to-eIF2a channel, interacts with PERK and is phosphorylated with the received message. Activation of the PERK-eIF2P branch of UPR causes a general inhibition of protein synthesis, but at the same time increases translation of specific mRNAs, such as transcription factor 4 (ATF4) synthesis, which in turn induces the transcription of genes that facilitate adaptation of cells to stress, through increasing the antioxidant capacity of the cell, or eliminating it, by activating apoptosis.

More specifically ATF4, induced by the PERK-eIF2 pathway up-regulates the expression of a proapoptotic factor, CHOP. CHOP is a member of the C/EBP family of bZIP transcription factors and upregulates a number of proapoptotic factors, including GADD34. CHOP seems to be a key player linking the accumulation of misfolded proteins to oxidative stress and apoptosis [33]. Results from further studies showed that ATF4 is the key signal for autophagy induced by ER-stress. Moreover, autophagy is switched to apoptosis by subsequent CHOP up-regulation, suggesting that the changeover switch between autophagy and apoptosis is located between ATF4 to CHOP in the PERK pathway [25]. However, the signal for selection of one of these two protective responses is unknown. The functional relationship between autophagy, ATF4, and CHOP, and the shift mechanism between autophagy and apoptosis are not sufficiently understood. On the other hand, eliminating the PERK-mediator CHOP does not ameliorate the phenotype of R98C mutant mice [40]. Interestingly, translational control of ATF4 mediated by GCN2eIF2 phosphorylation appears important for hippocampal synaptic plasticity and memory, as targeting inactivation of ATF4 can enhance



synaptic plasticity and memory storage [8]. After exposure to ER stress, the pathway activated most rapidly is translational repression mediated by PERK. Cleavage of ATF6 also follows fairly rapidly after exposure to stress. However, expression of the genes controlled by this sensor protein requires nuclear translocation of its cytoplasmic domain, the induction of transcription and protein synthesis [37].

IRE1 also initiates a pathway of transcriptional induction, but the full activation of this response is delayed, relative to the activation of the ATF4 and ATF6 pathways [46]. IRE1 pathway activation induces XBP1 splicing. IRE1 cleaves XBP1 mRNA to a spliced form of XBP1 that translates XBP1s to up-regulate UPR genes encoding factors involved in ER protein folding and degradation [45]. When activated, Ire1 oligomerizes and this promotes trans-autophosphorylation and activation of the RNase [44].

Process IRE1 sends Release message to BiP via the shared channel bind-toIRE1. The splicing event of XBP1 creates a translational frameshift in XBP1 to produce an active transcription factor. IRE1 is also suggested to be a contributor to apoptosis during certain ER stress arrangements [42]. IRE1 can bind the scaffolding protein TRAF2, which serves to activate JNK, a potent inducer of apoptosis [36, 43]. Scientists in studies with a mouse model of early-onset CMT noted increased expression of JNK, a potential activator of c-Jun transcription. There is not full comprehension of how the MpzR98C arrests or slows myelination but it most likely involves regulation of the transcription factors c-Jun and Krox-20. Thus, authors assumed that induction of the UPR could promote the increased expression of c-Jun, an inhibitor of myelination, in R98C Schwann cells and drive their de-differentiation [40]. In order to model this hypothesis we define the processes JNK, C-JUN, KROX. Process IRE1 abolishes Xbp1 mRNA splicing and in combination with signalling mediated by ASK1 activates JNK [27]. Activated JNK phosphorylates c-Jun and can stimulate and maintain its expression [18]. Due to the complexity of the reactions we only present an elementary reaction model, shown in Fig. 7.2.

Further studies with additional crossing of R98C or R98C-CHOP null mice with Ire1-null animals could help define the sequence of reactions and test this assumption.

ATF6 is a type II ER transmembrane protein. Under conditions of ER stress, ATF6 is released from BiP and transported from the ER to the Golgi apparatus, where it is cleaved by Golgi-resident proteases, first by S1P (site 1 protease) and then in an intramembrane region by S2P (site 2 protease) to release the cytosolic DNA-binding portion, ATF6f (f for fragment) [17]. From there, ATF6f moves to the nucleus and works synergistically or separately with XBP1s to regulate UPR gene [36]. The process by which ATF6 translocate from the ER to the Golgi for cleavage to produce functional forms is termed regulated intramembrane proteolysis (RIP) [7]. In Fig. 7.3 is presented a multi-step communication between ATF6 and cleaved-ATF6.

In conclusion, an important question raised is why two transcription factors (ATF6 and XBP1) are involved in induction of ER chaperone. Probably with two

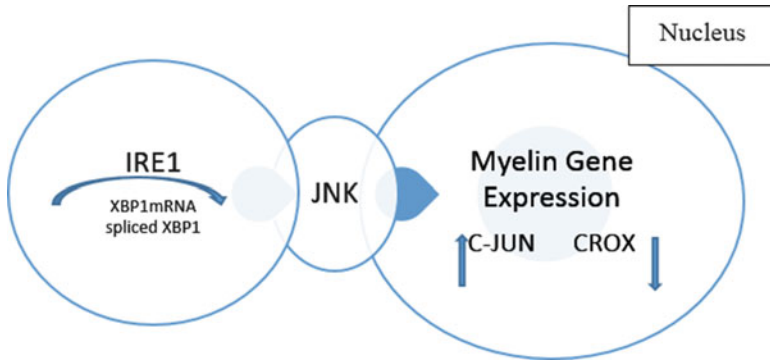


**Fig. 7.2** Activation of the IRE1 pathway leads to splicing of XBP1. Induced Jnk activity alters the expression of C-JUN and KROX, which regulate myelin gene expression

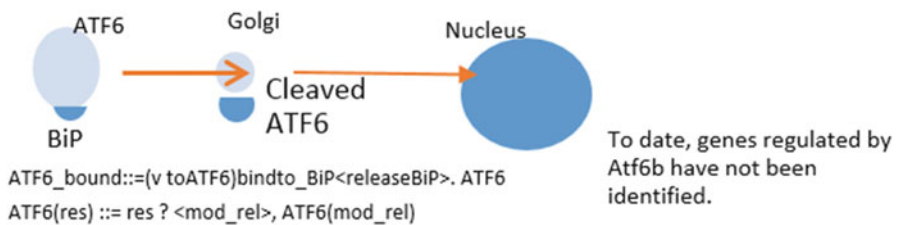


**Fig. 7.3** UPR activations induces ATF6 cleavage

transcriptional induction systems mammalian cells have become capable of coping with ER stress more effectively regardless the amount of unfolded proteins accumulated. It is suggested that mammalian protection cells have gained versatility by developing IRE1-dependent and -independent signaling pathways for activating the UPR [25].

**Conclusion**

Our aim is the development of an integrated model which will be able to interpret biological data and lead to new insights linking protein misfolding and clearance to demyelinating peripheral neuropathies. Our goal for future work will concentrate on developing models that will simulate biological functions in order to find new potential targets for improved diagnostics and treatment. The behavior of biomolecular systems is traditionally studied with Dynamical Systems Theory (described via differential equations) [13], which abstracts the cell and its molecular constituents to their quantifiable properties (e.g., concentration, position) and their couplings. In this work, we began to model this abstraction with the pi-calculus, a process algebra for the

(continued)

(continued)

representation and study of concurrent mobile systems. The development of a model will provide a framework to guide our research from theory to hypotheses. As a first step we tried to identify the basic entities of biomolecular systems and the events in which they participate. The next step is to develop general guidelines for the abstraction of these entities to the mathematical domain of the pi-calculus, which will then be employed for the modeling and study of real complex biomolecular systems. While the function of certain biomolecular systems may be abstracted in a qualitative or semi-quantitative way, the functionality of others critically depends on quantitative aspects. Moreover, different communications have different rates, and communications are selected based on probabilistic conditions. Thus, in order to study the stochastic behavior of specific systems, a stochastic extension of p-calculus will be used. A computable abstraction allows both the simulation of dynamic behavior and qualitative and quantitative reasoning on a biomolecular systems' properties. The only limitation of this computer language is when abstracting systems for which knowledge is limited and cannot be broken down to elementary processes. Recent evidence has implicated that protein misfolding and aggregation are implicated in the pathogenesis of CMT disease. Future studies will be able to identify how misfolding of these membrane proteins, with different topologies, contributes to demyelinating neuropathy.

## References

1. Alexiou AT, Psiha MM, Rekkas JA, Vlamos PM (2011) A stochastic approach of mitochondrial dynamics. *World Acad Sci Eng Technol* 79:77–81
2. Alexiou AT, Psiha MM, Vlamos PM (2011) A stochastic model for protein synthesis and activation through RNA-protein interaction in bioambients calculus. *Comput Technol Appl* 2:565–569
3. Barisic N, Claeys K, Sirotkovic-Skerlev M, Lfgren A, Nelis A, De Jonghe PEA (2008) Charcot–Marie–Tooth disease: a clinico-genetic confrontation. *Ann Hum Genet* 72 (Pt 3):41641
4. Berciano A, Garca E, Gallardo C, Ramn, Combarros O (2009) Phenotype and clinical evolution of Charcot–Marie–Tooth disease type 1A duplication. *Adv Exp Med Biol* 652:183200
5. Berger P, Young P, Suter U (2002) Molecular cell biology of Charcot–Marie–Tooth disease. *Neurogenetics* 4(1):1–15
6. Bertolotti A, Zhang Y, Hendershot LM, Harding HP, Ron D (2000) Dynamic interaction of BiP and ER stress transducers in the unfolded-protein response. *Nat Cell Biol* 2(6):326–332
7. Cao SS, Kaufman RJ (2012) Unfolded protein response. *Curr Biol* 22(16):R622–R626
8. Chen A, Muzzio IA, Malleret G, Bartsch D, Verbitsky M, Pavlidis P, Yonan AL, Vronskaya S, Grody MB, Cepeda I et al (2003) Inducible enhancement of memory storage and synaptic plasticity in transgenic mice expressing an inhibitor of atf4 (creb-2) and c/ebp proteins. *Neuron* 39(4):655–669

9. Chin L, Olzmann J, Li L (2008) Aggresome formation and neurodegenerative diseases: therapeutic implications. *Curr Med Chem* 15(1):47–60 (2008)
10. Chin LS, Lee SM, Li L (2013) Simple: a new regulator of endosomal trafficking and signaling in health and disease. *Commun Integr Biol* 6(3), 799–816 (2013)
11. Dyck PJ, Lambert EH (1968) Lower motor and primary sensory neuron diseases with peroneal muscular atrophy: I. neurologic, genetic, and electrophysiologic findings in hereditary polyneuropathies. *Arch Neurol* 18(6):603
12. Eylar EH, Uyemura K, Brostoff SW et al (1979) Proposed nomenclature for pns myelin proteins. *Neurochem Res* 4(2):289–293
13. Fontana W, Buss LW (1996) The barrier of objects: from dynamical systems to bounded organizations. Citeseer
14. Fortun WA, Dunn Jr S, Joy JL, Notterpek L (2003) Emerging role for autophagy in the removal of aggresomes in Schwann cells. *J Neurosci* 23(33):10672–10680
15. Fortun J, Go JC, Li J, Amici SA, Dunn Jr WA, Notterpek L (2006) Alterations in degradative pathways and protein aggregation in a neuropathy model based on PMP22 overexpression. *Neurobiol Dis* 22(1):153–164
16. Greenfield S, Brostoff S, Eylar EH, Morell P (1973) Protein composition of myelin of the peripheral nervous system. *J Neurochem* 20(4):1207–1216
17. Haze K, Yoshida H, Yanagi H, Yura T, Mori K (1999) Mammalian transcription factor atf6 is synthesized as a transmembrane protein and activated by proteolysis in response to endoplasmic reticulum stress. *Mol Biol Cell* 10(11):3787–3799
18. Jessen KR, Mirsky R (2008) Negative regulation of myelination: relevance for development, injury, and demyelinating disease. *Glia* 56(14):1552–1565
19. Juárez P, Palau F (2012) Neural and molecular features on Charcot–Marie–Tooth disease plasticity and therapy. *Neural Plast* 2012. Article ID 171636, 11 pages, 2012. doi:[10.1155/2012/171636](https://doi.org/10.1155/2012/171636)
20. Kamholz J, Awatramani R, Menichella D, Jiang H, Xu W, Shy M (1999) Regulation of myelin-specific gene expression: relevance to CMT1. *Ann N Y Acad Sci* 883(1):91–108
21. Krajewski K, Lewis R., Fuerst D et al (2000) Neurological dysfunction and axonal degeneration in Charcot–Marie–Tooth disease type 1a. *Brain* 44:1299–1304
22. Lee YC, Lin KP, Chang MH, Liao YC, Tsai CP, Liao KK, Soong BW (2010) Cellular characterization of mpz mutations presenting with diverse clinical phenotypes. *J Neurol* 257 (10):1661–1668
23. Lee SM, Olzmann JA, Chin LS, Li L (2011) Mutations associated with Charcot–Marie–Tooth disease cause SIMPLE protein mislocalization and degradation by the proteasome and aggresome–autophagy pathways. *J Cell Sci* 124(19):3319–3331
24. Lee SM, Chin LS, Li L (2012) Protein misfolding and clearance in demyelinating peripheral neuropathies: therapeutic implications. *Commun Integr Biol* 5(1):107–110
25. Matsumoto H, Miyazaki S, Matsuyama S, Takeda M, Kawano M, Nakagawa H, Nishimura K, Matsuo S (2013) Selection of autophagy or apoptosis in cells exposed to ER-stress depends on ATF4 expression pattern with or without chop expression. *Biol Open* 2(10):1084–1090
26. Milner R (1999) Communicating and mobile systems: the pi calculus. Cambridge University Press, Cambridge
27. Nishitoh H, Saitoh M, Mochida Y, Takeda K, Nakano H, Rothe M, Miyazono K, Ichijo H (1998) Ask1 is essential for JNK/SAPK activation by TRAF2. *Mol Cell* 2(3):389–395
28. Pareek S, Notterpek L, Snipes GJ, Naef R, Sossin W, Laliberté J, Iacampo S, Suter U, Shooter EM, Murphy RA (1997) Neurons promote the translocation of peripheral myelin protein 22 into myelin. *J Neurosci* 17(20):7754–7762
29. Pareyson D, Marchesi C (2009) Diagnosis, natural history, and management of Charcot–Marie–Tooth disease. *Lancet Neurol* 8(7):654–667
30. Patzkó Á, Bai Y, Saporta MA, Katona I, Wu X, Vizzuso D, Feltri ML, Wang S, Dillon LM, Kamholz J et al (2012) Curcumin derivatives promote Schwann cell differentiation and improve neuropathy in R98C CMT1B mice. *Brain* 135(12):3551–3566

31. Pennuto M, Tinelli E, Malaguti M, Del Carro U, D'Antonio M, Ron D, Quattrini A, Feltri ML, Wrabetz L (2008) Ablation of the UPR-mediator CHOP restores motor function and reduces demyelination in Charcot–Marie–Tooth 1b mice. *Neuron* 57(3):393–405
32. Pennuto M, Tinelli E, Malaguti M et al (2008) Ablation of the UPR-mediator CHOP restores motor function and reduces demyelination in Charcot–Marie–Tooth 1b mice. *Neuron* 57(3):393–405
33. Rajesh K, Papadakis AI, Kazimierczak U, Peidis P, Wang S, Ferbeyre G, Kaufman RJ, Koromilas AE (2013) eIF2 $\alpha$  phosphorylation bypasses premature senescence caused by oxidative stress and pro-oxidant antitumor therapies. *Aging* 5(12):884
34. Regev A, Shapiro E (2004) The  $\pi$ -calculus as an abstraction for biomolecular systems. In: *Modelling in molecular biology*. Springer, Berlin, pp 219–266
35. Regev A, Silverman W, Shapiro E (2001) Representation and simulation of biochemical processes using the pi-calculus process algebra. *Pac Symp Biocomput* 6:459–470
36. Ron D, Walter P (2007) Signal integration in the endoplasmic reticulum unfolded protein response. *Nat Rev Mol Cell Biol* 8(7):519–529
37. Rutkowski DT, Kaufman RJ (2004) A trip to the ER: coping with stress. *Trends Cell Biol* 14(1):20–28
38. Ryan MC, Shooter EM, Notterpek L (2002) Aggresome formation in neuropathy models based on peripheral myelin protein 22 mutations. *J Peripher Nervous System* 7(4):246–246 (2002)
39. Samali A, FitzGerald U, Deegan S, Gupta S (2010) Methods for monitoring endoplasmic reticulum stress and the unfolded protein response. *Int J Cell Biol* p 830307
40. Saporta MA, Shy BR, Patzko A, Bai Y, Pennuto M, Ferri C, Tinelli E, Saveri P, Kirschner D, Crowther M et al (2012) Mpzr98c arrests Schwann cell development in a mouse model of early-onset Charcot–Marie–Tooth disease type 1b. *Brain* 135(7):2032–2047
41. Shen J, Chen X, Hendershot L, Prywes R (2002) Er stress regulation of ATF6 localization by dissociation of BiP/GRP78 binding and unmasking of Golgi localization signals. *Dev Cell* 3(1):99–111
42. Teske BF, Wek SA, Bunpo P, Cundiff JK, McClintick JN, Anthony TG, Wek RC (2011) The eIF2 kinase PERK and the integrated stress response facilitate activation of ATF6 during endoplasmic reticulum stress. *Mol Biol Cell* 22(22):4390–4405
43. Urano F, Wang X, Bertolotti A, Zhang Y, Chung P, Harding HP, Ron D (2000) Coupling of stress in the ER to activation of JNK protein kinases by transmembrane protein kinase IRE1. *Science* 287(5453):664–666
44. Verfaillie T, Salazar M, Velasco G, Agostinis P (2010) Linking ER stress to autophagy: potential implications for cancer therapy. *Int J Cell Biol* 2010, Article ID 930509, 19 pages, 2010. doi:[10.1155/2010/930509](https://doi.org/10.1155/2010/930509)
45. Wang S, Kaufman RJ (2012) The impact of the unfolded protein response on human disease. *J Cell Biol* 197(7):857–867
46. Yoshida H, Matsui T, Hosokawa N, Kaufman RJ, Nagata K, Mori K (2003) A time-dependent phase shift in the mammalian unfolded protein response. *Dev Cell* 4(2):265–271
47. Züchner S, Vance JM (2006) Molecular genetics of autosomal-dominant axonal Charcot–Marie–Tooth disease. *Neuromol Med* 8(1–2):63–74

# Chapter 8

## The Effect of the Shape and Size of Gold Seeds Irradiated with Ultrasound on the Bio-Heat Transfer in Tissue

Ioannis Gkigkitzis, Carlos Austerlitz, Ioannis Haranas, and Diana Campos

**Abstract** The aim of this report is to propose a new methodology to treat prostate cancer with macro-rod-shaped gold seeds irradiated with ultrasound and develop a new computational method for temperature and thermal dose control of hyperthermia therapy induced by the proposed procedure. A computer code representation, based on the bio-heat diffusion equation, was developed to calculate the heat deposition and temperature elevation patterns in a gold rod and in the tissue surrounding it as a result of different therapy durations and ultrasound power simulations. The numerical results computed provide quantitative information on the interaction between high-energy ultrasound, gold seeds and biological tissues and can replicate the pattern observed in experimental studies. The effect of differences in shapes and sizes of gold rod targets irradiated with ultrasound is calculated and the heat enhancement and the bio-heat transfer in tissue are analyzed.

### 8.1 Introduction

Available methods to kill cancer cells may involve X-rays [36],  $\gamma$ -rays [7], beta rays [34], neutrons [38], high-energy electrons [15], protons [40], light and photosensitizers [24], light and gold nanoparticles, surgery, cryosurgery [16], chemicals [39], and hyperthermia [44] and thermoablation [17]. Hyperthermia is heating of certain

---

I. Gkigkitzis

Department of Mathematics and Physics, East Carolina University, Greenville, NC, USA  
e-mail: [gkigkitzisi@ecu.edu](mailto:gkigkitzisi@ecu.edu)

C. Austerlitz • D. Campos  
Clinica Diana Campos, Recife, PE, Brazil

I. Haranas (✉)

Physics and Computer Science, Wilfrid Laurier University, Science Building, Room N2078  
75 University Ave. W, Waterloo, ON, N2L 3C5, Canada  
e-mail: [yiannis.haranas@gmail.com](mailto:yiannis.haranas@gmail.com)

organs or tissues to temperatures between 41 and 48 °C as a treatment of cancer. Thermoablation is the attempt to heat tissues to temperatures above 47 °C (up to 56 °C). Thermoablation is characterized by acute necrosis, coagulation, or carbonization of the tissue. In clinical hyperthermia, thermoablation is mostly undesired [33]. Many institutions have used a target dose 42–43 °C for 60 min at some point within the tumor volume [6]. However, the goal of hyperthermia is to raise the entire tumor volume to 43 °C or above [6]. In ultrasound surgery the cancerous tissue can be destroyed by rising the temperature to cytotoxic level. The desired temperature in tumor is often 50–60 °C. Although lower temperatures could also be used, the use of high temperatures can reduce the treatment time significantly.

Hyperthermia cancer treatment has proven to be an effective method in cancer treatment compare to surgery, chemotherapy and radiation. Hyperthermia has been used on the treatment of many types of cancer, including sarcoma, melanoma, and cancers of the head and neck, brain, lung, esophagus, breast, bladder, rectum, liver, appendix, cervix, peritoneal lining, and prostate [12, 32, 48]. Hyperthermia may include local, regional, and whole-body hyperthermia [3, 48]. In local hyperthermia, heat is applied to a tumor by using external applicators positioned around or near the appropriate region, and energy focused on the tumor to raise its temperature; intraluminal or endocavitary probes placed inside the cavity and inserted into the tumor to deliver energy and heat the area directly [13]; and interstitial probes or needles [4, 5, 13] inserted into the tumor. In this case, the heat source is inserted into the probe. Radiofrequency ablation (RFA) is a type of interstitial hyperthermia that uses radio waves to heat and kill cancer cells. In regional hyperthermia, external applicators may be positioned around the body cavity or organ to be treated, and microwave or radiofrequency energy is focused on the area to raise its temperature. Whole-body hyperthermia is used to treat metastatic cancer that has spread throughout the body.

Hyperthermia in cancer treatment has been achieved by magnetic fluid [23], interstitial microwave probe [13, 14, 41], long frosted contact probe [29], magnetic nanoparticles [22], near-infrared-absorbing nanoparticles [28], gold nanospheres [45], gold nanorods [19], gold iron oxide [30], gold nanoshells [43], gold-coated brass [35], double-doped magnetic silica nanospheres [31], plasmonic photothermal [20], nonradioactive ferromagnetic seed [18] interstitial microwave antenna [26], interstitial laser [8], radiofrequency [41], ultrasound [9], diffuse focus ultrasound [25], focused ultrasound [46], and laser [42].

All such methods described so far make use of needles, probes, nanoparticles, optical fibers, and ferromagnetic alloys plated with gold. However, there is no find in the consulted literature about the use of macro gold rods irradiated with ultrasound to treat cancer tumor. Also, there is no find about hypothermia of normal tissue or organ near the lesion treated with hyperthermia.

This work has the objective to investigate a method and an analytical formalism to provide the optimization of the amount of pure solid gold rods implanted in prostate in terms of heat propagation when it is being irradiated with ultrasound, by measurements and/or analytical calculation, while avoiding hyperthermia of the urethra. The use of ultrasound is largely an effort to reduce the use of chemotherapy

and radiotherapy for treating cancer. Chemotherapy is considered to impose difficulties because drugs often produce harmful side effects. And radiotherapy is also problematic because X-rays travel through normal tissue to arrive at the tumor site and it is known that the X-rays sometimes damage normal tissue. Ultrasound has the ability to noninvasively concentrate energy into a controllable volume deep in tissue [47].

## 8.2 Material and Methods

The insufficiency of the response of single nanospheres to energy sources for the production of controllable hyperthermia and the need to use ensembles of nanoparticles to augment the contribution have been theoretically demonstrated [11, 19]. Heating of surrounding matrix becomes possible if particle size is large enough (in the presence of an amplified electric field enhancement). Gold seeds are the “hot” spots where the heating intensity is greatly enhanced. In this study, the attempt is to initiate a theoretical computational analysis for the optimization of spatiotemporal temperature distribution due to hyperthermia induced by gold seeds, macro-rods and macrospheres, heated through ultrasound, over a square matrix domain. Heat conduction is described by partial differential heat diffusion equations. These macroscopic equations are no longer applicable in scales where the temperature fields are not considered continuous (length scale comparable to or smaller than the mean free path of the material) [19, 21]. However, the equations are applicable and describe the heat diffusion at larger scales, such as mm scale.

Modeling ultrasound heating of a single macro-rod surrounded by a water medium is a first step towards understanding the thermal processes of macro-rod heating in relation to possible imaging parameters. Ultrasound directed to a dissipative medium leads to energy transfer, partial absorption, and conversion to heat. At the power level considered in this study (less than  $1 \text{ W/cm}^2$ ), heating contributions due to direct linear and nonlinear absorption of ultrasonic pressure by water or tissue will be neglected. Phenomenological models for ultrasound wave amplitude attenuation account for wave amplitude loss due to various mechanisms (absorption, scattering, mode conversion) as ultrasound travels through materials. The higher the frequency, the more energy is consumed in the increase of molecular motion, and the less energy for the sound beam to propagate. However, since therapeutic ultrasound has a frequency range of 0.7 and 5.0 MHz and we are interested in tissue penetration of a few centimeters (prostate cancer), for simplicity, attenuation is described by a constant (attenuation coefficient) in the power rate equation. These effects will be considered in detail in future studies.

A temperature distribution model for either a fluid or tissue containing a heating source (gold Nano spheres heated by a laser beam) based on the Pennes’ bio-heat equation was introduced in [11] and we adjust this model to our domain:



$$\rho C_p \frac{\partial T}{\partial t} = \nabla(k \nabla T) + Q + Q_{vh} + W \quad (8.1)$$

where  $t$  is time,  $T$  is the temperature,  $C_p$  is the heat capacity,  $k$  is the thermal conductivity,  $\rho$  is the density,  $Q$  is the heat source,  $Q_{vh}$  is the viscous heating, and  $W$  is the work pressure. The last two terms can be set equal to 0 for simplicity. The metabolic heat generation is considered negligible. Since the heat conductivity of gold is high, temperature gradients across the rod are weak so that temperature inside it should remain essentially constant. An initial temperature,  $T_1 = T$  is assigned on the entire domain and the appropriate boundary condition for the tissue inward heat flux  $q_0$  is

$$q_0 = -\vec{n} \cdot \nabla(k \nabla T) = h (T_{EXT} - T) \quad (8.2)$$

The heat transfer coefficient  $h$  enters the equation, as unit power per Kelvin and unit area (SI unit:  $W/m^2K^1$ ). The exterior temperature of the cooling fluid is  $T_{EXT}$ . The heat transfer problem is solved with appropriate boundary conditions knowing that healthy tissues (urethra) surrounding the infected region should be preserved and its temperature should be maintained constant. The value of  $h$  depends on the geometry and the ambient thermal conditions. Since metabolic heat generation is negligible in this model,  $Q$  is determined by the absorbed ultrasound energy in the tissue given by [2]

$$Q = a \frac{|P|^2}{\rho c} \quad (8.3)$$

where  $c$  is the speed of sound in the medium,  $a$  is the attenuation coefficient and  $P$  is the acoustic pressure which is the time harmonic ultrasound field solution of the Helmholtz equation in an inhomogeneous medium [2]:

$$\nabla \left( \frac{1}{\rho} \nabla P \right) - \frac{1}{\rho c^2} \frac{\partial^2 P}{\partial t^2} = 0 \quad (8.4)$$

where  $k$ , the wave number, is given by  $k = (\rho c)^{-1/2}$ . It has been generally accepted that it is an extremely challenging task to solve the Helmholtz equation even numerically, in particular, for the high-frequency cases and for arbitrary domains and boundary conditions. For ultrasound solution waves, the acoustic pressure is related to quantities and properties such as the underlying wave velocity, the characteristic acoustic “impedance,” the particle velocity (particles of the medium that are set into oscillation by the frequency associated with the wave) and organ characteristic scatter signature due to its structure (scattered echoes originating from relatively small, weakly reflective, irregularly shaped objects such as blood cells) and the variable compressibility of the domain. The lack and/or uncertainties of measurements practically constrain the identifiability of these parameters and we

choose a simple pattern oriented thermal modeling of the bio-heat transfer equation where we sample over different values of the gold rod heat source values  $Q$  because it gives good agreement with the main features of the experimental data as described later in this section. Results on the applications of ultrasound have been published by other authors for 600, 300, 60, and 10 s into the heating procedure [21] and simulations have been obtained for 180–300 s [49]. The COMSOL Multiphysics program ([48] Royal Institute of Technology in Stockholm, Sweden) is used to compute the temperature spatial distribution at the nodes of a 2-D finite element mesh. The heat source  $Q$  (unit power per unit volume) describes heat generation within the domain.

Comparisons between experimental measurements and the heat transfer-predicted values are available in the literature [19] for models of hyperthermia induced by gold nanoparticle dispersions in different laser energy levels (0.008, 0.016, and 0.032 W/mm<sup>3</sup>) with good agreement in most cases, and the same scale of ultrasound energy levels is used for the simulations but results for higher and lower energies are analyzed. All constants and material properties used in the solution of the bio-heat diffusion can be found in the “built-in” databases of predefined materials for COMSOL Modules.

In the figures (Figs. 8.1a, b, 8.2a, b, 8.3a, b, 8.4a, b, 8.5a, b, 8.6a, b, 8.7a, b, 8.8a, b, and 8.9a–d) the corresponding simulations can be found for different sizes and shapes of gold seeds. One side of the domain corresponds to a cooling boundary (Fig. 8.10).

### 8.3 Results and Discussion

A theoretical computational analysis for the determination of the pattern of the spatiotemporal temperature distribution due to hyperthermia induced by gold seeds (macro-rods and macro-spheres) heated through ultrasound has been carried out. A 2-D simulation of the ultrasound induced hyperthermia in the tissue is demonstrated. The temperature distributions resulting from the heating of gold seeds are calculated using the bio-heat equation. For ultrasound generated heat at the gold seed of rates 10<sup>5</sup>–10<sup>6</sup> W/m<sup>3</sup> plots of temperature raise against time and against radial and axial coordinate, have shown that the endpoint temperature depends on the gold target size. The bio-heat transfer partial differential equation has been simulated over a square domain, with a side boundary condition to describe the cooling of the urethra that leads to minimal side effect of ultrasound-gold seed heating of the surrounded healthy tissue. Different irradiation times up to 1,000 s have been monitored, and the dimensions of the domain and the seed can vary according to the desired design. Relative deviations have now been studied in detail as in the case of 1 mm × 10 mm gold rod (with the experiment). When the heat of the gold seeds was raised to appropriate temperatures, the bio-heat transfer in tissue in the parallel axis of the rods to reach 43 °C was found to be in the order of 0.5–1 cm for the 1 mm × 10 mm rod. In the case of the

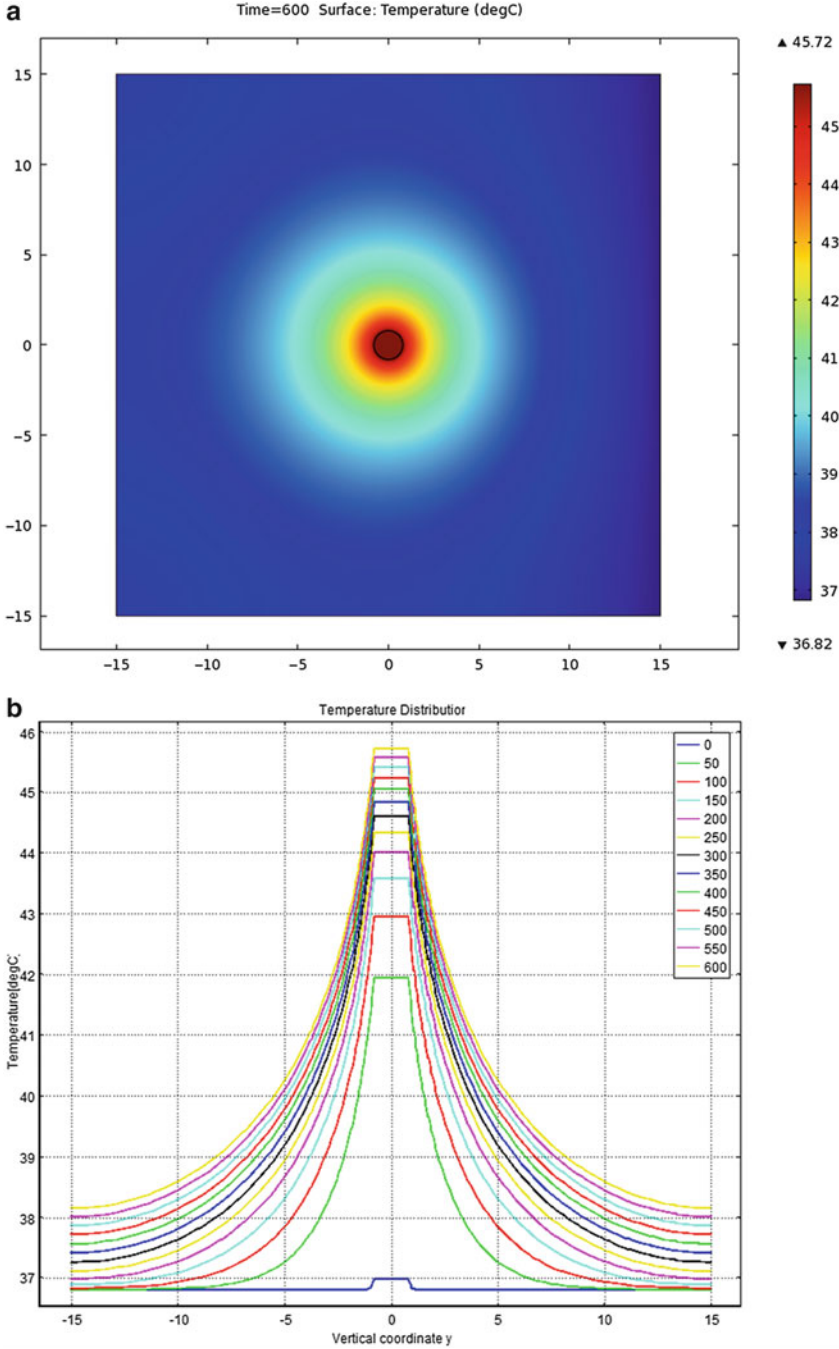


**Fig. 8.1** (a and b) Contour plot and temperature distribution plot of the temperature field of the temperature field in the target area at volumetric heat generation rate  $6 \times 10^6 \text{ W/m}^3$  and a run time of 600 s, for gold sphere of radius 0.8 mm in a  $30 \text{ mm} \times 30 \text{ mm}$  square domain

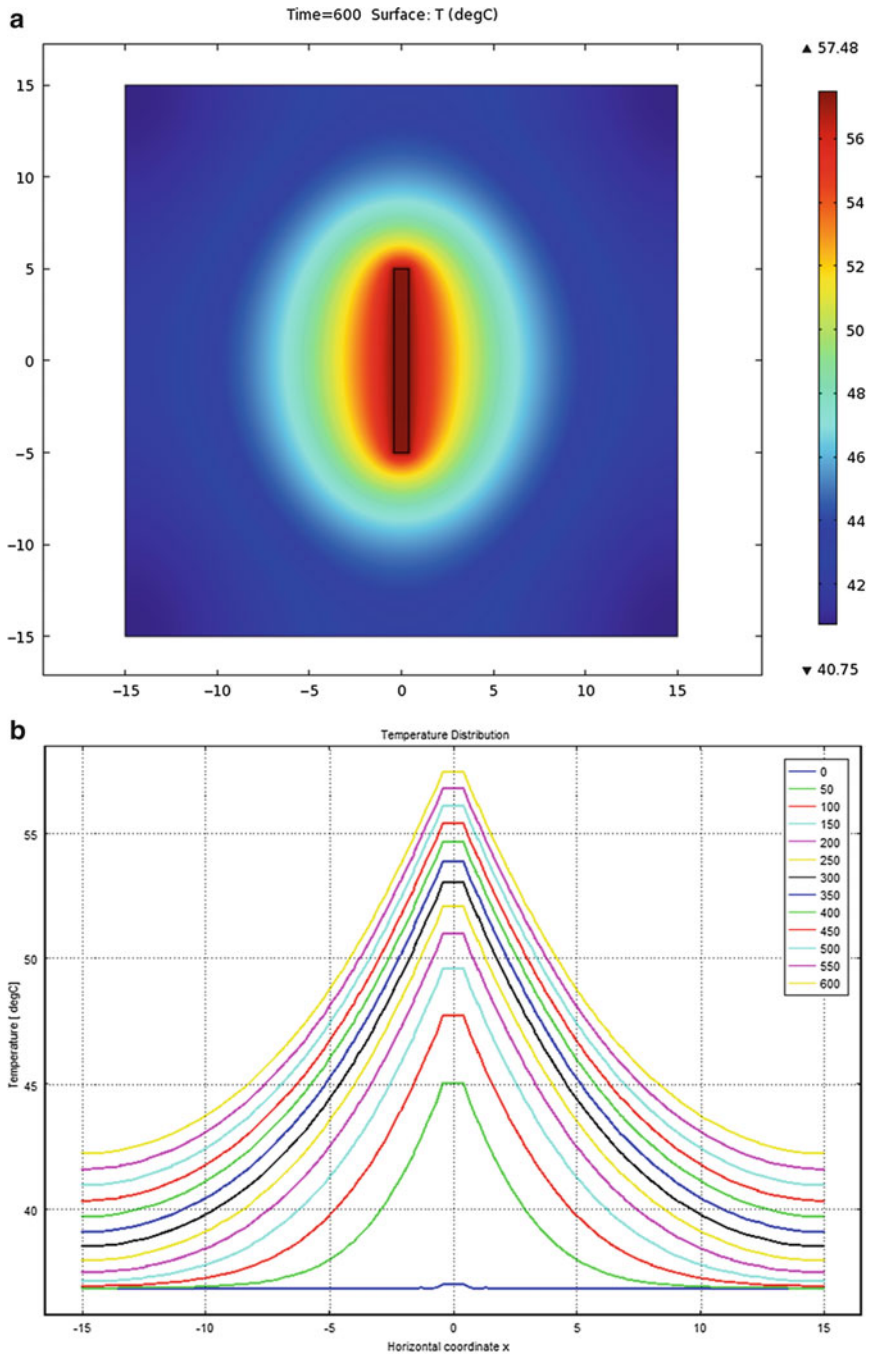


**Fig. 8.2** (a and b) Contour plot and temperature distribution plot of the temperature field of the temperature field in the target area at volumetric heat generation rate  $6 \times 10^6 \text{ W/m}^3$  and a run time of 600 s, for gold rod of  $0.8 \text{ mm} \times 10 \text{ mm}$  in a  $30 \text{ mm} \times 30 \text{ mm}$  square domain

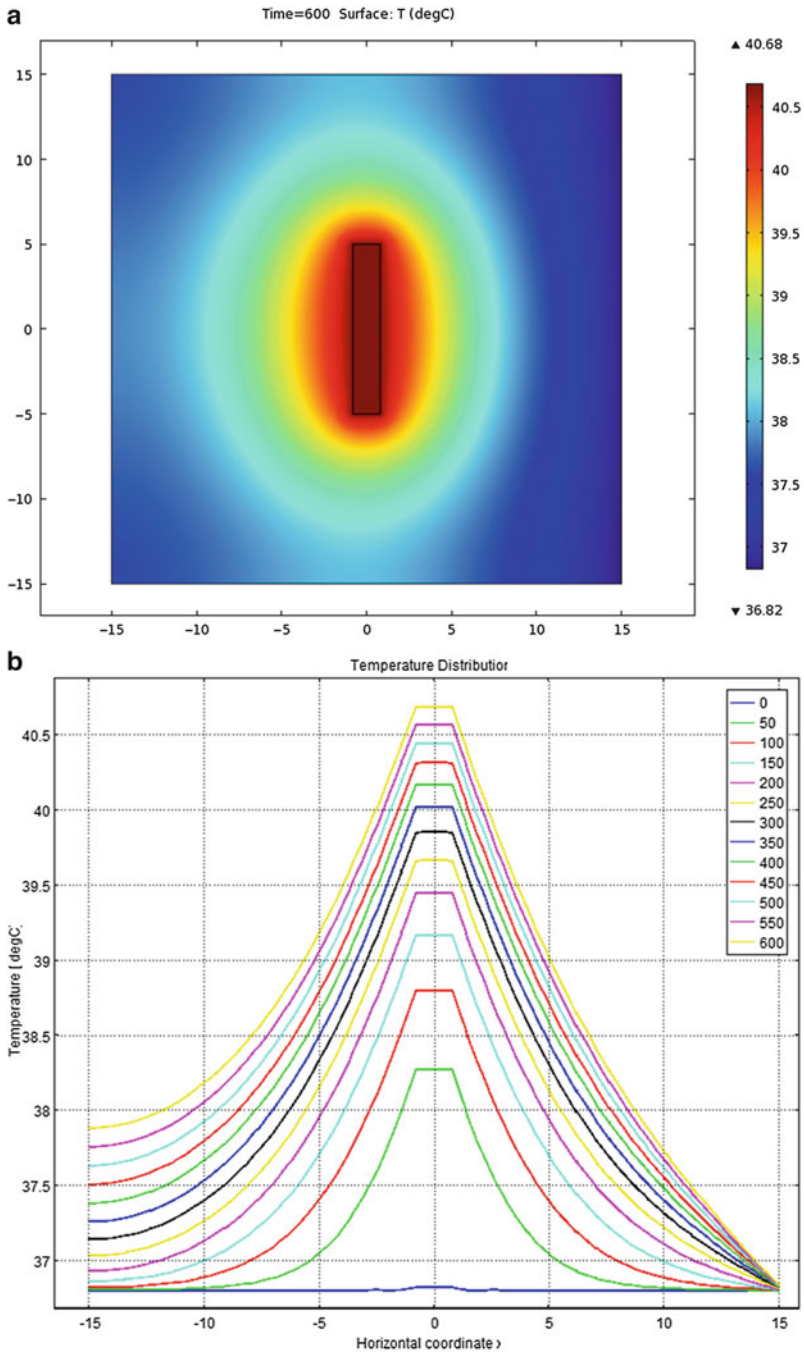


**Fig. 8.3** (a and b) Contour plot and temperature distribution plot of the temperature field of the temperature field in the target area at volumetric heat generation rate  $6 \times 10^5 \text{ W/m}^3$  and a run time of 600 s, for gold rod of  $1.6 \text{ mm} \times 10 \text{ mm}$  in a  $30 \text{ mm} \times 30 \text{ mm}$  square domain

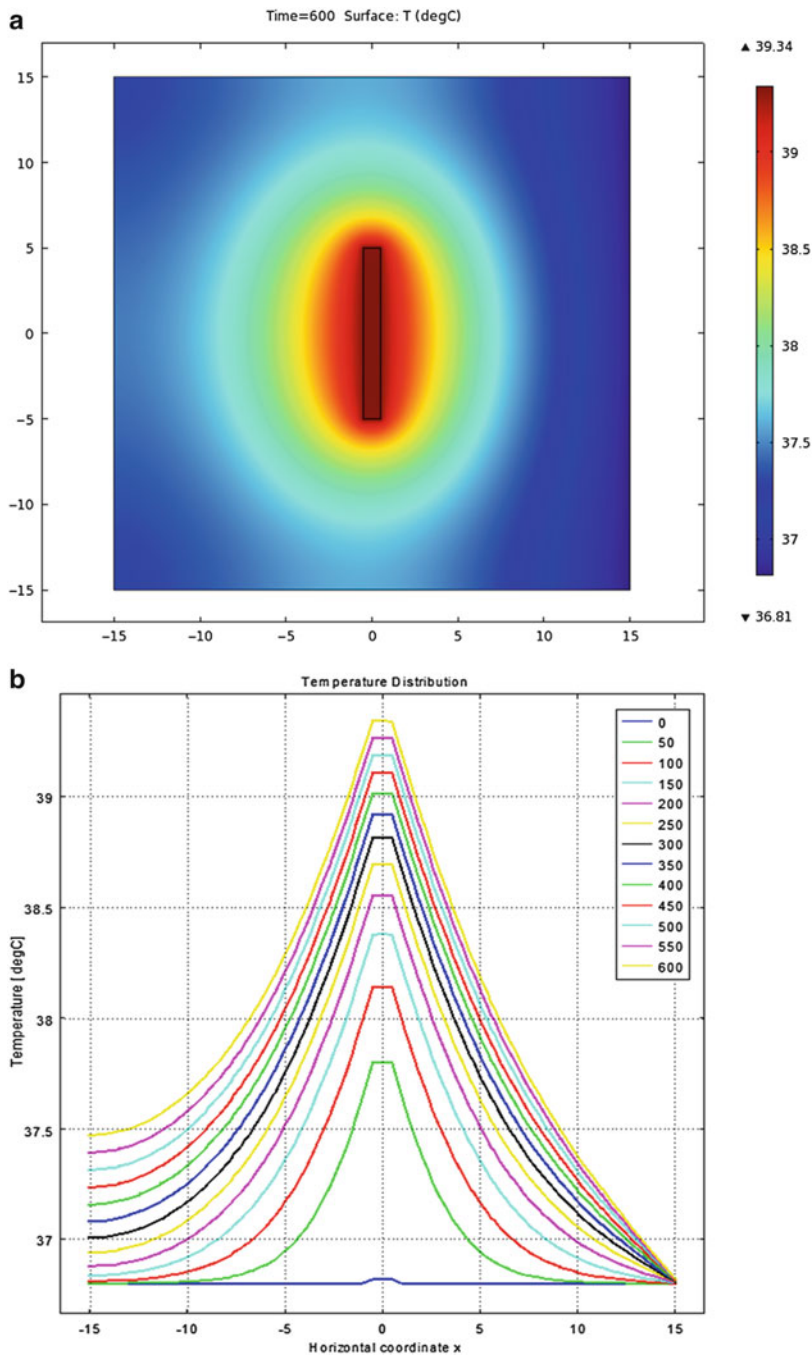
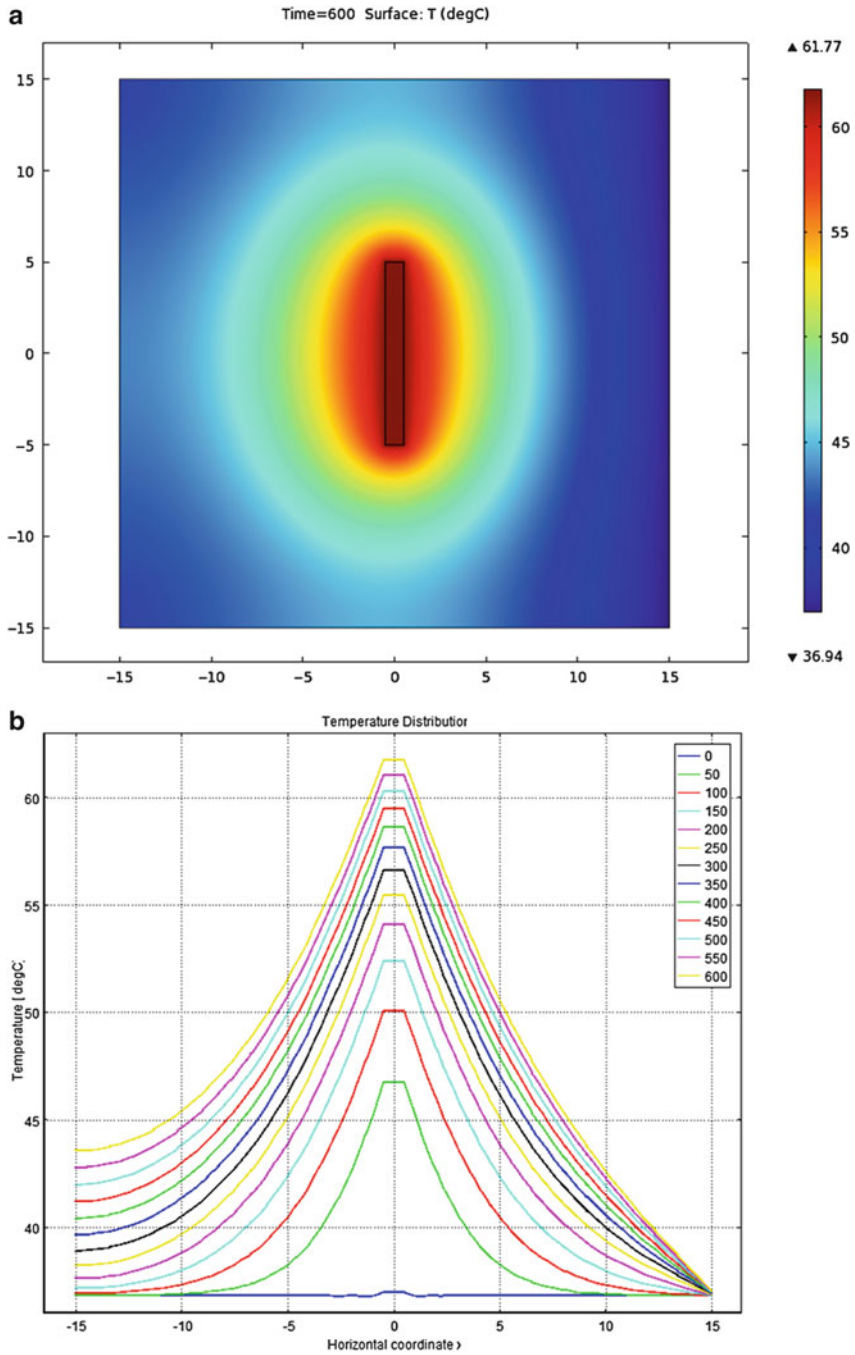
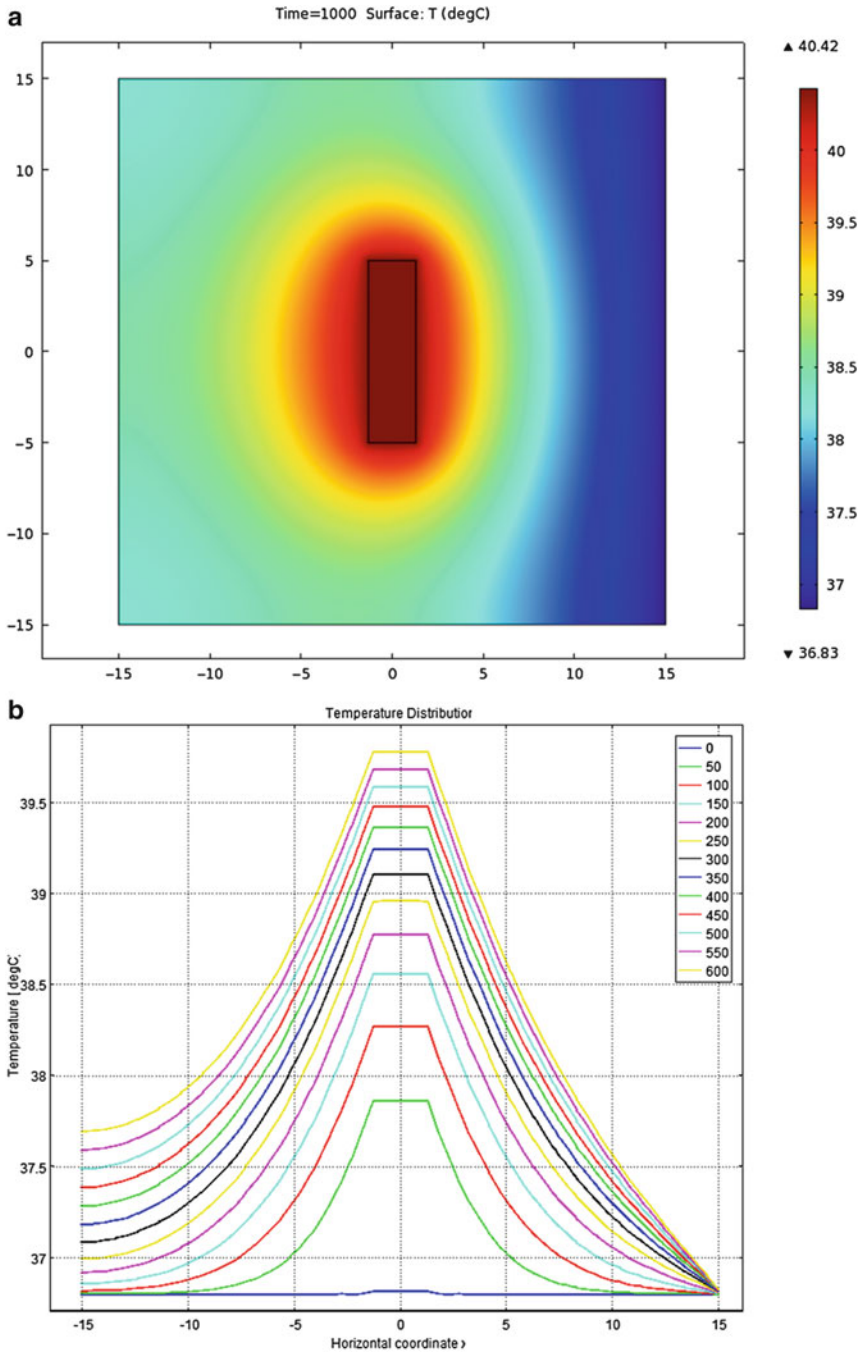


Fig. 8.4 (a and b) Contour plot and temperature distribution plot of the temperature field of the temperature field in the target area at volumetric heat generation rate  $6 \times 10^5 \text{ W/m}^3$  and a run time of 600 s, for gold rod of  $1.0 \text{ mm} \times 10 \text{ mm}$  in a  $30 \text{ mm} \times 30 \text{ mm}$  square domain





**Fig. 8.5** (a and b) Contour plot and temperature distribution plot of the temperature field of the temperature field in the target area at volumetric heat generation rate  $Q = 6 \times 10^6 \text{W/m}^3$  and a run time of 600 s, for gold rod of 1.0 mm  $\times$  10 mm in a 30 mm  $\times$  30 mm square domain



**Fig. 8.6** (a and b) Contour plot and temperature distribution plot of the temperature field of the temperature field in the target area at volumetric heat generation rate  $Q = 3 \times 10^5 \text{ W/m}^3$  and a run time of 1,000 s, for gold rod of  $2.6 \text{ mm} \times 10 \text{ mm}$  in a  $30 \text{ mm} \times 30 \text{ mm}$  square domain



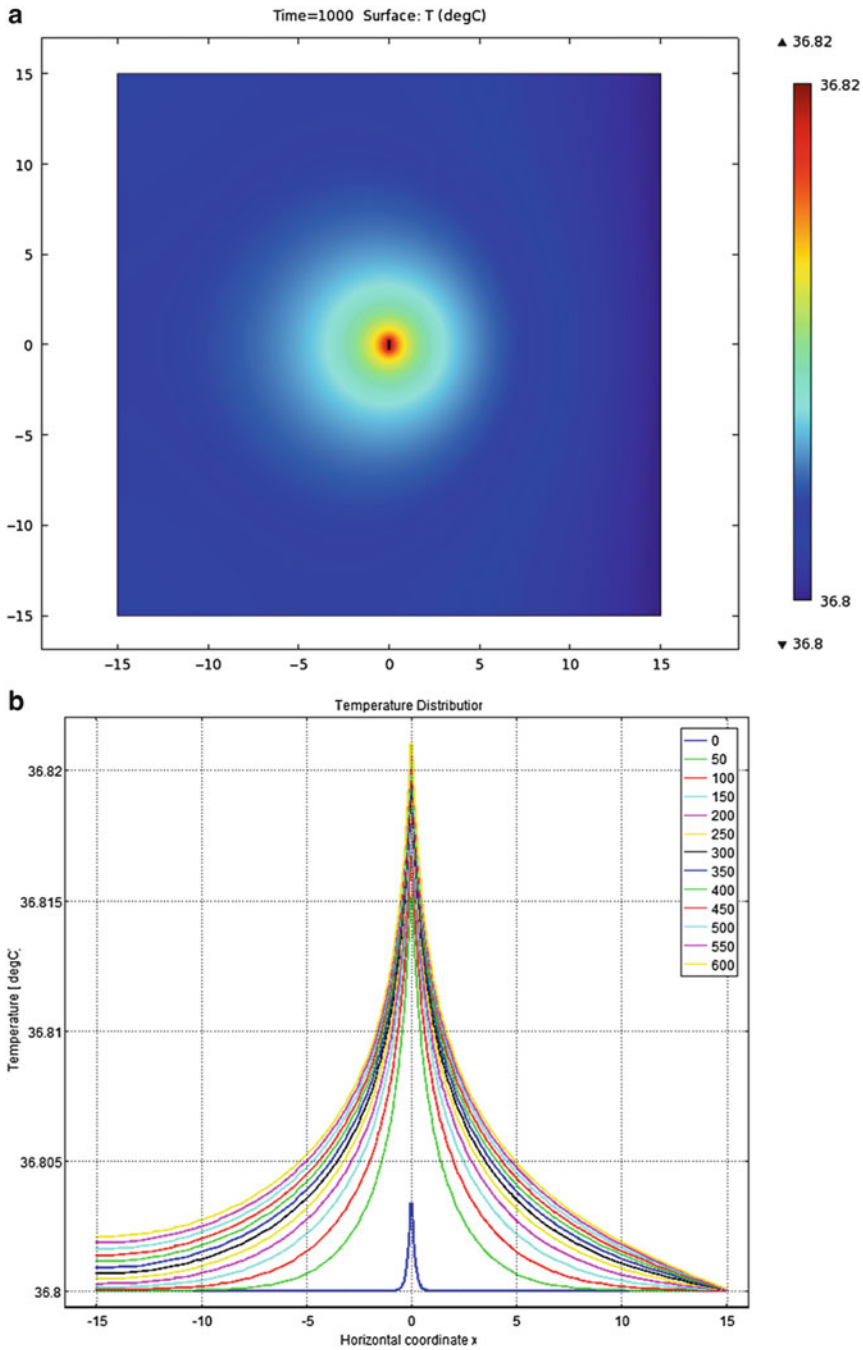


**Fig. 8.7** (a and b) Contour plot and temperature distribution plot of the temperature field of the temperature field in the target area at volumetric heat generation rate  $Q = 6 \times 10^5 \text{W/m}^3$  and a run time of 1,000 s, for gold rod of  $6 \mu\text{m} \times 50 \mu\text{m}$  in a  $30 \text{mm} \times 30 \text{mm}$  square domain

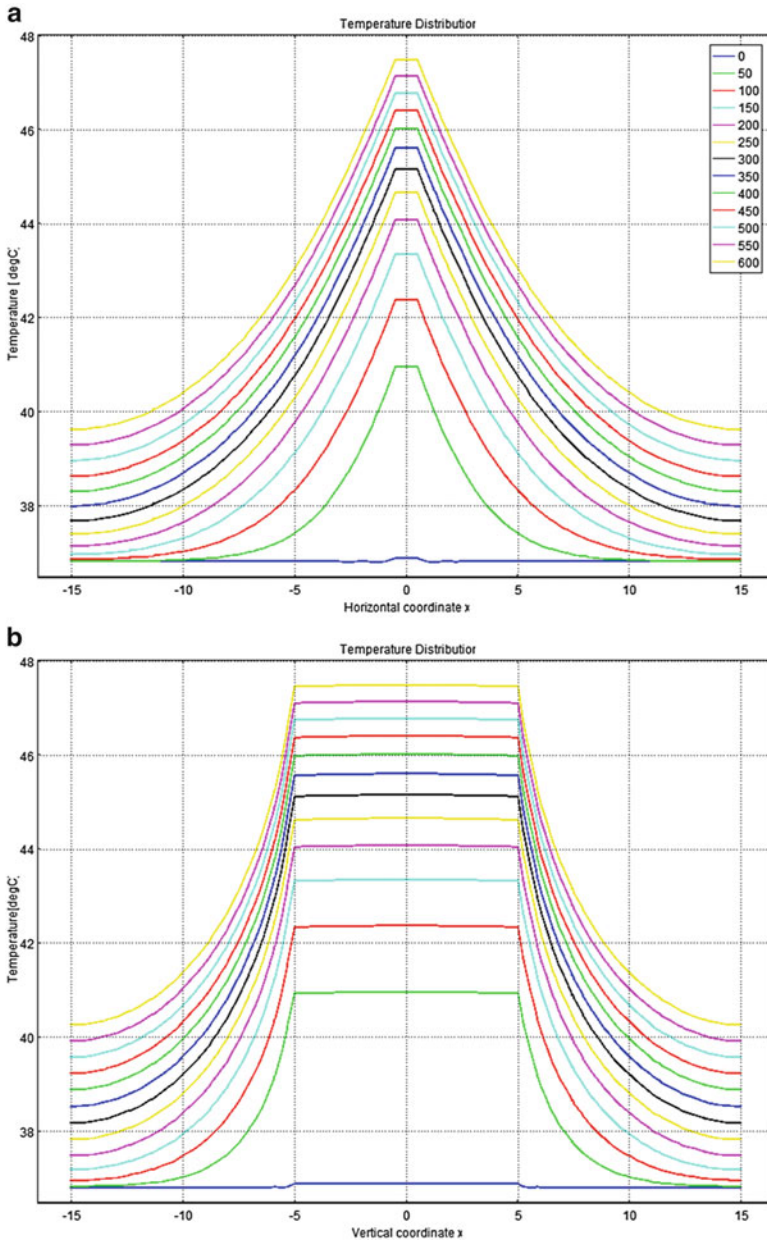


**Fig. 8.8** (a and b) Temperature distribution plot of the temperature field of the temperature field in the target area at volumetric heat generation rate  $Q = 2.4 \times 10^6 \text{W/m}^3$  and a run time of 600 s, for gold rod of 1 mm  $\times$  10 mm in a 30 mm  $\times$  30 mm square domain

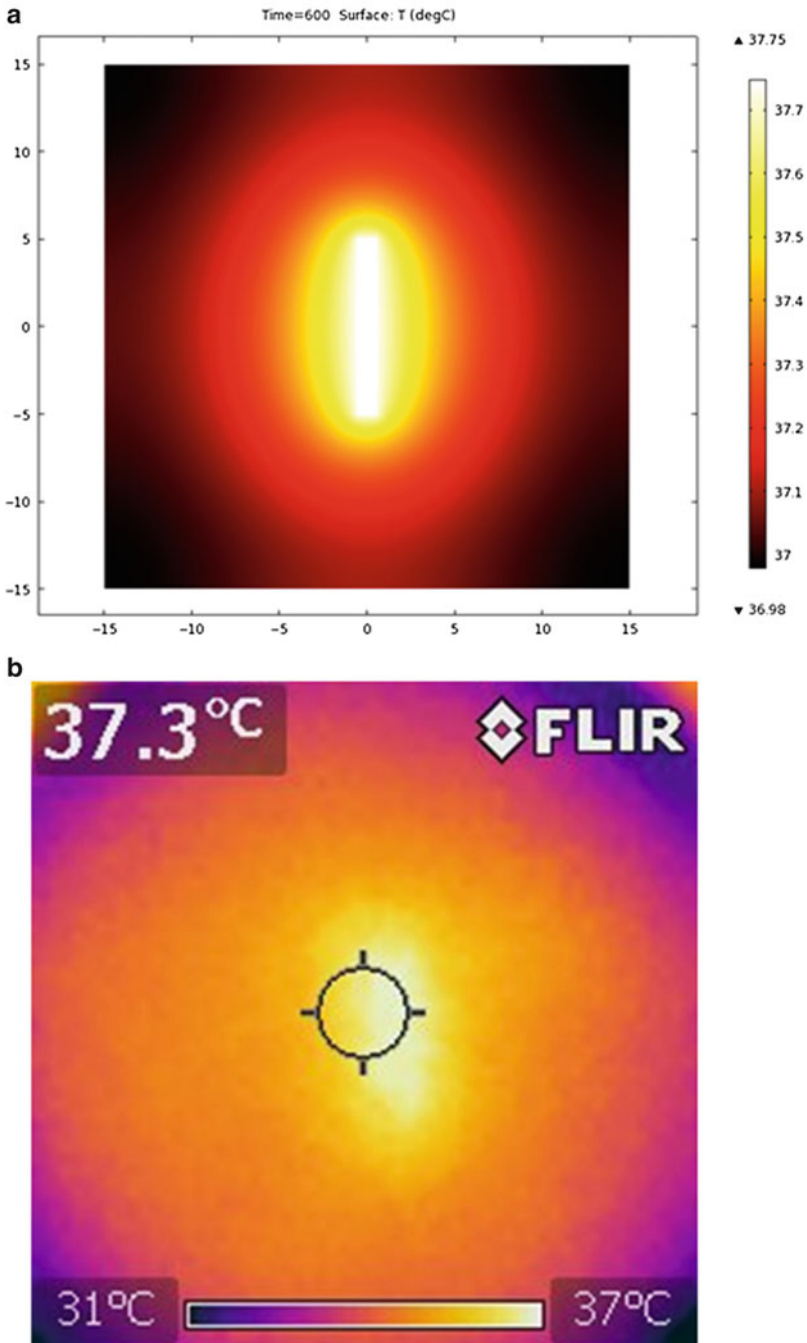


**Fig. 8.9 (a–d)** Contour plot and temperature distribution plot of the temperature field of the temperature field in the target area at volumetric heat generation rate  $Q = 2.2 \times 10^5 \text{ W/m}^3$  and a run time of 1,000 s, for gold rod of 1 mm  $\times$  10 mm in a 30 mm  $\times$  30 mm square domain. No boundary condition for this graph. Comparison of theoretical results (*left column*) vs. experimental results (*right column*) (communicated by Austerlitz, experiment with gold rod inserted in chicken breast and irradiated with ultrasonic energy of the given heat generation rate and run time)

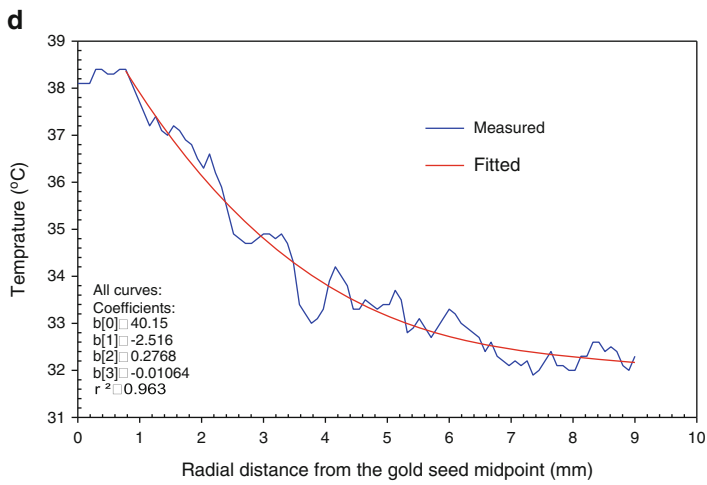
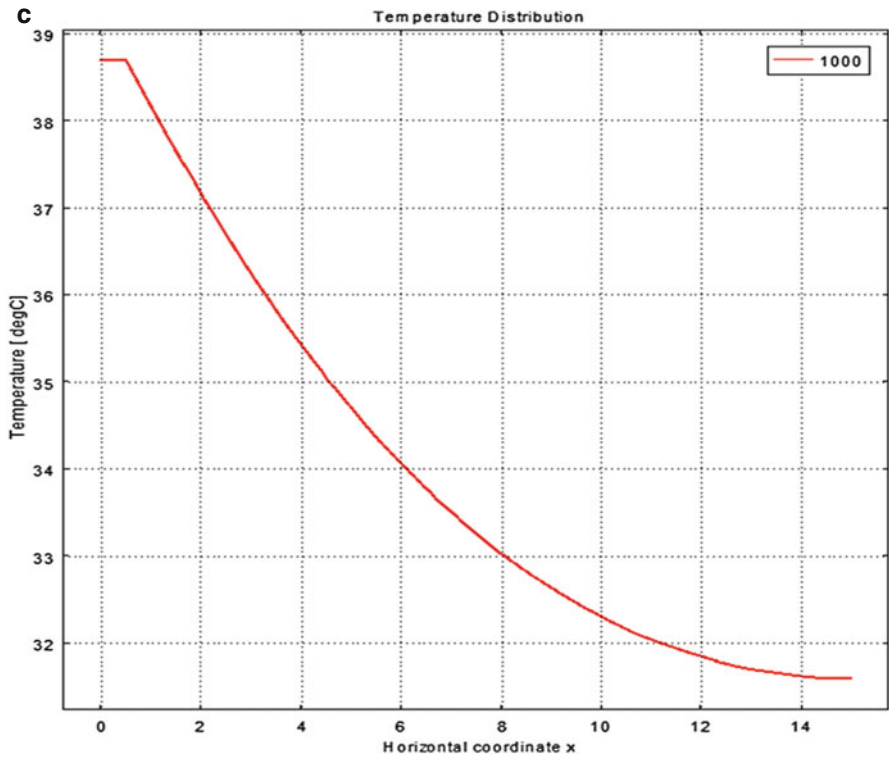
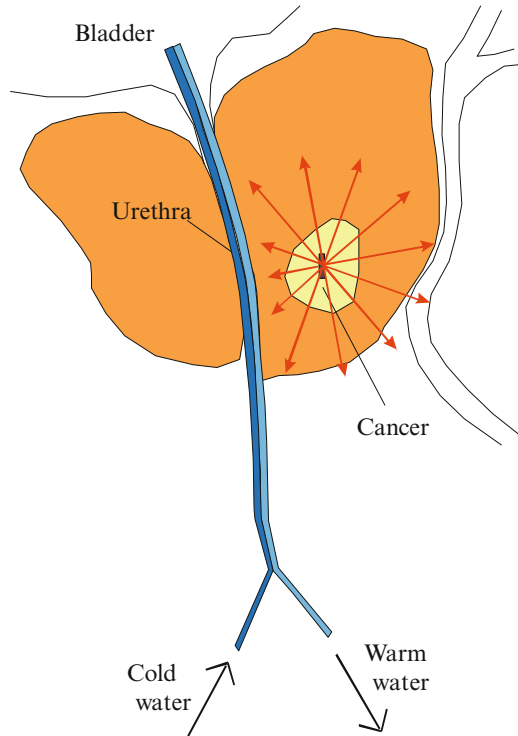


Fig. 8.9 (continued)

**Fig. 8.10** One side of the domain corresponds to a cooling boundary



orthogonal axis, the radial distances to reach this same temperature were more than 10 mm, respectively. Within 10 %, the radial temperature distribution in tissue emanating from the 1 mm × 10 mm rod, agrees with predicted experimental data (personal communication, Austerlitz). As expected, the radial temperature distribution for the 0.8 mm diameter sphere was less than that observed for the parallel axis of the 0.8 mm diameter but with 10 mm height rod. The simulations indicate that the methodology of ultrasound heated gold seeds may have therapeutic powers similar to radioactive substances. With the use of gold seed gun and needles of appropriate lengths and curvatures, uniform distributions of seeds can be obtained throughout the area of an implant, the seeds being small causing minimal trauma, and little disturbance to the patient. This procedure can be repeated rather easily and gold seeds are reusable. Furthermore, sound energy is non ionizing radiation and therefore its use does not impose the hazards, such as cancer production, attributed to ionizing radiation. Ultrasound kinetic energy when absorbed by tissues can also be converted into heat.

Currently, we study the use of other possible (gold-coated) materials: aluminum, copper, granite, high-strength alloy steel, iron, lead zirconate titanate, silicon, silica glass, structural steel, titanium beta-21S, and tungsten. Relative comparison will be made versus the case of nanoparticles (in preparation). The

use of ultrasonic vibrations in heat-treating metals and alloys is based on the transmission of elastic vibrations to the parts either through the surrounding medium (water, oil, emulsion, molten metal, or salt) or by firm contact with the wave guide. It has been shown that in austenite, the influence of elastic vibrations and the absorption of part of the energy of elastic vibrations leads to a certain increase in the temperature of samples. As was shown in [1], samples may heat up greatly under the influence of ultrasonic vibrations. In [1] the possibility of any influence of elastic ultrasonic vibrations on diffusion, ionic mobility, viscosity, or thermal diffusion was denied. The mechanism of the action of ultrasonic vibrations probably consists of changes in the conditions of evaporation on the surfaces of the parts being treated. The use of ultrasonic vibrations is especially effective for parts made of steels with low hardenability. The passage of ultrasonic vibrations through a solid body is accompanied by a series of effects such as intense heating of the samples to the melting temperature, the appearance of traces of residual deformation, and accumulations of structural fatigue and even fatigue destruction. Application of high-power 20 kHz ultrasound resulted in temperature increases of the order of 200 °C occurring 20–30 s after initiation of insonation in resonant specimens of fine-grained polycrystalline brass, copper, and steel [27]. Typically, the nanoparticles have a size of the order of a few tens of nanometers, because as mentioned above the particle has to be small for the SPR effect. If the radiation pulse width is short enough, heating is limited to the vicinity of the nanoparticle. Thus generally a large number of nanoparticles would be needed to effectively heat an entire cell, for example, the size of which can be of the order of microns to tens of microns. Recent studies have suggested the complementary use of sub-micron silicon carbide (SiC) particles as photothermal agents for the heating of bacteria by pulsed mid-infrared (MIR) radiation [37]. If a material is a good conductor of heat then the heat will move quickly. Metals are widely used for heat transfer purposes because they have properties which allow for propagation (movement in a line) of heat while being able to withstand the temperature extremes sometimes associated with heating. Conduction is when the heat moves through an object or from one object to another because the two objects are in contact with one another. It is the only mode of heat travel throughout solids. The ability to transfer heat within an object is called thermal conductivity “ $k$ ” (measured in W/m K). It varies for different materials. Gold, silver, and copper have high thermal conductivity.

The spatial temperature distribution in a multi-tissue arrangement is computed at three different frequencies and simulation times. Figure 8.1b shows a contour plot of the temperature distribution in the skin, breast and tumor tissues at 0.75 MHz at the end of 180 s. The maximum temperature (hot spot) occurred in the tumor and decreased when moving farther in other tissues. Increasing the time allowed for ultrasound therapy up to 300 s raised the temperature observed in the tumor and the surrounding tissues (Fig. 8.1a). The temperature distribution, employing a therapeutic transducer at a higher frequency of 1.5 MHz, at the end of 180- and 300-s

ultrasound therapy is shown in Figs. 8.2a and 8.3a. The highest temperature observed in the tumor was 45 °C which is suitable for destroying cancerous cells without a noticeable damage to the surrounding tissues. Simulation results using a transducer at a frequency of 2.75 MHz and at the end of 180 and 300 s, respectively is illustrated in Figs. 8.3a and 8.4a. It is observed that the temperature predicted in the tumor is about 51.04 °C. The surrounding area near the tumor has been affected by higher temperatures compared to previous simulation results at lower frequencies. Increasing the time allowed for ultrasound raised the temperature of the tumor as well as the surrounding tissues. This rise in the temperature of the surrounding healthy tissue leads to their destruction, which is a drawback of the therapeutic process. In addition, the temperature distribution is observed to be more localized, thus indicating better transducer focusing capabilities at higher frequencies. Numerical computations and analytical calculations of temperatures in various tissues are summarized. A good agreement was only observed at a frequency of 1.5 MHz.

First, we validated our model by simulating the heating of spherical particles and comparing the results with the lattice expansion measurements of Austerlitz (work in progress). Numerical simulations are compared with analytical results. An elevation in the temperature (hot spot) of the skin tissue was observed in all computations. Thus, a bolus of degassed water of temperature 10 °C is used as a cooling system in farther simulations. It acts as a heat sink, so as to avoid any pain or burning of the skin. In order to calculate the temperature field in the multi-tissue system, the uniform pressure of ranges from 0.045 to 0.0354 MPa is assumed to be applied on the surface of the breast tissue at the time from 180 to 300 s, so the spatial temperature profiles are very similar for both solutions. The numerical results show that employing a transducer at a frequency of 1.5 MHz is the most suitable for a successful ultrasound therapy. At this frequency, the highest temperature observed in the tumor was 45.5 °C which is favorable for destroying cancerous cells without a noticeable damage to the surrounding tissues. On the other hand, analytical results show that the highest temperature predicted in the tumor was 47.77 °C. The two solutions are considered in good agreement. The difference between the two solutions is minimized when a lower thermal conductivity value (e.g.,  $k$  less than 0.5 W/m °C) for the tumor in the FEM computations is used. The discrepancy between the numerical and analytical results is more noticeable at the two other frequencies. This is caused by the fact that heat conduction is ignored in the analytical method. As the frequency of simulation increases, the ultrasound intensities increases and the specific absorption rate increases. Thus, the heat generation in tissues is increased, and the surrounding area near the tumor has been affected by higher temperatures, but the temperature distribution is more localized, as shown in Figs. 8.3a and 8.4a.

## Conclusion

Computer modeling has been used to determine the likely temperature distribution of a given treatment and to plan the future of hyperthermia treatments. So, the goal of computer simulation is extremely useful in providing a firm scientific basis for the future of clinical investigation of focused ultrasound.

In this report, we propose a methodology that has the goal of sustaining hypothermia in the urethra and treat prostate cancer with macro-rod-shaped gold and ultrasound. Experimental studies that monitor the interaction of therapeutic ultrasound with heat-conducting material such as gold seeds in biological tissues can be a demanding research task. Numerical modeling of bio-heat transfer resulting from gold seed irradiation and seed size effect comparison can be very important and useful in non-invasive cancer therapy. A model-based analysis of these interactions and the corresponding temperature distribution was carried out, for time and irradiation rate found in current literature. Therapy design can be integrated into a predictive treatment planning model for prostate cancer ultrasound hyperthermia-hypothermia therapy by specifying the most appropriate ultrasound and gold seed parameters based on desired levels of temperature distribution both on tumor and healthy tissue. Utilization of this optimization model will enable a physician to evaluate tumor hyperthermia treatment and to better design a patient-specific therapy to achieve maximum destruction of the tumor and injury minimization of healthy tissue by controlling size, shape, and location of gold seeds implanted in tissue, and ultrasound parameters. In order to fully make use of numerical modeling results for the application of ultrasound on tissue containing seeds, and generation of hyperthermia to cancer control, physiological factors such as pH, oxygen consumption, nutrients, and blood flow of both tumor and normal host tissue should be measured in vivo and the analysis of these factors needs to be documented not only at normal temperatures but also under hyperthermic conditions to further elucidate the proper conditions for a selective destruction of tumor tissue with normal tissue sparing. Heating tissues using ultrasound decreases the viscosity of fluid elements, increases metabolic rate, increases blood flow which assists in the reduction of swelling, and stimulates the immune system. All these factors might play a significant role in the final outcome.

The experimental study of the interaction of therapeutic ultrasound with biological tissues and the monitoring of the temperature distribution is a very expensive and difficult task. Thus, numerical modeling of ultrasound hyperthermia treatment at different simulation frequencies and therapy durations is a very important therapeutic demand. A model-based analysis of the interaction of ultrasound intensity with breast tissue including a tumor was carried out in an effort to predict the path of the sound waves and the temperature

(continued)



(continued)

field in the regions of interest. Numerical and analytical calculations of temperature in various tissues were in good agreement at a certain frequency of 1.5 MHz. The computed results form a foundation for a better understanding of the interaction of ultrasound with biological tissues. More complex and extensive analytical methods including all aspects of heat conduction and wave attenuation should be considered in the future.

## References

- Balalaev GA (1966) Zashchita stroitel'nykh konstruksii i khimicheskikh apparatov ot korrozii [http://books.google.com/books/about/Za%C5%A1%C4%8Dita\\_stroitel\\_nyh\\_konstrukcij\\_ot\\_ko.html?id=prY\\_OQAACAAJ](http://books.google.com/books/about/Za%C5%A1%C4%8Dita_stroitel_nyh_konstrukcij_ot_ko.html?id=prY_OQAACAAJ)
- Bhatia AB (1985) Ultrasonic absorption: an introduction to the theory of sound absorption and dispersion in gases, liquids, and solids. Dover Publications, New York
- Chang E, Alexander HR, Libutti SK, Hurst R, Zhai S, Figg WD, Bartlett DL (2001) Laparoscopic continuous hyperthermic peritoneal perfusion1. *Journal of the American College of Surgeons* 193:225–229
- Chang I (2003) Finite element analysis of hepatic radiofrequency ablation probes using temperature-dependent electrical conductivity. *Biomedical Engineering Online* 2:12
- Cosman ER, Rittman W (2002) Ablation treatment of bone metastases. US Patent 6,478,793
- Coughlin CT (1992) Prospects for interstitial hyperthermia. *Interstitial Hyperthermia: Physics, Biology and Clinical Aspects* 3:1
- Critz FA, Tarlton RS, Holladay DA (1995) Prostate specific antigen-monitored combination radiotherapy for patients with prostate cancer. I-125 implant followed by external-beam radiation. *Cancer* 75:2383–2391
- Dowlatshahi K (1993) Apparatus for interstitial laser therapy having an improved temperature sensor for tissue being treated. Google Patents
- Ebbini ES, Umemura SI, Ibbini M, Cain CA (1988) A cylindrical-section ultrasound phased-array applicator for hyperthermia cancer therapy. *IEEE Transactions on Ultrasonics, Ferroelectrics and Frequency Control* 35:561–572
- Fasla B, Benmouna R, Benmouna M (2010) Modeling of tumor's tissue heating by nanoparticles. *Journal of Applied Physics* 108:124703
- Fenn AJ (2007) Breast cancer treatment by focused microwave thermotherapy. Jones & Bartlett Learning, Burlington, MA
- Fessenden P, Lee ER, Samulski TV (1984) Direct temperature measurement. *Cancer Research* 44:4799s
- Fetter RW, Gadsby PD, Kabachinski JL (1989). Microwave hyperthermia probe. US Patent 4,841,988
- Frischbier HJ, Thomsen K (1971) Treatment of cancer of the vulva with high energy electrons. *Am J Obstet Gynecol* 111(3):431–5
- Gage AA (1992) Cryosurgery in the treatment of cancer. *Surgery, Gynecology & Obstetrics* 174:73
- Hafeli U (1997) Scientific and clinical applications of magnetic carriers. Springer, New York
- Haider SA, Cetas TC, Wait JR, Chen JS (1991) Power absorption in ferromagnetic implants from radiofrequency magnetic fields and the problem of optimization. *IEEE Transactions on Microwave Theory and Techniques* 39:1817–1827

18. Hassan OM, Hassan N, Kadah YM (2009). Modeling of ultrasound hyperthermia treatment of breast tumors. Radio Science Conference, 2009. NRSC 2009. National. <http://ieeexplore.ieee.org/xpl/articleDetails.jsp?reload=true&arnumber=5233463>
19. Huang HC, Rege K, Heys JJ (2010) Spatiotemporal temperature distribution and cancer cell death in response to extracellular hyperthermia induced by gold nanorods. *ACS nano* 4:2892–2900
20. Huang X, Jain PK, El-Sayed IH, El-Sayed MA (2008) Plasmonic photothermal therapy (PPTT) using gold nanoparticles. *Lasers in Medical Science* 23:217–228
21. Hynynen K, Watmough DJ, Mallard JR (1983) Local hyperthermia induced by focused and overlapping ultrasonic fields—an in vivo demonstration. *Ultrasound in Medicine and Biology* 9:621–627
22. Johannsen M, Gneveckow U, Eckelt L, Feussner A, Waldöfner N, Scholz R, Deger S, Wust P, Loening SA, Jordan A (2005) Clinical hyperthermia of prostate cancer using magnetic nanoparticles: presentation of a new interstitial technique. *International Journal of Hyperthermia* 21:637–647
23. Jordan A, Scholz R, Wust P, Fähling H (1999) Magnetic fluid hyperthermia (MFH): cancer treatment with AC magnetic field induced excitation of biocompatible superparamagnetic nanoparticles. *Journal of Magnetism and Magnetic Materials* 201:413–419
24. Kennedy JC, Pottier RH, Pross DC (1990) Photodynamic therapy with endogenous protoporphyrin: IX: basic principles and present clinical experience. *Journal of Photochemistry and Photobiology B: Biology* 6:143–148
25. Lele PP (1990) Diffuse focus ultrasound hyperthermia system. Google Patents
26. Lyons BE, Britt RH, Strohhahn JW (1984) Localized hyperthermia in the treatment of malignant brain tumors using an interstitial microwave antenna array. *IEEE Trans Biomed Eng* 31(1):53–62
27. Mignogna RB, Green RE, Duke JC, Henneke EG, Reifsnider KL (1981) Thermographic investigation of high-power ultrasonic heating in materials. *Ultrasonics* 19:159
28. O’neal DP, Hirsch LR, Halas NJ, Payne JD, West JL (2004) Photo-thermal tumor ablation in mice using near infrared-absorbing nanoparticles. *Cancer Letters* 209:171–176
29. Panjehpour M, Overholt BF, Milligan AJ, Swaggerty MW, Wilkinson JE, Klebanow ER (1990) Nd: YAG laser-induced interstitial hyperthermia using a long frosted contact probe. *Lasers in Surgery and Medicine* 10:16–24
30. Park DW, Kim KS (2011) Seed-mediated synthesis of iron oxide and gold/iron oxide nanoparticles. *Journal of Nanoscience and Nanotechnology* 11:7214–7217
31. Park SE, Lee JW, Haam SJ, Lee SW (2009) Fabrication of double-doped magnetic silica nanospheres and deposition of thin gold layer. *Bull Korean Chem Soc* 30:869
32. Perez, Brady’s Principles and Practice of Radiation Oncology (Perez and Bradys Principles and Practice of Radiation Oncology) LWW; Sixth edition (May 6, 2013), ISBN-13:978-1451116489
33. Ramanujan RV, Lao LL Magnetic particles for hyperthermia treatment of cancer. Available online: <http://www.ntu.edu.sg/home/ramanujan/reprints/IBECpaper2RVR.pdf>
34. Regueiro CA, Valcarcel FJ, Romero J, De La Torre A (2002) Treatment of conjunctival lymphomas by beta-ray brachytherapy using a strontium-90-yttrium-90 applicator. *Clinical Oncology* 14:459–463
35. Roberts DW (1992) Interstitial hyperthermia in brain: the clinical experience. *Interstitial Hyperthermia: Physics, Biology and Clinical Aspects* 3:231
36. Romestaing P, Lehingue Y, Carrie C, Coquard R, Montbarbon X, Ardiet JM, Mamelle N, Gerard JP (1997) Role of a 10-Gy boost in the conservative treatment of early breast cancer: results of a randomized clinical trial in Lyon, France. *Journal of Clinical Oncology* 15:963
37. Rosenberg M, Petrie TA (2012) Theoretical study on the possible use of SiC microparticles as photothermal agents for the heating of bacteria. *Nanotechnology* 23:055103
38. Russell KJ, Caplan RJ, Laramore GE, Burnison CM, Maor MH, Taylor ME, Zink S, Davis LW, Griffin TW (1994) Photon versus fast neutron external beam radiotherapy in the treatment

- of locally advanced prostate cancer: results of a randomized prospective trial. *International Journal of Radiation Oncology Biology Physics* 28:47–54
39. Schiller JH, Harrington D, Belani CP, Langer C, Sandler A, Krook J, Zhu J, Johnson DH (2002) Comparison of four chemotherapy regimens for advanced non-small-cell lung cancer. *New England Journal of Medicine* 346:92–98
  40. Slater JD, Rossi CJ, Yonemoto LT, Bush DA, Jabola BR, Levy RP, Grove RI, Preston W, Slater JM (2004) Proton therapy for prostate cancer: the initial Loma Linda University experience. *International Journal of Radiation Oncology Biology Physics* 59:348–352
  41. Stauffer PR, Sneed PK, Suen SA, Satoh T, Matsumoto K, Fike JR, PHILLIPS TL (1989) Comparative thermal dosimetry of interstitial microwave and radiofrequency-LCF hyperthermia. *International Journal of Hyperthermia* 5:307–318
  42. Steger AC, Lees WR, Walmsley K, Bown SG (1989) Interstitial laser hyperthermia: a new approach to local destruction of tumours. *British Medical Journal* 299:362
  43. Stern JM, Stanfield J, Lotan Y, Park S, Hsieh JT, Cadeddu JA (2007) Efficacy of laser-activated gold nanoshells in ablating prostate cancer cells in vitro. *Journal of Endourology* 21:939–943
  44. Stromberg J, Martinez A, Gonzalez J, Edmundson G, Ohanian N, Vicini F, Hollander J, Gustafson G, Spencer W, Yan D (1995) Ultrasound-guided high dose rate conformal brachytherapy boost in prostate cancer: treatment description and preliminary results of a phase I/II clinical trial. *International Journal of Radiation Oncology, Biology, Physics* 33:161
  45. Terentyuk GS, Maslyakova GN, Suleymanova LV, Khlebtsov NG, Khlebtsov BN, Akchurin GG, Maksimova IL, Tuchin VV (2009) Laser-induced tissue hyperthermia mediated by gold nanoparticles: toward cancer phototherapy. *Journal of Biomedical Optics* 14:021016
  46. Uchida T, Sanghvi NT, Gardner TA, Koch MO, Ishii D, Minei S, Satoh T, Hyodo T, Irie A, Baba S (2002) Transrectal high-intensity focused ultrasound for treatment of patients with stage T1b-2n0m0 localized prostate cancer: a preliminary report. *Urology* 59:394–398
  47. Wu J, Nyborg WLM (2006) *Emerging therapeutic ultrasound*. World Scientific, Hackensack, NJ
  48. Wust P, Hildebrandt B, Sreenivasa G, Rau B, Gellermann J, Riess H, Felix R, Schlag PM (2002) Hyperthermia in combined treatment of cancer. *The Lancet Oncology* 3:487–497
  49. COMSOL Multiphysics®. © 1997–2008 COMSOL AB

# Chapter 9

## Clinical Decision Support System for the Diagnosis of Adolescence Health

Irene Moutsouri, Amalia Nikou, Machi Pampalou, Maria Lentza,  
Paulos Spyridakis, Natassa Mathiopoulou, Dimitris Konsoulas,  
Marianna Lampou, and Athanasios Alexiou

**Abstract** It is common that children confront psychological problems when they reach puberty. These problems could easily be overcome, but in many cases they could be severe, leading to social estrangement or worse in madness or death. According to information collected we designed a questionnaire about the psychology of adolescents in order to help people in that age or their elders find out if they have health issues. We used already published researches and material concerning all the psychological problems a child can confront in order to make a reliable questionnaire and to develop the clinical decision support system. Our main objective is to publish and administrate a web-based free tool for sharing medical knowledge about any psychological disease a child can already have or develop during puberty.

**Keywords** Adolescence health • Psychological disorders • Daily functions • Addiction • Neurological disorders • Computer-aided diagnosis systems • Clinical decision support systems

### 9.1 Introduction

There are various severe neurological disorders that can present during childhood or birth and affect the psychological health of the child when reaching puberty. Some of the disorders are extremely severe like Autism, Huntington's, epilepsy,

---

I. Moutsouri (✉) • A. Nikou • M. Pampalou • M. Lentza • P. Spyridakis  
N. Mathiopoulou • D. Konsoulas • M. Lampou  
Department of Computer Sciences and Biomedical Informatics, University of Thessaly,  
Papasiopoulou 2-4, 53100 Lamia, Greece  
e-mail: [emoutsou@dib.uth.gr](mailto:emoutsou@dib.uth.gr); [anikou@dib.uth.gr](mailto:anikou@dib.uth.gr); [apabalou@dib.uth.gr](mailto:apabalou@dib.uth.gr); [mlentza@dib.uth.gr](mailto:mlentza@dib.uth.gr);  
[pspyrida@dib.uth.gr](mailto:pspyrida@dib.uth.gr); [amathiop@dib.uth.gr](mailto:amathiop@dib.uth.gr); [dkonsoul@dib.uth.gr](mailto:dkonsoul@dib.uth.gr); [mlampou@dib.uth.gr](mailto:mlampou@dib.uth.gr)

A. Alexiou  
Department of Informatics, Ionian University, Plateia Tsirigoti 7, 49100 Corfu, Greece  
e-mail: [alexiou@ionio.gr](mailto:alexiou@ionio.gr)

and Down syndrome that will cause social estrangement and ultimately psychological problems during puberty.

Excluding birth and childhood traumas and diseases, the main factors for getting a disease/disorder during puberty are neuropsychological and psychological. These particular disorders can be caused by specific events during adolescence or by external factors such as the family environment, other interpersonal relationships and habits among others. A number of disorders of this classification (depression, schizophrenia, alcoholism, sleeping disorders etc.) affect one another, sometimes having identical or similar symptoms.

There is an ongoing momentum with increasing research regarding adolescent psychological health; Adolescents behave in ways that have been proved harmful in the past by acting without thinking, while even more disciplined adolescents can have a dangerous behavior when around peers of their own age. There are a number of occasions and incidences in modern societies which affect how adolescents behave, such as family crises including separation and divorce, traditional media showing images of behavior which teenagers mimic, the generation gap and lack of communication between them and their parents [1–12].

Severe conditions affect only around 15–20 % of teenagers, the rest being healthy or facing adolescence issues that are easily dealt with. However, numerous studies regarding 15-year-old adolescents have provided crucial, yet overwhelming results. In a recent study about Internet usage [7–10], 53.4 % were sexually inactive and used the Internet as a means to engage in sexual activities, while 28.6 % were already sexually active. Additionally, a study looking into substance dependence [10–12] concluded that 42.1 % had smoked a cigarette at least once, 10 % smoke at least 6 cigarettes and 7.2 % have used cannabis. It has to be noted that the above older statistics are merely an indication and it is probable that today's responses would be more overwhelming. Our paper seeks to find ways to reduce the numbers of adolescents facing psychological health issues by reaching out to parents and other parties in an adolescent's environment sometimes far away the psychiatry's office.

This paper aims to introduce an integrated questionnaire (Appendix) based on a web-based clinical decision support system (CDSS) and well-known published symptoms [13–15, 21–38] where anonymous or registered users, interested in a specific disorders' group (psychological disorders, neurological disorders, daily functions and addictions), can search through indicated symptoms or risk factors. Consequently, based on the symptoms selected, the user can get causes and treatments for the specific disease or disorder.

Based on latest researches, concerning any possible disease or disorder an adolescent can develop during puberty, we classified these diseases/disorders (Fig. 9.1) that emerge from a neurotransmitter disorder, certain brain section damage, genetic disorders, psychological problems, environmental factors, behavioral and social problems or even an addiction, using ontology-based modeling on the Protégé platform [16].

## 9.2 Disorders and Risk Factors

Based on information collected regarding the psychological health of adolescents, we have designed a multi-task questionnaire via which the users can effortlessly ascertain whether they suffer from a disease or disorder, as well can get information on the causes and any options for treatments through different medical doctors. We have created four different groups (Fig. 9.1), each of which comprises diseases and treatments with identical or similar symptoms. Disorders that are congenital, meaning they develop during pregnancy or at birth, are caused by neurological or other factors; examples of such conditions include autism, dyslexia, alexia, and Down syndrome among others. Children with such conditions may suffer from a number of apparent symptoms but there are cases where symptoms are not as evident and children can be superficially healthy.

However, in cases where there are a number of severe symptoms, a child’s psychology and character can be affected. The group which includes these disorders in our CDSS is neurological disorders (Fig. 9.2). Most of these conditions are caused by neurological or genetic factors; for example, in the case of alexia the user can select some of the evident symptoms and can consequently find possible causes, such as brain or parietal lobe damage, and finally find possible treatments.

On the other hand, there are some conditions that develop during adolescence due to external factors such as family environment, other inter-personal relationships and formed habits. Examples, among others, include depression, schizophrenia, alcoholism, and anorexia. Such conditions are grouped into psychological disorders (Fig. 9.3), daily functions, and addictions. Depression, which falls under psychological disorders, is caused by a number of events such as sorrow from losing a close person through death, divorce or separation of parents and symptoms can include social isolation or feelings of being deprived, radical lifestyle changes, conflicts with professors or other superiors, and addictions or obsessive habits. Recommended treatments of depression include medical selective serotonin reuptake inhibitors (SSRIs), which work on increasing the amount of serotonin in the brain, and as researches have proven [13–15], these medications

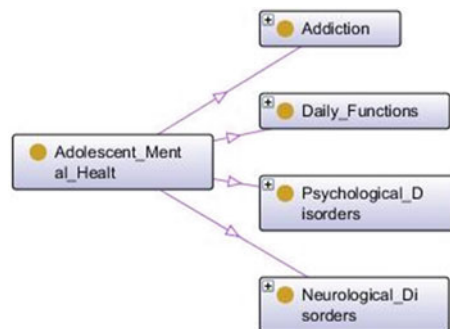


**Fig. 9.1** The four groups of Adolescence Mental health

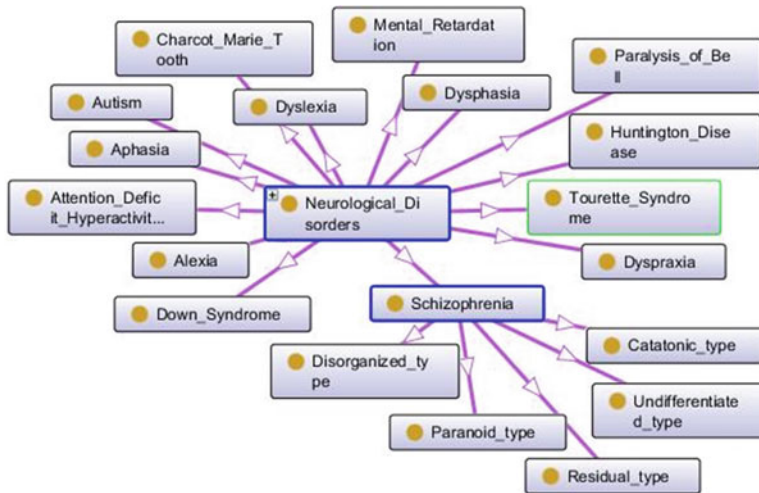


Fig. 9.2 Neurological disorders

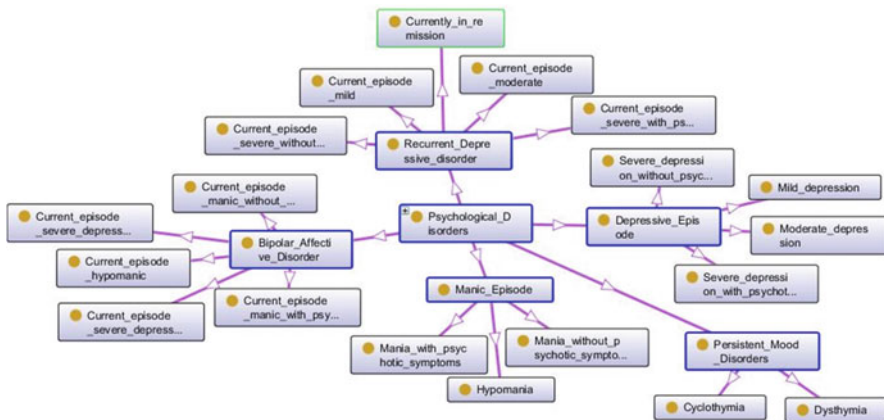


Fig. 9.3 Psychological disorders

improve mood. Other medications that can be helpful include nefazodone, trazodone, bupropion, and abilify.

Alternatively, there are many different types of effective therapeutic approaches used for the treatment of depression, including behavioral therapy, behavioral therapy ala Lewinsohn, interpersonal therapy, and rational emotive therapy [13–15]. Also individual and group are both used, depending on the severity of the depressive episode. In case of suicide attempts or of serious suicidal ideation the patient has to put in hospitalization in order to minimize the danger of harming himself or others [13–15].

The group of Daily Functions (Fig. 9.4) includes anorexia, which is caused by factors such as perfectionism, personality factors including being eager to please other people and high expectations for oneself, family history of eating disorders, living in an industrialized society, difficulty communicating negative emotions such as anger or fear, difficulty resolving problems or conflict, and low self-esteem. If the affected person’s medical condition has deteriorated, hospitalization may be required. There are no medications to treat anorexia and treatment for this disorder is often long term. Initially, treatment objectives are focused on reversing behavioral abnormalities and nutritional deficiencies. Any emotional support and the reassurance that eating as well as caloric restoration will not make the person overweight, are essential components during initial treatment sessions [24–26]. Psychosocial (both psychological and social) issues and family dysfunction are also addressed, which may reduce the risk of relapsing behaviors. Relapsing behaviors occur when an individual goes back to the old. At present, there is no standardized psychotherapeutic treatment model to address the multifactorial problems associated with anorexia. Cognitive-behavioral therapy (CBT) may help to improve and modify irrational perceptions and overemphasis of weight gain. Current treatment usually begins with behavioral interventions and should include family therapy (if age appropriate) [24–26]. Psychodynamic psychotherapy (also called exploratory psychotherapy) is often helpful in the treatment of anorexia [24–26].

Finally, in the case of addictions (Fig. 9.5), such as alcoholism, causes include the behavior of others and their attitude towards consumption of alcohol, namely the encouragement or criticism, pressure from peers, as an aid to relaxation and free

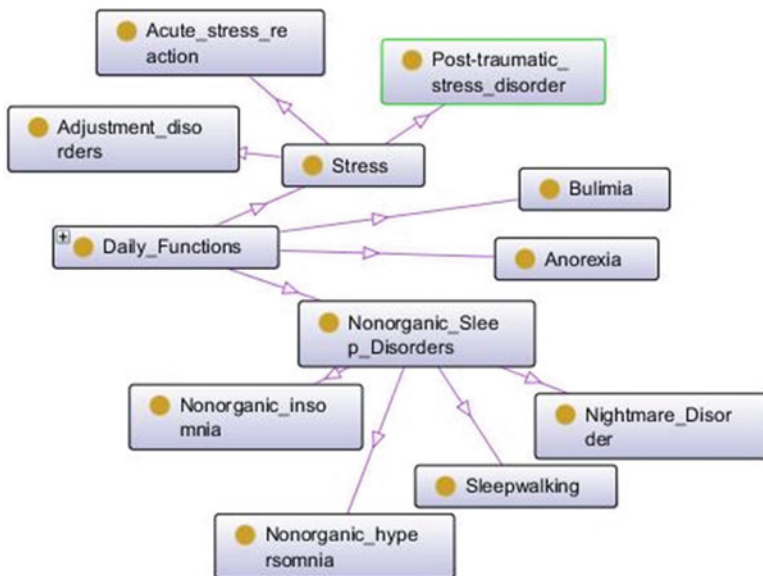
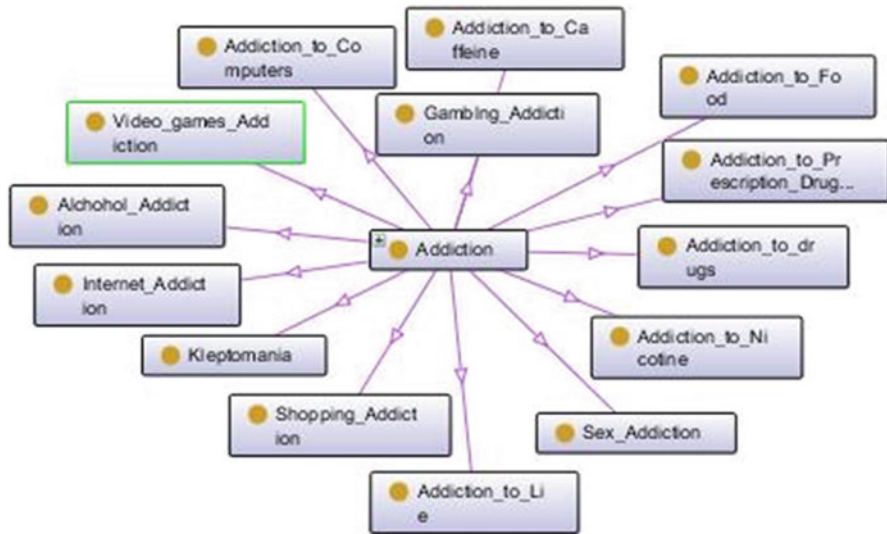


Fig. 9.4 Daily functions





**Fig. 9.5** Addictions

expression of emotions [27–29]. There is also a biological component, a neurotransmitter in the brain, dopamine, which plays an important role in the continued use of alcohol. Genetically, there is a gene that may cause alcohol dependence and usually transferred from fathers to sons [27–29]. Regarding the treatment of addictions, it has to be stressed that each case being different and there is no standardized treatment. The treatment has two parts, the first is detoxification, namely the elimination of the toxic effects of the body, and the second is restoration, that is, to stay healthy and avoid relapse [29]. Support worldwide groups like the Anonymous Alcoholics and use of CBT can also be helpful, as well as the use of drugs to reduce the craving for drink, like acamprosate and tonaltrexone. Other complementary therapies include dialogue, hypnotherapy, and support from family and friends [29].

There are increasing numbers of adolescents suffering from disorders and diseases and our project can facilitate the spread of knowledge effortlessly and each adolescent or their family can find out information about specific conditions and consequently learn about the causes and treatments. This process will be carried out through our website, the demo of which is illustrated below (Fig. 9.6).

### 9.3 The Clinical Decision Support System

In general computer-aided diagnosis (CAD) systems aim to enhance the ability to detect pathological structures in medical examinations and to support evaluation of pathological findings during the diagnostic procedure [17, 18]. CDSS are very

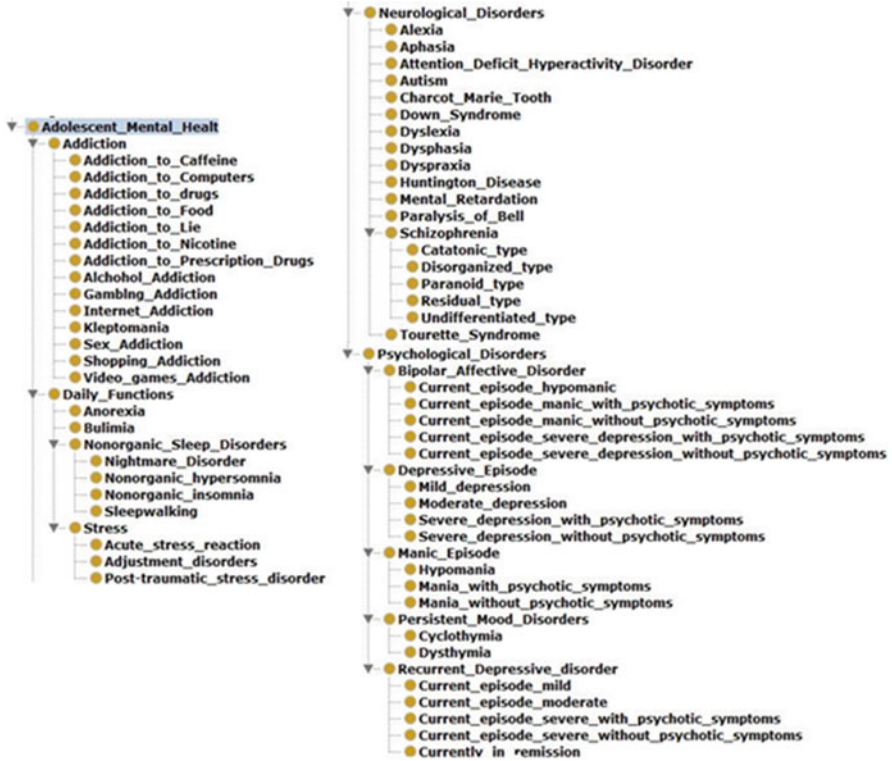


Fig. 9.6 The adolescent mental health CDSS

challenging and innovating interactive systems, designed to help doctors and other health professionals to take decisions regarding the condition a patient is facing, as well as to aid in keeping an updated patient record. As such, the principal function of the CDSS is to enable the doctor to interact with the system and consequently help in the diagnosis and analysis of patient data [19, 20]. The system we propose, however, has a fundamental modification as to its usage; apart from doctors and professionals, third parties such as a patient’s family can use the system in order to identify possible symptoms, risk factors, unusual attitudes or to help the patient in dealing with a specific condition. The proposed CDSS website can be used by anyone who wants to find out more about a specific condition. The website will offer the ability for signing up, so that users can be able to directly communicate with a specialized doctor, should they wish to do so. After choosing one of the four condition groups, the user will choose the disease or treatment that they wish to learn more about.

As each group of conditions contains diseases and disorders with similar or identical symptoms, the users might have to engage into the process more than once, in order to be sure of their condition. As shown below, if the users select one of the following conditions, they will have to choose only the symptoms that apply

in their case. Consequently, when the users finish the symptoms' selection process, a new window appears, advising for the possible causes and treatments for the specific condition. In the example of mania shown below, after the user has selected their symptoms, a result like the one in Fig. 9.7 will appear. As seen in Fig. 9.7, a user has selected a number of symptoms regarding a manic episode, like increased activity or physical restlessness, increased talkativeness, difficulty in concentration or distractibility, decreased need for sleep and mild spending sprees, or other types of reckless or irresponsible behavior. As a result, the user can view possible causes and treatments of the conditions they have chosen, in this case, the output concerns manic episode. At first, the causes of manic episode (Fig. 9.8) could be many and different. Manic episodes in adolescents are more likely to include psychotic features and may be associated with school truancy, antisocial behavior, school failure, or substance use [33–35]. A significant minority of adolescents appear to have a history of long-standing behavior problems that precede the onset of a frank

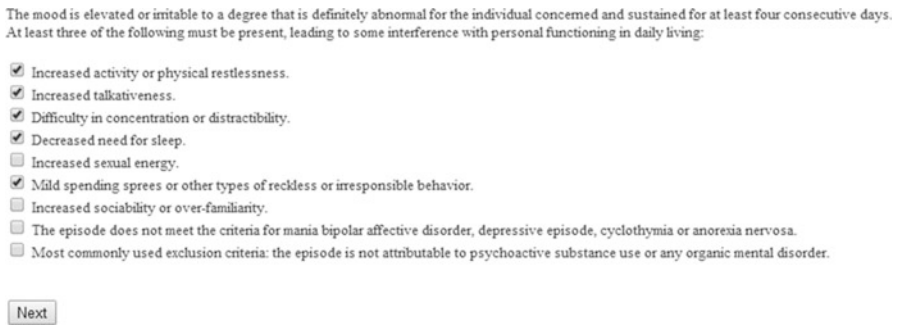


Fig. 9.7 Choosing symptoms of manic episode

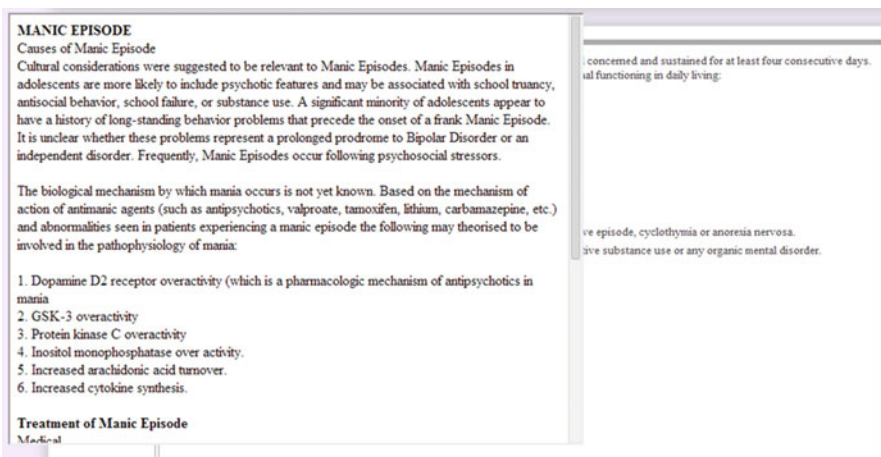


Fig. 9.8 CDSS output

manic episode. It is unclear whether these problems represent a prolonged prodromal to bipolar disorder or an independent disorder [19]. Frequently manic episodes occur following psychosocial stressors. The biological mechanism by which mania occurs is not yet known [33–35]. Based on the mechanism of action of antimanic agents (such as antipsychotics, valproate, tamoxifen, lithium, carbamazepine, etc.) and abnormalities seen in patients experiencing a manic episode the following may be theorized to be involved in the pathophysiology of mania such as dopamine D2 receptor overactivity (which is a pharmacologic mechanism of antipsychotics in mania), GSK-3 overactivity, protein kinase C overactivity, inositol monophosphatase overactivity, increased arachidonic acid turnover, and increased cytokine synthesis [36]. Also, the user could learn about the treatment of manic episode. Manic episodes in bipolar I disorder require treatment with drugs, such as mood stabilizers and antipsychotics, and sometimes sedative-hypnotics (benzodiazepines such as Ativan or Klonopin) [37]. Taking medicine on a regular basis can help to prevent future manic or depressive episodes. Regular therapy sessions with a psychologist or social worker can help people to identify factors that can destabilize mood (such as sleep deprivation, drug or alcohol abuse, and poor stress management), leading to fewer hospitalizations and feeling better overall [37, 38].

### Conclusion

In this chapter an integrated questionnaire concerning adolescent mental health is presented, in order to categorize every possible illness or symptom can be diagnosed in teen population. Neurological lesions, simple daily unusual symptoms, comorbidities, or other risk factors have been classified for the designing of the architecture of a web-based CAD system, easily to be accessible by patients, relatives, or medical doctors. Few examples have been presented in order to describe the importance and the usage of this free CDSS application. Our future study will concern clinical study in association with medical staff for the application of our tool in real time.

## Appendix: Questionnaire

### 1. Psychological Disorders

#### 1.1 Hypomania

- (a) Irrational euphoric for at least 4 days.
  - (b) Non-use of psychoactive substances.
  - (c) Absence of organic mental disorder.
- At least three of the following must be present:
    - Increased activity or physical restlessness.
    - Increased talkativeness.

- Difficulty in concentration or distractibility.
- Decreased need for sleep.
- Increased sexual energy.
- Reckless or irresponsible behavior.
- Increased sociability or over-familiarity.

### 1.2 *Mania without psychotic symptoms*

- (a) Abnormal elevated, expansive or irritable mood that is prominent for at least a week.
- (b) Non-use of psychoactive substances.
- (c) Absence of organic mental disorder.

- At least three of the following must be present:
  - Increased activity or physical restlessness.
  - Increased talkativeness.
  - Rapid flow of thought.
  - Loss of normal social inhibitions resulting in misbehavior.
  - Decreased need for sleep.
  - Inflated self-esteem or grandiosity.
  - Distractibility or constant changes in activity or plans.
  - Ignorance of the risk of reckless and daredevil acts.
  - Marked sexual energy or sexual indiscretions.

### 1.3 *Mania with psychotic symptoms*

- (a) Irrational euphoric for at least 4 days.
- (b) Noncondition of schizophrenia.
- (c) Existence of delusions or hallucinations.

- At least three of the following must be present:
  - Increased activity or physical restlessness.
  - Increased talkativeness.
  - Difficulty in concentration or distractibility.
  - Decreased need for sleep.
  - Increased sexual energy.
  - Reckless or irresponsible behavior.
  - Increased sociability or over-familiarity.

### 1.4 *Bipolar affective disorder*

#### 1.4.1. *Bipolar affective disorder, current episode hypomanic*

- (a) Irrational euphoric for at least 4 days.
- (b) Non-use of psychoactive substances.
- (c) Absence of organic mental disorder.
- (d) Existence of at least one other affective episode in the past, such as hypomanic or manic episode, depressive episode, or mixed affective episode.

- At least three of the following must be present:
  - Increased activity or physical restlessness.
  - Increased talkativeness.
  - Difficulty in concentration or distractibility.
  - Decreased need for sleep.
  - Increased sexual energy.
  - Reckless or irresponsible behavior.
  - Increased sociability or over-familiarity.

*1.4.2. Bipolar affective disorder, current episode manic without psychotic symptoms*

- (a) The depressive episode should last for at least 2 weeks.
  - (b) Nonexistence of hypomanic or manic symptoms.
  - (c) Non-use of psychoactive substances.
  - (d) Absence of organic mental disorder.
  - (e) Existence of at least one other affective episode in the past, such as hypomanic or manic episode, or mixed affective episode.
- At least two of the following three symptoms must be present:
    - Abnormal and constant depressed mood for at least 2 weeks.
    - Loss of interest or pleasure in activities that normally are pleasurable.
    - Decreased energy or increased fatigability.
  - At least one of the following three symptoms must be present:
    - Loss of confidence and self-esteem.
    - Unjustified feelings of guilt.
    - Recurrent thoughts of death or suicide.
    - Lack of concentration and indecision.
    - Change in psychomotor activity.
    - Sleep disturbance.
    - Change in appetite with corresponding weight change.

*1.4.3. Bipolar affective disorder, current episode severe depression without psychotic symptoms*

- (a) Existence of at least one other affective episode in the past, such as hypomanic or manic episode or mixed affective episode in the past.
- (b) Nonexistence of hallucinations, delusions, or depressive stupor.
- (c) Nonexistence of hypomanic or manic symptoms.
- (d) Non-use of psychoactive substances.
- (e) Abnormal and constant depressed mood for at least 2 weeks.
- (f) Loss of interest or pleasure in activities that normally are pleasurable.

- (g) Decreased energy or increased fatigability.
- (h) Loss of confidence and self-esteem.
- (i) Unjustified feelings of guilt.
- (j) Recurrent thoughts of death or suicide.
- (k) Lack of concentration and indecision.
- (l) Change in psychomotor activity.
- (m) Sleep disturbance.
- (n) Change in appetite with corresponding weight change.

*1.4.4. Bipolar affective disorder, current episode severe depression with psychotic symptoms*

- (a) Existence of at least one other affective episode in the past, such as hypomanic or manic episode or mixed affective episode in the past.
  - (b) Nonexistence of hypomanic or manic symptoms.
  - (c) Noncondition of schizophrenia.
  - (d) Non-use of psychoactive substances.
  - (e) Abnormal and constant depressed mood for at least 2 weeks.
  - (f) Loss of interest or pleasure in activities that normally are pleasurable.
  - (g) Decreased energy or increased fatigability.
  - (h) Loss of confidence and self-esteem.
  - (i) Unjustified feelings of guilt.
  - (j) Recurrent thoughts of death or suicide.
  - (k) Lack of concentration and indecision.
  - (l) Change in psychomotor activity.
- At least one of the following symptoms must be present:
    - Existence of delusions or hallucinations.
    - Depressive stupor.

*1.4.5. Bipolar affective disorder, current episode mixed*

- (a) Rapid alternation of hypomanic, manic and depressive mood for at least 2 weeks.
- (b) Existence of at least one hypomanic or manic episode, depressive or mixed affective episode in the past.

*1.4.6. Bipolar affective disorder, currently in remission*

- (a) Noncondition of manic episode in any severity, or for any other mood disorder.
- (b) Existence of at least one well-authenticated hypomanic or manic episode in the past.

## 1.5 Depressive episode

### 1.5.1. Mild depressive episode

- (a) Nonexistence of hypomanic or manic symptoms.
  - (b) Non-use of psychoactive substances.
  - (c) Absence of organic mental disorder.
- At least two of the following three symptoms must be present:
    - Abnormal and constant depressed mood for at least 2 weeks.
    - Loss of interest or pleasure in activities that normally are pleasurable.
    - Decreased energy or increased fatigability.
  - At least one of the following seven symptoms must be present:
    - Loss of confidence and self-esteem.
    - Unjustified feelings of guilt.
    - Recurrent thoughts of death or suicide.
    - Lack of concentration and indecision.
    - Change in psychomotor activity.
    - Sleep disturbance.
    - Change in appetite with corresponding weight change.

### 1.5.2. Moderate depressive episode

- (a) Nonexistence of hypomanic or manic symptoms.
  - (b) Non-use of psychoactive substances.
- At least two of the following three symptoms must be present:
    - Abnormal and constant depressed mood for at least 2 weeks.
    - Loss of interest or pleasure in activities that normally are pleasurable.
    - Decreased energy or increased fatigability.
  - At least six of the following seven symptoms must be present:
    - Loss of confidence and self-esteem.
    - Unjustified feelings of guilt.
    - Recurrent thoughts of death or suicide.
    - Lack of concentration and indecision.
    - Change in psychomotor activity.
    - Sleep disturbance.
    - Change in appetite with corresponding weight change.



### 1.5.3. Severe depressive episode without psychotic symptoms

- (a) Nonexistence of hallucinations, delusions, or depressive stupor.
- (b) Nonexistence of hypomanic or manic symptoms.
- (c) Non-use of psychoactive substances.
- (d) Abnormal and constant depressed mood for at least 2 weeks.
- (e) Loss of interest or pleasure in activities that normally are pleasurable.
- (f) Decreased energy or increased fatigability.
- (g) Loss of confidence and self-esteem.
- (h) Unjustified feelings of guilt.
- (i) Recurrent thoughts of death or suicide.
- (j) Lack of concentration and indecision.
- (k) Change in psychomotor activity.
- (l) Sleep disturbance.
- (m) Change in appetite with corresponding weight change.

### 1.5.4. Severe depressive episode with psychotic symptoms

- (a) Nonexistence of hypomanic or manic symptoms.
  - (b) Noncondition of schizophrenia.
  - (c) Non-use of psychoactive substances.
  - (d) Abnormal and constant depressed mood for at least 2 weeks.
  - (e) Loss of interest or pleasure in activities that normally are pleasurable.
  - (f) Decreased energy or increased fatigability.
  - (g) Loss of confidence and self-esteem.
  - (h) Unjustified feelings of guilt.
  - (i) Recurrent thoughts of death or suicide.
  - (j) Lack of concentration and indecision.
  - (k) Change in psychomotor activity.
- At least one of the following symptoms must be present:
    - Existence of delusions or hallucinations.
    - Depressive stupor.

## 1.6 Recurrent depressive disorder

### 1.6.1. Recurrent depressive disorder, current episode mild

- (a) Existence of at least one previous episode, mild, moderate, or severe depression episode, lasting for a minimum of 2 weeks and separated from the current episode by at least 2 months.
- (b) Nonexistence in the past or present hypomanic or manic episode.
- (c) Nonexistence of hallucinations, delusions, or depressive stupor.
- (d) Non-use of psychoactive substances.
- (e) Absence of organic mental disorder.

- At least two of the following three symptoms must be present:
  - Abnormal and constant depressed mood for at least 2 weeks.
  - Loss of interest or pleasure in activities that normally are pleasurable.
  - Decreased energy or increased fatigability.
- At least one of the following seven symptoms must be present:
  - Loss of confidence and self-esteem.
  - Unjustified feelings of guilt.
  - Recurrent thoughts of death or suicide.
  - Lack of concentration and indecision.
  - Change in psychomotor activity.
  - Sleep disturbance.
  - Change in appetite with corresponding weight change.

*1.6.2. Recurrent depressive disorder, current episode moderate*

- (a) Existence of at least one previous episode, mild, moderate, or severe depression episode, lasting for a minimum of 2 weeks and separated from the current episode by at least 2 months.
  - (b) Nonexistence in the past or present hypomanic or manic episode.
  - (c) Nonexistence of hallucinations, delusions, or depressive stupor.
  - (d) Non-use of psychoactive substances.
  - (e) Absence of organic mental disorder.
  - (f) Non-use of psychoactive substances.
- At least two of the following three symptoms must be present:
    - Abnormal and constant depressed mood for at least 2 weeks.
    - Loss of interest or pleasure in activities that normally are pleasurable.
    - Decreased energy or increased fatigability.
  - At least six of the following seven symptoms must be present:
    - Loss of confidence and self-esteem.
    - Unjustified feelings of guilt.
    - Recurrent thoughts of death or suicide.
    - Lack of concentration and indecision.
    - Change in psychomotor activity.
    - Sleep disturbance.
    - Change in appetite with corresponding weight change.

*1.6.3. Recurrent depressive disorder, current episode severe without psychotic symptoms*

- (a) Existence of at least one previous episode, mild, moderate, or severe depression episode, lasting for a minimum of 2 weeks and separated from the current episode by at least 2 months.
- (b) Nonexistence in the past or present hypomanic or manic episode.
- (c) Nonexistence of hallucinations, delusions, or depressive stupor.
- (d) Non-use of psychoactive substances.
- (e) Absence of organic mental disorder.
- (f) Non-use of psychoactive substances.
- (g) Abnormal and constant depressed mood for at least 2 weeks.
- (h) Loss of interest or pleasure in activities that normally are pleasurable.
- (i) Decreased energy or increased fatigability.
- (j) Loss of confidence and self-esteem.
- (k) Unjustified feelings of guilt.
- (l) Recurrent thoughts of death or suicide.
- (m) Lack of concentration and indecision.
- (n) Change in psychomotor activity.
- (o) Sleep disturbance.
- (p) Change in appetite with corresponding weight change.

*1.6.4. Recurrent depressive disorder, current episode severe with psychotic symptoms*

- (a) Existence of at least one previous episode, mild, moderate, or severe depression episode, lasting for a minimum of 2 weeks and separated from the current episode by at least 2 months.
- (b) Nonexistence in the past or present hypomanic or manic episode.
- (c) Non-use of psychoactive substances.
- (d) Non-use of psychoactive substances.
- (e) Abnormal and constant depressed mood for at least 2 weeks.
- (f) Loss of interest or pleasure in activities that normally are pleasurable.
- (g) Decreased energy or increased fatigability.
- (h) Loss of confidence and self-esteem.
- (i) Unjustified feelings of guilt.
- (j) Recurrent thoughts of death or suicide.
- (k) Lack of concentration and indecision.
- (l) Change in psychomotor activity.
- (m) Sleep disturbance.
- (n) Change in appetite with corresponding weight change.

### 1.6.5. *Recurrent depressive disorder, currently in remission*

- (a) Existence of at least one recurrent depressive episode in the past.
- (b) Nonexistence of depressive episode in the present.

## 1.7 *Persistent mood [affective] disorders*

### 1.7.1. *Cyclothymia*

- (a) Instability of mood for at least 2 years.
- (b) Several periods of both depression and hypomania.
- (c) Nonexistence of manic episode or depressive episode in the last 2 years.
  - During the depression stage at least three of the following should be present:
    - Decreased energy or activity.
    - Insomnia.
    - Loss of self-confidence or feelings of inadequacy.
    - Difficulty concentrating.
    - Social withdrawal.
    - Loss of interest or enjoyment in sex and other pleasurable activities.
    - Less talkative.
    - Pessimism.
  - During the mood elevation stage at least three of the following should be present:
    - Increased energy or activity.
    - Decreased need for sleep.
    - Inflated self-esteem.
    - Sharpened or unusually creative thinking.
    - Excessive sociability
    - Increased spirituality or talkativeness
    - Increased interest and involvement in sexual and other pleasurable activities.
    - Over-optimism.

### 1.7.2. *Dysthymia*

- (a) A period of at least 2 years of constant or constantly recurring depressed mood.
- (b) Nonexistence of hypomanic episode.
- (c) None or very few episodes of recurrent mild depressive disorder in the last 2 years.

- During the depression stage at least three of the following should be present:
  - A reduction in energy or activity.
  - Insomnia.
  - Loss of self-confidence or feelings of inadequacy.
  - Difficulty concentrating.
  - Often in tears.
  - Loss of interest or enjoyment in sex and other pleasurable activities.
  - Feeling of hopelessness or despair.
  - Failure to adapt the routine responsibilities of everyday life.
  - Pessimism.
  - Social withdrawal.
  - Less talkativeness.

## 2. Neurological disorders

### 2.1 Autism

- (a) Social adjustment difficulties.
- (b) Breakdown in communication.
- (c) Limited interests.
- (d) Repetitive kinetics behavior.
- (e) Eating certain foods.
- (f) Unresponsive on hearing their name.
- (g) Lack of visual contact.
- (h) Problematic interpersonal relationships.
- (i) Delayed speech and voice development.
- (j) Repetitive and stereotyped behaviors.

### 2.2 Dyslexia

- (a) Difficulties in writing skills.
- (b) Difficulty in speaking.
- (c) Difficulties in writing.
- (d) Problems in spelling.
- (e) Delay in learning to read.
- (f) Difficulties in mathematics.
- (g) Problems with memory.
- (h) Problems in reading.
- (i) Reciprocating skills event.
- (j) Problems in the estimation of distance and space.
- (k) Confusion with directions.
- (l) Time management problems.
- (m) Confusing similar-sounding words.

### 2.3 *Mental retardation*

- (a) Attention disorder.
  - (b) Hyperactivity.
  - (c) Impulsiveness.
  - (d) Psychoses.
- Existence of the following disorders:
    - Anxiety disorders.
    - Eating disorders.
    - Mental disorders.
    - Mood disorders.

### 2.4 *Aphasia*

- (a) Difficulty in speaking and hearing.
- (b) Difficulty in understanding and writing skills.
- (c) Difficulty in mathematical calculations.
- (d) Difficulty in communicating.

### 2.5 *Attention-Deficit Hyperactivity Disorder*

- (a) Inattention.
- (b) Distractibility.
- (c) Hyperactivity.
- (d) Nervousness.
- (e) Impulsiveness.
- (f) Impatience.

### 2.6 *Dyspraxia*

- (a) Tension.
- (b) Hyperactivity.
- (c) Poor mobility.
- (d) Absence of risk perception.
- (e) Confusing.
- (f) Trouble in body balance.
- (g) Distractibility.
- (h) Tendency to isolation.
- (i) Disturbances in speech.

### 2.7 *Dysphasia*

- (a) Difficulty with speech.
- (b) Difficulty in understanding.
- (c) Difficulty in hearing.
- (d) Difficulty in writing.
- (e) Difficulty in mathematical calculations.
- (f) Difficulty in communicating.

### 2.8 Huntington disease

- (a) Changes in personality.
- (b) Changes in physical skills.
- (c) Changes in cognitive function (loss of memory , abstract thinking).
- (d) Spasmodic random and uncontrollable movements (called chorea).
- (e) Lack of coordination.
- (f) Delayed eye movements.
- (g) Stiffness.
- (h) Volatility.
- (i) Difficulties in chewing, swallowing, and speech.
- (j) Difficulty feeding.
- (k) Sleep disorders.
- (l) Anxiety.
- (m) Depression.
- (n) Aggression.
- (o) Egocentrism.
- (p) Deterioration addictions.
- (q) Hallucinations.
- (r) Psychosis.
- (s) Dementia.

### 2.9 Tourette Syndrome

- (a) Physically teak.
  - (b) Blinking eye.
  - (c) Shaking head.
  - (d) Lifting shoulder.
  - (e) Grimacing face.
  - (f) Leaps.
  - (g) Swirled around himself.
  - (h) Vocal tics.
  - (i) Cleaning neck.
  - (j) Sucking nose.
  - (k) Shouts.
  - (l) Irrelevant words.
  - (m) Suicidal behavior.
  - (n) Hyperactivity.
- Existence of the following disorders:
    - Coprolalia.
    - Echolalia.
    - Palilalia.
    - Obsessive–compulsive disorder.
    - Attention-deficit disorder.
    - Learning disorders.
    - Sleep disorders.

### 2.10 Paralysis of Bell (Bell's Palsy)

- (a) Backlash.
- (b) Paralysis of one or both sides of the face.
- (c) Slowness of lower eyelid and corner of the mouth.
- (d) Inability to fully closing the eye.
- (e) Escape saliva.
- (f) Problems in taste.
- (g) Dry eyes or mouth.
- (h) Eye tearing.
- (i) Pain in the ear.
- (j) Headaches.
- (k) Difficulty chewing and swallowing.

### 2.11 Down Syndrome

- (a) Mental retardation.
- (b) Low stature.
- (c) Psychological disorders.
- (d) Tendency to obesity.
- (e) Damage to the digestive tract.
- (f) Congenital cardiac defects.
- (g) Endocrinopathies.
- (h) Musculoskeletal abnormalities.
- (i) Respiratory vulnerability.
- (j) Low-average life expectancy.
- (k) Eye problems.
- (l) Reproductive disorders.
- (m) Remote features in face.
- (n) Wide and flat face.
- (o) Microcephaly.
- (p) Small and round ears.
- (q) Hypoplastic pug nose.
- (r) Slant eyes with odd folds of skin.
- (s) No middle groove of the tongue.
- (t) Narrow and high palate.
- (u) Short lower jaw.
- (v) Short neck with an extra skin fold neck.
- (w) Flexibility.
- (x) The hands are near and wide.
- (y) Low stature.
- (z) Hyperkinesis.
- (aa) Depression.



### 2.12 *Charcot Marie Tooth*

- (a) Influence motor and sensory nerve.
- (b) Weakness of the muscles of the lower limbs.
- (c) Deformation of the legs.
- (d) Weakness in arms.
- (e) Abnormal and unreasonable pain.
- (f) Hammertoes.
- (g) Reduced ability to run.
- (h) Sensory disturbances.
- (i) Disorder mobility.
- (j) Erectile impotence.
- (k) Disorders of urination.
- (l) Diarrhea.

### 2.13 *Alexia*

- (a) Inability in reading and oral expression.
- (b) Partial or total blindness.
- (c) Problems in understanding and writing skills.
- (d) Failure or substituting words.
- (e) Transfer of letters in words.
- (f) Problems with spelling.
- (g) Delay in speech.
- (h) Confusion with directions.
- (i) Confusion with the opposite.
- (j) Problems in math.

### 2.14 *Multiple Sclerosis Center*

- (a) Problems in speech.
- (b) Problems in vision.
- (c) Problems in memory.
- (d) Weakness in arm or leg.
- (e) Loss of urine.
- (f) Numbness in face or arm or leg.
- (g) Vertigo.
- (h) Instability.

### 2.15 *Epilepsy and seizure disorders*

- (a) Loss of awareness.
- (b) Moving disorders.
- (c) Sensation disorders.

### 2.16 *Schizophrenia*

- (a) Somatic hallucinations.
- (b) Auditory hallucinations.

- (c) Disorganized speech and thinking.
- (d) Disorganized behavior.
- (e) Catatonic behavior.
- (f) Blunted or flattened affect.
- (g) Alogia.
- (h) Avolition.
- (i) Anhedonia.
- (j) Anosognosia.
- (k) High rates of substance-abuse disorders.
- (l) High risk of suicide.

### 3. Daily functions

#### 3.1. Anorexia

- (a) Constant starvation.
- (b) Data suggesting alterations in brain size.
- (c) Neurotransmitter unbalance.
- (d) Abnormal hormonal secretion signals originating from the brain.
- (e) Genital dysfunction.
- (f) Problem amenorrhea.
- (g) A chronic weakening of the heart.
- (h) Bradycardia.
- (i) Arrhythmias.
- (j) Digastric motility and delayed gastric emptying.
- (k) Bloating.
- (l) Constipation.
- (m) Problematic bone growth.
- (n) Development of osteoporosis.
- (o) Cold hands and feet.
- (p) Dry skin.
- (q) Hair loss.
- (r) Headaches.
- (s) Fainting.
- (t) Dizziness.
- (u) Lethargy.
- (v) Develop lanugo on the face or back.
- (w) Inability to concentrate.
- (x) Irrascibility.
- (y) Depression.
- (z) Socially withdrawn.
- (aa) Obsessively avoid food.
- (bb) Hypothermia.
- (cc) Lowered glucose and white blood cell rates.
- (dd) A loss of muscle mass.

### 3.2. *Bulimia*

- (a) Nausea.
- (b) Abdominal distension.
- (c) Cramping.
- (d) Slowed digestion.
- (e) Weight gain.
- (f) Self-induced vomiting.
- (g) Erosion of tooth enamel.
- (h) Enlargement of the salivary glands.
- (i) Scars and calloused areas on the knuckles from contact with the teeth.
- (j) Irritation of the throat and esophagus from contact with stomach acid.
- (k) Tearing of mucous membranes in the upper gastrointestinal tract or perforation of the esophagus and stomach wall.
- (l) Perforation of part of the digestive tract.
- (m) Loss of fluids.
- (n) Depletion of hydrogen chloride, potassium, sodium, and magnesium.
- (o) Hypokalemia.
- (p) Irregular menstrual periods.
- (q) Petechiae in the skin around the eyes and rectal prolapse.

### 3.3. *Nonorganic sleep disorders*

#### 3.3.1. *Nonorganic insomnia*

- (a) Difficulty in falling asleep.
- (b) Frequent sleep disturbances.
- (c) Awaken too early in the morning.
- (d) Too light sleeping.
- (e) Reduced ability to concentrate or pay attention.
- (f) Decreased alertness.
- (g) Mental sluggishness.

#### 3.3.2. *Nonorganic hypersomnia*

- (a) Problems with the morning waking.
- (b) Staying awake during the day.
- (c) Sleep for 18 or more hours a day.
- (d) Irrascibility.
- (e) Indiscriminate sexual advances.
- (f) Eat uncontrollably.
- (g) Rapidly gain weight.

### 3.3.3. *Sleepwalking:*

- (a) No memory of the sleepwalking events.
- (b) Great difficulty to awaken.
  - During the sleep:
    - Sitting up in bed.
    - Looking around and walking.
    - Attempts at communication.
    - Eyes open.
    - Dilated pupils.
    - A blank stare.
    - Not respond to another's attempts at communication.

### 3.3.4. *Nightmare disorder*

- (a) Symptoms of anxiety or fear.
- (b) Prominence of the dream images in the person's mind.
- (c) Waking from the nightmare with a profound sense of fear.
- (d) Good recall of the dream and what was so frightening about it.
- (e) Avoid going to sleep after a particularly intense.
- (f) Decreased mental clarity.
- (g) Problems paying attention.
- (h) Excessive daytime sleepiness.
- (i) Irritability.
- (j) Mild depression.
- (k) Problems with falling.
  - During the sleep:
    - The sleeper may moan, talk, or move slightly.
    - Increased heart rate.
    - Sweating.

### 3.4. *Stress*

- (a) Withdrawing from social activities.
- (b) Avoiding stimuli associated with the revival of the event.
- (c) Increased heart rate.
- (d) Alternations in the rhythm of the heart.
- (e) Release of extra clotting factors into the blood.
- (f) Release of fat into the bloodstream.
- (g) Diarrhea.
- (h) Constipation.
- (i) Bloating.
- (j) Irritable bowel syndrome.
- (k) Abnormal weight loss or gain.

- (l) Chronic pain of arthritis and other joint disorders.
- (m) Tension-type headaches.

#### 4. *Addiction*

##### 4.1. *Addiction to Caffeine*

- (a) Feeling nervousness.
- (b) Feeling excitement.
- (c) Feeling restlessness.
- (d) Sleep disturbances.
- (e) Diuresis.
- (f) Gastrointestinal disorders.
- (g) Muscle contractions.
- (h) Disturbed heartbeat.
- (i) Immunity to caffeine.
- (j) Ringing in the ears.
- (k) Flashes of light.
- (l) Seizures.
- (m) Respiratory failure.
- (n) Headache.
- (o) Fatigue.
- (p) Depression.
- (q) Difficulty concentrating.
- (r) Trouble sleeping.
- (s) Constipation.
- (t) Problems in school.
- (u) Flu-like symptoms such as stuffy nose and vomiting.
- (v) Inability in everyday responsibilities.

##### 4.2. *Addiction to computers*

- (a) Lack of sense of time.
- (b) Problems in their daily obligations.
- (c) Great change in progress at school.
- (d) Isolation from friends and family.
- (e) Creating a sense of joy and euphoria during use computers.
- (f) Carpal tunnel syndrome.
- (g) Pain in the neck and back.
- (h) Changes in sleep hours.
- (i) Severe headaches.
- (j) Blurred vision.
- (k) Intense weight change.
- (l) Unsuccessful attempts to restrict its use.
- (m) Telling lies for the reason that sits on the computer.
- (n) Excessive cash outlays for the purchase of products for the computer.
- (o) Possible disruption of school.

- (p) Lack of personal hygiene.
- (q) Many hours of isolation.
- (r) Withdrawal symptoms and anxiety when they do not use computers.

#### 4.3. *Addiction to Drugs*

- (a) Red eyes.
- (b) Frequent nose bleeds.
- (c) Itchy nose and runny.
- (d) Changes in sleeping routine.
- (e) Changes in appetite.
- (f) Changes in body weight.
- (g) Changes in clothing
- (h) Lack of personal hygiene.
- (i) Usual chills.
- (j) Changes in speech.
- (k) Loss of concentration.
- (l) Weakness.
- (m) Unusual hyperactivity.
- (n) Sudden irritability.
- (o) Outbursts.
- (p) Memory loss.
- (q) Nervousness.
- (r) Absenteeism at school.
- (s) Large change in behavior at school.
- (t) Drop in grades.
- (u) Indifference for extracurricular activities and a hobby.
- (v) Suspicious secretive behavior.
- (w) Sudden change in relationships with friends.
- (x) Sudden change on mood.
- (y) New friendships.
- (z) Unusual odor on breath.
- (aa) Unusual odor on body.
- (bb) Unusual odor on clothes.
- (cc) Signs of needles into specific points on the body.
- (dd) Abnormal heartbeat.
- (ee) Dry cough.
- (ff) Nausea.
- (gg) Vomiting.
- (hh) Sudden need for more money.
- (ii) Sudden secretive about things.
- (jj) Stays out unusually late.
- (kk) Unreasonable use of air conditioning.
- (ll) Cough

- When the use of drugs is already known.
  - Need a higher dose of drug to have the same result as before.
  - Theft to find money for drugs.
  - The use of drugs to withstand the deprivation of the substance.
  - Frequent respiratory infections.
  - Possible mental health decline.
  - Constipation.
  - Endocarditis.
  - Hepatitis.
  - HIV.
  - Inability to stop using.
  - Possession of various ancillary drug paraphernalia.
  - Fatal overdose.
  - Weight loss.
  - Insomnia.
  - Cardiac or cardiovascular complications.
  - Stroke.
  - Seizures.
  - Sleep disturbances.
  - Depression.
  - Impaired memory.
  - Hyperthermia.
  - Anxiety.
  - Tremors.
  - Numbness.
  - Memory loss.
  - Nausea.
  - Flashbacks.
  - Hallucinogen persisting perception disorder.
  - Hypertension.
  - Blood clotting.
  - Cholesterol changes.
  - Liver cysts.
  - Hostility.
  - Aggression.
  - Acne.
  - Stoppage of growth.
  - In males—prostate cancer.
  - In males—reduced sperm production.
  - In males—shrunken testicles.

- In males—breast enlargement.
- In females—menstrual irregularities.
- In females—development of beard and other masculine characteristics.

#### 4.4. *Addiction to food*

- (a) At least three of the following symptoms must be present:
- For certain foods, eat more than planned.
  - Eating certain foods even when not hungry.
  - Eating without limits.
  - Stress because of the lack of certain food.
  - Stress and depression for the act-eating.
  - Combat of negative feelings and euphoria because of eating certain foods.
  - Inability to control the amount of food and passion for some food.
  - Failed attempts with various weight loss diets.
  - Eating in secret.
  - Pay more attention to the food than to friends and relatives.
  - Eating all day or at short intervals several times.
  - Avoiding social events.
  - Embarrassment about the body image.
  - Steal food from others.
  - Inability to stop the large amount in particular foods.
  - Use of laxatives and diuretics.
  - Self-induced vomiting.
  - Fasting and excessive exercise to eliminate the food.
  - Unable to stop overeating even if wants to.
  - Weight loss or weight gain.
  - Determination of the mood by the appearance and the weight.
  - Frequent use of mirror and scale.
  - Use clothing that is loose.
  - Buying clothes in a different size than normal.
  - Fear for weighing.
  - Negative comments about their body to others.
  - Check for various defects in the body.
  - Removal from various activities due weight.
  - Hiding food in strange places.
  - Eat faster than normal.
  - Extreme emotions when eating addictive substances.
  - Reduce energy and intense fatigue.
  - Difficulty in concentration.
  - Sleep disorder.
  - Headache.
  - Digestive disorders.



- Low self-esteem.
- Heart problems.
- High cholesterol.
- Diabetes.
- Hypertension.
- Kidney disease.
- Arthritis.
- Obesity.
- Panic attacks.
- Isolation from other people.
- Unstable progress at school.

#### 4.5. *Addiction to lie*

- (a) Lack of confidence and low self-esteem.
- (b) Deservedness.
- (c) Propensity to say realistic and persuasive stories.
- (d) Ability to cover lies.
- (e) Successful disclaimer by blaming others.
- (f) Looking into other's eyes while lying.
- (g) Defensiveness.

#### 4.6. *Addiction to nicotine*

- (a) Unsuccessful attempts to quit smoking.
- (b) Continued smoking despite health problems.
- (c) Chronic lung disease.
- (d) Cardiovascular disease.
- (e) Stroke.
- (f) Cancer of the mouth.
  - Health problems in:
    - Pharynx.
    - Larynx.
    - Esophagus.
    - Stomach.
    - Pancreas.
    - Cervix.
    - Kidney.
    - Bladder.
    - Heart.
- (g) Acute myeloid leukemia.
- (h) Adverse pregnancy outcomes.
- (i) Problems increase in blood pressure.

- (j) Change habits and fun time to consistent with the possibility for smoking.
- (k) Smoking becoming priority.
- (l) Continues increase of the amount of nicotine.
- (m) Use of a greater amount than originally calculated for cigarettes.
  - During the break in their use:
    - Anxiety.
    - Frustration.
    - Anger.
    - Sleep disturbance.
    - Weakness concentration.
    - Increased appetite.
    - Weight gain.
    - Depression.
    - Decreased heart rate.
    - Headache.
    - Panic.
    - Redirecting.
    - Fatigue.
    - Constipation.
    - Loss of performance.

#### 4.7. Alcohol addiction:

- (a) Alcohol use until drunkenness.
- (b) Display problems in family, friendships, and school.
- (c) Immunity to alcohol.
- (d) Memory gaps after the drunkenness.
- (e) Refusal problems.
- (f) Unsuccessful attempts to quit drinking.
- (g) Distant from extracurricular activities.
- (h) Hidden alcohol use at school.
- (i) Emotional and physical problems.
- (j) Increased violence after drinking.
- (k) Hostility when they need to answer questions about alcohol.
- (l) Consume alcohol alone.
- (m) Excuses for drinking.
- (n) Engaging in dangerous and illegal situations.
- (o) Spend large amounts of money buying alcohol.
- (p) No clear speech.
- (q) Unbalance.
- (r) Reduction of reflexes.
- (s) Emotional volatility.
- (t) Change in appearance.
- (u) Changes in food and sleep routine.

- (v) Slow or uncontrollable eye movements.
- (w) Impaired vision.
  - During drunkenness:
    - Facial redness.
    - Delusions.
    - Hallucinations.
    - Insomnia.
    - Strong heartbeat.
    - Fever.
    - Nausea.
    - Tremors.
    - Nightmares.
    - Dilated pupils.
    - Anxiety.
    - Nervousness.
    - Depression.
    - Fatigue.
    - Pain.
    - Sweating.

#### 4.8. Gambling addiction

- (a) Persistence for gambling.
- (b) Lack of time for family and friends.
- (c) Use the entire tip for gambling.
- (d) Theft of money.
- (e) Non-control of the money and the time spending by playing.
- (f) Failed attempts to stop it.
- (g) Changes in lifestyle.
- (h) Differences in food and personal hygiene habits.
- (i) Persistence thoughts of finding money.
- (j) Lies to parents and friends.
- (k) Daily playing.
- (l) Relationship with “dangerous” people.
- (m) Puts aside his daily school obligations to play.
- (n) Anxiety.
- (o) Depression.
- (p) Alcohol and drug use.
- (q) A sudden desire to learn the value of the house.
- (r) Asking money from friends and family.
- (s) Thoughts or attempts of suicide.
- (t) Sleep deprivation.
- (u) Weight gain or loss.

- (v) Dark circles under the eyes.
- (w) Willing to play even when he have no money.
- (x) Irrascibility.
- (y) Angriiness.
- (z) Nervousness.

#### 4.9. Internet addiction

- (a) Internet use for extended periods.
- (b) Inability to stop using Internet.
- (c) Distance from family and friends.
- (d) Feelings of pleasure when using the Internet.
- (e) Major changes in grades.
- (f) Distance from school.
- (g) Lack of sleep.
- (h) Fatigue.
- (i) Change in external appearance.
- (j) Weight changes.
- (k) Headache.
- (l) Back pain syndrome carpal tunnel.
- (m) Not fed properly.
- (n) Lack of personal hygiene.
- (o) Reduce functionality outside Internet.
- (p) Reduced interest in hobbies.
- (q) Denial of reality.
- (r) Lies to close people.
- (s) When removed from the Internet have feelings of nervousness and melancholy.

#### 4.10. Kleptomania

- (a) Repeated theft of objects that are unnecessary.
- (b) Before the act of theft there is increasing excitement
- (c) During the theft feels pleasure and relief.
- (d) After the act feels shame and remorse.
- (e) Cravings for theft.
- (f) Inability to stop this desire after many attempts.
- (g) These products are not used to and sometimes returned back.

#### 4.11. Sex addiction

- (a) Large number of partners.
- (b) Cybersex or phone sex.
- (c) Excessive masturbation.
- (d) Resumption of sexual intercourse several times in a day.
- (e) Recurrent thoughts about the sexual act and everything has to do with this.
- (f) Nervousness and anxiety in idleness.

- (g) Often one-night stands.
- (h) Feeling demonstration and contacts with prostitutes.
- (i) Exhaustion.
- (j) Physical injuries.
- (k) Addiction to porn and voyeurism.
- (l) Cases of rape and sexual harassment.
- (m) Lies to friends and family for sexual acts.
- (n) Thoughts and fantasies about the sexual act.
- (o) Irresponsibility resulting unwanted pregnancies and aphrodisiac diseases.
- (p) Failure to stop and continued despite the adverse impact on it.
- (q) Isolation from friends and family.
- (r) Disregard for the school and its progress.
- (s) Unable to resist even in extreme and bizarre sexual acts.
- (t) Inability to control the wills.
- (u) Domination sense of insecurity for abandonment.
- (v) Constantly changing relationships.

#### 4.12. *Shopping addiction*

- (a) At least four symptoms must be present:
  - Large cash outlays.
  - Overcoming the initial budget.
  - Continuous buying of a product in a particular period.
  - Lies to parents.
  - Buying things on credit cards which they cannot cover.
  - Obsession with money.
  - Guilt and remorse at the end of a purchase.
  - Buy things every day or every week.
  - Feelings of joy and euphoria during operation.
  - Buying unnecessary things.
  - Repeated failed attempts to stop it.
  - Financial problems.
  - Defensive behavior when someone asks for shopping.
  - They spend more than they can financially.

#### 4.13. *Video games addiction*

- (a) Non-control of playing time.
- (b) Distance from friends and family.
- (c) Neglect of personal hygiene.
- (d) Feeling indifference to the complaints of friends and family for dereliction.
- (e) Spend large amounts of money for games.
- (f) Feelings of joy and elation when playing.
- (g) Feeling sadness, anger, and anxiety when cannot play.

- (h) Unusually weight increase and decrease.
- (i) Unsociality.
- (j) Conflicts with parents and friends.
- (k) Problems in school and grades.
- (l) Musculoskeletal disorders of the upper limb.
- (m) Fatigue.
- (n) Headache.
- (o) Red or dry eyes.
- (p) Syndrome carpal tunnel.
- (q) Changes in sleep schedules.
- (r) Lies for real-time playing.
- (s) Personality change.
- (t) Pain in the back.
- (u) Playing marathon games.
- (v) Not engaged in other activities.
- (w) Unable to stop a game in order to do the homework.
- (x) New online friends.
- (y) Increasing communication with Internet friends.
- (z) Wearing diapers for adults not to interrupt the game.
- (aa) Spend all the spare time in games.
- (bb) Dreams just for the game.
- (cc) Talking for the games even when not playing.

#### 4.14 *Addiction to prescription drugs*

- (a) Increased dose.
- (b) Continuous use.
- (c) Visits to numerous doctors to get more recipes.
- (d) Borrowing drugs.
- (e) Abnormal use.
- (f) Lying to friends and family.
- (g) Problems with friends and family.
- (h) Theft or forgery of prescriptions.
- (i) Theft drugs.
- (j) Mood swings depending on the use or not of drugs.
- (k) Changes in sleep.
- (l) Changes in food.
- (m) Unstable weight.
- (n) Sale of drugs for money.
- (o) Not convincing answers to doctors for the use of recipes.
- (p) Difficulty making decisions.
- (q) Appearing intoxicated or excessive energy or is lethargic.
- (r) Fear of the different.

- (s) Believing that without the substance cannot function properly.
  - (t) Lack of interest in hobbies.
  - (u) Unconsciousness and amnesia.
  - (v) Continued use despite its impact on their health.
  - (w) Immunity to drugs.
- Depending on the drugs may result in health problems such as:
    - Slowed breathing.
    - Tolerance.
    - Withdrawal.
    - Lowered pulse and blood pressure.
    - Unconsciousness.
    - Increased heart rate.
    - Metabolism disorders.
    - Reduced appetite.
    - Nervousness.
    - Insomnia.
    - Seizures.
    - Increased heart rate.
    - Dizziness.
    - Nausea.
    - Vomiting.
    - Confusion.
    - Paranoia.
    - Distorted visual perceptions.
    - Impaired motor function.

## References

1. Barnes G, Welte J, Hoffman J, Dintcheff B (2005) Shared predictors of youthful gambling, substance use, and delinquency. *Psychol Addict Behav* 19(2):165–174
2. Delfabbro P, Lahn J, Grabosky P (2006) Psychosocial correlates of problem gambling in Australian students. *Aust N Z J Psychiatry* 40(6):587–595
3. Derevensky JL, Gupta R, Winters K (2003) Prevalence rates of youth gambling problems: are the current rates inflated? *J Gambl Stud* 19:405–425
4. Dickson L, Derevensky J, Gupta R (2002) The prevention of gambling problems in youth: a conceptual framework. *J Gambl Stud* 18(2):97–159
5. Dickson L, Derevensky J, Gupta R (2008) Youth gambling problems: examining risk and protective factors. *Int Gambling Stud* 8(1):25–47
6. Gerdner A, Svensson K (2003) Predictors of gambling problems among male adolescents. *Int J Soc Welf* 12(3):182–192
7. Block JJ (2008) Issues for DSM-V: internet addiction. *Am J Psychiatry* 165(3):306–307. doi:[10.1176/appi.ajp.2007.07101556](https://doi.org/10.1176/appi.ajp.2007.07101556)
8. Byun S, Ruffini C, Mills JE, Douglas AC, Niang M, Stepchenkova S, Lee SK, Loutfi J, Lee JK, Atallah M, Blanton M (2009) Internet addiction: metasynthesis of 1996–2006 quantitative research. *Cyberpsychol Behav* 12(2):203–207

9. Young KS (1998) Internet addiction: the emergence of a new clinical disorder. *Cyberpsychol Behav* 1:237–244. doi:[10.1089/cpb.1998.1.237](https://doi.org/10.1089/cpb.1998.1.237)
10. Shapira N, Goldsmith T, Keck P, Khosla UM, McElroy SL (2000) Psychiatric features of individuals with problematic internet use. *J Affect Disord* 57(1):267–272. doi:[10.1016/S0165-0327\(99\)00107-X](https://doi.org/10.1016/S0165-0327(99)00107-X)
11. Taintor Z (2004) Telemedicine, telepsychiatry, and online therapy. In: Sadock BJ, Sadock VA (eds) *Kaplan and Sadock's comprehensive textbook of psychiatry*. Lippincott Williams & Wilkins Publishers, Philadelphia, PA, pp 955–963
12. Young KS, Rogers RC (1998) The relationship between depression and internet addiction. *Cyberpsychol Behav* 1(1):25–28. doi:[10.1089/cpb.1998.1.25](https://doi.org/10.1089/cpb.1998.1.25)
13. Appendix D—DSM-IV-TR Mood Disorders.(2012) (n.d.) Managing depressive symptoms in substance abuse clients during early recovery. <http://www.ncbi.nlm.nih.gov/books/NBK64063/>. 1 Aug 2012
14. Bhatia SK, Bhatia SC (2007) Childhood and adolescent depression. *Am Fam Physician* 75 (1):73–80. <http://www.aafp.org/afp/2007/0101/p73.html>. Retrieved 1 Aug 2012
15. FAQs on Child and Adolescent Depression (n.d.) American Academy of Child & Adolescent Psychiatry. [http://www.aacap.org/cs/child\\_and\\_adolescent\\_depression\\_resource\\_center/faqs\\_on\\_child\\_and\\_adolescent\\_depression](http://www.aacap.org/cs/child_and_adolescent_depression_resource_center/faqs_on_child_and_adolescent_depression). Retrieved 1 Aug 2012
16. <http://protege.stanford.edu/>
17. Brown NL, Gletsos M, Mougiakakou S, Matsopoulos G, Nikita KS, Nikita A, Kelekis D (2003) A computer-aided diagnostic system to characterize CT focal liver lesions: design and optimisation of a neural network classifier. *IEEE Trans Inf Technol Biomed* 7:153–162
18. Goldberg DE (1989) *Genetic algorithms in search, optimization and machine learning*. Addison-Wesley Publishing, Redwood City, CA
19. Golemati S, Sassano A, Lever MJ, Bharath AA, Dhanjil S, Nicolaidis AN (2003) Carotid artery wall motion estimated from B-mode ultrasound using region tracking and block-matching. *Ultrasound Med Biol* 29:387–399
20. Golemati S, Tegos TJ, Sassano A, Nikita KS, Nicolaidis AN (2004) Echogenicity of B-mode sonographic images of the carotid artery – work-in-progress. *J Ultrasound Med* 23:659–669
21. Anxiety Disorders and Stress (n.d.) American Psychological Association. [http://www.apa.org/divisions/div12/rev\\_est/anxiety.html](http://www.apa.org/divisions/div12/rev_est/anxiety.html). Retrieved 12 Jul 2012
22. Nutrition and Mental Health (2011) FamilyDoctor.org. <http://familydoctor.org/familydoctor/en/prevention-wellness/emotional-wellbeing/mental-health/nutrition-and-mental-health.html>. Retrieved 12 Jul 2012
23. Rogge T (2011) Stress and anxiety. National Library of Medicine - National Institutes of Health. <http://www.nlm.nih.gov/medlineplus/ency/article/003211.htm>. Retrieved 12 Jul 2012
24. Anorexia Nervosa (n.d.) NAMI: National Alliance on Mental Illness. [http://www.nami.org/Template.cfm?Section=By\\_Illness&template=/ContentManagement/ContentDisplay.cfm&ContentID=7409](http://www.nami.org/Template.cfm?Section=By_Illness&template=/ContentManagement/ContentDisplay.cfm&ContentID=7409). Retrieved 19 Apr 2012
25. Anorexia nervosa (n.d.) Mayo Clinic. <http://www.mayoclinic.com/health/anorexia/DS00606>. Retrieved 19 Apr 2012
26. Anorexia nervosa - PubMed Health (n.d.) National Center for Biotechnology Information. <http://www.ncbi.nlm.nih.gov/pubmedhealth/PMH0001401/>. Retrieved 19 Apr 2012
27. Alcoholics Anonymous (2012) Alcoholics Anonymous. <http://www.aa.org/?Media=PlayFlash> <http://www.aa.org/?Media=PlayFlash>. Retrieved 13 Jul 2012
28. Alcoholism (2010) Mayo Clinic. <http://www.mayoclinic.com/health/alcoholism/DS00340>. Retrieved 11 Jul 2012
29. Alcoholism (2011) University of Maryland Medical Center. <http://www.umm.edu/altmed/articles/alcoholism-000002.htm>. Retrieved 11 Jul 2012
30. Dysthymia (2005) Harvard Medical School. <http://www.health.harvard.edu/newsweek/Dysthymia.htm>. Retrieved 28 Jun 2012
31. Dysthymia (2010) Mayo Clinic. <http://www.mayoclinic.com/health/dysthymia/DS01111>. Retrieved 28 Jun 2012



32. Dysthymia (2010) National Library of Medicine – National Health Institutes. <http://www.nlm.nih.gov/medlineplus/ency/article/000918.htm>. Retrieved 28 Jun 2012
33. Bipolar disorder: treatments and drugs - MayoClinic.com (n.d.) Mayo Clinic. <http://www.mayoclinic.com/health/bipolar-disorder/DS00356/DSECTION=treatments-and-drugs>. Retrieved 11 Sep 2013
34. CQAIMH - STABLE measures: bipolar disorder or depression: assessment for risk of suicide. (n.d.). CQAIMH - center for quality assessment and improvement in mental health. [http://www.cqaimh.org/measure\\_ROS.html](http://www.cqaimh.org/measure_ROS.html). Retrieved 11 Sep 2013
35. NIMH - Bipolar Disorder (n.d.) NIMH - Home. <http://www.nimh.nih.gov/health/topics/bipolar-disorder/index.shtml>. Retrieved 11 Sep 2013
36. Nurnberger JI Jr, Foroud T (2000) Genetics of bipolar affective disorder. *Curr Psychiatry Rep* 2(2):147–157
37. Kessler RC, Chiu WT, Demler O, Walters EE (2005) Prevalence, severity, and comorbidity of twelve-month DSM-IV disorders in the National Comorbidity Survey Replication (NCS-R). *Arch Gen Psychiatry* 62(6):617–627
38. Kessler RC, Berglund P, Demler O, Jin R, Merikangas KR, Walters EE (2005) Lifetime prevalence and age-of-onset distributions. *Arch Gen Psychiatry* 62(6):593–602

# Chapter 10

## Mitochondrial Fusion Through Membrane Automata

Konstantinos Giannakis and Theodore Andronikos

**Abstract** Studies have shown that malfunctions in mitochondrial processes can be blamed for diseases. However, the mechanism behind these operations is yet not sufficiently clear. In this work we present a novel approach to describe a biomolecular model for mitochondrial fusion using notions from the membrane computing. We use a case study defined in BioAmbient calculus and we show how to translate it in terms of a P automata variant. We combine brane calculi with (mem)brane automata to produce a new scheme capable of describing simple, realistic models. We propose the further use of similar methods and the test of other biomolecular models with the same behaviour.

### 10.1 Introduction

During the last few decades, interdisciplinary research between the fields of Computer Science and Biology has brought forth a wide variety of results. Biological systems and their functions involve large numbers of (nested) components with complex, highly intrinsic parallel and stochastic behaviour. It is well known that biomolecular processes play an essential role for the regular function of an organism, whereas cells are the basic unit of life. In particular, mitochondria and their functions in eukariotic cells are under constant study [5, 13, 14, 20] in various scientific fields aside from biology and medicine. Furthermore, recent studies have revealed that malfunctions in mitochondrial processes such as fusion and fission can potentially be a factor to blame for neurodegenerative diseases [5, 14], e.g. Alzheimer's disease [21].

Mitochondria typically consist of enzymes, ribosomes, mitochondrial DNA and RNA, among others. They are surrounded by two membranes, the inner one and the outer one. Their main responsibility is the production of adenosine triphosphate (ATP), that is essential for the organism. The preservation of their population in a

---

K. Giannakis (✉) • T. Andronikos  
Department of Informatics, Ionian University, Corfu, Greece  
e-mail: [kgiann@ionio.gr](mailto:kgiann@ionio.gr); [andronikos@ionio.gr](mailto:andronikos@ionio.gr)

cell is crucial for the wealth of the whole organism. The main functions mitochondria perform in order to regulate their population in a cell are fusion and fission.

As far as the mitochondrial fusion is concerned, it can be depicted as a parallel structure where several units operate concurrently interacting with one another. Formal methods of modeling are used to simulate these intrinsic concurrent systems and in general they include typical mathematical methods to describe the behaviour of parallel structure. For example, many of them include stochastic models, such as *Markov processes* [12].

In this paper we consider P automata and their implementation on modeling a biological function (mitochondrial fusion) based on a previously described model in [2]. P systems (indicative references can be found in [17, 18]) and P automata [6–8, 10] are formal tools originating from the concept of membrane computing, with enhanced power and efficiency. Previous related work can be found in [4] where the membrane computing was combined with concepts from brane calculus [3], a process calculus of the same family with BioAmbients calculus.

The contribution of this paper lies on the fact that for the very first time P automata are combined with the BioAmbients calculus. We discuss the pros and cons of using our approach in describing biological models of this kind. Moreover, we demonstrate our proposed scheme using a realistic biomolecular model of mitochondrial fusion as a case study demonstrating the potential of our method. The use of P automata notions in describing a mitochondrial model is, also, a novelty of our study. The motivation behind our work is the importance of biomolecular functions for human's health, as stated above.

In Sect. 10.2, we introduce the concept of P automata and in Sect. 10.3 we briefly present the summary of Alexiou et al. [2] model which is described in BioAmbients calculus [19]. In Sect. 10.4 our main contribution is being analysed and finally in Sect. 10.5 we summarize our conclusion and directions for future work.

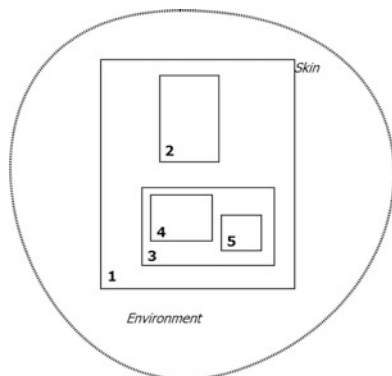
## 10.2 P Systems and P Automata

In this section we present a short review of notions inspired from the concept of *membrane computing* [15, 17, 18]. We start by introducing P systems, presenting the most notable works on them in relation with our study and, then we proceed into the analysis of P automata.

Computer science has a long tradition of getting inspiration from physical and biological processes and the bioinspired models are widely used. P systems and membrane computation, inspired from organic cells and their membranes, were used to model several systems and problems in computer science. When one uses P systems to model biological processes, he sees them in terms of dynamical systems. The focus of our work is on the (deterministic or probabilistic) evolution of these systems.

In brief, membrane computing was initiated in the late 1990s by G. Păun [17]. Since then, the field has widely spread and many variants have been proposed

**Fig. 10.1** A figure depicting a general hierarchical nested membranes as a Venn diagram



(e.g. [15, 17, 18]). Current literature has identified three main types of P systems: cell-like P systems, tissue-like P systems and neural-like P systems. In general, objects are represented by symbols from a alphabet. In addition, there are evolution rules on these objects, acting in specified compartments or even membranes.

There are different types of evolution rules in P systems. The most common type are rewriting rules on multisets imitating natural chemical reactions in biological system. These rules are of the form  $u \rightarrow v$  ( $u, v$  are multisets of objects). On the other hand, there are transport rules (e.g. symport and antiport rules). Moreover, the hierarchical status of membranes can evolve by constantly creating and destroying membranes, by membrane division, etc. Similarly to rules, objects themselves can be of various types usually denoted by letters from an alphabet.

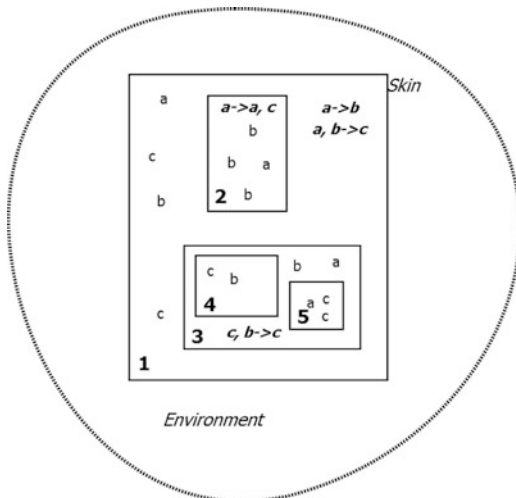
The outer membrane is called *skin* and the space which surrounds the membrane system is called *environment*. Membranes can contain other membranes creating a hierarchical structure. In addition, each membrane contains a series of objects and rules. Objects can be proteins or whatever can be inside a cell-like system (in our case a mitochondrion). Figure 10.1 shows a simple example of a P system.

P systems evolve via non deterministic, parallel rules, while the system being synchronized by a global clock. Current literature is full of P systems' variants and extensions. There are three fundamental characteristics that membrane systems possess: the membrane structure, multisets of objects, and rules [17, 18]. Mathematically P systems can be represented by a string of labelled matching parentheses and objects are on the region of each membrane (Fig. 10.2).

Membrane communication defines the passing of an object through a membrane. By using rules, transitions among configurations are made and a sequence of transitions is interpreted as computation. Accepted computations are those which halt and a successful computation can be associated with a result. There are three types of rules: objects evolving rules, objects communicating rules through membranes and membranes handling rules.

A membrane structure can be represented either by a Venn diagram or by a tree where the root represents the skin membrane. The main variants of P systems are P systems with active membranes, P systems with symport/antiport rules,

**Fig. 10.2** The membrane structure of Fig. 10.1, containing simple objects and rules. These objects may represent proteins, catalysts, etc.



communicating P systems, and tissue P system. There are two main types of communication rules among membranes: symport rules (the passing through a membrane strictly in the same direction) and antiport rules (the passing through a membrane in opposite directions).

P automata are variants of P systems with automata-like accepting behaviour [6–8, 10]. The first variants of P automata were one-way P automata having only symport rules [8], and analysing P systems, which accept a computation by halting configurations [11]. Nevertheless, the generic model of P automata is a P system with antiport rules. An input sequence is a sequence of multisets of objects which enters the system from the environment.

The computation starts from an initial configuration and acceptance is defined by a set of final states as in classic automata theory, except that these states define an computable set of configurations satisfying certain conditions. The language accepted by a P automaton is obtained from the set of accepted input sequences, like classic automata [7]. A configuration of a (simple) P automaton having  $n$  membranes at a step of the computation process is defined a  $n$ -tuple of multisets of object presented in each membrane space.

A run of a P automaton is defined as a process of altering its configurations in each step. This state changing is driven by a transition function which directly depends on the computational mode that is used. For example, there is the maximally parallel mode (which constrains the system to consume all the available resources during a single transition), the sequential mode, etc.

Another variant of the accepting P system is the analyzing P system introduced in [11]. A lot of variants of accepting P systems or P automata have been developed and studied; for detailed information the reader is referred to the survey [6] and the textbook of [18]. A  $P_{pp}$  automaton is a P automaton with marked membranes. In this model the system accepts objects as inputs from its surrounding

environment. Using non-empty marking of the skin membrane the system absorbs objects (e.g. proteins) from the environment.

### 10.3 A Mitochondrial Fusion Model

There are plenty of tools and mechanisms to choose from in order to formally describe biomolecular models. We chose the work of Alexiou et al. in [2] where a simple biological model of mitochondrial fusion was suggested. In future, our approach can be adapted to other similar models. In [2] the authors proposed a model describing the fusion of two mitochondria. In particular, they used the BioAmbient calculus [19], a process calculus based on the pi-calculus proposed by Milner in the early 1990s [16]. They investigated the distribution of mitochondrial fusion in the renewal of mitochondrial population within an eukariotic cell. Their model tries to explain the fusion process and it is described in terms of BioAmbients calculus.

BioAmbient calculus uses the notion of hierarchical compartments (i.e. *Ambients*) and their mobility mechanisms inside a cell. The morphology of the cell is divided into nested ambients under a predefined hierarchical structure. Specifically, proteins, membranes and communication channels take the role of separated and (if necessary) nested ambients. The four main characteristics of BioAmbients calculus are actions, directions, capabilities and processes, where capabilities and communications are synchronous.

Three mammalian proteins are required (Mfn1, Mfn2 and OPA1) for the successful fusion process [5, 20]. There are two ways fusion can occur. Firstly and most typically is by the merging of two membrane-bound segments, where two separated segments become one, with their contents shared. Merging is also divided in complete and transient fusion (known as *kiss-and-run*) [1]. Secondly, segments may enter or exit one another (e.g. mitophagy) or entry of a complex molecule into an organelle can occur. Synchronized capabilities that can alter the ambients' current state are entry, exit, or merge of other compartments.

To sum up, in this model, the proteins Mfn1 and Mfn2 in the outer mitochondrial membrane and OPA1 in the inner mitochondrial membrane are initially created. Then, OPA1 is being activated by Mfn1 and Mfn2 and finally, the merge of two independent mitochondria is occurred completing the process of mitochondrial fusion. At first, the creation of the Mfn1–Mfn2 begins with the transcription of DNA into mRNA. At the same time RNAMfn1–Mfn2 is able to react with Transl which contributes to the translation process. The mRNA translation is completed in two steps and the production of protein OPA1 follows a similar process. Note that the production process of the above two proteins is independent. Afterwards, the activating of protein OPA1 follows. It must be noted that the above procedure takes place using specific communication channels in each step (and sub steps) which are included in the definition of the model in BioAmbient calculus.

## 10.4 Our Approach

A first attempt to connect membrane computing notions with a biological process calculus was described in [4, 9]. In [3] brane calculi were proposed, a variation of process calculi aiming to describe biomolecular models with focus on membrane structures and membrane mobility, rather than the compartments they surround.

Both have in common the fact that they are inspired by the same cell section (membranes) but they differ in their core functions. Membrane computing is a pure computing model (using automata and language theoretic tools) motivated from the structure and the functioning of the biological cell, whereas brane calculi focus on the fidelity of the biological reality, thus having as a primary target strictly biological systems. In membrane computing, membranes are just separators of compartments and the main data structure used is the multiset of abstract objects whereas in the case of brane calculi the structure, properties, and evolution of membranes themselves matter.

The procedure of modeling particular biological activities through P systems' notions is neither obvious nor straightforward. Different variants of P systems simulate different aspects of the cellular biology depending on their behaviour and characteristics (types of rules, attention on skin's boundaries, etc.).

In [3, 4] six biological operations are discussed (*pino*, *exo*, *phago*, *drip*, *mate* and *bud*) acting among membranes. It turns out that the latter three operations (*drip*, *mate* and *bud*) can be expressed in terms of the other three operations using the appropriate sequence of *pinos/exos/phagos*.

In [4] the six different biological operations of brane calculi are transformed into membrane computing terms. Specifically, they analyze the *pino* (and its complementary process *exo*) and *mate* (and its complementary process *drip*). In our case study's model there is a mitochondria fusion mechanism that includes specific actions and communications. A main characteristic in a such procedure is the attachment of different objects' membranes. These objects are mitofusins and other proteins.

We demonstrate the transcription of some indicative parts of the model stated in Sect. 10.3 expressed in BioAmbient calculus in terms of P automata using notions from brane calculi and brane automata. Firstly, every ambient has to be translated into a membrane subsystem. The fact that the fusion process of a mitochondrion includes many parts whose membranes have to merge enhances our symbolism and our concept. Also, biomolecular rules have to be transformed from Bioambient calculus to P automata rewriting rules in an appropriate way. While there are other works with similar goal, our work is the first that combines BioAmbient calculus with a type of P automata.

Our test model consists of three mammalian proteins named Mfn1, Mfn2 and OPA1. As we briefly described in the previous section, fusion occurs in two ways. Either two segments merge, mixing their contents or one individual segment enters to (or exits from) another compartment (e.g. mitophagy). There are three actions that are capable of altering the ambients' state, namely entry, exit or merge.

**Table 10.1** Table explaining the abbreviations used

Abbreviation	Full name
PM1M2	ProteinMfn1–Mfn2
RM1M2	RNAMfn1–Mfn2
GM1M2	GeneMfn1–Mfn2
OMOM1M2	OuterMembraneOfM1& M2
RD	RNAdeg
PD	Proteindeg
K	Kinase
PO1	ProteinOPA1
RO1	RNAOPA1
GO1	GeneOPA1
IMOM1M2K	InnerMembraneOfM1& M2
BO1	BountOPA1
AO1	ActiveOPA1

Next we represent the schematic depiction of the model using the membrane system's mode. The partition into membrane-like segments is similar to the hierarchical structure of ambient.

Consequently, we have the following initial configuration of the system, where each pair of “[ ]” states a distinct membrane and the symbols in its right corner define its abbreviated name. For simplicity we ignore the transcription and translation processes that occur using the ambients *Transcr* and *Transl* in the model.

$$[[[[[[[AO1]K]PM1M2]RM1M2]GM1M2]OMOM1M2 \quad [[[[[BO1]PO1]RO1]GO1]IMOM1M2]skin/cell$$

Where Table 10.1 explains the abbreviations used.

The final configuration of the model would look like:

$$[[PM1M2]RM1M2]GM1M2]OMOM1M2]PO1]RO1]GO1]IMOM1M2]K]AO1]BO1]skin/cell$$

The fact that most of the activation processes are independent to each other increases the use of a mechanism with intrinsic parallel, non-deterministic behaviour. Now we show how one can describe the production of the protein Mfn1–Mfn2. The procedure to create the OPA protein follows a similar methodology. The system begins in the initial configuration and after consecutive use of appropriate rules the system reaches a final configuration and halts. In the same way the subsystem responsible for the production of the OPA runs.

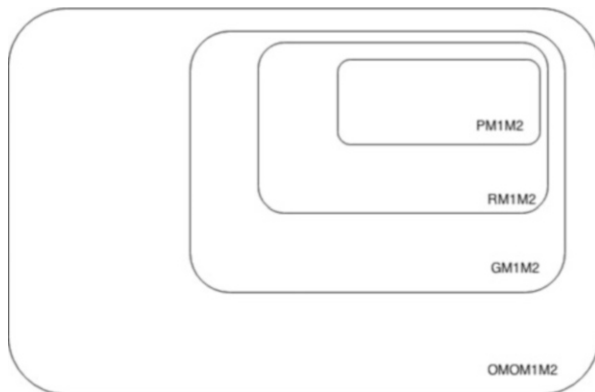
Initial configuration:  $[[[[[PM1M2]RM1M2]GM1M2]OMOM1M2$

Final configuration:  $[[PM1M2]RM1M2]GM1M2]OMOM1M2$

The rules to obtain the halting configuration include consecutive *exo* operations of the nested membranes, one in each step of the computation. In BioAmbient calculus the *exit/expel* actions are used for the unfolding of the nested ambients.



**Fig. 10.3** The initial configuration for the production of protein Mfn1–Mfn2



The *exo* operation is complementary to the *pino* operation in  $P_{pp}$  automata. Communication channels in the biomolecular model can be treated as objects acting as catalysts in the evolution of the model over time. The *exo* operation is not included in [9] semantics but through [4] it can easily be constructed. In every configuration we omit the skin membrane of the system which includes all the nested membranes and it represents the outer membrane of the mitochondrion. Thus, we have:

$$\begin{aligned}
 & \left[ \left[ \left[ PM1M2 \right]_{RM1M2} \right]_{GM1M2} \right]_{OMOM1M2} \xrightarrow{exo} \\
 & \left[ \left[ PM1M2 \right]_{RM1M2} \right]_{GM1M2} \sqcup OMOM1M2 \xrightarrow{exo} \\
 & \left[ PM1M2 \right]_{RM1M2} \sqcup GM1M2 \sqcup OMOM1M2 \xrightarrow{exo} \\
 & PM1M2 \sqcup RM1M2 \sqcup GM1M2 \sqcup OMOM1M2
 \end{aligned}$$

In a similar manner the rest of the biomolecular model described previously can be expressed in another way besides BioAmbient calculus. We use membrane computing notions (specifically P automata with marked membranes) and parts of the brane calculus (Figs. 10.3 and 10.4).

## 10.5 Conclusion and Future Work

There are several features of P systems that make them ideal models of biological processes. Most important among them are the inherent compartmentalization, the easy extensibility and the direct intuitive appearance for biologists (through Venn diagrams). Moreover, membrane systems are particularly suitable in cases of few number of objects involved in the process or slow reactions, which is not rare in the study of biological phenomena.

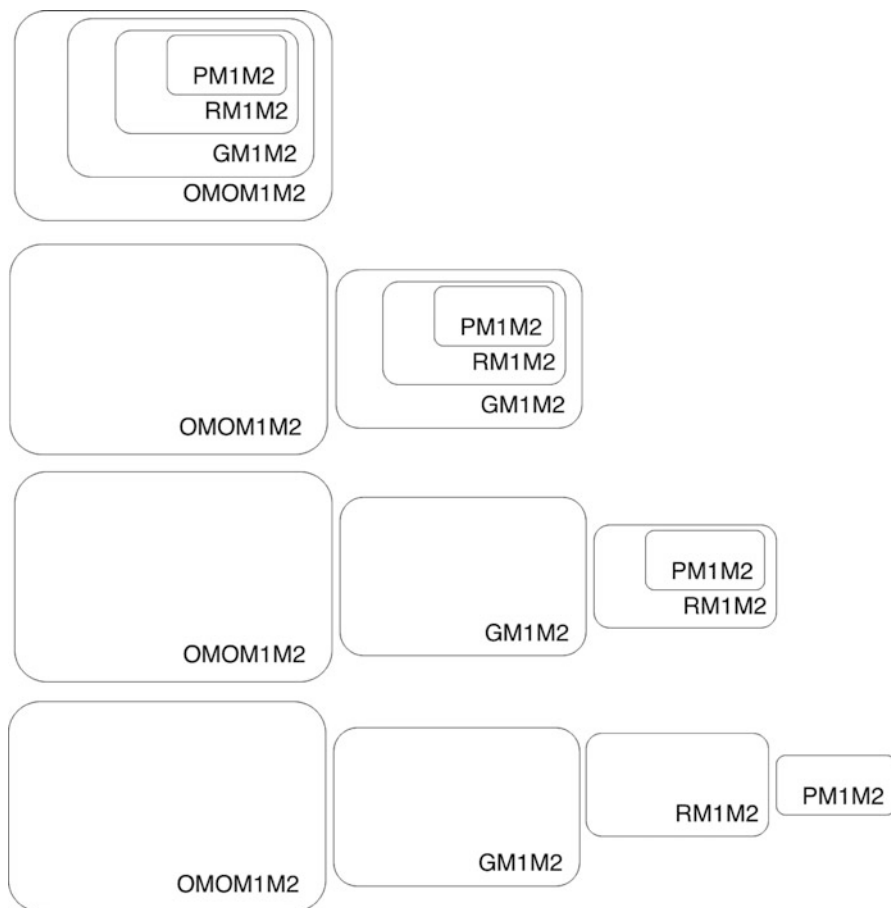


**Fig. 10.4** The step by step process through consecutive uses of the *exo* operation

In this work we combined P systems and a biological calculus in order to present a novel version of an already defined biomolecular model from the current literature. The wealth of many membrane computing models leaves ample space for future work in this direction. Besides the modeling capabilities of these mechanisms, they can potentially act as computation devices, especially the automata-like variants of membrane systems with accepting behaviour. The fact that these computation devices are inspired from the biomolecular world is obviously a factor in favour of this approach.

Our case study was a model of mitochondrial fusion. The need for deeper understanding of these natural processes is vital in studying plenty of diseases and malfunctions in the human neurodegenerative systems. As we briefly described in our introduction, mitochondria processes and their population dynamics play an important role and bioinformatics can be a useful tool towards the study of these phenomena.

The intrinsic infinite behaviour of similar biomolecular functions should be further investigated by implementing and using elements from the computation theory on infinite objects, searching the most appropriate structure in each case. This proposal can be combined with the probability theory since many biological functions are of stochastic nature.

## References

1. Alexiou A, Vlamos P (2012) A cultural algorithm for the representation of mitochondrial population. *Adv Artif Int* 2012:ID 457351. doi:[10.1155/2012/457351](https://doi.org/10.1155/2012/457351)
2. Alexiou AT, Psiha MM, Rekkas JA, Vlamos PM (2011) A stochastic approach of mitochondrial dynamics. *World Acad Sci Eng Technol* 55, pp 77–80
3. Cardelli L (2005) Brane calculi. In: *Computational methods in systems biology*. Springer, New York, pp 257–278
4. Cardelli L, Păun G (2006) An universality result for a (mem) brane calculus based on mate/drip operations. *Int J Found Comput Sci* 17(01):49–68
5. Chen H, Chan DC (2009) Mitochondrial dynamics-fusion, fission, movement, and mitophagy-in neurodegenerative diseases. *Hum Mol Genet* 18(R2):R169–R176
6. Csuhaj-Varjú E (2005) P automata. In: *Membrane computing*. Springer, New York, pp 19–35
7. Csuhaj-Varjú E (2010) P automata: concepts, results, and new aspects. In: *Membrane computing*. Springer, New York, pp 1–15
8. Csuhaj-Varjú E, Vaszil G (2003) P automata or purely communicating accepting p systems. In: *Membrane computing*. Springer, New York, pp 219–233
9. Csuhaj-Varjú E, Vaszil G (2008) (Mem) brane automata. *Theor Comput Sci* 404(1):52–60
10. Csuhaj-Varjú E, Vaszil G (2013) On the power of p automata. In: *Unconventional computation and natural computation*. Springer, New York, pp 55–66
11. Freund R, Oswald M (2002) A short note on analysing p systems with antiport rules. *Bull EATCS* 8:231–236
12. Koski T (2001) *Hidden Markov models for bioinformatics, vol 2*. Springer, New York
13. Kubli DA, Gustafsson ÅB (2012) Mitochondria and mitophagy the yin and yang of cell death control. *Circ Res* 111(9):1208–1221
14. Longo DL, Archer SL (2013) Mitochondrial dynamics-mitochondrial fission and fusion in human diseases. *New England J Med* 369(23):2236–2251
15. Martin-Vide C, Păun G, Pazos J, Rodríguez-Patón A (2003) Tissue p systems. *Theor Comput Sci* 296(2):295–326
16. Milner R, Parrow J, Walker D (1992) A calculus of mobile processes, I. *Inf Comput* 100(1):1–40
17. Păun G (2000) Computing with membranes. *J Comput System Sci* 61(1):108–143
18. Paun G, Rozenberg G, Salomaa A (2010) *The Oxford handbook of membrane computing*. Oxford University Press, Inc., Oxford
19. Regev A, Panina EM, Silverman W, Cardelli L, Shapiro E (2004) Bioambients: an abstraction for biological compartments. *Theor Comput Sci* 325(1):141–167
20. van der Bliek AM, Shen Q, Kawajiri S (2013) Mechanisms of mitochondrial fission and fusion. *Cold Spring Harbor Persp Biol* 55:a011072
21. Ye X, Tai W, Zhang D (2012) The early events of Alzheimer’s disease pathology: from mitochondrial dysfunction to bdnf axonal transport deficits. *Neurobiol Aging* 33(6):1122–e1

# Chapter 11

## A Mathematical Model for the Blood Plasma Flow Around Two Aggregated Low-Density Lipoproteins

Maria Hadjinicolaou

**Abstract** The rheological behaviour of low-density lipoprotein (LDL) particles within the blood plasma and their role in atherogenesis, as well as their ability to aggregate under certain circumstances, is the subject of many clinical tests and theoretical studies aiming at the prevention of atherosclerosis. In the present study we develop a mathematical model that describes the flow of the blood plasma around two aggregated LDLs. We consider the flow as a creeping steady incompressible axisymmetric one, while the two aggregated LDLs are described by an inverted oblate spheroid. The mathematical methods of Kelvin inversion and the semi-separation of variables are employed and analytical expressions for the stream function are derived. These expressions are expected to be useful for further model developing and screening as well as the theoretical justification and validation of laboratory results.

**Keywords** Low-density lipoproteins (LDL) • Atherogenesis • Inverted oblate spheroid • Mathematical model • Stokes flow • Kelvin inversion • Analytical solution

### 11.1 Introduction

Lipoprotein aggregation and deposition in artery walls initiates atherosclerosis which is a serious cardiovascular disease [1–4]. The molecules of lipoprotein allow the transportation of lipids such as cholesterol, phospholipids, and triglycerides, within the plasma. Low-density lipoprotein (LDL) is one of the five categories of lipoproteins, which are, with respect to their molecular size and in ascending order: arechylomicrons, very low-density lipoprotein (VLDL), intermediate-density lipoprotein (IDL), LDL, and high-density lipoprotein (HDL). Studies have shown that higher levels of type-B LDL particles (as opposed to type-A

---

M. Hadjinicolaou (✉)  
School of Science and Technology, Hellenic Open University,  
11 Sahtouri str., GR-26 222 Patras, Greece  
e-mail: [hadjinicolaou@eap.gr](mailto:hadjinicolaou@eap.gr)

LDL particles) are associated with health problems, including cardiovascular diseases [2, 3]. In atherogenesis, molecules of low-density lipoprotein (LDL, diameter 22 nm) accumulate in the extracellular space of the arterial intima forming aggregates of lipid droplets (droplet diameter up to 400 nm). The effects of various modifications on LDL aggregation and fusion were studied in [5].

Through scanning force microscopy, it has been shown that Lipoprotein(a), Lp(a), consists of low-density lipoprotein (LDL) and apolipoprotein(a), apo(a), in a “belt-like structure with two ends”. Apo(a) bounds the LDL sphere at two distant sites. In certain cases, these are attached to two touching spheres of LDL [6]. The roles of apoA and apoB are discussed in [7], where some pictures of the LDLs and HDL structure are also available. The non-destructive identification of the physical characteristics of small coated spherical particles can be achieved through low-frequency inverse scattering techniques, as it is shown in [8]. Recent results indicate that the absorbent of lipoproteins in the sub-endothelium initiates the development of atherosclerosis, but the involved molecular mechanisms are not well understood. More accurate techniques such as Trp-fluorescence and NMR (nuclear magnetic resonance) have shown that apolipoprotein B (apoB) in electro-negative LDL(-) conforms in an abnormal configuration (misfolding). Therefore it is believed that LDL(-) could play a pertinent role in atherogenesis by stimulating the lipoprotein aggregation [9, 10].

Aiming for a better understanding of the role that LDL plays to atherogenesis, we present in this manuscript a model that describes the blood plasma flow around two aggregated LDLs. The flow of blood plasma around a fixed red blood cell (RBC) has been studied analytically in [11], while the sedimentation of RBCs is modelled an analytically solved in [12]. In these studies, the RBC is described mathematically as an inverted prolate spheroid having its axis of symmetry along the direction of the flow. Taking into account the physical characteristics and scales involved, the plasma flow was considered to be uniform, steady and creeping, i.e. Stokes flow. In the present work, analogous physical assumptions have been made. Accordingly, the method of the Kelvin inversion for Stokes flow [13], as it is applied to non-convex domains [14–16] along with the method of semiseparable and the R-semiseparable decomposition of Stokes flow operators [17, 18], is also employed.

In the present work, the two aggregated molecules of LDL are described as an inverted oblate spheroid. Then the flow around them is obtained as follows. First, we derive the analytical solution for the Stokes flow in the interior of an oblate spheroid. Then, through the Kelvin transformation, we obtain the stream function for the plasma flow at the exterior of two aggregated molecules of LDL.

The structure of the manuscript is as follows: the statement of the flow problem in the interior of the oblate spheroid is presented in Sect. 11.2. The Kelvin inversion method and the necessary mathematical background are presented in Sect. 11.3. The solution of the transformed and of the original problem is given in Sect. 11.4, along with sample calculations. Concluding remarks are summarized in Sect. 11.5.

### 11.2 Statement of the Problem

We consider the plasma axisymmetric creeping flow around two aggregated stationary, isolated LDL molecules, represented by an inverted oblate spheroid, having its centre at the origin of a Cartesian coordinate system  $(x_1, x_2, x_3)$ , as it shown in Fig. 11.1. The blood plasma is assumed to flow with an approaching uniform velocity of magnitude  $U$ , which is parallel to the  $x_3$ -axis in the negative direction. Taking into account the size of the LDL molecule, we may also assume that the fluid is unbounded. In what follows, the prime quantities stand for the problem at hand, while the unprimed ones stand for its image under the Kelvin inversion. The governing equation of the steady, axisymmetric, creeping flow of an incompressible, viscous fluid [19] is

$$E'^4 \psi_b(\mathbf{r}') = 0, \quad \mathbf{r}' \in V', \tag{11.1}$$

where  $V'$  is the exterior fluid domain,  $\partial V'$  denotes the surface of the aggregated molecules of LDL (Ag-LDL),  $V$  stands for the interior of the inverted oblate spheroid,  $E'^2$  is the Stokes operator,  $E'^4 = E'^2 \circ E'^2$  and  $\psi_b$  is the stream function.

The surface of the Ag-LDL is assumed to be non-slipping and impenetrable; therefore the boundary conditions [19] are

$$\psi_b(\mathbf{r}') = 0, \quad \mathbf{r}' \in \partial V', \tag{11.2}$$

$$\frac{\partial \psi_b(\mathbf{r}')}{\partial n} = 0, \quad \mathbf{r}' \in \partial V'. \tag{11.3}$$

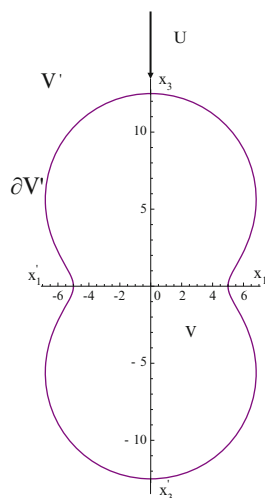


**Fig. 11.1** Two aggregated LDLs—statement of the problem

Due to the characteristic dimensions of the quantities involved in the physical problem (i.e. size of the proteins, velocity of the plasma, viscosity), we further impose that the presence of the neighbouring molecules do not affect the flow field and thus  $V'$  is assumed to be unbounded. The condition to be satisfied then, from [19], is

$$\psi_b(\mathbf{r}') \rightarrow \frac{1}{2}\varpi'^2 U, \quad r' \rightarrow +\infty, \quad (11.4)$$

where  $U$  is the fluid velocity and  $\varpi'$  is the radial cylindrical coordinate. The problem at hand is described through Eqs. (11.1)–(11.4). A classical method for solving the problem is to use the spectral decomposition of the differential operators  $E^2, E^4$ , as these are expressed in the appropriate system of coordinates. This method is adopted here.

## 11.3 Mathematical Methods and Background

### 11.3.1 Kelvin's Inversion

Let  $V$  denote the interior of a closed, bounded, smooth surface  $S$  in  $\mathbb{R}^3$ . Considering a sphere of radius  $b > 0$ , located at the centre of the system, as being the sphere of inversion, the Kelvin inversion  $K$  of any point  $\mathbf{r}$  in  $\mathbb{R}^3$  is defined [11, 13, 16] as

$$K : \mathbb{R}^3 \rightarrow \mathbb{R}^3, \quad \mathbf{r}' := K(\mathbf{r}) := \left(\frac{b}{r}\right)^2 \mathbf{r}, \quad \mathbf{r} \neq \mathbf{0}, \quad (11.5)$$

where  $|\mathbf{r}| = r$ . Hence  $K = K^{-1}$ . The origin is mapped to infinity, the surface  $S$  is mapped to the surface  $S'$  and  $V'$  is the image of  $V$ .

The effect of the Kelvin inversion on the stream and the bistream operators  $E^2$  and  $E^4$  is thoroughly presented by Dassios [13]. The basic result is that every stream function  $\psi$  in  $\Omega \subseteq \mathbb{R}^3$  with enough smoothness can be obtained from the analogous form of the stream function in  $\Omega'$  modified appropriately through the relation

$$E^4 \psi(\mathbf{r}) = \frac{r'^5}{b^5} E'^4 \left[ \frac{r'^3}{b^3} \psi \left( \frac{b^2}{r'^2} \mathbf{r}' \right) \right], \quad \mathbf{r} \in \Omega, \quad \mathbf{r}' \in \Omega', \quad (11.6)$$

where  $\mathbf{r}'$  is given by the Kelvin transformation,  $\Omega' \subseteq \mathbb{R}^3$  denotes the Kelvin image of  $\Omega$ ,  $E^4$  is the bistream operator in  $\Omega$  and  $E'^4$  is the bistream operator in  $\Omega'$ .

### 11.3.2 The Inverted Oblate Spheroidal System of Coordinates

The position vector  $\mathbf{r}$  of every point  $(x_1, x_2, x_3)$  in Cartesian coordinates [19] can be represented in the modified inverted oblate spheroidal coordinates  $(\lambda', \zeta', \varphi)$ , by

$$\mathbf{r} = \left( \bar{c} \sqrt{\lambda'^2 + 1} \sqrt{1 - \zeta'^2} \cos \varphi, \bar{c} \sqrt{\lambda'^2 + 1} \sqrt{1 - \zeta'^2} \sin \varphi, \bar{c} \lambda' \zeta' \right), \quad (11.7)$$

where  $\bar{c} > 0$  denotes the semifocal distance and  $0 \leq \varphi < 2\pi$ .

Using the modified oblate spheroidal coordinates  $(\lambda, \zeta, \varphi)$  the position vector yields

$$\mathbf{r} = \left( \frac{b^2 \sqrt{\lambda^2 + 1} \sqrt{1 - \zeta^2} \cos \varphi}{\bar{c}(\lambda^2 - \zeta^2 + 1)}, \frac{b^2 \sqrt{\lambda^2 + 1} \sqrt{1 - \zeta^2} \sin \varphi}{\bar{c}(\lambda^2 - \zeta^2 + 1)}, \frac{b^2 \lambda \zeta}{\bar{c}(\lambda^2 - \zeta^2 + 1)} \right), \quad (11.8)$$

where  $\lambda \in \mathbb{R}$ ,  $-1 \leq \zeta \leq 1$ ,  $b > 0$ , while the radial cylindrical coordinate  $\varpi'$  becomes

$$\varpi' = \frac{b^2 \sqrt{\lambda^2 + 1} \sqrt{1 - \zeta^2}}{\bar{c}(\lambda^2 - \zeta^2 + 1)}. \quad (11.9)$$

Also, we can easily prove that

$$\zeta' \lambda' = \frac{b^2}{r^2} \zeta \lambda \quad (11.10)$$

and

$$(1 - \zeta'^2)(\lambda'^2 + 1) = \frac{b^4}{r^4} (1 - \zeta^2)(\lambda^2 + 1). \quad (11.11)$$

Furthermore, the Stokes stream operator in the inverted oblate system is

$$E'^2 = \frac{\bar{c}^2(\lambda^2 - \zeta^2 + 1)}{b^4(\lambda^2 + \zeta^2)} \left\{ 2\lambda(\lambda^2 + 1) \frac{\partial}{\partial \lambda} + (\lambda^2 + 1)(\lambda^2 - \zeta^2 + 1) \frac{\partial^2}{\partial \lambda^2} - 2\zeta(1 - \zeta^2) \frac{\partial}{\partial \zeta} + (1 - \zeta^2)(\lambda^2 - \zeta^2 + 1) \frac{\partial^2}{\partial \zeta^2} \right\}. \quad (11.12)$$



## 11.4 Solution

### 11.4.1 The Transformed Problem

Due to the geometry of the (Ag-LDL), the problem (11.1)–(11.4) is formulated in the inverse modified oblate spheroidal coordinates. Thus it is written as

$$E^4 \psi_b(\lambda', \zeta') = 0, \quad (\lambda', \zeta') \in V', \quad (11.13)$$

$$\psi_b(\lambda', \zeta') = 0, \quad (\lambda', \zeta') \in \partial V', \quad (11.14)$$

$$\frac{\partial \psi_b(\lambda', \zeta')}{\partial \lambda'} = 0, \quad (\lambda', \zeta') \in \partial V', \quad (11.15)$$

$$\psi_b \rightarrow \frac{1}{2} \bar{c}^2 (\lambda'^2 + 1) (1 - \zeta'^2) U, \quad r' \rightarrow +\infty, \quad (11.16)$$

where  $\psi_b(\lambda', \zeta')$  is the stream function in the inverted spheroidal system. Furthermore, due to the imposed symmetry of the flow with respect to the  $x'_3 x_3$  axis, the stream function is also azimuthally independent.

As it is stated in (11.6), that the stream function in the inverted system,  $\psi_b(\lambda', \zeta')$  is related to the stream function in the oblate spheroidal coordinate system  $\psi(\lambda, \zeta)$ , through the relation

$$\psi_b(\lambda', \zeta') = \frac{b^3}{r^3} \psi(\lambda, \zeta), \quad (11.17)$$

where the relations between  $\lambda, \zeta$  and  $\lambda', \zeta'$  are given in [20] and are derived through (11.10) and (11.11).

Therefore the problem (11.13)–(11.16) which solves Stokes flow in the exterior of the inverted oblate spheroid, expressed in the system  $(\lambda, \zeta, \varphi)$ , is translated to

$$E^4 \psi(\lambda, \zeta) = 0, \quad (11.18)$$

$$\psi(\lambda_0, \zeta) = 0, \quad (11.19)$$

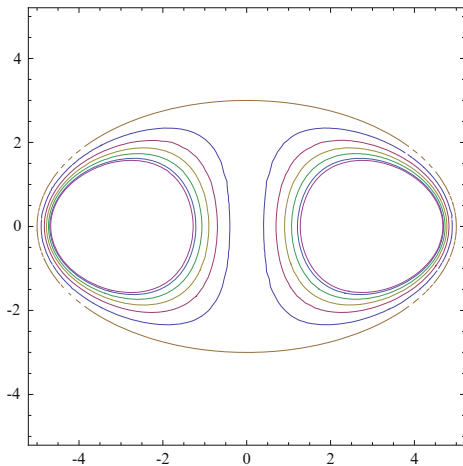
$$\left. \frac{\partial \psi(\lambda, \zeta)}{\partial \lambda} \right|_{\lambda=\lambda_0} = 0, \quad (11.20)$$

$$\psi(\lambda, \zeta) \rightarrow \frac{1}{2} \frac{b \bar{c} (1 - \zeta^2) (\lambda^2 + 1)}{\sqrt{\lambda^2 - \zeta^2 + 1}} U, \quad \text{as } (\lambda, \zeta) \rightarrow (0, 1), \quad (11.21)$$

where  $\lambda = \lambda_0 = \text{constant}$  denotes the surface of the oblate spheroid.

The solution of the problem (11.18)–(11.21) is derived explicitly in the [Appendix](#). The obtained analytical expression for the stream function is then

**Fig. 11.2** Streamlines in the plane  $x_2 = 0$ . From the surface of the oblate spheroid to the centre, the stream function values are:  
 $10^{-4}$ ,  $3 \times 10^{-4}$ ,  
 $5 \times 10^{-4}$ ,  $7 \times 10^{-4}$ ,  
 $9 \times 10^{-4}$ ,  $10^{-3}$



$$\psi(\lambda, \zeta) = \sum_{n=1}^{\infty} g_{2n}(i\lambda)G_{2n}(\zeta), \tag{11.22}$$

where  $G_{2n}$  are Gegenbauer functions of the first kind and  $g_{2n}$  is a sum of products of order  $n - 2$ ,  $n$ ,  $n + 2$  Gegenbauer functions [19] of angular and radial dependence, of the first and the second kind  $G_n$  and  $H_n$  respectively.

Next we depict various streamlines for the Stokes flow problem in the interior of oblate spheroid, using only the first term of the series, assuming dimensionless plasma velocity  $U = 0.01$ , radius of the sphere of inversion  $b = 4$  and axes ratio  $5/3$  (Fig. 11.2).

### 11.4.2 The Original Problem

Following the proposed methodology, the stream function of the original problem is obtained by substituting (11.22) in to (11.17) and it assumes the form

$$\psi_b(\lambda', \zeta') = \frac{b^3}{\bar{c}^3 \sqrt{\lambda'^2 - \zeta'^2 + 1}} \sum_{n=1}^{\infty} g_{2n}(i\lambda)G_{2n}(\zeta), \tag{11.23}$$

where  $g_{2n}(i\lambda)$  have been calculated in the [Appendix](#).

### 11.4.3 Sample Calculations

Next we demonstrate streamlines for the flow around an Ag-LDL with plasma velocity  $U = 0.01$ , sphere radius  $b = 4$ , and different length/thickness ratio, i.e. axes ratio,  $k$ , assumed in each graph. We use the first three terms of the stream function in order to have better accuracy, so we define

$$\psi_b^{(3)}(\lambda', \zeta') = \frac{b^3}{\bar{c}^3 \sqrt{\lambda^2 - \zeta^2 + 1}} [g_2(i\lambda)G_2(\zeta) + g_4(i\lambda)G_4(\zeta) + g_6(i\lambda)G_6(\zeta)]. \quad (11.24)$$

In Figs. 11.3 and 11.4 we present the streamlines assuming stream function values equal to 0.03, 0.05, 0.07, 0.09, 0.11, depicted from infinity towards the surface of the inverted oblate spheroid respectively by using three terms of the series.

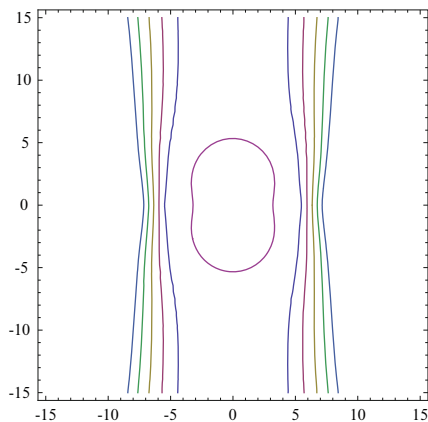


**Fig. 11.3** Streamlines in the plane  $x_2 = 0$  with  $k = 5/3$

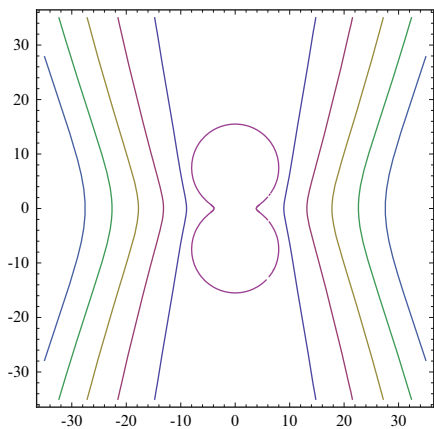


**Fig. 11.4** Streamlines in the plane  $x_2 = 0$  with  $k = 4$

## Conclusions

A serious problem that may cause cardiovascular diseases is the atherosclerosis. Many studies and experimental works along with clinical tests are focused on the prevention of this formation. Towards this direction, we developed a mathematical model aiming for a better understanding of the rheological behaviour of two aggregated LPL. The aggregated molecules were mathematically described as an inverted oblate spheroid while the plasma flow around it was considered to be creeping, steady and azimuthally independent, i.e. Stokes flow. This is justified by taking into account the characteristic scales of the problem. The governing equation for the stream function is a fourth order partial differential equation with respect to two variables. Non-slip conditions have been assumed on the surface of the LDLs, while an asymptotic one holds away from the molecules. An analytical solution of the problem is obtained using the Kelvin inversion method and the concept of R-semi-separation of variables. First we solve the analogous problem in the interior of an oblate spheroid, and then, the solution of the original problem results as its image under the Kelvin transformation. The stream function is expressed through a series expansion of Gegenbauer functions of even order. Sample stream lines are depicted showing the flow field patterns at two different stages of aggregation. The analytical solution is expected to be useful in studying transport phenomena regarding apolipoproteins apoA and apoB and their role in atherogenesis. The obtained results can be also used for other medical, biological as well as physical problems.

**Acknowledgements** This research has been co-financed by the European Union (European Social Fund—ESF) and Greek national funds through the Operational Program “Education and Lifelong Learning” of the National Strategic Reference Framework (NSRF)—Research Funding Program: ARCHIMEDES III. Investing in knowledge society through the European Social Fund.

## Appendix

From [21] we have that

$$\frac{1}{r} = \frac{1}{\bar{c}} \sum_{n=0}^{\infty} \frac{(-1)^n (4n+1)(2n)!}{2^{2n} (n!)^2} i Q_{2n}(i\lambda) P_{2n}(\zeta). \quad (11.25)$$

Employing the relations connecting the Legendre functions with the Gegenbauer functions [22], using recurrence relations and after performing calculations, we arrive at

$$\begin{aligned}
\frac{(1-\zeta^2)(\lambda^2+1)}{\sqrt{\lambda^2-\zeta^2+1}} &= \left[ -2G_1(i\lambda) - \frac{18}{5}H_2(i\lambda) - \frac{12}{5}H_4(i\lambda) \right] iG_2(\zeta) \\
&+ \sum_{n=2}^{\infty} w_{n-1}e_{n-1}d_{n-1}H_{2n-2}(i\lambda) iG_{2n}(\zeta) \\
&+ \sum_{n=2}^{\infty} (-w_{n-1}e_{n-1}^2 - w_n d_n^2) H_{2n}(i\lambda) iG_{2n}(\zeta) \\
&+ \sum_{n=2}^{\infty} w_n d_n e_n H_{2n+2}(i\lambda) iG_{2n}(\zeta), \tag{11.26}
\end{aligned}$$

where

$$d_n = \frac{2n(2n-1)}{4n+1}, \quad e_n = \frac{2(2n+1)(n+1)}{4n+1}, \quad w_n = \frac{(-1)^n(4n+1)(2n)!}{2^{2n}(n!)^2}. \tag{11.27}$$

We know from [17] that the solution of (11.18) is

$$\psi(\tau, \zeta) = g_0(i\lambda)G_0(\zeta) + g_1(i\lambda)G_1(\zeta) + \sum_{n=2}^{\infty} [g_n(i\lambda)G_n(\zeta) + h_n(i\lambda)H_n(\zeta)], \tag{11.28}$$

with

$$g_2(\tau) = A_2G_2(\tau) + B_2H_2(\tau) + C_2G_0(\tau) + D_2G_1(\tau) + E_2G_4(\tau) + F_2H_4(\tau), \tag{11.29}$$

and

$$\begin{aligned}
g_{2n}(\tau) &= A_{2n}G_{2n}(\tau) + B_{2n}H_{2n}(\tau) + C_{2n}G_{2n-2}(\tau) + D_{2n}H_{2n-2}(\tau) \\
&+ E_{2n}G_{2n+2}(\tau) + F_{2n}H_{2n+2}(\tau), \quad n \geq 2. \tag{11.30}
\end{aligned}$$

Using orthogonality arguments in (11.28) from (11.26) we can calculate coefficients  $B_{2n}$ ,  $D_{2n}$ ,  $F_{2n}$ , while we have to calculate  $A_{2n}$ ,  $C_{2n}$ ,  $E_{2n}$  and we have only two equations to apply. Therefore we need one more condition. We use the fact that the oblate spheroid becomes a sphere when the semifocal distance tends to zero, so the solution in the oblate coordinates becomes the solution in the spherical coordinates. This allows us to find the solution of which is given in (11.24) with

$$g_2(i\lambda) = A_2 G_2(i\lambda) + i \frac{9b\bar{c}U}{5} H_2(i\lambda) + ib\bar{c}U G_1(i\lambda) + E_2 G_4(i\lambda) + i \frac{6b\bar{c}U}{5} H_4(i\lambda), \quad (11.31)$$

$$g_{2n}(i\lambda) = A_{2n} G_{2n}(i\lambda) + i \frac{b\bar{c}U}{2} (w_{n-1} e_{n-1}^2 + w_n d_n^2) H_{2n}(i\lambda) - i \frac{b\bar{c}U}{2} w_{n-1} e_{n-1} d_{n-1} H_{2n-2}(i\lambda) + E_{2n} G_{2n+2}(i\lambda) - i \frac{b\bar{c}U}{2} w_n d_n e_n H_{2n+2}(i\lambda), \quad (11.32)$$

$$A_2 = -ib\bar{c}U \frac{\begin{vmatrix} \frac{9}{5}H_2(i\lambda_0) + G_1(i\lambda_0) + \frac{6}{5}H_4(i\lambda_0) & G_4(i\lambda_0) \\ \frac{9}{5}H'_2(i\lambda_0) + G'_1(i\lambda_0) + \frac{6}{5}H'_4(i\lambda_0) & G'_4(i\lambda_0) \end{vmatrix}}{\begin{vmatrix} G_2(i\lambda_0) & G_4(i\lambda_0) \\ G'_2(i\lambda_0) & G'_4(i\lambda_0) \end{vmatrix}}, \quad (11.33)$$

$$E_2 = -ib\bar{c}U \frac{\begin{vmatrix} G_2(i\lambda_0) & \frac{9}{5}H_2(i\lambda_0) + G_1(i\lambda_0) + \frac{6}{5}H_4(i\lambda_0) \\ G'_2(i\lambda_0) & \frac{9}{5}H'_2(i\lambda_0) + G'_1(i\lambda_0) + \frac{6}{5}H'_4(i\lambda_0) \end{vmatrix}}{\begin{vmatrix} G_2(i\lambda_0) & G_4(i\lambda_0) \\ G'_2(i\lambda_0) & G'_4(i\lambda_0) \end{vmatrix}}, \quad (11.34)$$

$$A_{2n} = -i \frac{b\bar{c}U}{2} \frac{\begin{vmatrix} (w_{n-1} e_{n-1}^2 + w_n d_n^2) H_{2n}(i\lambda_0) - w_{n-1} e_{n-1} d_{n-1} H_{2n-2}(i\lambda_0) & G_{2n+2}(i\lambda_0) \\ -w_n d_n e_n H_{2n+2}(i\lambda_0) & G_{2n+2}(i\lambda_0) \\ (w_{n-1} e_{n-1}^2 + w_n d_n^2) H'_{2n}(i\lambda_0) - w_{n-1} e_{n-1} d_{n-1} H'_{2n-2}(i\lambda_0) & G'_{2n+2}(i\lambda_0) \\ -w_n d_n e_n H'_{2n+2}(i\lambda_0) & G'_{2n+2}(i\lambda_0) \end{vmatrix}}{\begin{vmatrix} G_{2n}(i\lambda_0) & G_{2n+2}(i\lambda_0) \\ G'_{2n}(i\lambda_0) & G'_{2n+2}(i\lambda_0) \end{vmatrix}}, \quad (11.35)$$

and

$$E_{2n} = -i \frac{b\bar{c}U}{2} \frac{\begin{vmatrix} G_{2n}(i\lambda_0) & (w_{n-1} e_{n-1}^2 + w_n d_n^2) H_{2n}(i\lambda_0) & \\ & -w_{n-1} e_{n-1} d_{n-1} H_{2n-2}(i\lambda_0) - w_n d_n e_n H_{2n+2}(i\lambda_0) & \\ G'_{2n}(i\lambda_0) & (w_{n-1} e_{n-1}^2 + w_n d_n^2) H'_{2n}(i\lambda_0) & \\ & -w_{n-1} e_{n-1} d_{n-1} H'_{2n-2}(i\lambda_0) - w_n d_n e_n H'_{2n+2}(i\lambda_0) & \end{vmatrix}}{\begin{vmatrix} G_{2n}(i\lambda_0) & G_{2n+2}(i\lambda_0) \\ G'_{2n}(i\lambda_0) & G'_{2n+2}(i\lambda_0) \end{vmatrix}}. \quad (11.36)$$

## References

1. Xu S, Lin B (2001) The mechanism of oxidation-induced low-density lipoprotein aggregation: an analogy to colloidal aggregation and beyond? *Phys J* 81(4):2403–2413
2. [http://en.wikipedia.org/wiki/Low-density\\_lipoprotein](http://en.wikipedia.org/wiki/Low-density_lipoprotein)
3. Cromwell WC, Otvos JD (2004) Low-density lipoprotein particle number and risk for cardiovascular disease. *Curr Atheroscler Rep* 6(5):381–387. doi:10.1007/s11883-004-0050-5, PMID: 15296705
4. O’Keefe JH, Cordain L, Harris WH, Moe RM, Vogel R (2004) Optimal low-density lipoprotein is 50 to 70 mg/dl: lower is better and physiologically normal. *J Am Coll Cardiol* 43(11):2142–2146
5. Pentikäinen MO, Lehtonen EM, Kovanen PT (1996) Aggregation and fusion of modified low density lipoprotein. *J Lipid Res* 37(12):2638–2649
6. Xu S (1998) Apolipoprotein(a) binds to low-density lipoprotein at two distant sites in lipoprotein(a). *Biochemistry* 37(26):9284–9294
7. Lu M, Gursky O (2013) Aggregation and fusion of low-density lipoproteins in vivo and in vitro. *Biomol Concepts* 4(5):501–518
8. Hadjinicolaou M (2000) Non-destructive identification of spherical inclusions. *Adv Compos Lett* 9(1):25–33
9. Ursini F, Davies KJ, Maiorino M, Parasassi T, Sevanian A (2002) Atherosclerosis: another protein misfolding disease? *Trends Mol Med* 8(8):370–374
10. Sánchez-Quesada JL, Villegas S, Ordóñez-Llanos J (2012) Electronegative low-density lipoprotein. A link between apolipoprotein B misfolding, lipoprotein aggregation and proteoglycan binding. *Curr Opin Lipidol* 23(5):479–486
11. Dassios G, Hadjinicolaou M, Protopapas E (2012) Blood plasma flow past a red blood cell: mathematical modeling and analytical treatment. *Math Methods Appl Sci* 35(13):1489–1612
12. Hadjinicolaou M, Kamvyssas G, Protopapas E (2014) Stokes flow applied to the sedimentation of a red blood cell. *Q Appl Math*. Online ISSN 1552-4485
13. Dassios G (2009) The Kelvin transformation in potential theory and Stokes flow. *IMA J Appl Math* 74:427–438
14. Baganis G, Hadjinicolaou M (2009) Analytic solution of an exterior Dirichlet problem in a non-convex domain. *IMA J Appl Math* 74(5):668–684
15. Baganis G, Hadjinicolaou M (2010) Analytic solution of an exterior Neumann problem in a non-convex domain. *Math Methods Appl Sci* 33(17):2067–2075
16. Baganis G, Dassios G, Hadjinicolaou M, Protopapas E (2013) The Kelvin transformation as a tool for analyzing problems in medicine and technology. *Math Methods Appl Sci*. doi:10.1002/mma.2903
17. Dassios G, Hadjinicolaou M, Payatakes AC (1994) Generalized eigenfunctions and complete semiseparable solutions for Stokes flow in spheroidal coordinates. *Q Appl Math LII* (1):157–191
18. Hadjinicolaou M, Protopapas E (2013) On the R-semiseparation of the Stokes bi-stream operator in the inverted prolate spheroidal coordinates. *Math Methods Appl Sci*. doi:10.1002/mma.2841
19. Happel J, Brenner H (1991) *Low Reynolds number hydrodynamics*. Kluwer Academic Publishers, London
20. Hadjinicolaou M, Protopapas E (2014) Translation of two aggregated low density lipoproteins. A mathematical model, *Advances in Experimental Medicine and Biology*\_820, DOI 10.1007/978-3-319-09012-2-12
21. Dassios G, Kleinman R (1989) On the capacity and Rayleigh scattering for a class of non-convex bodies. *Q J Mech Appl Math* 42(3):467–475
22. Lebedev NN (1972) *Special functions and their applications*. Dover Publications, New York

# Chapter 12

## Translation of Two Aggregated Low-Density Lipoproteins Within Blood Plasma: A Mathematical Model

Maria Hadjinicolaou and Eleftherios Protopapas

**Abstract** Arteriosclerosis is a disease in which the artery walls get thicker and harder. Atherosclerosis is a specific form of arteriosclerosis which allows less blood to travel through the artery and increases blood pressure. Low-density lipoproteins (LDLs) and their ability to aggregate are important in atherosclerosis. In the present study we develop a mathematical model that describes the translation of two aggregated LDSs through blood plasma. We model the two aggregated LDLs as an inverted oblate spheroid and the flow as a creeping steady incompressible axisymmetric one. The mathematical tools that we used are the Kelvin inversion and the semi-separation of variables in the spheroidal coordinate systems. The stream function is given as a series expansion of even order terms of combinations of Gegenbauer functions of angular and radial dependence. The analytical solution is expected to give insight into the study of the various chemical precipitation methods used for the precipitation of lipoproteins, as this is the first step for the measurement of their concentration within blood plasma.

**Keywords** Stokes flow • Aggregation • Low-density lipoproteins (LDLs) • Blood plasma flow • Mathematical model • Stream function • Precipitation of lipoproteins • Inverse oblate spheroid

### 12.1 Introduction

According to [1], aggregates of low-density lipoprotein (LDL) are formed by subjecting small vortexes to LDL molecules. The role of high-density lipoprotein (HDL) or apolipoprotein A-I in preventing LDL aggregation and in inhibiting the atherosclerosis is presented in [2, 3]. LDL aggregation along with fusion and the formation of lipid droplets are considered to be the initial state for atherogenesis. A summary of the relevant up-to-date studies concerning the in vivo and in vitro

---

M. Hadjinicolaou (✉) • E. Protopapas  
School of Science and Technology, Hellenic Open University,  
11 Sahtouri str., Patras, Greece, GR-26 222  
e-mail: [hadjinicolaou@eap.gr](mailto:hadjinicolaou@eap.gr)



mechanisms that are leading to these formations is presented in [3–5]. The effects of various modifications on LDL aggregation and fusion are studied in [4, 5].

As it is shown in [6], apolipoprotein(a), apo(a), bounds the LDL sphere at two distant sites in a belt-like structure and in certain cases, LDLs are attached and thus are modelled as two touching spheres. All this knowledge is expected to be helpful in establishing new therapeutics. Towards this aim, we developed in [7] a mathematical model for the blood plasma flow around two aggregated LDLs employing inverted oblate spheroidal coordinates and assuming steady, creeping axisymmetric flow. In the present study we further modify our previous model in order to describe the translation of two aggregated LDSs through blood plasma. The two aggregated LDLs are modelled again as an inverted oblate spheroid and the blood plasma flow as Stokes flow. Analogous assumptions have been made for the study of the relative blood plasma flow around a red blood cell, through mathematical models [8–10]. The Kelvin transformation method as it is applied to Stokes flow [11] is also employed here. The Stokes stream function is given through Gegenbauer functions as in [7]. For a further study on the Kelvin inversion in various curvilinear systems one can see [12–14], while on the structure of the eigenspace of the Stokes operators  $E^2$  and  $E^4$ , one may read [7, 15, 16].

In the present study, we provide analytical expression for the stream function. This is expected to give an insight into the chemical precipitation methods used for the separation of lipoproteins in order to be measured in laboratories.

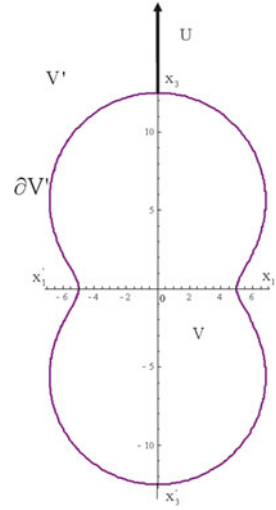
The structure of the manuscript is as follows. The mathematical formulation of the problem and its solution is given in Sect. 12.2. A brief discussion and further possible applications of the obtained results are included in Sect. 12.3.

## 12.2 The Mathematical Model and Solution

The physical statement and the mathematical formulation of the problem is similar to the one presented in [7]. Specifically, we consider that the two aggregated molecules of LDLs are represented geometrically by an inverted oblate spheroid. Moreover, we assume that its centre coincides with the origin of a Cartesian coordinate system  $(x_1, x_2, x_3)$ , as it shown in Fig. 12.1. The two aggregated LDLs are moving through an unbounded quiescent fluid  $V'$ , with constant velocity  $U$ , parallel to the  $x_3$ -axis in the positive direction. We denote by  $\partial V'$  the surface of the aggregated molecules of LDL (Ag-LDL) while the interior of the inverted oblate spheroid is denoted by  $V$ .

The Stokes operator in axisymmetric low Reynolds number flow is the fourth-order partial differential operator,  $E'^4$ , with  $E'^4 = E'^2 \circ E'^2$ , and the problem at hand reads

**Fig. 12.1** Translation of two aggregated LDLs—statement of the problem



$$E'^4 \psi_t(\mathbf{r}') = 0, \quad \mathbf{r}' \in V', \tag{12.1}$$

$$\psi_t(\mathbf{r}') + \frac{1}{2} \varpi'^2 U = 0, \quad \mathbf{r}' \in \partial V', \tag{12.2}$$

$$\frac{\partial}{\partial n} \left[ \psi_t(\mathbf{r}') + \frac{1}{2} \varpi'^2 U \right] = 0, \quad \mathbf{r}' \in \partial V', \tag{12.3}$$

$$\frac{\psi_t(\mathbf{r}')}{r'^2} \rightarrow 0, \quad r' \rightarrow +\infty, \tag{12.4}$$

where  $\psi_t$  is the stream function and  $\varpi'$  is the cylindrical coordinate. Specifically, Eq. (12.1) is the governing equation of the flow, relation (12.2) denotes that there is no relative tangential velocity component on the surface of the aggregated LDLs, relation (12.3) implies that the aggregated LDLs are impenetrable ( $n$  here denotes the radial coordinate of any axisymmetric system) and relation (12.4) expresses the assumption that the blood plasma extends to infinity where it is at rest.

Using the modified inverted oblate spheroidal coordinate system  $(\lambda', \zeta')$ , the problem (12.1)–(12.4), becomes

$$E'^4 \psi_t(\lambda', \zeta') = 0, \quad (\lambda', \zeta') \in V', \tag{12.5}$$

$$\psi_t(\lambda', \zeta') = -\frac{1}{2} \bar{c}^2 (\lambda'^2 + 1) (1 - \zeta'^2) U, \quad (\lambda', \zeta') \in \partial V', \tag{12.6}$$

$$\frac{\partial \psi_t(\lambda', \zeta')}{\partial \lambda} = -\frac{U}{2} \frac{\partial}{\partial \lambda} \left[ \bar{c}^2 (\lambda'^2 + 1) (1 - \zeta'^2) \right], \quad (\lambda', \zeta') \in \partial V', \tag{12.7}$$

$$\frac{\psi_t(\lambda', \zeta')}{r'^2} \rightarrow 0, \quad r' \rightarrow +\infty, \quad (12.8)$$

where  $\psi_t(\lambda', \zeta')$  is the stream function in the inverted system,  $\bar{c} > 0$  is the semifocal distance,  $(\lambda', \zeta') \in \partial V'$  denotes the surface of the aggregated LDLs and

$$r' = \bar{c} \sqrt{\lambda'^2 - \zeta'^2 + 1}. \quad (12.9)$$

It is known from [17] that the stream function  $\psi_b(\lambda', \zeta')$  for the Stokes flow past a stationary solid and the stream function  $\psi_t(\lambda', \zeta')$  for the translating solid satisfy the relation

$$\psi_t(\lambda', \zeta') = \psi_b(\lambda', \zeta') - \psi_\infty(\lambda', \zeta'), \quad (12.10)$$

where  $\psi_\infty(\lambda', \zeta')$  is the stream function for the unperturbed flow at infinity, which in our case is

$$\psi_\infty(\lambda', \zeta') = \frac{b^4(\lambda^2 + 1)(1 - \zeta^2)}{2\bar{c}^2(\lambda^2 - \zeta^2 + 1)^2} U, \quad (12.11)$$

where  $(\lambda, \zeta)$  denote the modified oblate spheroidal coordinates. Using results from [7] we arrive to

$$\psi_t(\lambda', \zeta') = \frac{b^3}{\bar{c}^3 \sqrt{\lambda'^2 - \zeta'^2 + 1}} \sum_{n=1}^{\infty} [A_{2n} G_{2n}(i\lambda) + E_{2n} G_{2n+2}(i\lambda)] G_{2n}(\zeta), \quad (12.12)$$

where  $G_{2n}$  are the Gegenbauer functions of the first kind [18],  $\lambda = \lambda_0$  denotes the surface of the oblate spheroid and

$$A_2 = -ib\bar{c}U \frac{\begin{vmatrix} \frac{9}{5}H_2(i\lambda_0) + G_1(i\lambda_0) + \frac{6}{5}H_4(i\lambda_0) & G_4(i\lambda_0) \\ \frac{9}{5}H'_2(i\lambda_0) + G'_1(i\lambda_0) + \frac{6}{5}H'_4(i\lambda_0) & G'_4(i\lambda_0) \end{vmatrix}}{\begin{vmatrix} G_2(i\lambda_0) & G_4(i\lambda_0) \\ G'_2(i\lambda_0) & G'_4(i\lambda_0) \end{vmatrix}}, \quad (12.13)$$

$$E_2 = -ib\bar{c}U \frac{\begin{vmatrix} G_2(i\lambda_0) & \frac{9}{5}H_2(i\lambda_0) + G_1(i\lambda_0) + \frac{6}{5}H_4(i\lambda_0) \\ G'_2(i\lambda_0) & \frac{9}{5}H'_2(i\lambda_0) + G'_1(i\lambda_0) + \frac{6}{5}H'_4(i\lambda_0) \end{vmatrix}}{\begin{vmatrix} G'_2(i\lambda_0) & G_4(i\lambda_0) \\ G_2(i\lambda_0) & G_4(i\lambda_0) \end{vmatrix}}, \quad (12.14)$$

$$A_{2n} = -i \frac{b\bar{c}U}{2} \frac{\begin{vmatrix} (w_{n-1}e_{n-1}^2 + w_n d_n^2)H_{2n}(i\lambda_0) - w_{n-1}e_{n-1}d_{n-1}H_{2n-2}(i\lambda_0) \\ -w_n d_n e_n H_{2n+2}(i\lambda_0) & G_{2n+2}(i\lambda_0) \\ (w_{n-1}e_{n-1}^2 + w_n d_n^2)H'_{2n}(i\lambda_0) - w_{n-1}e_{n-1}d_{n-1}H'_{2n-2}(i\lambda_0) \\ -w_n d_n e_n H'_{2n+2}(i\lambda_0) & G'_{2n+2}(i\lambda_0) \end{vmatrix}}{\begin{vmatrix} G_{2n}(i\lambda_0) & G_{2n+2}(i\lambda_0) \\ G'_{2n}(i\lambda_0) & G'_{2n+2}(i\lambda_0) \end{vmatrix}}, \quad (12.15)$$

$$E_{2n} = -i \frac{b\bar{c}U}{2} \frac{\begin{vmatrix} G_{2n}(i\lambda_0) & (w_{n-1}e_{n-1}^2 + w_n d_n^2)H_{2n}(i\lambda_0) - w_{n-1}e_{n-1}d_{n-1}H_{2n-2}(i\lambda_0) \\ & -w_n d_n e_n H_{2n+2}(i\lambda_0) \\ G'_{2n}(i\lambda_0) & (w_{n-1}e_{n-1}^2 + w_n d_n^2)H'_{2n}(i\lambda_0) - w_{n-1}e_{n-1}d_{n-1}H'_{2n-2}(i\lambda_0) \\ & -w_n d_n e_n H'_{2n+2}(i\lambda_0) \end{vmatrix}}{\begin{vmatrix} G_{2n}(i\lambda_0) & G_{2n+2}(i\lambda_0) \\ G'_{2n}(i\lambda_0) & G'_{2n+2}(i\lambda_0) \end{vmatrix}}, \quad (12.16)$$

$$w_n = \frac{(-1)^n (4n+1)(2n)!}{2^{2n}(n!)^2}, \quad d_n = \frac{2n(2n-1)}{4n+1}, \quad e_n = \frac{2(2n+1)(n+1)}{4n+1}. \quad (12.17)$$

In all the above relations, the modified oblate spheroidal coordinates  $(\lambda, \zeta)$  are related to the modified inverted oblate spheroidal coordinates ones,  $(\lambda', \zeta')$  via the following relations, that are taken into account for the calculations.

$$\lambda^2 = \frac{b^4 - \bar{c}^2 r'^2 + \sqrt{(b^4 - \bar{c}^2 r'^2)^2 + 4b^4 \bar{c}^4 \lambda'^2 \zeta'^2}}{2c^2 r'^2}, \quad (12.18)$$

$$\zeta^2 = \frac{2\bar{c}^2 b^4 \lambda'^2 \zeta'^2}{r'^2 \left[ b^4 - \bar{c}^2 r'^2 + \sqrt{(b^4 - \bar{c}^2 r'^2)^2 + 4b^4 \bar{c}^4 \lambda'^2 \zeta'^2} \right]}. \quad (12.19)$$

In the next graphs, we demonstrate sample streamlines, assuming  $U = 0.01$  and radius of the sphere of inversion  $b = 5$ , for various values of the aspect ratio  $k$  (length/thickness). Since the series solution converges fast, we next use only the first term of the series, so the stream function which is

$$\psi_i^{(1)}(\lambda', \zeta') = \frac{b^3}{\bar{c}^3 \sqrt{\lambda^2 - \zeta^2 + 1}} [A_2 G_2(i\lambda) + E_2 G_4(i\lambda)] G_2(\zeta). \quad (12.20)$$

In Figs. 12.2 and 12.3 we illustrate indicatively, for aspect ratio of the axis of the oblate spheroid  $k = 2.5$  and  $k = 4$  sample streamlines, when the stream function gets

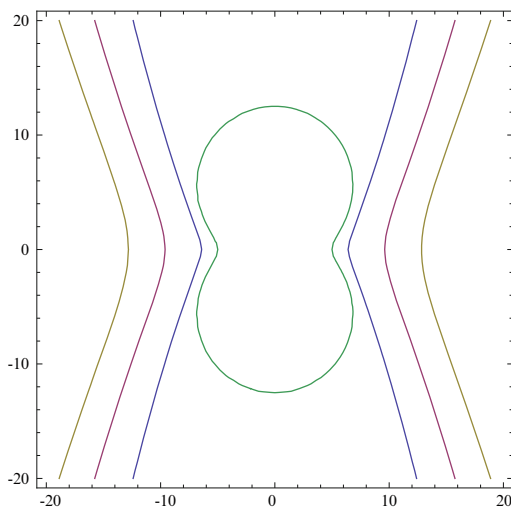


**Fig. 12.2** Streamlines in the plane  $x_2 = 0$  with  $k = \frac{5}{2}$

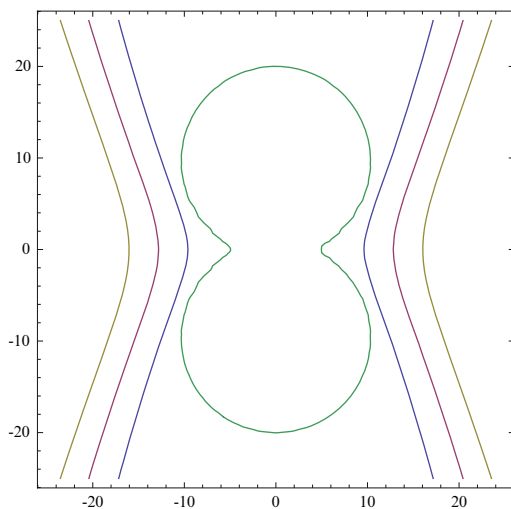


**Fig. 12.3** Streamlines in the plane  $x_2 = 0$  with  $k = 4$

successively the values:  $-0.2$ ,  $-0.3$ ,  $-0.4$ . These are shown respectively as they emanate from the surface of the inverted oblate spheroid towards infinity, and by employing only the first term of the series.

### 12.3 Discussion

Aiming in the better understanding of the processes induce atherogenesis, and in particular the hydrodynamic behaviour of aggregated LDLs, we solve analytically the axisymmetric Stokes flow problem for an inverted oblate spheroid that moves with constant velocity within a Newtonian fluid. The fluid resembles the blood plasma which, moreover, is assumed to be at rest far away of the spheroid. We used an inverted oblate spheroid to model the two aggregated LDLs. This is a quite new approach, since the only geometry used so far was the spherical one which was not adequate to describe aggregated spherical objects.

We derive the stream function, employing the methods and some results developed in previous works of the authors [11, 12], where the stream function for Stokes flow past a stationary inverted oblate spheroid was derived explicitly.

Employing the stream function, we can calculate important hydrodynamic quantities, such as the drag force exerted by the fluid on the surface of the inverted oblate spheroid, the drag coefficient and the terminal settling velocity. Thus we aim to contribute to the studies concerning HDL and LDL measurements and the chemical precipitation methods for the separation of HDL. The proposed analytical expressions may also help to validate relative laboratory practices and quantitative methods. To this end, the provided analytical results are expected to be useful not only for the aggregated LDLs but also for any similar flow problem involving inverted oblate spheroid of various geometrical characteristics.

**Acknowledgments** This research has been co-financed by the European Union (European Social Fund—ESF) and Greek national funds through the Operational Program “Education and Lifelong Learning” of the National Strategic Reference Framework (NSRF)—Research Funding Program: ARCHIMEDES III. Investing in knowledge society through the European Social Fund.

### References

1. Khoo J C, Miller E, McLoughlin P, Steinberg D (1990) Prevention of low density lipoprotein aggregation by high density lipoprotein or apolipoprotein A-I. *J Lipid Res* 31:645–652
2. Steinberg D (1978) The rediscovery, of high density lipoprotein: a negative risk factor in atherosclerosis. *Eur J Clin Invest* 8:107–109
3. Cromwell W C, Otvos J D (2004) Low-density lipoprotein particle number and risk for cardiovascular disease. *Curr Atheroscler Rep* 6(5):381–387. doi:10.1007/s11883-004-0050-5, PMID: 15296705
4. Lu M, Gursky O (2013) Aggregation and fusion of low-density lipoproteins in vivo and in vitro. *Biomol Concepts* 4(5):501–518

5. Pentikäinen M O, Lehtonen E M, Kovanen P T (1996) Aggregation and fusion of modified low density lipoprotein. *J Lipid Res* 37(12):2638–2649
6. Xu S (1998) Apolipoprotein(a) binds to low-density lipoprotein at two distant sites in lipoprotein(a). *Biochemistry* 37(26):9284–9294
7. Hadjinicolaou M (2014) A mathematical model for the blood plasma flow around two aggregated low density lipoproteins. GENEDIS 2014, Advances in Experimental Medicine and Biology\_820, DOI [10.1007/978-3-319-09012-2-11](https://doi.org/10.1007/978-3-319-09012-2-11)
8. Dassios G, Hadjinicolaou M, Protopapas E (2012) Blood plasma flow past a red blood cell: mathematical modeling and analytical treatment. *Math Methods Appl Sci* 35(13):1489–1612
9. Hadjinicolaou M, Kamvyssas G, Protopapas E (2014) Stokes flow applied to the sedimentation of a red blood cell. *Q Appl Math* (to appear)
10. Baganis G, Dassios G, Hadjinicolaou M, Protopapas E (2013) The Kelvin transformation as a tool for analyzing problems in medicine and technology. *Math Methods Appl Sci*. doi:[10.1002/mma.2903](https://doi.org/10.1002/mma.2903)
11. Dassios G (2009) The Kelvin transformation in potential theory and Stokes flow. *IMA J Appl Math* 74:427–438
12. Baganis G, Hadjinicolaou M (2009) Analytic solution of an exterior Dirichlet problem in a non-convex domain. *IMA J Appl Math* 74(5):668–684
13. Baganis G, Hadjinicolaou M (2010) Analytic solution of an exterior Neumann problem in a non-convex domain. *Math Methods Appl Sci* 33(17):2067–2075
14. Dassios G, Kleinman R (1989) On the capacity and Rayleigh scattering for a class of non-convex bodies. *Q J Mech Appl Math* 42(3):467–475
15. Dassios G, Hadjinicolaou M, Payatakes AC (1994) Generalized eigenfunctions and complete semiseparable solutions for Stokes flow in spheroidal coordinates. *Q Appl Math LII* (I):157–191
16. Hadjinicolaou M, Protopapas E (2013) On the R-semiseparation of the Stokes bi-stream operator in the inverted prolate spheroidal coordinates. *Math Methods Appl Sci*. doi:[10.1002/mma.2841](https://doi.org/10.1002/mma.2841)
17. Happel J, Brenner H (1991) *Low Reynolds number hydrodynamics*. Kluwer Academic Publishers, London
18. Lebedev N N (1972) *Special functions and their applications*. Dover Publications, New York

# Chapter 13

## Chaotic Attractors in Tumor Growth and Decay: A Differential Equation Model

Michael Harney and Wen-sau Yim

**Abstract** Tumorigenesis can be modeled as a system of chaotic nonlinear differential equations. A simulation of the system is realized by converting the differential equations to difference equations. The results of the simulation show that an increase in glucose in the presence of low oxygen levels decreases tumor growth.

### 13.1 Introduction

Cancer growth and decay can be modeled as a system of chaotic nonlinear differential equations. The system is based on a reaction-diffusion cancer growth model, expressed by

$$\frac{\partial n}{\partial t} = d_n \nabla^2 - \rho \nabla \cdot (n \nabla f) \tag{13.1}$$

$$\frac{\partial f}{\partial t} = \alpha \eta (m - f) \tag{13.2}$$

$$\frac{\partial m}{\partial t} = d_m \nabla^2 m + \kappa n - \sigma m \tag{13.3}$$

$$\frac{\partial c}{\partial t} = d_c \nabla^2 c + \nu f - \omega n - \phi c \tag{13.4}$$

The above model will be simplified by Ivancevic et al. [1] so as to allow useful parameters to be applied for simulation and then recreated in C/Java, to directly compare with its predecessor project created by Ivancevic et al. (simulated in Wolfram CDF and Mathematica).

---

M. Harney (✉)  
Health Catalyst, Salt Lake City, UT, USA  
e-mail: [mharney1@jhu.edu](mailto:mharney1@jhu.edu)

W.-s. Yim (✉)  
Life Technologies, San Francisco, CA, USA  
e-mail: [wylim2@jhu.edu](mailto:wylim2@jhu.edu)



Varying input parameters of glucose and oxygen levels will be examined to determine chaos behavior. Ultimately, the result will be the development of a bifurcation graph to characterize the chaotic behavior of the system.

## 13.2 Methodology

From the reaction-diffusion cancer growth model above, a simplified non-dimensional nonspatial derivative model was found. This model was further modified by adding four additional parameters ( $\alpha$ ,  $\beta$ ,  $\gamma$ ,  $\delta$ ) which represent tumor cell volume, glucose level, number of tumor cells, and diffusion saturation level from the surface, respectively. The starting point of the generation C/Java simulations is expressed by

$$\dot{n} = 0 \quad (13.5)$$

$$\dot{f} = \alpha\eta(m - f) \quad (13.6)$$

$$\dot{m} = \beta\kappa n + f(\gamma - c) - m \quad (13.7)$$

$$\dot{c} = \nu fm - \omega n - \delta\phi c \quad (13.8)$$

Calculations can be found in Appendix 1. For a unit dimensionless time change, the following was solved for  $f_{\text{new}}$ ,  $m_{\text{new}}$ , and  $c_{\text{new}}$ :

$$f_{\text{new}} = (1 - \alpha\eta)f_{\text{old}} + \alpha\eta m_{\text{old}} \quad (13.9)$$

$$m_{\text{new}} = \beta\kappa n + f_{\text{old}}(\gamma - c) \quad (13.10)$$

$$c_{\text{new}} = (1 - \delta\phi)c_{\text{old}} + \nu f_{\text{old}} m_{\text{old}} - \omega n \quad (13.11)$$

The methodology in finding a chaotic system is to analyze the set of constant parameters that describe the system. The constants hypothesized to exhibit chaotic behavior include  $\alpha$ ,  $\beta$ ,  $\gamma$ ,  $\delta$ ,  $\eta$ ,  $\beta$ ,  $\kappa$ ,  $\gamma$ ,  $\nu$ ,  $\omega$ ,  $\delta$ ,  $\phi$ , where  $\alpha$  = tumor cell volume,  $\beta$  = glucose level,  $\gamma$  = number of tumor cells,  $\delta$  = diffusion saturation, and  $\eta$ ,  $\beta$ ,  $\kappa$ ,  $\gamma$ ,  $\nu$ ,  $\omega$ ,  $\delta$ ,  $\phi$  are non-dimensional constants.

## 13.3 Implementation

The equations in (13.9)–(13.11) are translated into a high-level programming pseudo-code:

```
// Set initial conditions
n = 50; // tumor cell density in the simulation
m = 0; // matrix-degradative enzyme concentration
f = 0; // matrix-metalloproteinases concentration
c = 0; // Oxygen concentration
```

```
// Start the simulation loop for N loops
Start Loop
    f[i+1] = (1-alpha * eta)*f[i] + alpha * eta* m[i];
    m[i+1] = beta * kappa * n + f[i]*(gamma - c[i])
    c[i+1] = (1 - delta * phi)*c[i] + nu * f[i] * m[i] - omega * n
End Loop
```

Sample C and Java source codes are provided in Appendix 2.

## 13.4 Software

Three programming software packages were utilized:

- The C simulation was written and compiled using Pelles C, version 6.50 (<http://www.smorgasbordet.com/pelleesc/>).
- The Java simulation was written and compiled with Java SE Version 6 Update 27 and Java SE Development Kit (JDK) 6, provided by Oracle (<http://www.oracle.com/technetwork/java/javase/downloads/index.html>).
- Wolfram Alpha CDF (<http://www.wolframalpha.com/cdf-experiment/>) and Wolfram Alpha Mathematica.

## 13.5 Summary

Case 1:  $\Gamma = \Delta = 0$

As it has been found from our C and Java simulation that decreasing  $\Gamma$  and  $\Delta$  increases bifurcations for an increase in tumor cell density, we start the CDF simulation with  $\Gamma$  and  $\Delta$  set to 0 and we use the  $m, f$  phase plot results in Fig. 13.1 for comparison.

Case 2:  $\Gamma = \Delta = 0$ , decreased oxygen

By decreasing oxygen (variable  $c$ ), we find that the average  $m, f$  phase plot has a lower trajectory density than in Fig. 13.1. This would be expected—decreasing oxygen slows growth and moves trajectories away from the attractor. Note that the two trajectory points in Fig. 13.1 have decreased to one trajectory in Fig. 13.2. Also, the  $(f, c)$  phase plot shows reduced activity, which is to be expected as  $c$  is the oxygen concentration variable.

Case 3:  $\Gamma = \Delta = 0$ , decreased oxygen, decreased glucose

Starting with Case 2 and decreasing glucose (variable  $\beta$ ), we find that the second trajectory point returns in the  $m, f$  phase plot of Fig. 13.3, showing an increase in attractor stability.

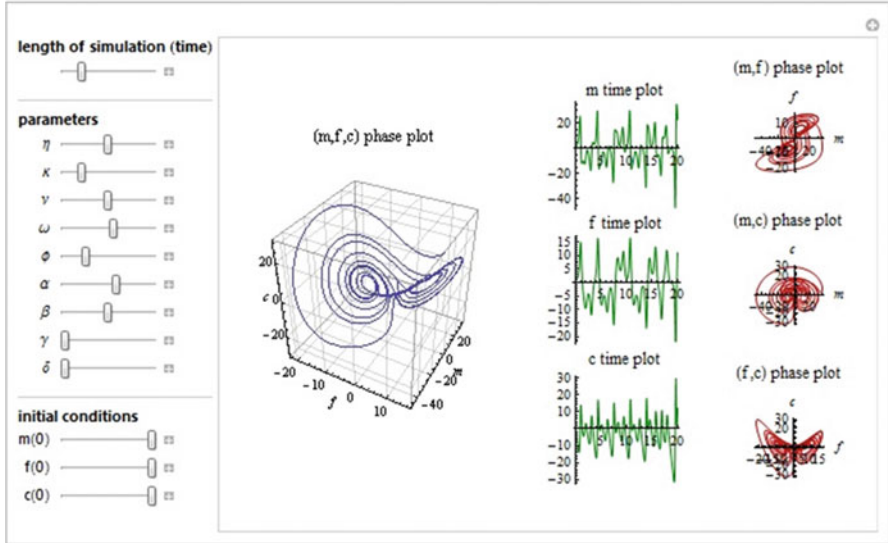


Fig. 13.1 Case 1, Gamma = Delta = 0

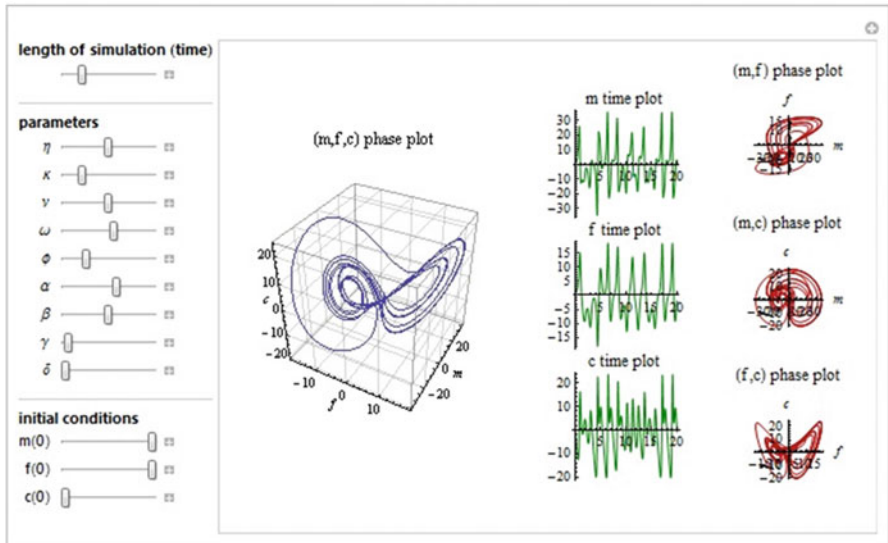


Fig. 13.2 Case 2, Gamma = Delta = 0 with decreased oxygen levels

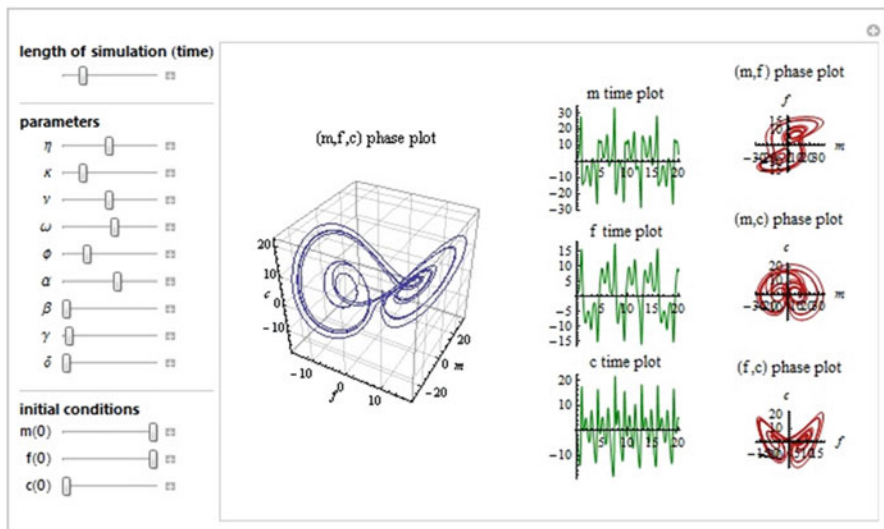


Fig. 13.3 Case 3, Gamma = Delta = 0 with decreased oxygen and glucose

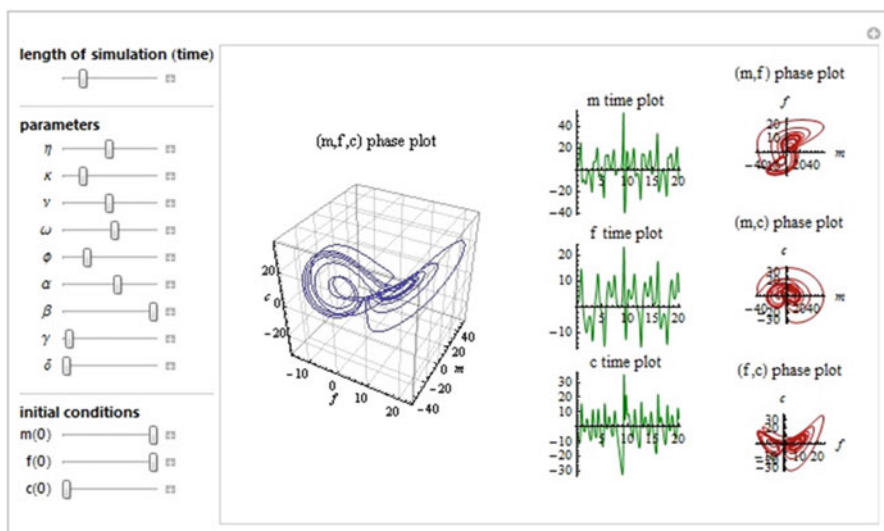


Fig. 13.4 Case 4, Gamma = Delta = 0 with decreased oxygen and increased glucose

Case 4: Gamma = Delta = 0, decreased oxygen, increased glucose

Starting with Case 3 and increasing glucose significantly, we find that the lower left trajectory point in Fig. 13.4 of the  $m,f$  plot is decreasing in size and density. This may indicate that the attractor is becoming less stable. The  $f,c$  phase plot also shows reduced activity, similar to when oxygen concentration was initially decreased in Case 2.

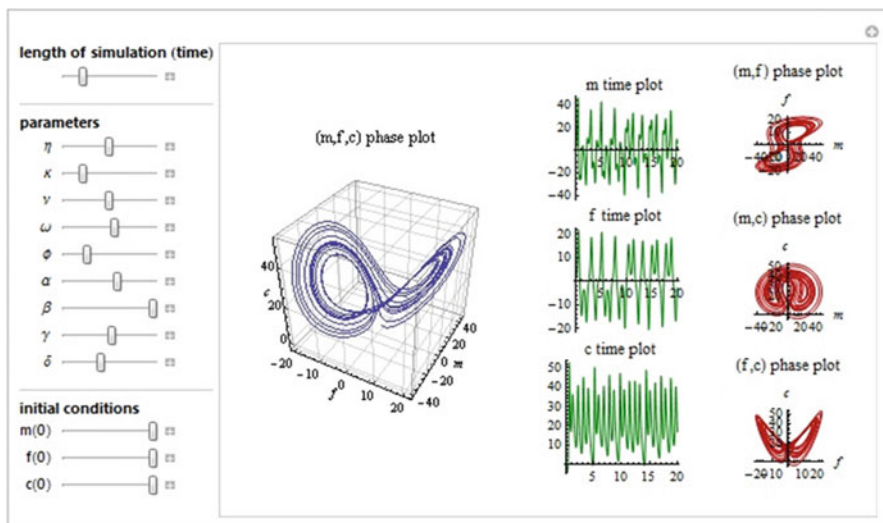


Fig. 13.5 Case 5, maximized glucose

#### Case 5: Glucose maximized

For comparison to the above simulations where gamma and delta were set equal to 0, we restore gamma, delta and the oxygen concentration to significant values and we also increase glucose. The results show a robust attractor with two well defined trajectory points in the  $m,f$  plot of Fig. 13.5. This is typical of a textbook definition of tumor growth—high oxygen and glucose concentration yield strong tumor growth.

#### Case 6: Glucose minimized

From Case 5 settings, we decrease glucose and find that the trajectory points in the  $m,f$  plot of Fig. 13.5 shows some reduction (as expected from a standard cell growth model) but not as significant a reduction as shown in Case 3, where gamma and delta were set to 0 and glucose was increased (Fig. 13.6).

## 13.6 Validation

To validate the C/Java/CDF model used in this study, the 3D chaotic attractor generated by Ivancevic et al. was recreated. The original attractor taken in Fig. 13.1 from Ivancevic is shown in Fig. 13.7.

By inserting the original conditions in the C/Java/CDF model, the following 3D model was generated, illustrated in Fig. 13.8.

By manipulating the values of the constants of gamma and delta (in the C/Java source code found in Appendix 2), which represent the number of tumor cells and

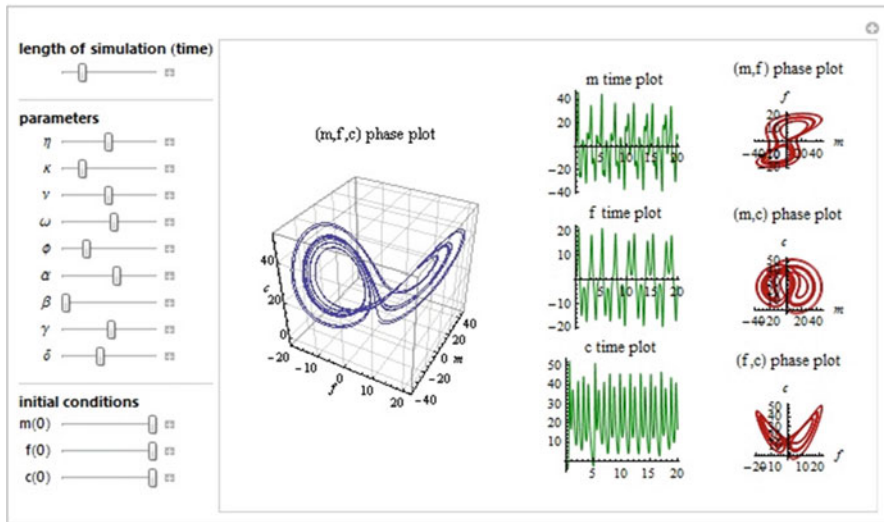
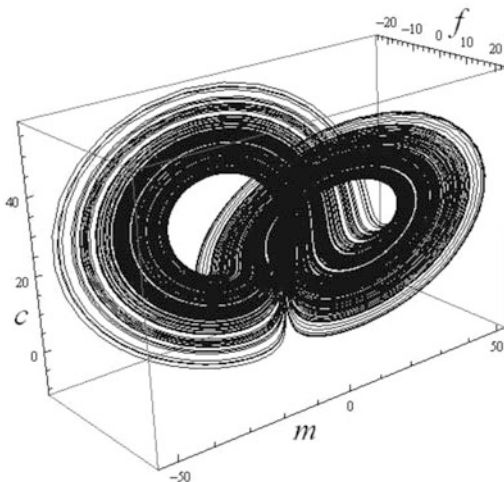


Fig. 13.6 Case 6, minimized glucose

Fig. 13.7 3D Lorenz-like chaotic attractor from Ivancevic



the diffusion from the surface respectively, the system was found to produce increasing bifurcations as is shown in Fig. 13.9, which shows bifurcation levels for matrix-degradative enzyme concentration (MDE), matrix-metalloproteinases concentration, and oxygen concentration (which hypothetically changes due to rapid and then slower growth rates). The system modeled with the C and Java simulation produces results that approach the plots in Fig. 13.1 of the CDF time domain simulations.

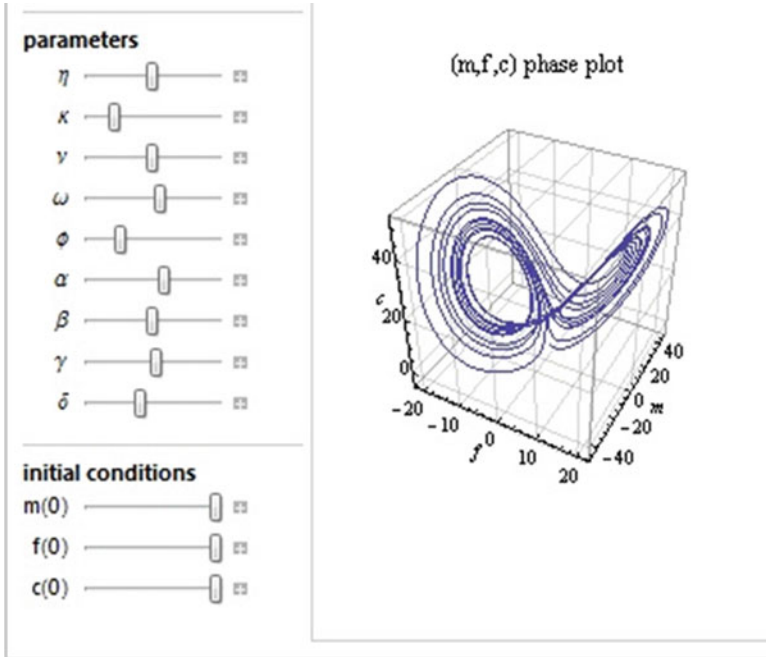


Fig. 13.8 Validation  $(m,f,c)$  phase plot

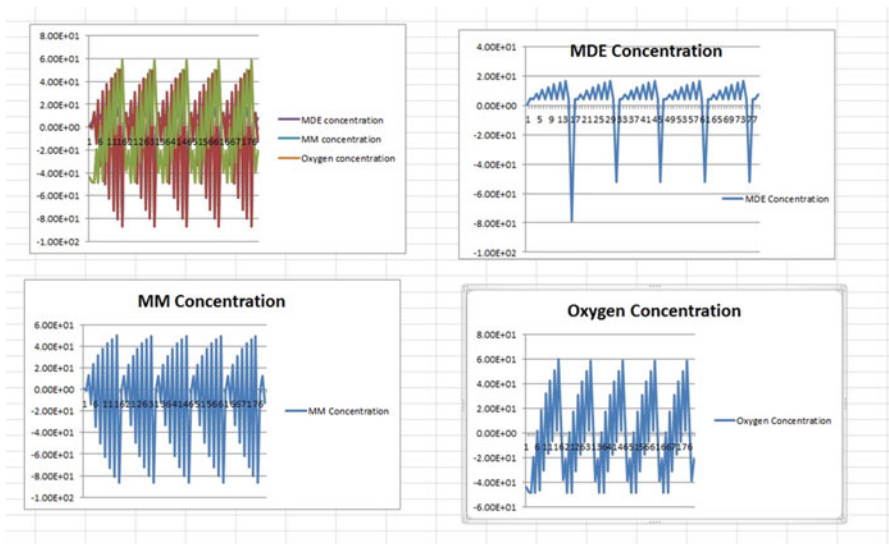


Fig. 13.9 C/Java Simulation Results with  $\gamma = 0.265$  (low),  $\delta = 0.4$  (low), and  $\beta = 0.05$  (low)

### Conclusions

Bar-Yam's definition of a chaotic system is a deterministic system that is difficult to predict. Chaotic systems are often associated with the butterfly effect or "sensitivity to initial conditions." Both characteristics stem from the behavior of chaotic systems to evolve into unpredictable paths. This study aimed to characterize the chaotic behavior in the case of cancer tumor growth and decay. The terms "deterministic" and "characterize" may seem out of place when referring to chaotic systems, especially for tumor growth. Using a simplified non-dimensional non-spatial differential equation model, a stable (non-chaotic) system was found by manipulating the system parameters:  $\delta$ ,  $\beta$ .

A bifurcating system that approaches a chaotic system was found by defining decreased values of gamma (number of tumor cells) and delta (diffusion constant):  $\gamma = 0.265$ ,  $\delta = 0.40$ . In this modified system, a key finding was that the increased glucose in the presence of lowered oxygen levels decreased the tumor growth. Biologically speaking, this deviates from the current literature that argues that increase in glucose levels leads to increase of tumor growth, which is shown for comparison in Case 5 (Fig. 13.5) and Case 6 (Fig. 13.6). Annibaldi and Widmann show that glucose deprivation can activate oncogenes which can up-regulate proteins involved in aerobic glycolysis which can in turn render tumor cells more resistant to apoptosis [5]. It is therefore reasonable to assume that a downregulation in these same proteins initiated by an increase in glucose concentration could render the same cells vulnerable to apoptosis, decreasing tumorigenesis, which supports the results from the simulations in Sect. 13.5. The decrease in the number of tumor cells and the decrease in the diffusion constant are expected to decrease tumor growth, but it would still be assumed that an increase in glucose would increase tumor growth and there is evidence from Case 1–4 examples that this is not the case. Our C/Java simulation also provides evidence of an increase in activity as glucose is decreased when gamma and delta have low values.

## Appendix 1: Calculations for DE Model

The derivations for the C/Java model are provided below:

$$\int \frac{dn}{dt} dt = 0$$

$$\dot{f} = \frac{f_{\text{new}} - f_{\text{old}}}{t} = \alpha\eta(m - f)$$



$$\dot{m} = \frac{m_{\text{new}} - m_{\text{old}}}{t} = \beta\kappa n + f(\gamma - c) - m$$

$$\dot{c} = \frac{c_{\text{new}} - c_{\text{old}}}{t} = \nu f m - \omega n - \delta\phi c$$

For a unit time change of 1, solve for  $f_{\text{new}}$ ,  $m_{\text{new}}$ , and  $c_{\text{new}}$ :

$$f_{\text{new}} = (1 - \alpha\eta)f_{\text{old}} + \alpha\eta m_{\text{old}}$$

$$m_{\text{new}} = \beta\kappa n + f_{\text{old}}(\gamma - c)$$

$$c_{\text{new}} = (1 - \delta\phi)c_{\text{old}} + \nu f_{\text{old}} m_{\text{old}} - \omega n$$

## Appendix 2: Sample Source Code

### C Programming Language

```
#include <math.h>
#include <stdio.h>
#include <stdlib.h>

#define ITERATIONS 900

int main ()
{
    inti;
    FILE *F1;

    floatn_old = 0.50; // tumor cell density 50
    floatf_old = 0.0; // matrix-metalloproteinases concentration
    floatf_new = 0.0;
    floatm_old = 0.0; // matrix-degradative enzyme concentration
    floatm_new = 0.0;
    floatc_old = 0.0; // Oxygen concentration
    floatc_new = 0.0;

    float alpha = 0.06; // tumor cell volume
    float beta = 0.05; // glucose level
    float gamma = 0.265; // number of tumor cells 26.5
    float delta = 0.40; // diffusion from the surface 40

    floatdn = 0.0005;
    float dm = 0.0005;
    float dc = 0.5;
    float rho = 0.01;
    float eta = 0.50; //was 50
    float kappa = 1.0;
```

```

float sigma = 0;
float nu = 0.5;
float omega = 0.57;
float phi = 0.025;

F1 = fopen("chaotumor.txt", "w");
for (i = 0; i < ITERATIONS; i++)
{
    f_new = alpha*eta*(m_old - f_old) + f_old;
    m_new = beta*kappa*n_old - f_old*c_old + gamma*f_old;
    c_new = nu*f_old*m_old - omega*n_old - delta*phi*c_old + c_old;

    f_old = f_new;
    m_old = m_new;
    c_old = c_new;

    fprintf (F1, "%f", m_new);
    fprintf (F1, "%f\n", f_new);
    fprintf (F1, "%f\n", c_new);
}
fclose(F1);
}

```

### Java Programming Language

```

import java.util.Scanner;
import java.io.*;
import java.lang.Math.*;
import java.util.Random;
import java.util.*;

public class ChaosTumor
{
    // initialize system parameters
    static double alpha = 0.06; //tumor cell volume
    static double beta = 0.05; // glucose level
    static double gamma = 0.265; // number of tumor cells, 26.5
    static double delta = 0.40; // diffusion from surface, 40

    // initialize system constants
    static double n = 50;
    static double dn = 0.0005;
    static double dm = 0.0005;
    static double dc = 0.5;
    static double rho = 0.01;

```

```

static double eta = 50;
static double kappa = 1.0;
static double sigma = 0;
static double nu = 0.5;
static double omega = 0.57;
static double phi = 0.025;

public static void main (String[] args)
{
    // initialize parameters
double f; // matrix-metalloproteinases concentration
double m; // matrix-degradative enzyme concentration
double c; // oxygen concentration

    // ask user input for growth, capacity, and initial population
    Scanner scan = new Scanner (System.in);
System.out.println("Chaos in Tumor Growth Dynamics Study");
System.out.println("*****");
System.out.print("Enter MM concentration, f: ");
    f = scan.nextDouble();
System.out.print("Enter MDE concentration, m: ");
    m = scan.nextDouble();
System.out.print("Enter the oxygen concentration, c: ");
    c = scan.nextDouble();
System.out.println("*****");

    // open file
try
{
    // open output file
    File outFile = new File("ChaosTumor.txt");
BufferedWriter writer = new BufferedWriter(new FileWriter
(outFile));

    // print out the inital condition
writer.write("Initial conditions :"+m+" "+f+" "+c);
System.out.println("Initial population: "+m+" "+f+" "+c);
writer.newLine();

double [] temp = new double[3];
for(int i=1; i<51; i++)
{
    temp = compute(m, f, c);
    f = temp[0];
    m = temp[1];
    c = temp[2];
}
}
}

```

```

// remove negative values
if(m<0)
    m=0;
if(f<0)
    f=0;
if(c<0)
    c=0;

writer.write("Iteration "+i+": "+m+" "+f+" "+c);
writer.newLine();
System.out.println("Iteration "+i+": "+m+" "+f+" "+c);
}
// close output file
writer.close();
}
catch (IOException e)
{
System.err.println(e);
System.exit(1);
}
// close file
} // endmain

/**
 * method: compute(float m, float f, float c)
 * computes an array containing [m, f, c] at t+1
 * @param: float m, float f, float c
 * @precondition: none
 * @postcondition: none
 * @return: returns m, f, and c concentrations at t+1
 */
public static double[] compute(double m, double f, double c)
{
    double[] array = new double[3];
array[0] = (1-alpha*eta)*f + alpha*eta*m;
    array[1] = beta*kappa*n + (gamma-c)*f;
    array[2] = (1-delta*phi)*c + nu*f*m - omega*n;
return array;
}
}

```

## References

1. Ivancevic TT, Bottema MJ, Jain LC (2008) [A theoretical model of chaotic attractor in tumor growth and metastasis](#). arXiv: 0807.4272 in Cornell University Library's arXiv.org
2. Sole R, Goodwin B (2000) Signs of life: how complexity pervades biology. Basic Books, New York, NY
3. Bar-Yam Y (2011) Concepts: chaos. New England Complex Systems Institute. <http://www.necsi.edu/guide/concepts/chaos.html>
4. Guiot C, Degiorgis PG, Delsanto PP, Gabriel P, Deisboeck TS. Does tumor growth follow a universal law? <http://arxiv.org/ftp/physics/papers/0303/0303050.pdf>
5. Annibaldi A, Widmann C (2010) Glucose metabolism in cancer cells. PubMed: <http://www.ncbi.nlm.nih.gov/pubmed/20473153>

# Chapter 14

## Modeling $k$ -Noncrossing Closed RNA Secondary Structures via Meandric Compression

Antonios Panayotopoulos and Panayiotis Vlamos

**Abstract** In this chapter we present the transformation of a meander to its compression and we apply this new formulation for the modeling of  $k$ -noncrossing closed RNA secondary structures. We obtain this by using curves which consist parts of their meandric curve. We prove basic properties and produce generating procedures. Two new types of meanders arise: the simple and the perpendicular, in order to be used as representatives of  $k$ -noncrossing closed RNA secondary structures.

### 14.1 Introduction

The ultimate goal of RNA structure prediction problem is to obtain the three-dimensional structure of these biomolecules through computation. The key concept for solving the above problem is the appropriate representation of the biological structures. RNA secondary structure is often assumed to be sufficient for being able to predict the RNA function. RNA secondary structure has already been studied as  $k$ -noncrossing set of partitions, which corresponds to the base pairs and no base pairs, respectively [1]. In this chapter, we present the mathematical formulation for modeling of  $k$ -noncrossing closed RNA structures with meandric compression.

A closed meander of order  $n$  is a closed self-avoiding curve crossing an infinite horizontal line  $2n$  times [2]. The meanders were also independently introduced as planar permutations by P. Rosenstiehl [3]. Considered as planar permutations, meanders have been studied with nested sets and parentheses [3], Motzkin words [4], and polygons [5].

---

A. Panayotopoulos  
University of Piraeus, Karaoli & Dimitriou 80, 18534 Piraeus, Greece  
e-mail: [antonios@unipi.gr](mailto:antonios@unipi.gr)

P. Vlamos (✉)  
Department of Informatics, Ionian University, Plateia Tsirigoti 7, 49100 Corfu, Greece  
e-mail: [vlamos@ionio.gr](mailto:vlamos@ionio.gr)

Our motivation for introducing the compression of a meander was considered both in mathematical and physical context. Each meander has a unique compression, thus we can create representatives of large classes of meanders of different orders. If the representative compressions of these classes could be decompressed, then we could obtain significant results on the problem of enumerating meanders. From the biological point of view, it is clear that a given RNA sequence has many potential structures which grow exponentially with the length of the RNA sequence [1]. The challenge is to identify whether structure plays a functional role for a given RNA sequence and, if yes, to predict this functional RNA structure. Using the proposed meandric compression classes we reduce the RNA  $k$ -noncrossing set of partitions, which is the starting point of many combinatorial-based algorithms for the RNA structure prediction problem [6].

In this chapter, we obtain the compression as the determination of a unique simple meander. In Sect. 14.2, we cut the RNA  $k$ -noncrossing set of partitions vertically at a given position and create two specific forms of meanders: the simple and the perpendicular. We study the properties of their numbers of cuttings and cutting degree [5]. In Sect. 14.3, we define the compression geometrically, using the flow of curves of the meander. In order to deduce the simple meander, we need a total order on the set of the curves and then, after suitable transformations, with the help of the perpendicular meander, we obtain the compression.

## 14.2 Meanders

The set of all the meanders of order  $n$  is denoted by  $\mathcal{M}_{2n}$ . Let  $\mu \in \mathcal{M}_{2n}$  be a meander crossing a horizontal line. Following [5], for any  $i \in [2n - 1]$  we consider the vertical line, which shall be called the  $i$ -line, passing through the middle point of the segment  $(i, i + 1)$  of the horizontal line of the meandric curve. The number of those arcs of the meandric curve, which are intersected by the  $i$ -line and lie above and beneath the horizontal line of  $\mu$ , is called the *numbers of cuttings*  $\theta(i)$  and  $\theta'(i)$ , respectively.

The sum  $\varepsilon(i) = \theta(i) + \theta'(i)$  of the number of those arcs of the meandric curve which are intersected by the  $i$ -line is called the *cutting degree* of the meander at  $i$ . We notice that  $\theta(i)$  and  $\theta'(i)$  are of the same parity; hence  $\varepsilon(i)$  is always even.

The meandric curve always has points of intersection with the  $i$ -line, which we call *traces*. Obviously, the number of the traces is equal to  $\varepsilon(i)$ . Starting below the horizontal line, we label the traces with the numbers  $1, 2, 3, \dots, \varepsilon(i)$ , knowing that  $\theta(i)$  (resp.  $\theta'(i)$ ) of them are lying above (resp. beneath) the horizontal line.

From now on, we will consider that the traces are identical to their corresponding labels. For example, for the meander of Fig. 14.1 and for  $i = 14$ , we have  $\theta(14) = 4$ ,  $\theta'(14) = 6$  and  $\varepsilon(14) = 10$ .

Beginning from trace 1 and moving clockwise upon the meandric curve, following its “natural flow”, we obtain the set of open curves  $C(i) = \{c_1^i, c_2^i, \dots, c_{\varepsilon(i)}^i\}$ ,

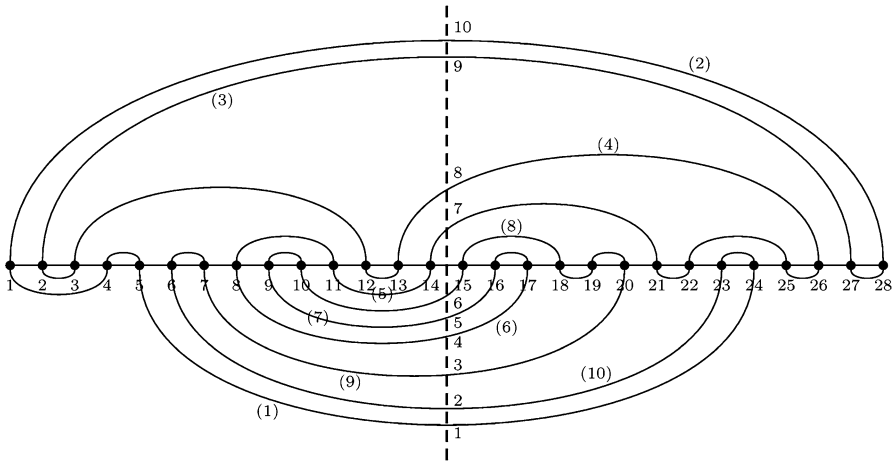


**Fig. 14.1** Representation of a  $k$ -noncrossing closed RNA structure as a meander of order 14

where each  $c_k^i$ ,  $k \in [ei]$ , belongs entirely in one of the two semiplanes defined by the  $i$ -line and has as its ends two traces, i.e. the “entrance” trace denoted by  $\tau_i(k)$  and the “exit” trace denoted by  $\tau_i(k + 1)$ .

We observe that for a curve  $c_k^i$ , if  $k$  is odd (resp. even), then the curve lies on the left (resp. right) of the  $i$ -line. All the curves of the set  $C_i$  do not cross each other.

In Fig. 14.1, we denote the curve  $c_k^i$  by  $(k)$ .

At each curve  $c_k^i$ ,  $k \in [ei]$ , we correspond a number  $b_k^i$  such that

$$b_k^i = \begin{cases} 1, & \text{if the curve } c_k^i \text{ crosses the horizontal line at an odd number of points} \\ 2, & \text{if the curve } c_k^i \text{ crosses the horizontal line at an even number of points} \end{cases}$$

The set  $C_i$  can be partitioned into three classes  $C_1i$ ,  $C_2i$  and  $C'_2i$ :

The set  $C_1i$  consists of the curves  $c_k^i$  with  $b_k^i = 1$ ; that is, their traces lie the one above and the other beneath the horizontal line.

The set  $C_2i$  (resp.  $C'_2i$ ) consists of the curves  $c_k^i$  with  $b_k^i = 2$ ; that is, their traces lie both above (resp. beneath) the horizontal line.

We classify the curves  $c_k^i$  of  $C_i$  by comparing their traces with the number of cuttings  $\theta^i$ :

1. If  $\theta^i < \tau_i(k), \tau_i(k + 1)$ , then  $c_k^i \in C_2i$ .
2. If  $\tau_i(k), \tau_i(k + 1) \leq \theta^i$ , then  $c_k^i \in C'_2i$ .
3. If  $\tau_i(k) \leq \theta^i < \tau_i(k + 1)$  or  $\tau_i(k + 1) \leq \theta^i < \tau_i(k)$ , then  $c_k^i \in C_1i$ .

The meanders for which there exists at least one  $i \in [2n - 1]$ , such that every curve of the sets  $C_1i$  (resp.  $C_2i$ ,  $C'_2i$ ) has exactly one point (resp. two points) on the horizontal line, which will be called *simple at  $i$* . For example, the meander of Fig. 14.2 is simple at  $i = 8$ .



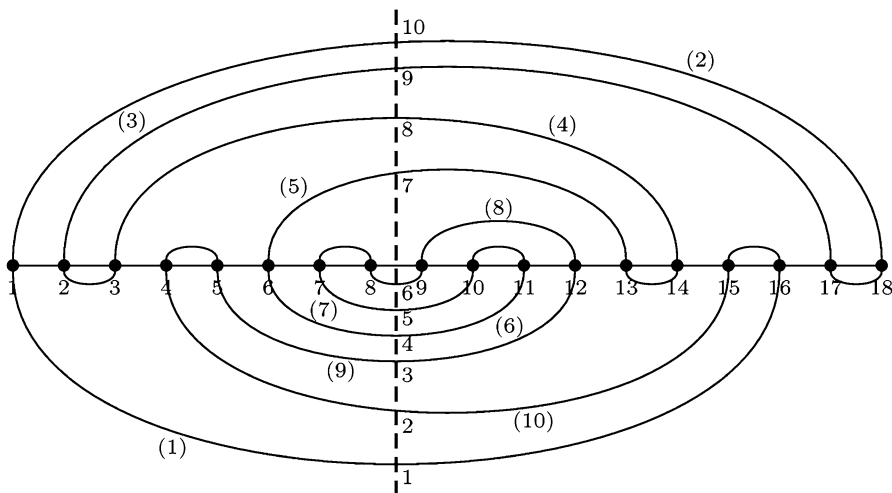


**Fig. 14.2** A meander of order 9, simple at  $i = 8$

Following the “natural flow” of the meander  $\mu$ , through its open curves  $c_k^i$ , described as before, its traces  $\tau_i(k)$ ,  $k \in [ei]$ , define a self-avoiding closed curve by neglecting its isotopies on the plane; that is, they form a meander  $\tau_i$  of order  $ei/2$ . Indeed, this meandric curve is deduced by the open curves  $c_k^i$  which are non-crossing.

The  $i$ -line of  $\mu$  is the line of  $\tau_i$  and the line of  $\mu$  is the  $\ell$ -line of  $\tau_i$ , where  $\ell = \theta' i$ .

So, at each pair  $(\mu, i)$  corresponds a meander  $\tau_i$ , which we call *perpendicular meander of  $\mu$  at  $i$* , due to the relation of perpendicularity between the  $i$ -line and the  $\ell$ -line.

For example, the meander of Fig. 14.3 is the perpendicular of the meander of Fig. 14.1 at  $i = 14$ , where the pair  $\{\tau_i(k), \tau_i(k + 1)\}$  is denoted by  $(k)$ .

We denote the numbers of cuttings of the meander  $\tau_i$  by  $\tilde{\theta}(\ell), \tilde{\theta}'(\ell)$  and its cutting degree by  $\tilde{\varepsilon}(\ell)$ . We can easily obtain that:

1.  $\tilde{\theta}(\ell) = \sum_{k \in K} b_k^i$ , where  $K = \{k \in [ei] : b_k^i = 1 \text{ and } k \text{ odd}\}$
2.  $\tilde{\theta}'(\ell) = \sum_{k \in K'} b_k^i$ , where  $K' = \{k \in [ei] : b_k^i = 1 \text{ and } k \text{ even}\}$
3.  $\tilde{\varepsilon}(\ell) = \sum_{k \in K \cup K'} b_k^i$

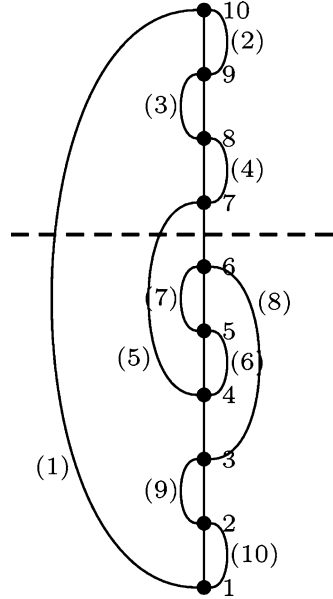
For example, considering the meander of Fig. 14.1 and taking  $i = 14$ , we have that  $\ell = \theta'(14) = 6$ , whereas for the meander of Fig. 14.3 and for  $\ell = 6$ , we have that  $\tilde{\theta}(6) = 2, \tilde{\theta}'(6) = 0$  and  $\tilde{\varepsilon}(6) = 2$ .

Following Proposition 3.1 of [5], we obtain:

**Proposition 1** For the numbers of cuttings  $\tilde{\theta}(\ell), \tilde{\theta}'(\ell)$  we have that:

1.  $\ell, \tilde{\theta}(\ell)$  and  $\tilde{\theta}'(\ell)$  have the same parity

**Fig. 14.3** The perpendicular meander of the meander of Fig. 14.1 at  $i = 14$



2.  $\max\{\tilde{\theta}(\ell), \tilde{\theta}'(\ell)\} \leq \min\{\theta(i), \theta'(i)\}$
3.  $|\tilde{\theta}(\ell + 1) - \tilde{\theta}(\ell)| = |\tilde{\theta}'(\ell + 1) - \tilde{\theta}'(\ell)| = 1$

This meander is defined by the permutation  $\tau = \tau(1)\tau(2) \cdots \tau(2\nu)$ . The set  $T(\ell)$  of the pairs  $\{\tau(k), \tau(k + 1)\}$  is partitioned into the classes  $T_1(\ell)$ ,  $T_2(\ell)$  and  $T_2'(\ell)$ , according to the following relations:

1.  $\tau(k) < \ell < \tau(k + 1)$  or  $\tau(k + 1) < \ell < \tau(k)$
2.  $\ell < \tau(k), \tau(k + 1)$
3.  $\tau(k), \tau(k + 1) < \ell$   
respectively.

### 14.3 Compression

Let  $\mu \in \mathcal{M}_{2n}$  be a meander who is not simple at  $n$ , and let  $C(n) = \{c_1, c_2, \dots, c_{2\nu}\}$  be its already defined set of open curves, where  $2\nu = \varepsilon(n)$  (and  $c_k = c_k^n$  for simplicity). Each curve  $c_k \in C(n)$  starts from the trace  $\tau(k)$  (where  $\tau(k) = \tau_n(k)$  for simplicity) and ends at the trace  $\tau(k + 1)$ . We distinguish two points of  $c_k$  on the horizontal line: the first after the entrance trace  $\tau(k)$  and the last before the exit trace  $\tau(k + 1)$ . From these two points, the one which is the most distant from the  $n$ -line for  $k \in I_1 = \{1, 3, \dots, 2\nu - 1\}$  (resp. the closest to the  $n$ -line for  $k \in I_2 = \{2, 4, \dots, 2\nu\}$ ) is called the *compression point* (*c-point* for simplicity) of the curve  $c_k \in C(n)$ ,  $k \in [2\nu]$ .

For each curve  $c_k \in C(n)$ , we denote by  $\gamma_k, k \in [2\nu]$ , the closed interval of  $[2\nu]$  with ends the traces  $\tau(k), \tau(k + 1)$ . Given a pair of curves  $c_k, c_\lambda \in C(n), k, \lambda \in I_1$  or  $k, \lambda \in I_2$ , with  $\gamma_\lambda \subset \gamma_k$ , then the curve  $c_\lambda$  is called *internal* of the curve  $c_k$ , and the curve  $c_k$  is called *external* to the curve  $c_\lambda$ . We can easily deduce that the number of the internal curves of a curve  $c_k \in C(n)$  is equal to  $\frac{1}{2}(|\tau(k) - \tau(k + 1)| - 1)$ .

If we transform the curves  $c_k, k \in [2\nu]$ , of the meander  $\mu$  into curves having only one point (resp. two points) on the horizontal line if  $b_k = 1$  (resp.  $b_k = 2$ ) (where  $b_k = b_k^n$  for simplicity), by cutting and rejecting the extra arcs of the corresponding curves of the set  $C(n)$  (similarly to the topological method of surgery), then at least one simple meander is deduced.

Each simple meander defined as above is of order  $\frac{1}{2} \sum_{k \in [2\nu]} b_k$  (since its curves have one or two points of intersection with the horizontal line) and simple at  $u = \sum_{k \in I_1} b_k$  (counting the points of intersection with the horizontal line to the left of the  $n$ -line). The result of the above transformation is the set of open curves  $\bar{C}(u) = \{\bar{c}_1, \bar{c}_2, \dots, \bar{c}_{2\nu}\}$  (where  $\bar{c}_k = \bar{c}_k^u$  for simplicity), for which a bijection is established with the set  $C(n)$ ; that is, each open curve  $c_k$  corresponds to a unique open curve  $\bar{c}_k$  passing from the same traces and reversely, for every  $k \in [2\nu]$ .

We denote with a dash the corresponding elements which characterize this simple meander. The set  $\bar{C}(u)$  can be partitioned into the classes  $\bar{C}_1(u), \bar{C}_2(u), \bar{C}'_2(u)$  corresponding to the classes  $C_1(n), C_2(n), C'_2(n)$  of the set  $C(n)$ .

We notice that  $u, n$  are of the same parity. Indeed, if  $n$  is odd, then there exists an odd number of curves of  $C_1(n)$  to the left, so the same will hold for  $\bar{C}_1(u)$  and  $u$  is odd.

We can easily deduce that

- (a)  $\bar{\varepsilon}(u) = 2\nu, \bar{\theta}(u) = \theta(n), \bar{\theta}'(u) = \theta'(n)$
- (b) Their perpendicular meanders at  $n$  for the meander  $\mu$  and at  $u$  for the corresponding simple meander, respectively, coincide. This common perpendicular meander is denoted by  $\tau$ .
- (c) If  $c_k \in C_2(n)$  (resp.  $c_k \in C'_2(n)$ ) and  $|\tau(k) - \tau(k + 1)| = 1$ , then its corresponding  $\bar{c}_k \in \bar{C}_2(u)$  (resp.  $\bar{c}_k \in \bar{C}'_2(u)$ ) contains one short pair of  $\bar{L}$  (resp.  $\bar{U}$ ). If  $c_k \in C_1(n)$ , then its corresponding curve  $\bar{c}_k \in \bar{C}_1(u)$  is an arc with ends the traces  $\tau(k), \tau(k + 1)$ .

Now, we will confront the problem of finding the curves of the set  $\bar{C}(u)$ . If we follow the flow  $s$  of the meander  $\mu$ , then the creation of these curves, will produce many difficulties. For example, for the meander of Fig. 14.1, the points of the pair of curves  $\bar{c}_1$  and  $\bar{c}_3$  must be properly selected so that the two curves do not cross each other. The same holds for the pairs  $\bar{c}_5$  and  $\bar{c}_7, \bar{c}_3$  and  $\bar{c}_9, \bar{c}_4$  and  $\bar{c}_{10}$ .

Hence, we introduce in the set  $\bar{C}(u)$ , the binary relation “ $<$ ” of preceding for its curves, i.e.  $\bar{c}_p < \bar{c}_q$ , with  $p, q \in I_1$  or  $p, q \in I_2$ , when the  $c$ -point of the curve  $\bar{c}_p$  precedes the  $c$ -point of the curve  $\bar{c}_q$  (i.e. the  $c$ -point of  $\bar{c}_p$  lies at the left of the  $c$ -point of  $\bar{c}_q$  at the horizontal line).

From the above, we can easily deduce the following (1)–(4) results:

1. If  $c_p \in C_1(n)$ ,  $c_q \in C(n)$ , with  $\gamma_q \subset \gamma_p$  and  $p, q \in I_1$  (resp.  $p, q \in I_2$ ), then  $\bar{c}_p < \bar{c}_q$  (resp.  $\bar{c}_q < \bar{c}_p$ ), since the curve  $\bar{c}_q$  is internal of the curve  $\bar{c}_p$ .
2. If  $c_p \in C_2(n) \cup C'_2(n)$ ,  $c_q \in C_1(n)$ , with  $\gamma_q \cap \gamma_p = \emptyset$  and  $p, q \in I_1$  (resp.  $p, q \in I_2$ ), then  $\bar{c}_p < \bar{c}_q$  (resp.  $\bar{c}_q < \bar{c}_p$ ), since this is imposed by the nature of the meander.
3. If  $c_p, c_q \in C_2(n) \cup C'_2(n)$ , with  $\gamma_q \subset \gamma_p$  and  $p, q \in I_1$  or  $p, q \in I_2$ , then  $\bar{c}_p < \bar{c}_q$ , since the curve  $\bar{c}_q$  is internal of the curve  $\bar{c}_p$ .
4. If  $c_p, c_q \in C_2(n)$ , with  $\gamma_q \cap \gamma_p = \emptyset$ ,  $\min \gamma_q < \min \gamma_p$  and  $p, q \in I_1$  (resp.  $p, q \in I_2$ ), then  $\bar{c}_p < \bar{c}_q$  (resp.  $\bar{c}_q < \bar{c}_p$ ), since this is imposed by the nature of the meander. The case where  $c_p, c_q \in C'_2(n)$  is similar.

Obviously, the above results do not cover the cases of two curves, the one belonging to the set  $C_2(n)$  and the other to the set  $C'_2(n)$ , where none of them corresponds to a curve which is internal to some other curve. Consequently, we can deduce more than one solutions, from the perpendicular meander.

In order to obtain a unique solution, we have to make the following choice:

5. If  $c_p \in C_2(n)$ ,  $c_q \in C'_2(n)$ , with  $p, q \in I_1$  or  $p, q \in I_2$  and the  $c$ -point of the curve  $c_p$  precedes the  $c$ -point of  $c_q$ , then  $\bar{c}_p < \bar{c}_q$ . For these curves, we always have  $\gamma_p \cap \gamma_q = \emptyset$ .

We observe that the internal curves of every curve of  $C(n)$  should remain internal of the corresponding transformed curve of  $\bar{C}(u)$ .

The above relation of preceding gives, together with the conditions (1)–(4) and the previous conclusions for the internal curves, a total order  $\bar{c}_{r(1)}, \bar{c}_{r(2)}, \dots, \bar{c}_{r(2\nu)}$ , for the curves of the set  $\bar{C}(u)$ . We can easily understand that the  $\nu$  first elements (resp. the  $\nu$  last elements) of the permutation  $r = r(1)r(2) \dots r(2\nu)$  on  $[2\nu]$  belong to the set  $I_1$  (resp.  $I_2$ ).

For example, applying the above conditions (1)–(5) for the meander of Fig. 14.1, we obtain two total orders:  $\bar{c}_1 < \bar{c}_3 < \bar{c}_9 < \bar{c}_5 < \bar{c}_7$  and  $\bar{c}_8 < \bar{c}_6 < \bar{c}_4 < \bar{c}_{10} < \bar{c}_2$ . Indeed,  $\bar{c}_1 < \bar{c}_3, \bar{c}_5, \bar{c}_7, \bar{c}_9$  due to the condition (1),  $\bar{c}_3 < \bar{c}_5$  due to the condition (2),  $\bar{c}_3 < \bar{c}_9$  due to the condition (5),  $\bar{c}_5 < \bar{c}_7$  due to the condition (1) and finally  $\bar{c}_9 < \bar{c}_5$  due to the condition (2). Similarly, we obtain the ordering for the right curves.

In the general case, the ordering is deduced from a Hamiltonian path of the directed graphs with vertices the elements of the set  $I_1$  (resp.  $I_2$ ) and edges the pairs  $(p, q) \in I_1^2$  (resp.  $(p, q) \in I_2^2$ ) such that  $\bar{c}_p < \bar{c}_q$ .

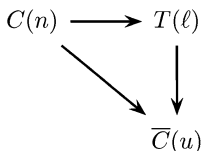
For the permutations  $\tau$  and  $r$  of  $[2n]$ , which correspond to each meander  $\mu$  of  $\mathcal{M}_{2n}$ , we can easily deduce the following proposition:

**Proposition 2** *The permutations  $\tau$  and  $r$  of a meander  $\mu$  of  $\mathcal{M}_{2n}$  define a unique simple meander  $\bar{\mu}$ .*

The pair  $(\bar{\mu}, u)$  is called *central compression* or simply *compression* of the meander  $\mu$ . The simple meander  $\bar{\mu}$  has as same invariants with the meander  $\mu$  the traces and the flow of curves, and hence they have the same perpendicular meander, while  $\bar{\mu}$  has the minimum possible order. Obviously, many meanders of the same or

different order can have the same compression. Two meanders  $\mu_1, \mu_2$  of order  $n_1, n_2$ , of the same parity, respectively, are called *equivalent* according to their compressions (for simplicity *c-equivalent*) iff they have as compression the meander  $\bar{\mu}$  of order  $\bar{n}$ , simple at  $u$ .

Practically, the whole procedure of finding the meander  $\bar{\mu}$  of the compression can be significantly simplified with the help of the perpendicular meander  $\tau$ , according to the following scheme:



Indeed, we have that each curve  $\bar{c}_k \in \bar{C}_1(u)$  coincides with the arc  $(k)$  joining the pairs  $\{\tau(k), \tau(k+1)\}$  of the set  $T_1(\ell)$ . The curves of the set  $\bar{C}_2(u)$  (resp.  $\bar{C}'_2(u)$ ) are deduced from the pairs of the set  $T_2(\ell)$  (resp.  $T'_2(\ell)$ ), if we connect them by extending their arcs in order to intersect the horizontal line on the remaining pairs of points, according to the total order of the curves of the set  $\bar{C}(u)$ .

For example, if we apply the above procedure to the total orders

$$\bar{c}_1 < \bar{c}_3 < \bar{c}_9 < \bar{c}_5 < \bar{c}_7 \quad \text{and} \quad \bar{c}_8 < \bar{c}_6 < \bar{c}_4 < \bar{c}_{10} < \bar{c}_2,$$

we deduce from the perpendicular meander  $\tau$  (Fig. 14.3) the meander  $\bar{\mu}$  of the compression (Fig. 14.2).

We complete the above construction with

**Proposition 3** *For the order  $\bar{n}$  of the meander  $\bar{\mu}$ , we have that  $\nu + 1 \leq \bar{n} \leq n$ .*

**Proof** For the meander  $\mu$  we have

$$2\nu = |C_1(n)| + |C_2(n)| + |C'_2(n)|$$

and for the meander  $\bar{\mu}$

$$2\bar{n} = |\bar{C}_1(u)| + 2|\bar{C}_2(u)| + 2|\bar{C}'_2(u)|$$

Hence,

$$2\bar{n} = |C_1(n)| + |C_2(n)| + |C'_2(n)| = 2\nu + |C_2(n)| + |C'_2(n)| \geq 2\nu + 2$$

given that  $\bar{\mu}$  is simple and has  $\bar{n} \geq 2$ , so  $|C_2(n)|, |C'_2(n)|$  cannot be equal to zero. The relation  $\bar{n} \leq n$  is the result of the definition of the meander of the compression.

**Corollary 1** *If  $n = \nu + 1$ , then the meander  $\mu$  is incompressible.*

Obviously, the inverse argument is not always true.

**Proposition 4** *If  $n$  is even, then there do not exist meanders of  $\mathcal{M}_{2n}$  having compression with  $\bar{n} = 1$ .*

**Proof** A compression of order  $\bar{n} = 1$  means that  $\theta(n) = \theta'(n) = 1$ , which holds only if  $n$  is odd, which is a contradiction.

**Proposition 5** *If  $n$  is odd, then*

1. There do not exist meanders of  $\mathcal{M}_{2n}$  having compression with  $\bar{n} = 2$  and  $u = 2$ .
2. There exist  $M_{\frac{n+1}{2}}^2$  meanders of  $\mathcal{M}_{2n}$  having compression with  $\bar{n} = 1$ .

**Proof**

1. A compression of order  $\bar{n} = 2$  at  $u = 2$  means that  $\theta(n) = 2$  and  $\theta'(n) = 0$ , or  $\theta(n) = 0$  and  $\theta'(n) = 2$ , which holds only if  $n$  is even, which is a contradiction.
2. A compression of order  $\bar{n} = 1$  means that  $\theta(n) = \theta'(n) = 1$ . Since the meandric curve is separated at  $n$ , then two open meanders (where an open meander of order  $n$  is a self-avoiding curve that travels from left to right, crossing an infinite horizontal line  $n$  times [2]) are formed. Each one of those meanders needs one extra point in order to become a closed meander of order  $\frac{n+1}{2}$ . Thus, we have  $M_{\frac{n+1}{2}}$  meanders from each part of the  $n$ -line sewed to produce the compression.

## 14.4 Conclusion

We have introduced the compression of a meander geometrically. We also applied this mathematical formulation for the representation of  $k$ -noncrossing closed RNA secondary structures. The uniqueness of the compression is established by the ordering of the corresponding open curves, which is deduced according to the flow of the meander. The preservation of invariants gives us new types of meanders: the simple and the perpendicular.

In this way, we have a two-level classification of all the meanders of order  $n$ , according to their perpendicular meander with or without information on the ordering of its corresponding open curves. This classification could be a topic of future study. In parallel, the next step of our research is the algorithmic interpretation of the compression directly from the meandric permutations.

Finally, the main open problem is the reverse procedure of compression. The decompression of a meander to others of larger order having the same traces, number of cuttings and flow, seems to be the final step for integrating the procedures of cutting and compressing meanders, and in parallel being very promising not only for enumeration results but also for applications in the related biological problems.

## References

1. Alexiou A, Psiha M, Vlamos P (2011) Combinatorial permutation based algorithm for representation of closed RNA secondary structures. *Bioinformatics* 7(2):91–95, PubMed: 21938211
2. Lando S, Zvonkin A (1993) Plane and projective meanders. *Theor Comput Sci* 117:227–241
3. Rosentiel P (1984) Planar permutations defined by two intersecting Jordan curves. *Graph theory and combinatorics*, Academic Press, pp 259–271
4. Panayotopoulos A, Tsikouras P (2003) Properties of meanders. *J Comb Math Comb Comput* 46:181–190
5. Panayotopoulos A, Vlamos P (2008) Meandric polygons. *Ars Combin* 87:147–159
6. Zhan Y, Guo M (2005) A permutation-based genetic algorithm for predicting RNA secondary structure—a practicable approach. In: Wang L, Jin Y (eds) *Fuzzy systems and knowledge discovery*, vol 3. Springer, Berlin, pp 861–864

# Chapter 15

## Exploring the Online Satisfaction Gap of Medical Doctors: An Expectation-Confirmation Investigation of Information Needs

Panos E. Kourouthanassis, Patrick Mikalef, Margarita Ioannidou, and Adamantia Pateli

**Abstract** This research explores the satisfaction gap between the expectations of medical doctors when using the Internet to search for health-related information, and the confirmations they receive following the use of specific information sources to meet their information needs. We executed a quantitative study on 303 medical doctors to capture their online information-seeking behavior. Results suggest that authoritative online information sources are strongly related with the derived satisfaction of medical doctors' online information needs, whilst expectation fulfillment is not related with usage of non-authoritative sources. Nevertheless, doctors' perceptions regarding the information quality of online sources, and discerning personal constraints regarding Internet use, moderate the relationship between online source usage and the effectuation of their expectations.

### 15.1 Introduction

Extant research on the online information-seeking behavior of doctors primarily emphasizes around three interweaved themes: (a) exploring the needs or motives that underpin the use of the Internet by medical professionals, (b) pinpointing the online information sources utilized by doctors and their frequency of use, and (c) framing the barriers or obstacles that hinder the use of digital sources. Research findings in these themes suggest that there are commonalities in the online search behavior of doctors and in the factors that discourage Internet usage. In effect, doctors primarily use the Internet to retrieve information that would help them in

---

P.E. Kourouthanassis (✉) • P. Mikalef (✉) • M. Ioannidou • A. Pateli  
Department of Informatics, Ionian University, 7 Tsirigoti Square, Corfu 49100, Greece  
e-mail: [pkour@ionio.gr](mailto:pkour@ionio.gr); [mikalef@ionio.gr](mailto:mikalef@ionio.gr); [margaritaioannidou@gmail.com](mailto:margaritaioannidou@gmail.com); [pateli@ionio.gr](mailto:pateli@ionio.gr)



work-related activities (such as medication, treatment, and expanding their knowledge and awareness on new protocols and prescriptions), education, or research activities [1, 2, 3, 5]. Search engines, scientific journals, and medical databases comprise the most popular and frequently used online information sources by professionals to supplement their expertise and to keep themselves up to date [4–6]. Interestingly, scholars also report a growing use of social media by medical professionals in order to expand their knowledge and develop more effective communication bridges with their patients [7].

However, the online search behavior of doctors is influenced by a variety of inherent factors that deter the use of digital sources. Personal barriers (i.e., computer illiteracy, lack of time, and difficulty in searching or comprehending information in a language other than the native one of the user) are important reasons that diminish Internet use [8]. Likewise, the quality of online information (i.e., information credibility, accuracy, and timeliness) plays an important role in the selection of digital sources. Because professionals express concerns regarding the existence of inaccurate health-related information on the Web, they tend to downplay the value of sources that they do not perceive as trustworthy or credible [9, 10]. This behavior creates a paradox on the information search behavior of doctors. On the one hand, doctors tend to seek authoritative information on the Internet when they exhibit low perceptions of personal skills and available online information quality [5]. On the other hand, this hinders a narrowly restrictive approach in their online search strategies since they will most likely visit on a recurring basis sources that they are familiar with or they trust [10, 11].

Whilst our theoretical understanding of the online needs and search strategies of medical professionals has been well documented, the relation between the overall information seeking behavior of doctors and the degrees of derived satisfaction from the consumed information remains largely understudied. Arguably, medical professionals will select their online sources based on their information needs. The combination of information needs, coupled with the selected information sources, will generate expectations, which will be confirmed (or disconfirmed) following the use of online sources by medical professionals. Confirmation of the perceived expectations will result to post-usage satisfaction and subsequent reuse intention of the Internet [12]. Drawn on the above, this study attempts to shed light on the following research questions:

- Are there discrepancies between the expectations of doctors from using the Internet and the actual post-usage satisfaction that they receive?
- What is the relation between usage intensity of the Internet and post-usage satisfaction of doctors' online information needs?
- Are there variations between the online satisfaction paths of medical doctors as a result of their perceived barriers of accessing and using the Internet?

To address these questions we performed a quantitative study on 303 medical doctors in Greece. Our theoretical model was grounded on established theories from such disciplines as psychology, management science, and information systems. The structure of this chapter delineates the research questions in the

following. Section 15.2 briefly discusses the theoretical models that underpin our analysis space. Section 15.3 outlines the research design and profile of the study respondents. Section 15.4 presents the results of our empirical study. Section 15.5 concludes the chapter with a discussion of the practical and theoretical implications.

## 15.2 Theoretical Grounding

We rely our investigation lenses on two models that have been extensively used in information science and information systems literature to capture individuals' information behavior and perceived satisfaction when using information resources.

### 15.2.1 *Wilson's Macro-Model Model of Information Seeking Behavior*

Wilson's [13, 14] model posits that the information behavior of individuals is decomposed to three elements: (a) capturing the information goals that direct a certain seeking behavior (commonly referred to as 'information needs'); (b) identifying personal, social, or environmental interventions that reinforce or create resistances to the information seeking behavior; and (c) framing the properties of the information acquisition process (i.e., which information channels or sources are used, whether individuals follow passive or active usage behavior, and so on). The model has been used to explain the online information-seeking behavior of individuals on several usage contexts [15, 16].

### 15.2.2 *Expectation-Confirmation Theory*

The expectation-confirmation theory was originally proposed by Oliver [17] to explain loyalty behavior for consumer products or services. According to the theory, consumers form initial expectations of products or service which are then confirmed (or disconfirmed) following the purchase and consumption processes. Expectations are considered key satisfaction goals because they provide consumers with the reference level for the configuration of alternative evaluations. The impact of positive or negative disconfirmation leads to post-purchase satisfaction (or dissatisfaction), which determines the subsequent behavior. Hence, satisfied consumers are likely to formulate repurchase intentions. Dissatisfied consumers are likely to shift to other alternative products or services. The expectation-confirmation theory has been adapted from Bhattacharjee [12] to explain

**Table 15.1** Operationalization of the study investigation lenses

Theoretical articulations	Operationalization
Information needs expectations and confirmations	Work-related information needs related to epidemiology, diagnosis, and therapy. Knowledge expansion information needs related to drugs/medicine, scientific developments and developments in the field of medical equipment. Research information needs related to scientific studies and educational work.
Information barriers	Personal barriers: Individual shortcomings that discourage Internet usage (computers illiteracy, information processing illiteracy, lack of time). Information quality barriers: Perceptions that online information sources provide incomplete, inaccurate or outdated information.
Information sources	Authoritative sources: Regulated medical information sources that adhere to predefined quality criteria or standards (e.g., scientific databases, medical associations' websites). Non-authoritative sources: Unstructured or non-regulated medical information sources (e.g., blogs, search engines, web portals).

individuals' continuance intention to use information systems and services. In this case, expectations are met through the perceived performance of the information system or service. In accordance to the original model, positive disconfirmations are likely to lead to satisfied users. The model has been extensively employed by information systems scholars to explain post-usage satisfaction and reuse behavior of various online information services (e.g., [18, 19]).

Table 15.1 summarizes the operationalization of our investigation directions under the prescriptions of the underlying theoretical models.

### 15.3 Research Design and Profile of Respondents

To understand how the usage of online information sources impacts the confirmation of expectations regarding medical knowledge, we collected primary data through questionnaires distributed to doctors of medicine (M.D.). The questionnaire was developed specifically for the purpose of this study and comprised four main parts. The first part contained questions relating to demographic and professional information. Part two revolved around the expectations that doctors develop regarding the potential value of information sources and to what degree these are fulfilled. The third part measured the frequency of use for a number of authoritative and non-authoritative information sources, whilst the final part of the questionnaire contained questions asking respondents to evaluate the perceived barriers they face when searching for medical information.

**Table 15.2** Demographics of study ( $n = 303$ )

Gender	
Male	61.7 %
Female	38.3 %
Age	
<40	62.4 %
40–50	25.1 %
50–60	8.9 %
>60	3.6 %
Additional education	
Related master degree	20.1 %
Related doctoral degree	20.1 %
Unrelated master degree	4.6 %
Unrelated doctoral degree	1.7 %
None	53.5 %
Current work facility	
University hospital	23.4 %
Public hospital	41.3 %
Primary healthcare unit	3.3 %
Public medical office	0.7 %
Private hospital	0.7 %
Healthcare services group	1.0 %
Private medical office	27.1 %
Other	2.6 %
Internet usage frequency for medical information search	
Never	0.3 %
Once a month	3.0 %
Once a week	17.2 %
Everyday	79.5 %

The questionnaire was distributed to four major hospitals operating in Greece in order to be filled out by medical doctors of varying specializations. Respondents were given the choice to fill out the questionnaire either in printed form, or through an online survey. The data collection was open between November 2013 and January 2014. Out of the 800 questionnaires handed out, a total of 310 were returned, from which 303 were rendered as suitable for further analysis, yielding a valid response rate of 37.8 %. Table 15.2 outlines the demographic profile of the study respondents.

The majority of responses were from male doctors (61.7 %), with female doctors accounting for the remaining 38.3 %. The age group with the largest proportion of responses belonged to doctors aged below 40 years (62.4 %), with the next in sequence being the age group ranging from 40 to 50 (25.1 %). In our sample there was an approximately even dichotomization between respondents with an additional related degree (Masters 20.1 % and Doctoral 20.1 %) to ones with no further education (53.5 %) or unrelated further studies (6.3 %). Most subjects were currently employed in public hospitals (41.3 %), and the vast majority were very

frequent users of online medical information sources (79.5 %). The most appeared specializations in our sample were cardiologists (20.5 %  $n = 62$ ), pathologists (12.5 %  $n = 38$ ), and orthopedists (7.3 %  $n = 22$ ).

In order to examine the effectiveness of various online information sources on satisfying doctors' knowledge requirements, questionnaire items developed on the basis of the expectation-confirmation model were formulated. Respondents were asked to evaluate on 9-point Likert scale (1—Not at all, 9—Totally) the degree to which they expected their professional requirements to be fulfilled by online information sources (expectation), and then the level to which these expectations were realized (Confirmation). To capture the full range of requirements we distinguished between elements relating to: (1) work, (2) knowledge, and (3) research needs. Additionally, for each type of information source, questions measuring the frequency of use were employed. These questions followed a 9-point Likert scale, from 1—Never use, to 9—Always use, with items being grouped into Authoritative and Non-Authoritative sources (Table 15.3).

**Table 15.3** Descriptive statistics for frequency of usage and expectation–confirmation

Frequency of information source usage			Expectation–confirmation of information requirements				
			Expectation		Confirmation		
Mean	Std. Dev.		Mean	Std. Dev.	Mean	Std. Dev.	
<i>Authoritative</i>			<i>Work</i>				
Scientific digital databases	6.87	1.98	Epidemiology	6.84	1.95	6.41	1.96
Medical corporation websites	6.40	2.29	Diagnosis	6.50	1.94	6.09	2.02
Online scientific journals (specialized)	6.35	2.35	Therapy	7.06	1.72	6.57	1.88
Online scientific journals	6.21	2.32	<i>Knowledge</i>				
Digital books	5.24	2.50	Drugs/medicine	7.48	1.53	6.96	1.76
Public authorities websites	5.11	2.35	Scientific developments	8.00	1.44	7.41	1.71
<i>Non-authoritative</i>			Medical equipment	7.11	1.68	6.36	1.92
Search engines	7.72	1.71					
Medical portals	5.31	2.41	<i>Research</i>				
Pharmaceutical company Websites	4.16	2.20	Scientific studies	7.23	1.79	6.62	1.94
Medical equipment provider websites	4.00	2.19	Educational work	6.80	1.75	6.32	1.86
Social networking websites	3.88	2.73					
Online forums	3.52	2.56					
Medical doctors personal websites	3.39	2.29					

## 15.4 Results

### 15.4.1 *Disconfirmations of Doctors' Online Information Expectations*

The first step of our analysis was aimed at determining whether the expectations of medical doctors regarding the fulfillment of their requirements are actually confirmed. To do so, we calculated the difference between expectation and confirmation for a number of requirements relating to the medical profession. For each of these requirements we performed a paired difference *t*-test in which the value of [Expectation – Confirmation] is computed and then evaluated on the degree of its significance. Results depicted in Table 15.4, indicate that for requirements pertaining to each of the three categories, expectations are significantly different from confirmations. Since *t*-values are positive, this signifies that when searching on online information sources for medical information, expectations are not satisfied. This outcome provided a basis for further examination as to which types of information sources fulfill the different classifications of requirements.

### 15.4.2 *Relating Online Information Sources with Post-usage Satisfaction*

We employed partial least squares (PLS) analysis to obtain path weights for relationships, and coefficients of determination for the dependent variables that measure doctors' post-usage satisfaction. Significance of associations was determined by

**Table 15.4** Paired samples *t*-test for all medical requirements

	Paired differences				<i>t</i> -value	df
	Mean	Std. Dev.	95 % Confidence interval of difference			
			Lower	Upper		
<i>Work</i>						
Epidemiology	0.428	1.501	0.258	0.597	4.968**	303
Diagnosis	0.414	1.446	0.251	0.578	4.997**	303
Therapy	0.490	1.340	0.339	0.641	6.378**	303
<i>Knowledge</i>						
Drugs/medicine	0.516	1.300	0.370	0.663	6.928**	303
Scientific developments	0.586	1.177	0.453	0.718	8.674**	303
Medical equipment	0.743	1.567	0.567	0.920	8.272**	303
<i>Research</i>						
Scientific studies	0.618	1.460	0.454	0.783	7.386**	303
Educational work	0.474	1.653	0.287	0.660	4.997**	303

\*\**p* < 0.01

running a bootstrapping procedure with 500 samples. Using two-tailed significance values, significance intervals are set as  $p < 0.05$  ( $t \geq 1.968$ ),  $p < 0.01$  ( $t \geq 2.592$ ), and  $p < 0.001$  ( $t \geq 3.323$ ) for 303 degrees of freedom.

Prior to empirically examining our associations we performed an evaluation of measurement model. We conceptualized the constructs by using formative indicators since each item represents a unique facet of the underlying factor. In contrast to reflective measurement models in which reliability, convergent and discriminant validity are assessed, formative measures require a different approach. Since items comprising a formative construct are considered as being an integral part of the overall construct, it is imperative that content validity is covered. This requires that every facet of the construct is included through the various items to measure it. We established content validity through an extensive literature review, and based on an aggregation of past studies that conceptualized each latent variable we developed items accordingly. Additionally, we tested for multicollinearity, which in contrast with reflective constructs is a problem for formative measures [20]. We assessed multicollinearity through the Variance Inflation Factor (VIF). For all constructs VIF was slightly above 1 and below 3, thus indicating an absence of collinearity between items [21]. With absence of multicollinearity, and content validity of constructs confirmed, we proceeded to analyze the structural model. The results of the PLS algorithm with significance of weights are depicted in Fig. 15.1 below.

The outcomes of the PLS analysis confirm the positive and significant association between the frequency of use of authoritative information sources and confirmation of expectations. Contrarily, the prevalence of non-authoritative information sources use is not found to significantly impact confirmation of expectations. More specifically, we found that when authoritative information sources use

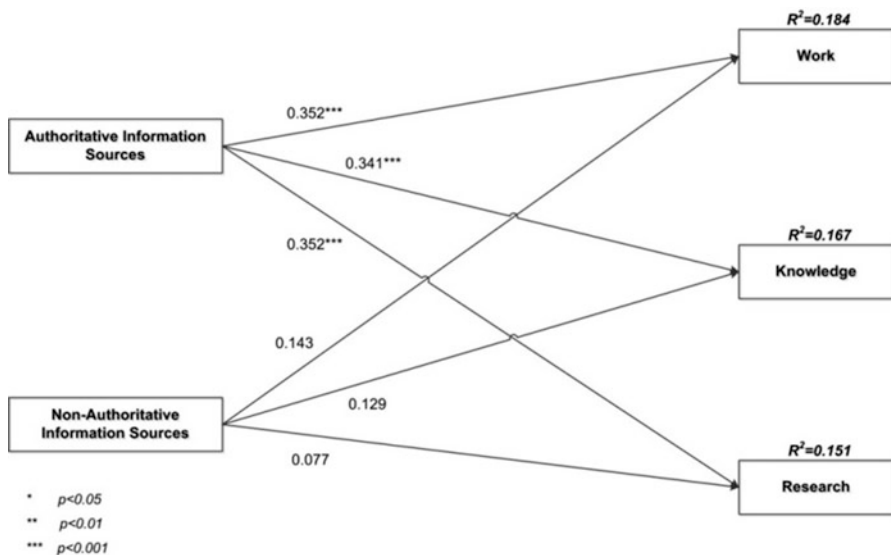


Fig. 15.1 Structural model with path coefficients and confidence intervals

increases, so does the fulfillment of expectations for work-related requirements ( $\beta = 0.352$   $t = 4.577$ ). Moreover, doctors that were more inclined to use authoritative information sources were found to have a greater degree of requirement realization for aspects relating to enhancement of knowledge for their supporting tasks ( $\beta = 0.341$   $t = 3.798$ ). Finally, the positive association of authoritative information sources use is confirmed for need fulfillment of research-related aspects ( $\beta = 0.352$   $t = 4.807$ ). Contrariwise, despite the positive association of non-authoritative use with work ( $\beta = 0.143$   $t = 1.599$ ), knowledge ( $\beta = 0.129$   $t = 1.462$ ), and research ( $\beta = 0.077$   $t = 1.034$ ) oriented requirement fulfilment, the level of significance does not indicate a valid relation. Therefore, we can conclude that non-authoritative information sources do not facilitate doctors' expectation realization when searching for information online. The coefficient of determination values indicate that 18.4 % ( $R^2 = 0.184$ ) of variation is explained for work related medical information needs, 16.7 % ( $R^2 = 0.167$ ) for research, and 15.1 % ( $R^2 = 0.151$ ) for research by the frequency of use of authoritative and non-authoritative information sources. These values indicate a moderate explanatory power hinting that there are factors that are not included in the conceptual model that may have a significant effect on confirmation of expectations.

Taking into account the various barriers that doctors face when attempting to search medical information online, we perform two split sample analysis based on (1) doctors' perceptions of information quality, and (2) personal constraints relating to lack of knowledge or sources. For each barrier, the sample is split into two sub-samples of equal size, using the median as the threshold value. Hence, the sample is split into doctors that are with high/low perceptions regarding online medical information quality, and high/low personal barriers when seeking for such data. The weights and significance levels for each subgroup of the two control barriers are illustrated in Table 15.5.

**Table 15.5** Split sample path coefficients, significance levels, and coefficients of determination

	Information quality perceptions				Personal barriers			
	High		Low		High		Low	
	Beta	R <sup>2</sup>	Beta	R <sup>2</sup>	Beta	R <sup>2</sup>	Beta	R <sup>2</sup>
<i>Work</i>								
Authoritative	0.492***	0.278	0.045	0.047	0.404***	0.309	-0.049	0.027
Non-authoritative	0.056		0.199		0.217***		0.170	
<i>Knowledge</i>								
Authoritative	0.409***	0.341	0.086	0.265	0.323***	0.284	0.376**	0.292
Non-authoritative	0.238***		0.483		0.280***		0.305	
<i>Research</i>								
Authoritative	0.542***	0.319	0.302	0.096	0.405***	0.303	-0.286	0.085
Non-authoritative	0.036		-0.201		0.209***		0.165	

\* $p < 0.05$   
 \*\* $p < 0.01$   
 \*\*\* $p < 0.001$



From the split sample analysis it is evident that there are considerable differences in the effect of frequency of online information sources usage on confirmation of expectations. The outcomes show that this association is dependent on the perceptions regarding the quality of online information as well as on personal constraints of doctors. This indicates that fulfillment of requirements is dependent on factors which are contingent upon personal beliefs of doctors about the value of online medical information, and on their competence in using computers and effectively utilizing digital repositories. Indicative of this is the finding that users with high perceptions regarding the quality of online medical information tend to have a stronger relation between the frequency of use of information sources and fulfillment of their expectations than those with low perceptions. Strikingly, the frequency of usage of information sources on fulfillment of requirements is found to be significant only for doctors who perceive themselves as having high personal barriers.

### **Conclusions**

This study provides a first insight into the perceived discrepancy between doctors' online expectations for seeking health-related information and the satisfaction they receive after using different types of information sources. To our knowledge this is the first study that reports a satisfaction gap in doctors' online information seeking behavior; expectations for meeting their information needs through online sources are apparently higher than the satisfaction they receive.

Delving on this observation, our research confirms that doctors replicate their contemporary information search strategies in the online environment. Specifically, usage of authoritative sources is likely to lead to high degrees of satisfaction for doctors' work-related, knowledge expansion-related, and research- and education-related information needs. In contrast, satisfaction of doctors' information needs through online means does not seem to be related with the intensity of using non-authoritative online information sources.

This finding is contradicted if we factor for the perceived information barriers of the sample. Interestingly, doctors that are highly discouraged to use the Internet because of personal insufficiencies (e.g., lack of computer skills) or low trust on the quality of available information on the Internet tend to exhibit a match of their online information satisfaction through both authoritative and non-authoritative sources. This outcome implies that doctors perceiving high degrees of information barriers may be inclined to unveil a restrictive online information search behavior by repeatedly visiting the same websites and, consequently, narrowing their knowledge space. On the opposite side, doctors that perceive they possess the necessary skills to search and process online information tend to demonstrate an inconsistency in

(continued)

(continued)

matching their online satisfaction through any type of information source. This is a first indication that devising actions that mitigate the information barriers may help medical doctors to exit from their 'online comfort zone' and explore with a critical perspective the available online sources of health-related information.

## References

1. Masters K (2008) For what purpose and reasons do doctors use the Internet: a systematic review. *Int J Med Inform* 77(1):4–16. <http://dx.doi.org/10.1016/j.ijmedinf.2006.10.002>
2. Younger P (2010) Internet-based information-seeking behaviour amongst doctors and nurses: a short review of the literature. *Health Info Libr J* 27(1):2–10. doi:10.1111/j.1471-1842.2010.00883.x
3. Davies K (2007) The information-seeking behaviour of doctors: a review of the evidence. *Health Info Libr J* 24(2):78–94. doi:10.1111/j.1471-1842.2007.00713.x
4. Clarke MA, Belden JL, Koopman RJ, Steege LM, Moore JL, Canfield SM, Kim MS (2013) Information needs and information-seeking behaviour analysis of primary care physicians and nurses: a literature review. *Health Info Libr J* 30(3):178–190. doi:10.1111/hir.12036
5. Kostagiolas P, Korfiatis N, Kourouthanasis P, Alexias G (2014) Work-related factors influencing doctors search behaviors and trust toward medical information resources. *Int J Inf Manage* 34(2):80–88. <http://dx.doi.org/10.1016/j.ijinfomgt.2013.11.009>
6. Krizt M, Gschwandtner M, Stefanov V, Hanbury A, Samwald M (2013) Utilization and perceived problems of online medical resources and search tools among different groups of European physicians. *J Med Internet Res* 15(6):e122
7. Antheunis ML, Bates K, Nieboer TE (2013) Patients' and health professionals' use of social media in health care: motives, barriers and expectations. *Patient Educ Couns* 92(3):426–431. <http://dx.doi.org/10.1016/j.pec.2013.06.020>
8. Bernard E, Arnould M, Saint-Lary O, Duhot D, Hebbrecht G (2012) Internet use for information seeking in clinical practice: a cross-sectional survey among French general practitioners. *Int J Med Inform* 81(7):493–499
9. Falagas ME, Pitsouni EI, Malietzis GA, Pappas G (2008) Comparison of PubMed, Scopus, web of science, and Google scholar: strengths and weaknesses. *FASEB J* 22(2):338–342
10. Hughes B, Wareham J, Joshi I (2010) Doctors' online information needs, cognitive search strategies, and judgments of information quality and cognitive authority: how predictive judgments introduce bias into cognitive search models. *J Am Soc Inf Sci Technol* 61(3):433–452. doi:10.1002/asi.21245
11. Jerome PK (2011) We should encourage browsing. *BMJ* 342. doi:10.1136/bmj.d2182
12. Bhattacharjee A (2001) Understanding information systems continuance: an expectation-confirmation model. *MIS Quart* 25(3):351–370
13. Wilson TD (1999) Models in information behaviour research. *J Documentation* 55(3):249–270
14. Wilson TD (1997) Information behaviour: an interdisciplinary perspective. *Inf Process Manage* 33(4):551–572
15. Spink A (2002) A user-centered approach to evaluating human interaction with Web search engines: an exploratory study. *Inf Process Manage* 38(3):401–426. [http://dx.doi.org/10.1016/S0306-4573\(01\)00036-X](http://dx.doi.org/10.1016/S0306-4573(01)00036-X)
16. Kellar M, Watters C, Shepherd M (2007) A field study characterizing Web-based information-seeking tasks. *J Am Soc Inf Sci Technol* 58(7):999–1018. doi:10.1002/asi.20590

17. Oliver RL (1980) A cognitive model of the antecedents and consequences of satisfaction decisions. *J Market Res* 17:460–469
18. Lin CS, Wu S, Tsai RJ (2005) Integrating perceived playfulness into expectation-confirmation model for web portal context. *Inf Manage* 42(5):683–693. <http://dx.doi.org/10.1016/j.im.2004.04.003>
19. Venkatesh V, Thong JYL, Chan FKY, Hu PJH, Brown SA (2011) Extending the two-stage information systems continuance model: incorporating UTAUT predictors and the role of context. *Inf Syst J* 21(6):527–555
20. Jarvis CB, MacKenzie SB, Podsakoff PM (2003) A critical review of construct indicators and measurement model misspecification in marketing and consumer research. *J Consum Res* 30(2):199–218
21. Petter S, Straub D, Rai A (2007) Specifying formative constructs in information systems research. *MIS Quart* 31(4):623–656

# Chapter 16

## A Cloud-Based Data Network Approach for Translational Cancer Research

Wei Xing, Dimitrios Tsoumakos, and Moustafa Ghanem

**Abstract** We develop a new model and associated technology for constructing and managing self-organizing data to support translational cancer research studies. We employ a semantic content network approach to address the challenges of managing cancer research data. Such data is heterogeneous, large, decentralized, growing and continually being updated. Moreover, the data originates from different information sources that may be partially overlapping, creating redundancies as well as contradictions and inconsistencies. Building on the advantages of elasticity of cloud computing, we deploy the cancer data networks on top of the CELAR Cloud platform to enable more effective processing and analysis of Big cancer data.

### 16.1 Introduction

Translational cancer research builds on incorporating multiple levels of biological information within clinical data with aim of gaining better understanding of how cancer works and developing new ways for identifying, preventing and treating the disease. The first challenge in conducting translational studies is that the data is heterogeneous, including phenotype, genotype, expression profiling, proteomics, protein interaction, metabolic analysis data as well as physiological measurements, etc. The second key challenge is that the data is large, decentralized, growing and continually being updated. It originates from different sources, e.g. different

---

W. Xing (✉)

Cancer Research UK Manchester Institute, University of Manchester,  
Manchester M20 4BX, UK  
e-mail: [wei.xing@cruk.manchester.ac.uk](mailto:wei.xing@cruk.manchester.ac.uk)

D. Tsoumakos

Computing Systems Laboratory, National Technical University of Athens,  
Athens 15773, Greece  
e-mail: [dtsouma@cslab.ece.ntua.gr](mailto:dtsouma@cslab.ece.ntua.gr)

M. Ghanem

School of Science and Technology, Middlesex University, Hendon, London NW4 4BT, UK  
e-mail: [m.ghanem@mdx.ac.uk](mailto:m.ghanem@mdx.ac.uk)

experiments and different labs. It is also stored in different distributed databases that are managed by different organizations. The content of such databases is thus typically overlapping, creating redundancies as well as contradictions and inconsistencies.

In this paper, we develop a new cancer data network (CDN) model and associated technology for constructing and managing **self-organizing** content in order to support the integration of biological and clinical data with the research it is spawned from. In addition, CDN offers the ability of track several aspects of patient care according to genetic and molecular profiles to facilitate tailoring of treatment.

The proposed CDN architecture is based on a novel content management model that supports end users in managing distributed, dynamic and evolving data sets. Within CDN, we shift the view of **content** from being a static resource, and introduce it as a **dynamic and intelligent entity** that is able to perform operations such as linking itself to other relevant content. In doing so, the intelligent content can discover implied relationships with other content, identifying redundancies and overlap as well as updating its links with the ecosystem when new content is added or old content is removed or depreciated.

Within the CDN approach, data content is represented as an active object equipped semantic mechanisms that allow a greater degree of flexibility towards automating the procedure of content management and organization. To this end, we define **Active Cancer Data Content** as a logical container that contains the digital data content (i.e., patient data, clinical data, research experiment data, publications, public gene or protein databases, etc.) together with intelligent and autonomic, self-organizing mechanisms for automating content management.

The remainder of this paper is organized as follows. Section 16.2 introduces the underlying principles and design of the CDN; Sect. 16.3 presents the architecture of CDN, focusing on its software components, and on the main interactions between them, and describing how each of them is instantiated for the implementation with EU CELAR cloud platform; Sect. 16.4 describes the related work; and finally, “Conclusion” section provides conclusions, and describes open issues and our planned future work.

## 16.2 The Design of CDN

CDN is designed to bridge the gap between translational research and targeted patient treatment. Hence, the design goals of CDN are (1) to better analyse data obtained dynamically from various bio-instrument sources in order to answer biological question at a system level; and (2) to better translate data obtained from in vitro and in vivo discoveries into the clinic.

## ***16.2.1 Problems and Requirements***

The key challenge CDN addresses is that information stored or published over the web and other specialized data sources is heterogeneous, decentralized, growing and continually being updated. Furthermore, the content living or archiving on different information sources partially overlaps creating redundancies as well as contradictions and inconsistencies. In this section we describe the current issues of the area of personalized medicine research.

### **16.2.1.1 Redundant or Irrelevant Information of Protein and Gene Sequence**

Currently, well over a thousand accessible data sources provide information pertaining to any gene, mRNA or protein sequence (estimated by the number of known SRS “Sequence Retrieval System”) such as polymorphisms, protein interactions and expression levels. The vast majority of the data sources are specialized and are therefore maintained and updated by different organizations. In addition, data sources with the same emphasis (such as nucleotide or protein sequences) are updated and curated at different intervals and with various benchmarks and standards. As a result, many databases contain outdated, redundant or irrelevant information pertaining to the scientific question at hand.

Also, our continually expanding knowledge base adds new dimensions to the content. For example, the cataloging and assessment of functional impact of recently discovered mechanisms of dynamic biological regulation, including but not restricted to microRNAs and our knowledge of protein modification types and permutations, is incomplete. New categorical discoveries and their related information detail will need to be progressively built into any comprehensive content structure.

### **16.2.1.2 Evolving Methods of Data Generation from Multiple Instrument Platforms**

Translational cancer research requires the integration of data from state-of-the-art technologies, for which the methods of translating and interpreting raw instrument data into relevant contextualized biological outputs are continually improving. An example of this is the interpretation of mass spectrometry peptide fragmentation data into qualitative and quantitative peptide and protein data in proteomics experiments. Different instruments produce data with different technical characteristics, including signal-to-noise ratios, raw signal intensities, and data accuracy, precision and resolution. These characteristics are continually changing for the better, but will continue to vary depending on the type and generation of instruments used, new hardware innovations, and the data acquisition and experiment style.

The bioinformatic translation of the raw fragmentation data into peptide and protein identities is also evolving. Current strategies typically employ probabilistic, stochastic or descriptive models to pattern match fragment ion profiles against theoretical profiles generated against assumed protein sequences and modification content. Personalized medicine will dictate a drift away from this data interrogation strategy since each individual labours genomic and proteomic differences that would not be represented in an assumed protein sequence database. This may involve fundamental changes to the data interrogation strategy, for example a migration towards *de novo* sequencing tools, or at the very least changes to scoring of genepeptideprotein sequence assignments and the specific identification of mutations, polymorphisms or variables specific to individuals.

### 16.2.1.3 Creating Genomic Networks

To elucidate the wiring of cellular information processes, current research requires integration of quantitative and dynamic data from several sources. Such information sources could be genomic public database-based, sequence-based or clinical information-based and require various algorithms and software package for data analysis. For maximal output from such data, it is important that the multidimensionality is taken into account and the data can be visualized with differential weighting of individual data sources. For example, gene mutation and gene function interactions can be measured in a static manner using techniques such as yeast 2 hybrid and complement assays as well as the dynamic and quantitative abundances can be included through platforms such as COSMIC, VerScan and Meerkat runs. While each source provides important information, the sources provide complementary aspects of information, which is important to integrate and visualize.

To address the above issues, we design CDN system to support:

1. **Integrating heterogeneous and unstructured content.** It allows scientists to incorporate multiple levels of background information within their studies, such as phenotype, genotype, expression profiling, proteomics, protein–protein interactions, biochemical metabolic studies, and physiology measurement, etc.
2. **Decentralized control and collaborative communities.** The content itself either arises from biological experiments conducted by individual groups or as a result of data integration and analysis studies using data published by other groups.
3. **Multi-discipline.** The information is highly relevant to researchers working on other topics can be shared easily, between specialized data sources (including scientific literature) and databases focusing on specific topics, e.g. organisms, diseases, genes, proteins, metabolic pathways, chemical compounds or on relationships between them.

Our special focus is on addressing the issues of overwhelming and continuous flood of complex information generated and published on a daily basis through the use of Semantic Web Technology. We illustrate our approach in the next section.

## ***16.2.2 Semantic Approach***

CDN aim to develop novel mechanisms for constructing and generating symbiotic, semantically described, self-aware and self-organizing content technology that enables distributed digital objects to be linked together into **CDNs**.

### **16.2.2.1 The CDNs**

A key feature of scientific information is that it is continually evolving. For example, new information about scientific entities (e.g. proteins, genes or diseases) is being published on a daily basis. Furthermore, the decentralized authority over the content, whereby scientists in different organizations publish and manage their own findings, means that information about the same, similar or related entities, may be stored on different sources that evolve in different ways. This inevitably results in partial overlaps in the coverage of the data sources creating redundancies as well as contradictions and inconsistencies at both the entity and the concept level.

We design CDN to link individual elements of the digital content together. By using semantic data model and ontology, we define two types of links among the CDN nodes (i.e. content): explicit links and conceptual links.

Explicit links between different elements are typically stored with the content. At the simplest level an entry on a specific protein on a particular data source can make explicit references to other protein, gene or disease entries on other sources, or to specific supporting scientific publications. Ontologies can be used to either manually or automatically assign scientific papers, genes, proteins to different categories.

Conceptual links between different elements are typically not stored with the content, but can traditionally be inferred by using either statistical/probabilistic analysis techniques or domain knowledge. At the simplest level, users may wish to group proteins together based on the similarity of specific properties such as their effect on the same cellular function, or their causal implication to a similar disease phenotype.

### **16.2.2.2 Retrieval, Integration and Update**

In [1], we developed a semantic information integration approach to integrate and update information from distributed, heterogeneous data sources dynamically.



CDN employs ActOn as a means to retrieve, integrate and manage the CDN Content in an intelligent, active manner.

ActOn is an ontology-based information integration approach that is suitable for highly dynamic distributed resources. To deal with this issue, i.e. that information changes frequently and information requests have to be answered quickly in order to provide up-to-date information, ActOn employs an information cache that works with an update-on-demand policy. Due to the multitude of databases and information sources, the most appropriate sources have to be selected for each query to ensure optimal and relevant data retrieval. To deal with this issue that the most suitable information sources have to be selected from a set of different distributed information sources that can provide the information needed, ActOn adds an information source selection step to the ontology-based information integration. Thereby, the most suitable information source database will be selected for a user query.

### 16.2.3 *CDN Architecture*

Figure 16.1 shows three-tier view of CDN architecture. At the core of the middleware (in blue) lies the CDN ActOn Information Manager that represents the Cancer Data Content and its associated information extraction tools. The CDN ActOn contains the semantic metadata and knowledge management tools that enable modeling and analysing its life cycle and that support reasoning about the content. CDN also contains the workflow tools (Workflow engine) that enable the statistical analysis of the content enabling it to self-organize when linking with other content. Finally, the CDN also includes semantic-aware and peer-to-peer based networking functionality that enables the content to discover other content and communicate with it.

#### 16.2.3.1 **System Components**

We use a bottom-up description of the components shown in Fig. 16.1.

**CDN Semantic Model.** The bottom layer represents existing and traditional data sources that will be used within CDN. Digital content elements on the sources will be identified and extracted and represented as Knowledge Cells (KC) that represent the core of an Data Content object and that represent nodes in abstract CDNs. Data sources can be accessed through the middleware and be offered to the application platform.

**ActOn Information Manager.** CDN middleware employs ActOn [1, 2], a semantic information integration system, to connect the data sources to the CDN system in order to: (a) deploy the Data Content and place it inside CDN which contain extra information about the content that make it both self-aware and context-aware together, and (b) to link the Data Content in multiple Data Content

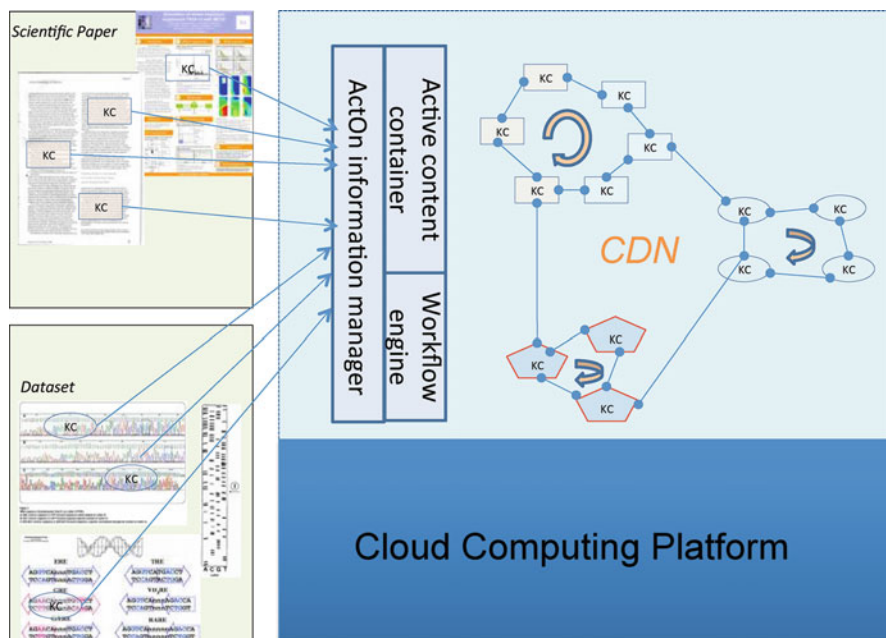


**Fig. 16.1** Overview of the CDN architecture

Networks. During system operation, the links (the edges in the network graph shown in Fig. 16.1) between Data Content entities (the nodes in the network graph in Fig. 16.1) can be re-organized based on statistical analysis, user preferences or other types of runtime information.

**Workflow Engine.** The Workflow engine enables data document access over preprocessing, tokenization, parsing, named entity recognition to the final consumer. It implements specialized workflows that support the different types of users of the system (data publishers, curators and end users) in combining data retrieval, integration, semantic annotation and deployment of Data Content within data analysis tasks in end user applications. The starting point for implementing the workflow engine is to employ Tarverna [3] workflow system (authoring tools and execution engines) for the integration and analysis of a wide variety cancer data (including genomic, proteomic data sets, as well as free text publications).

**Semantic Web User Interface.** At the top-level, a user interface includes functions that can be used to connect to the CDN middleware in order to: (a) Retrieve content from the distributed data sources (shown as different databases in the bottom of Fig. 16.1) in order to create the relevant Data Content. When Data Content is created, it is passed to the CDN middleware in order to be deployed in CDNs. (b) Interact with the user, i.e. issue user-queries and get back results which CDN can present to the users in an advanced way, showing the Knowledge Cells (KC) inside the retrieved content. This way, the user can use the KC in order to issue/refine further queries or even browse based on a given KC in order to find similar KCs and iteratively refine his/her queries within CDN in order to get satisfactory results.

## 16.3 Related Work

In the life sciences area there are several systems available that add semantic annotations, primarily these are done through Medline or similar literature databases. Some examples include iHop2, WhatIzIt3 and EBIMed4, and BioAlma5 [4–6]. Entities (such as gene names, protein names, drug names) are recognized, and links are added, however a disadvantage is that the recognition is not **active**, it is done once, off-line, and is not active in the CDN sense. Since the semantic framework to recognize entity identity across different services is currently missing, these services all point to a small subset of the data that is available for these entities, i.e. these systems are like isolated silos, compared to CDN’s model of self-organizing, distributed structure. Adding semantic markups to more structured data is a relatively new area that has not been systematically explored in the biosciences. Such a system would take as input structured texts, such as protein sequence files, or entire databases, such as the EMBL, PDB, etc., then would add database cross-reference information based, in a way similar to SRS or MRS, then also add semantic annotations, similar to iHop [6–8].

## 16.4 Implementation

We prototyped the CDN system (shown in Fig. 16.2) using Java Spring Framework and RDF Jena API. Spring is a software toolkit that can be used to program web-based application and data management system. Jena is a Java API that can be used to create and manipulate RDF models. By using Spring framework, we are able to code the system in Java following the WSRF specification. We use Jena OWL toolkit for creating, manipulating and querying the semantic metadata of Data Content.

Given the volume of the cancer data is large, we use CELAR cloud platform, an elastic cloud computing platform [9], to process and build the CDN networks. The EU CELAR cloud can deliver a fully automated and highly customizable system for elastic provisioning of resources within cloud computing infrastructures. It therefore can provide large-scale computation resources required by CDN. In addition, the CELAR platform can also provision particular types of computing resources

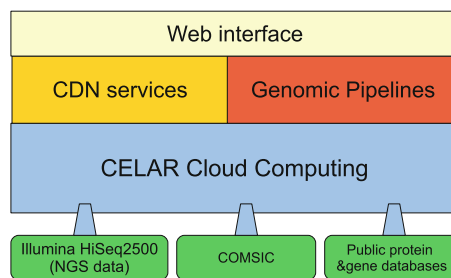


Fig. 16.2 The CDN implementation



**Fig. 16.3** An example of CDN network

required by CDN dynamically, such as windows system with large memory or large amount CPU resources of linux systems, etc. Currently our prototype implementation is mainly for creating and managing gene mutation data and the NGS variation detection data. The initial results are shown in Fig. 16.3.

## Conclusion

In this paper we have presented CDN an active content management system for personalized medicine research. CDN is based on a semantic content network approach which overcomes some of the limitations of current other content management approaches when dealing with dynamic, distributed and redundant bio-data sources.

Our main contribution over the state of the art in content management systems is that we have proposed Cancer Data Content architecture supporting deployment of Cancer Data Content, defining Cancer Data Content containers and the networking capabilities that allow remote interactions between Data Content entities. We also prototyped CDN as a cloud-based, networking middleware for Cancer Data Content discovery and communication.

The initial results show that CDN can facilitate both the cataloguing of samples collected during routine research and manage datasets generated by numerous multi-step experiments carried out from a single sample. For example, the CDN can provide a platform whereby all tissue samples, experimental step samples, datasets and analysis can be compiled and linked allowing ease of access to every stage in an open manner in order to streamline research and increase productivity.

**Acknowledgements** This work is supported by EU FP7 CELAR project.

## References

1. Xing W, Corcho O, Goble C, Dikaiakos MD (2010) An ActOn-based semantic information service for grids. *J Future Gen Comput Syst* 26(3):324–336. doi:10.1016/j.future.2009.10.003
2. Xing W, Corcho O, Goble C, Dikaiakos M (2007) Active ontology: an information integration approach for highly dynamic information sources. In: European semantic Web conference 2007 (ESWC-2007), Innsbruck, June 2007 (Poster)
3. Oinn T, Addis M, Ferris J, Marvin D, Senger M, Greenwood M, Carver T, Glover K, Pocock MR, Wipat A et al Taverna: a tool for the composition and enactment of bioinformatics workflows. *Bioinformatics* 20(17):3045–3054
4. Rebholz-Schuhmann D, Kirsch H, Gaudan S, Arregui M, Nenadic G (2006) Annotation and disambiguation of semantic types in biomedical text: a cascaded approach to named entity recognition. In: Proceedings of the EACL workshop on multi-dimensional markup in NLP, Trento
5. Bioalma (2009). <http://www.bioalma.com>
6. Fernandez JM, Hoffmann R, Valencia A (2010) ihop web services family. In: JBI, pp 102–107
7. Sequence Retrieval System (2010). <http://srs.ebi.ac.uk>
8. Hekkelman ML, Vriend G (2005) Mrs: a fast and compact retrieval system for biological data. *Nucleic Acids Res* 33(Web-Server-Issue):766–769
9. EU CELAR Project (2013–2015). <http://www.celarcloud.eu/>

# Index

## A

Addiction, 126, 127, 129, 144, 150–160  
Adolescence health, 125–160  
Aggregation, 100, 173, 174, 181, 186, 224  
Analytical solution, 174, 181  
Artificial intelligence (AI), 80, 81  
Atherogenesis, 174, 181, 185, 191

## B

Balance disorders, 61–67  
Blood plasma flow, 173–183

## C

Cardiovascular diseases (CDs),  
50, 71, 72, 74, 80, 88, 154, 173,  
174, 181  
Clinical decision support systems (CDSS),  
70, 125–160  
Computer-aided diagnosis (CAD)  
program, 70  
systems, 69–76  
Cybernetics, 5, 43, 45

## D

Daily functions, 71, 72, 127, 129, 147–150  
Decision making, 70, 80  
Decision support system, 61–67  
Deposition probability, 3–45  
Disordered proteins, 49–58

## E

Elderly, 67, 70, 71, 73

## F

Frailty, 69–76, 125

## G

Geriatric clinical medicine, 71  
Gravitational acceleration, 5, 8–12, 14, 43

## H

Human diseases, 81, 96

## I

Information, 4, 5, 38–40, 42–45, 51, 58,  
62, 63, 73, 80, 81, 93, 127, 130, 160,  
215, 217–227, 229, 231–236  
Inverted oblate spheroid, 174, 175, 177, 178,  
180, 181, 186–191

## K

Kelvin inversion, 174–176, 181, 186

## L

Low-density lipoproteins (LDLs), 173–183,  
185–191

## M

Mathematical model, 64, 173–183, 185–191  
Multi-scale modeling, 62, 63

## N

Neurological disorders, 91, 125–128, 142–147

**P**

Pattern extraction, 81  
Posttranslational modifications, 50, 55, 57  
Precipitation of lipoproteins, 186  
Psychological disorders, 126–128, 133–142

**R**

Respiratory system, 5, 7, 8, 43–45

**S**

Sedimentation, 3–45, 174  
Stokes flow, 174, 178, 179, 181, 186,  
188, 191  
Stream function, 174–181, 186–188, 190, 191

**Z**

Zonal harmonic, 8, 45